Investigating the mechanisms underlying Alzheimer's disease using a novel organotypic brain slice culture model

Croft, Cara Louise

Awarding institution:
King's College London

Investigating the mechanisms underlying Alzheimer's disease using a novel organotypic brain slice culture model

Cara Louise Croft

Thesis submitted in fulfilment of the degree of Doctor of Philosophy

Department of Basic and Clinical Neuroscience

Institute of Psychiatry, Psychology and Neuroscience

King's College London

March 2016

Declaration

I hereby declare that all of the work presented in this thesis is my own.

Cara Louise Croft

March 2016

Acknowledgements

I would first like to thank Dr. Wendy Noble, my primary supervisor, for her outstanding support and encouragement over the course of my PhD project. Wendy was always there to provide guidance and positive advice throughout the project but also allowed me to drive the project independently, and for that I am truly grateful. I would also like to extend thanks to Dr. Diane Hanger, my secondary supervisor, for her excellent additional support, guidance and input to the project. I would also like to thank the National Centre for the Replacement, Refinement and Reduction of Animals in Research (NC3Rs) for funding this work. I am also thankful to members of team tau for their positivity, energy and warmth in the laboratory, office (and in the pub!). I am eternally grateful to my parents and family for their constant support of my career and life goals and their loving and caring nature. I am also thankful to have such fabulous friends whose support and encouragement enables me to work hard but play hard too.

Lastly, this thesis is dedicated in loving memory of Miss Dorothy Knowles, one of the strongest, most independent women to have played a part in my life.

Abstract

Alzheimer's disease is a devastating progressive neurodegenerative disorder characterised by deposits of amyloid-β in extracellular plaques, intracellular neurofibrillary tangles comprising highly phosphorylated and aggregated tau species, synaptic dysfunction and neuronal death. Although several transgenic mouse models of Alzheimer's disease have been developed, *in vivo* studies using transgenic mice are time- and cost- consuming, and it is imperative that more ethically sustainable alternatives, which allow faster translation to the clinic, are developed. This thesis aims to determine if organotypic brain slice cultures from 3xTg-AD mice recapitulate key features of *in vivo* brain and can be used in mechanistic and pre-clinical Alzheimer's disease studies.

Organotypic brain slice cultures prepared from 3xTg-AD mouse pups and maintained in culture for several weeks developed highly phosphorylated and high molecular weight tau species, increased amounts of β-amyloid and showed increased activation of cyclin-dependent kinase 5 over time. These biochemical changes closely recapitulate the molecular changes observed in *in vivo* models and post-mortem Alzheimer's disease brain. In addition, brain slices from wild-type and 3xTg-AD mice showed altered tau release characteristics, indicating a distinction in the mechanisms underlying physiological and pathological tau release. These data support the notion that brain slice cultures can be used to understand the mechanisms and pathways underlying the development and progression of Alzheimer's disease.

Furthermore, the utility of brain slice cultures for pre-clinical drug discovery was demonstrated following the application of tau-based therapies that rescued key disease features in brain slice cultures in a similar manner to that previously reported *in vivo*. In addition, treatment of 3xTg-AD organotypic slice cultures with the amyloid-binding agent, BTA-EG_4, revealed novel effects of this compound on tau that were associated with the inhibition of glycogen synthase kinase-3.

The findings of this thesis therefore support the use of organotypic brain slice culture models as an alternative to, at least some, *in vivo* research for investigations into the molecular mechanisms underpinning Alzheimer's disease and related neurodegenerative tauopathies, as well as their use as a platform for pre-clinical drug screening and development for these disorders.

Contents

List of Figures

List of Tables

Publications arising from this thesis

Croft CL, Wade MA, Kurbatskaya K, Hughes MM, Phillips EC, Hanger DP, Noble W. (2016) Altered physiological and pathological tau release in a novel organotypic brain slice culture model of Alzheimer's disease. *In preparation.*

Croft CL, Wade MA, Kurbatskaya K, Hughes MM, Phillips EC, Hanger DP, Noble W. (2016) Inhibition of GSK-3 with the amyloid-binding agent BTA-EG_4 reduces tau phosphorylation in a model of Alzheimer's disease. *In preparation.*

Kurbatskaya K, Dentoni G, Hughes MM, Phillips EC, **Croft CL**, Wade MA, Al-Sarraj S, Troakes C, Hanger DP, Noble W. (2015) Early upregulation of calpain activity precedes tau phosphorylation and loss of synaptic proteins in Alzheimer's disease brain. *Acta Neuropathologica Communications. Submitted*.

Phillips EC, **Croft CL**, Kurbatskaya K, O'Neill MJ, Hutton ML, Hanger DP, Garwood CJ, Noble W (2014) Astrocytes and neuroinflammation in Alzheimer's disease. *Biochemical Society Transactions,* 42, 1321-1325.

Atherton J, Kurbatskaya K, Bondulich M, **Croft CL**, Garwood CJ, Chhabra R, Wray S, Jeromin A, Hanger DP, Noble W (2013) Calpain cleavage and inactivation of the sodium calcium exchanger-3 occur downstream of Aβ in Alzheimer's disease. *Aging Cell,* 13, 49-59.

Abbreviations

AAV	Adeno-associated virus
Aβ	beta-amyloid
AD	Alzheimer's disease
ADAM	a disintegrin and metalloprotease
ADNF	activity-dependent neurotrophic factor
AICD	amyloid precursor protein intracellular domain
ALS	amyotrophic lateral sclerosis
AMPA	α-amino-3-hydroxy-5-methyl-4-isoxazolepropionic acid
ApoEε2	apolipoprotein E ε2
ApoEε4	apolipoprotein E ε4
APH-1	anterior pharynx-defective 1
ApoE	apolipoprotein E
APP	amyloid precursor protein
APS	ammonium persulphate
asp	aspartate
BCA	bicinchoninic acid
BIN-1	bridging integrator 1
BME	basal medium eagle
BSA	bovine serum albumin
CAST	calpastatin
cdk5	cyclin-dependent kinase 5

CLU	clusterin
CSF	cerebrospinal fluid
CTF	C-terminal fragment
DAB	3.3’-diaminobenzidine tetrahydrochloride
DIV	days *in vitro*
DMSO	dimethyl sulfoxide
DNase	deoxyribonuclease
EDTA	ethylenediaminetetraacetic acid
EOAD	early onset Alzheimer's disease
FCS	fetal calf serum
FTD	Fronto-temporal dementia
GFAP	glial fibrillary acidic protein
GSK-3	glycogen synthase kinase-3
HBSS	Hank’s balanced salt solution
HRP	horseradish peroxidase
iPSC	induced pluripotent stem cell
ISF	interstitial fluid
LiCl	lithium chloride
LDH	lactate dehydrogenase
LOAD	late onset Alzheimer's disease
LSS	low speed supernatant
LTP	long-term potentiation
MAP	microtubule-associated protein

MCI	mild cognitive impairment
mEPSCs	miniature excitatory postsynaptic currents
MTBD	microtubule-binding domain
NaCl	sodium chloride
NFT	neurofibrillary tangle
NMDA	N-methyl-D-aspartate
NR2B	NMDA receptor 2B
PBS	phosphate-buffered saline
PEN-2	presenilin enhancer 2
PFA	paraformaldehyde
PICALM	phosphatidylinositol binding clathrin assembly protein
PIPES	piperazine-N,N'-bis (2-ethane-sulfonic acid)
PP2A	protein phosphatase 2A
PRD	proline-rich domain
PS	presenilin
PSD-95	postsynaptic density protein 95
SDS-PAGE	SDS-polyacrylamide gel electrophoresis
ser	serine
TBS	tris-buffered saline
TEMED	N,N,N',N', tetramethylethylenediamine
thr	threonine
TMB	tetramethylbenzidine
TREM2	triggering receptor expressed on myeloid cells 2

TTX	tetrodotoxin
tyr	tyrosine
WT	wild-type

Chapter 1 : Introduction

1.1 Alzheimer's disease

1.1.1 Background

History

Alzheimer's disease (AD) is a devastating progressive neurodegenerative disorder, first reported in 1906 by Alois Alzheimer following post-mortem analysis of the brain of a 51 year old woman presenting with cognitive, memory and mood problems (Alzheimer, 1906). Brain atrophy was reported as well as the presence of 'abnormal clumps' and 'tangled bundles of fibres' in the cortex (Alzheimer, 1906). These features are what we now identify as extracellular beta-amyloid (Aβ) plaques and intracellular neurofibrillary tau tangles, respectively. Over 100 years has passed since this initial report of AD, yet it still remains incompletely understood, untreatable and the only available therapeutics treat the symptoms of AD only. At present, several clinical trials targeting different aspects of the development and pathogenesis of AD are underway (Broadstock et al., 2014). Decades of research into this disease has shed light on some of the underlying mechanisms, as well as molecular pathways, which may be suitable therapeutic targets; however, work into this debilitating condition must continue to allow the development of new therapeutic strategies, particularly since the prevalence of AD continues to rise.

Symptoms and diagnosis

Biochemical and physiological changes occur in the brain well before the onset of the symptoms of AD. This can begin up to 20 years before receiving an official diagnosis of AD. AD patients suffer symptoms of progressive loss of cognition and memory decline,

often concurrent with changes in mood and problems with communication and daily living (Yates and McLoughlin, 2008). These clinical features appear to correlate with the areas of the brain affected by pathology in Alzheimer's disease (Terry and Davies, 1980, Yates and McLoughlin, 2008). A diagnosis of mild cognitive impairment (MCI) is usually the first point in which decline in cognition and memory are detected, and this condition often precedes AD dementia, but is not itself classed as dementia and does not guarantee AD onset in all cases (Gagnon and Belleville, 2011).

Diagnosis of AD requires neurological and psychiatric examinations in addition to neuropsychological testing. Definitive diagnosis of AD occurs only upon post-mortem examination of the brain to detect both Aβ and tau lesions. Although misdiagnosis is common, research into faster recognition and detection of AD is ongoing, with progress in cerebrospinal fluid (CSF) and blood-based markers of AD being made, with introduction of novel PET biomarkers and other imaging techniques that show promise of more rapid diagnosis (Schaffer et al., 2015).

Statistics on the prevalence and economic burden of AD

AD is the most common cause of dementia. Current figures report that 800,000 men and women are living in the UK with dementia, with projections suggesting that this will rise to over 1 million people by 2025. At present, one in three people over 65 will die with dementia (Alzheimer's Society, 2015). Worldwide, this stretches to an estimated 35.6 million people living with dementia, with these numbers set to increase to 115.4 million in 2050. As lifespan increases due to advancements in other areas of medical research,

the prevalence of AD is expected to continue rising. In contrast, recent evidence suggests that the prevalence of AD may actually be in decline as the incidence of AD has actually declined over the past three decades (Satizabal et al., 2016). However, finding novel therapeutics to treat or prevent AD still remains a very important goal.

As the number of individuals being diagnosed with AD continues to rise, the associated costs will also increase. AD causes a strain on worldwide economies due to increasing demand in unpaid and paid care, days of work lost and rising healthcare costs. It is estimated that AD currently costs the UK economy £26 billion every year, of which £4.3 billion is in costs to the National Health Service, £10.3 billion is spent on social care and £11.6 billion is contributed by the work of unpaid carers (Prince et al., 2014). These statistics highlight the socioeconomic burden of this disease, and the urgent need to work towards rapidly understanding and treating AD.

1.1.2 Neuropathology of AD

Plaques

Neuritic or senile plaques composed of proteolytic fragments of amyloid precursor protein (APP) and other associated protein and cell fragments can accumulate in the extracellular space in affected AD brain regions (Yates and McLoughlin, 2008). Senescence in normal individuals can also cause the accumulation of these plaques composed of Aβ (Villemagne et al., 2011); however observed alongside neurofibrillary tangles (NFTs), neuritic Aβ plaques are hallmark pathologies of AD brain. The formation of these extracellular plaques in brain regions follows a somewhat unpredictable

spatiotemporal development in the brain. In general, Aβ plaques tend to occupy the association areas of the neocortex in AD before developing in the entorhinal cortex, hippocampus and then to a lesser extent in the primary sensory, motor and visual neocortex. Despite this unpredictable development of pathology, Braak and Braak distinguished three stages for the spread of neuritic plaques in AD (Braak and Braak, 1991). At stage A, Aβ plaques are found mainly found in the frontal, temporal, and occipital neocortex. At Stage B, all association areas of the neocortex contain Aβ plaques whilst the hippocampus becomes mildly affected. By the final stage, stage C, the primary sensory, motor and visual neocortex are likely to be positive for Aβ plaques, and plaques can also be present in the cerebellum, striatum, hypothalamus, thalamus and subthalamic nuclei (Braak and Braak, 1991). An example of human AD brain stained for Aβ plaques is shown in Figure 1.1.

Tangles

Conclusive diagnosis of AD also requires the post-mortem detection of NFTs. Intracellular NFTs are typically composed of aggregated tau species arranged in the form of paired helical filaments (PHFs) or straight filaments (Grundke-Iqbal et al., 1986). It is speculated that highly phosphorylated tau or truncated tau species drive tau aggregation and subsequent tangle formation (Hanger et al., 2009). Tangle pathology in Alzheimer's disease spreads through the brain in a predetermined spatiotemporal pattern along anatomically connected pathways, and the regions which are affected by NFTs in Alzheimer's disease are characterised by Braak staging (Braak and Braak, 1995). Braak stage I is characterised by the presence of NFTs in the transentorhinal cortex; this

pathology then spreads to the entorhinal cortex and CA1 region of the hippocampus in stage II during the asymptomatic, preclinical AD phase (potentially up to 20 years before diagnosis). By Braak stage III, AD is usually diagnosed as mild to moderate over a period of 2 to 10 years, and at this stage NFTs are found in the limbic system including the rest of the hippocampal formation, the amygdala, claustrum and thalamus (stage IV). Braak stages V and VI represent severe or advanced AD, and typically occur over 1 to 5 years. Most of the association areas of the neocortex are occupied by NFTs and show considerable atrophy (stage V), and severe atrophy of the primary sensory, motor and visual areas of the neocortex (stage VI), concurrent with the presence of tangles in these regions. Regions of the brain including the basal ganglia and cerebellum do not accumulate neurofibrillary tangles and remain relatively unaffected by tau pathology in AD (Braak and Braak, 1991, Braak and Braak, 1995). Human AD brain stained for NFTs is shown in Figure 1.1.

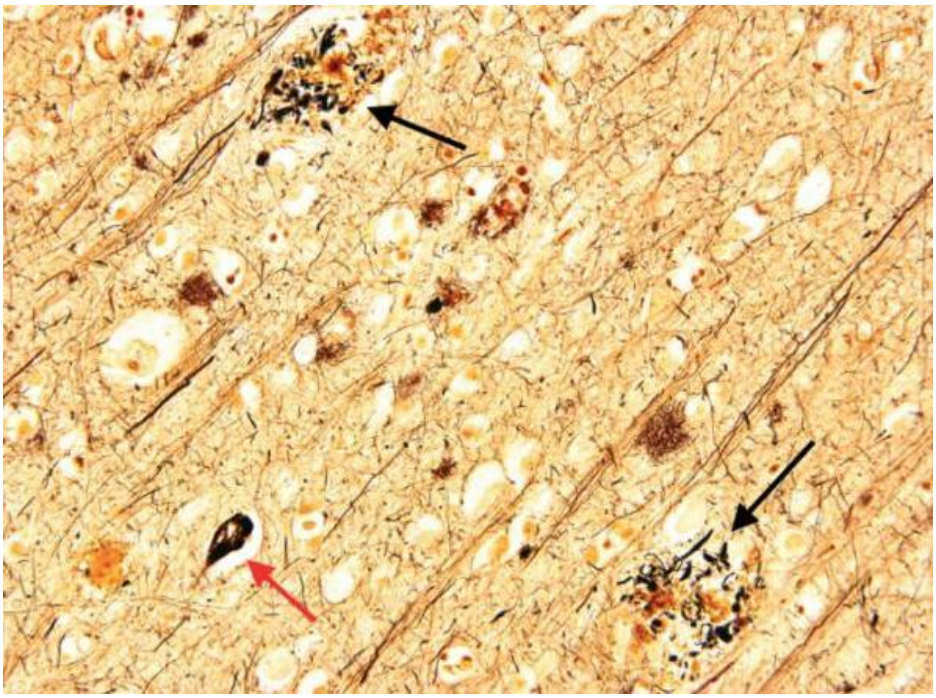

Figure 1.1: Bielschowski-stained Aβ plaques and a neurofibrillary tangle in AD human post-mortem brain.
The presence of both extracellular Aβ-containing plaques (black arrows) and intracellular NFTs (red arrow) stained with a modified Bielschowski stain and imaged at 100x in post-mortem human AD brain. Taken from (Perl, 2010).

1.1.3 Genetics of Alzheimer's disease

Two defined forms of AD exist; the first generally presents later in life (over 65 years) occurring sporadically, and is known as late onset AD (LOAD). The second presents earlier in life, usually in the late 40s or early 50s, has a genetic (familial) link and is known as early onset AD (EOAD) (Tanzi, 2012).

Early onset AD

A genetic link to AD was first reported in 1952 when familial clustering of AD was identified (Sjogren et al., 1952). Familial AD, or EOAD, accounts for only approximately 1-5% of all AD cases. Familial AD is typically caused by rare, highly penetrant mutations in

three genes encoding proteins involved in APP processing and Aβ generation. In 1991, the first mutation in the *APP* gene, V717I, on chromosome 21 was reported and was found to increase the production of a 42 amino acid Aβ species - Aβ-42 (Goate et al., 1991). At present there are 52 known mutations in *APP* (Cruts et al., 2012). Most of these mutations are positioned in the region of the β-secretase and γ-secretase cleavage sites and they affect normal APP proteolytic processing to increase Aβ production, the ratio of Aβ-42 to Aβ-40, and/or the aggregatory properties of the Aβ that is generated (Tanzi, 2012). Not all mutations in *APP* promote AD, indeed the Icelandic mutation (A673T) protects against cognitive decline and AD, and *in vitro* reduces the production of Aβ (Jonsson et al., 2012). The other mutations that cause EOAD are in the presenilin 1 and 2 genes – *PSEN1* (chromosome 14) and *PSEN2* (chromosome 1), which encode presenilin (PS)1 and PS2 proteins, respectively. The first mutations in *PSEN1* and *PSEN2* were identified in 1995 (Sherrington et al., 1995, Levy-Lahad et al., 1995). At present there are 205 known mutations in *PSEN1* and 14 known mutations in *PSEN2* (Cruts et al., 2012, Tanzi, 2012). Together with nicastrin, anterior pharynx-defective 1 (APH-1) and presenilin enhancer 2 (PEN-2), the presenilins comprise the integral units of the γ-secretase complex, and mutations in PS1 and PS2 are believed to act predominantly by increasing the ratio of pro-aggregatory Aβ-42 production relative to Aβ-40 (Tanzi, 2012).

Late onset Alzheimer's disease

LOAD or sporadic AD accounts for greater than 95% of AD cases. The cause of LOAD is likely due to a combination of genetic, lifestyle and environmental risk factors. Possession of one or two copies of the Apolipoprotein E ε4 (ApoEε4) allele is the biggest

genetic risk factor for AD, increasing the risk of sporadic AD by 4-fold and 12-fold, respectively (Corder et al., 1993). In contrast, possession of the ApoEε2 allele is protective against AD (Corder et al., 1994). The physiological roles of ApoE include lipoprotein metabolism and transport. In the pathogenesis of AD, ApoE is believed to play a role in Aβ clearance, as deposits of Aβ are more abundant in post mortem brains of those possessing one or two copies of the APOEε4 allele (Schmechel et al., 1993). Over 20 other genetic risk factors for AD have been identified in recent large genome-wide association studies, most notably, bridging integrator 1 (*BIN-1*) (Lambert et al., 2013), phosphatidylinositol binding clathrin assembly protein (*PICALM*), clusterin (*CLU*) (Seshadri S. et al., 2010) and triggering receptor expressed on myeloid cells 2 (*TREM2*) (Guerreiro et al., 2012). Mutations in *TREM2* disrupt microglial clearance of Aβ and inflammatory responses (Guerreiro and Hardy, 2014, Rivest, 2015). Mutations in *PICALM* and *BIN-1* are associated with the disruption of endocytosis, and mutations in *CLU* affect the immune response and lipid metabolism (Guerreiro and Hardy, 2014).

1.2 APP and Aβ

1.2.1 Background

APP was identified as the precursor of Aβ-40 and Aβ-42 in the 1980s (Kang et al. 1987). APP is a large single-pass transmembrane protein with a large extracellular domain which can undergo proteolytic cleavage to form the major component of neuritic plaques - Aβ (Glenner and Wong, 1984). Alternate splicing of the *APP* gene generates 8 isoforms, 3 of which are more common than the others. A 695 amino acid isoform of APP is expressed mainly throughout the central nervous system, with the 751 and 770

amino acid isoforms found ubiquitously (Bayer et al., 1999). The precise physiological function of APP still remains unclear, but a role for APP has emerged in the modulation of cell growth, motility, neurite outgrowth, and cell survival (Dawkins and Small, 2014). In addition, full length APP holds a clear physiological role at the synapse in promoting proper spine formation and development, as well as promoting surface expression of N-methyl-D-aspartate (NMDA) and α-amino-3-hydroxy-5-methyl-4-isoxazolepropionic acid (AMPA) receptors – important for long-term potentiation (LTP) and memory (Lee et al., 2010, Hoe et al., 2012).

1.2.2 APP processing

Large amounts of APP are produced in neurons and this is usually metabolised very rapidly (Lee et al., 2008). Two main pathways of APP proteolysis exist and can either cause the generation of Aβ peptides or preclude their formation. APP is normally sorted in the endoplasmic reticulum and the trans golgi network, before being trafficked along axons, and to synapses (Koo et al., 1990). Most APP processing is believed to occur at the cell surface or in the trans-golgi network (Choy et al., 2012); however, pathogenic intracellular pools of Aβ have also been reported, suggesting processing of APP may also occur in intracellular compartments (LaFerla et al., 2007).

On the cell surface, APP is sequentially proteolytically cleaved by α-secretases and then γ-secretases, the former of which cleave APP through the Aβ sequence, thereby precluding the formation of Aβ. This pathway is therefore termed as non-amyloidogenic, cleavage of APP by the aforementioned secretases produces a soluble

APP ectodomain – sAPPα - an α C-terminal fragment (CTF) - $C83$ - and subsequently, $p83$ and an intracellular C-terminal fragment (AICD) (Sheng et al., 2012). The ADAM (a disintegrin and metalloproteinase) family of proteases act as α-secretases, predominantly act at the cell surface but also show some activity in the trans-golgi network (Zhang et al., 2011b). γ-secretases exist as multiprotein complexes containing PS1 or PS2 as described above.

Alternatively, APP can be proteolytically cleaved by β-secretases and then γ-secretases in the amyloidogenic pathway. This is thought to occur in endosomes as a result of APP not being cleaved at the cell surface by α-secretases and instead being internalised in clathrin-coated pits. Cleavage by β-secretases produces the soluble APP ectodomain - sAPPβ - and a β-CTF -$C99$. Subsequent cleavage of the β-CTF by γ-secretase results in the generation of Aβ peptides ranging from 38 to 44 amino acids in length (1–40 and 1–42 being most common) and an AICD (Zhang et al., 2011b). BACE1, a transmembrane aspartic protease, is the predominant β-secretase which cleaves APP to produce Aβ (Vassar et al., 1999). A schematic diagram describing amyloidogenic and non-amyloidogenic processing of APP is shown in Figure 1.2.

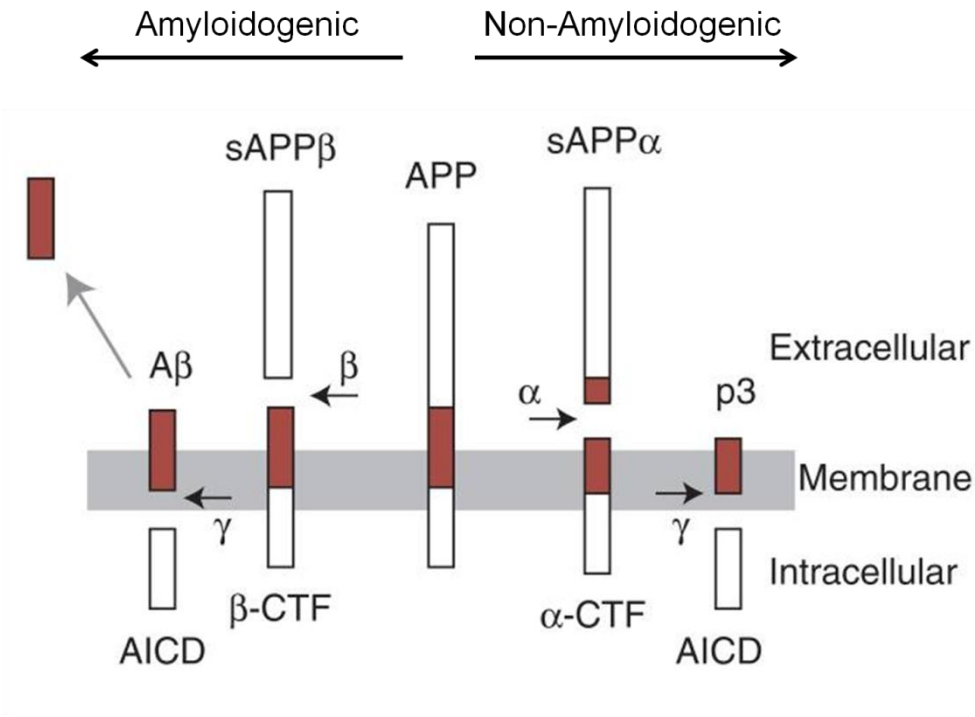

Figure 1.2: APP processing and the formation of Aβ peptide.
The full-length human amyloid precursor protein (APP) is a single transmembrane protein with an intracellular carboxyl terminus which is sequentially cleaved in amyloidogenic and non-amyloidogenic pathways. In the amyloidogenic pathway, cleavage of APP by β-secretase produces the carboxy-terminal fragment of APP (β-CTF [C99]) and releases the soluble extracellular domain of APP (sAPPβ), before cleavage by γ-secretase produces the Aβ peptide, and the intracellular carboxy-terminal domain of APP (AICD). In the non-amyloidogenic pathway, cleavage by α-secretase precludes formation of Aβ, and instead results in the production of the soluble extracellular domain of APP sAPPα and α -CTF [C83] before cleavage by γ-secretase produces the AICD and p3 peptide. Figure adapted from (Sheng et al., 2012).

More recently, other forms of APP processing have been identified and implicated in AD. Specifically asparagine endopeptidase, termed δ-secretase has been shown to cleave APP prior to cleavage by β-secretase (Zhang et al., 2015b). In addition, another novel secretase, deemed η-secretase cleaves APP to form η-CTFs and long and short Aη peptides. These long and short Aη peptides created by η-secretase cleavage are synaptotoxic *in vivo* and *in vitro* (Willem et al., 2015).

Aβ-40 and Aβ-42 are the main components of neuritic plaques and are generated via cleavage of APP along the amyloidogenic pathway (Glenner and Wong, 1984). However, increased levels of Aβ-40 and Aβ-42 and neuritic plaques can be found in healthy aged brains (Villemagne et al., 2011) as well as pathologically in AD, and Aβ is physiologically important for synaptic physiology (Abramov et al., 2009). It is not known for certain which form of Aβ is the most toxic in AD; however mutations in PS1 and PS2 promote the production of Aβ-42 relative to Aβ-40 (Fernandez et al., 2014), Aβ-42 aggregates much more readily than shorter species and *in vitro* studies reveal a higher toxicity of Aβ-42 relative to Aβ-40 to neurons (Klein et al., 1999, Ahmed et al., 2010). Aβ oligomerizes via an unknown mechanism, adopting several higher order conformations such as soluble dimers, trimers, dodecamers, higher order oligomers, protofibrils, and fibrils (Walsh et al., 2000). Extracellular neuritic plaques are shown to contain Aβ in the form of soluble Aβ-40 and Aβ-42 monomers (Butterfield et al., 2002) oligomeric or dimeric Aβ (Shankar et al., 2008), multimeric pore-like complexes of Aβ monomers and truncated, insoluble species of Aβ (Yankner and Lu, 2009). All of these Aβ species show neurotoxic properties in various cell and animal models of AD, and identifying the "toxic" species of Aβ remains a controversial and much debated topic in the field (Mucke and Selkoe, 2012). In addition, whether intracellular Aβ or extracellular Aβ is more toxic is also not clear. This is due, at least in part, to a debate about the specificity of antibodies to detect intracellular Aβ rather than APP; nevertheless, intracellular Aβ is thought to accumulate in the early stages of disease in transgenic AD models, as mentioned above (LaFerla et al., 2007).

1.2.3 Mechanisms of Aβ toxicity

As described earlier, there are several species of Aβ which exert synaptotoxic and neurotoxic effects in models of AD, and ongoing research is designed to determine which of these species are the most critical in AD. Several deleterious effects of Aβ relevant to AD have been described including:

- Neurotoxicity and synaptotoxicity. Application of soluble Aβ1-42 oligomers causes neurotoxicity *in vitro* (Atherton et al., 2014, Garwood et al., 2011) and application or accumulation of Aβ-42 in rodents leads to neuronal loss and cognitive dysfunction (Walsh et al., 2002, Bayer and Wirths, 2008). Aβ also causes detrimental effects at the synapse (Selkoe, 2002). These synaptotoxic effects of Aβ are further described in section 1.5.1.
- Neuroinflammation. Inflammation is likely a crucial driver in the pathogenesis of AD (Sastre et al., 2011, Phillips et al., 2014). Aβ can trigger a number of inflammatory events (Butterfield et al., 2002) and also promote astrocytic (Hu et al., 1998) and microglial (Meda et al., 1995, Maezawa et al., 2011) activation.
- Caspase activation. The activity of caspases is known to be upregulated in AD and caspase cleavage of tau is an early event in AD (Rissman et al., 2004). Aβ has been shown to upregulate the activity of caspases (Mattson et al., 1998).
- Kinase activation. Aβ can increase the activation of cdk5 (Lee et al., 2000) and GSK-3 (Townsend et al., 2007, Magdesian et al., 2008), which are both implicated in increased tau phosphorylation in AD (Hanger et al., 2009).

- Oxidative damage. Aβ can drive increases in oxidative DNA damage and stress both *in vitro* and *in vivo* which is an important feature in AD (Smith et al., 1998, Yatin et al., 1999, Butterfield, 2002).
- Calcium dysregulation. Aβ disrupts calcium homeostasis (Mattson et al., 1993, Mark et al., 1995) and upregulates calcium-sensitive calpains (Lee et al., 2000), which are shown to play a key role in AD (Atherton et al., 2014, Egorova et al., 2015).

1.3 Tau

1.3.1 Background

The best recognised function of tau as a promoter of microtubule assembly and stability was first determined when it was isolated in association with tubulin in the 1970s and identified as a microtubule-associated protein (MAP), essential for dimers of α- and β-tubulin to polymerise and form microtubules (Weingarten et al., 1975). Tau is the most common MAP and accounts for approximately 80% of total MAPs (Wang et al., 2014). Tau is abundantly expressed throughout the central nervous system and is found primarily in a soluble state in the axonal compartment of neurons, with small amounts also expressed in astrocytes (Papasozomenos and Binder, 1987) and oligodendrocytes (Lopresti et al., 1995).

Human tau is encoded by the *MAPT* gene on chromosome 17q.21.31 and consists of 16 exons. Mutations in *MAPT* do not cause AD, but are causative for frontotemporal dementia (FTD), demonstrating the importance of tau for neurodegeneration (Hanger et

al., 2009, Hutton et al., 1998). Alternative splicing of exons 2, 3 and 10 gives rise to six different tau isoforms. Exclusion or inclusion of exon 10 results in tau containing either three or four microtubule repeat domains (3R or 4R tau, respectively) towards the C-terminus (Himmler et al., 1989). The number of microtubule repeat domains determines the affinity of tau for microtubules, with 4R tau having greater binding capacity. Exclusion, or inclusion of exon 2 and 3 gives rise to tau isoforms containing 0, 1 or 2 N-terminal inserts (0N, 1N or 2N, respectively) (Goedert et al., 1989, Himmler, 1989). 0N3R tau is only found in the foetal brain (Takuma et al., 2003). A diagram showing the six different tau isoforms is shown in Figure 1.3.

In the mature CNS, human tau is composed of 352 to 441 amino acid residues (Himmler et al., 1989) and is natively unfolded, lacking a defined 3D structure (Schweers et al., 1994). Tau protein contains four main regions which drive certain functions of tau: an N-terminal projection region, a proline-rich domain (PRD), a microtubule-binding domain (MTBD) and a C-terminal region (Figure 1.3). The N-terminus of tau can associate with the cell membrane and may also control other cytoskeletal dynamics (Brandt et al., 1995). Phosphorylation of tau at the N-terminus can control its dynamic association with plasma membranes (Pooler et al., 2012). The PRD contains many phosphorylation sites which are the targets of the proline-directed and non-proline directed serine(ser)/threonine(thr) kinases, including glycogen synthase kinase 3 (GSK-3) and cyclin dependent kinase 5 (cdk5) (Hanger et al., 2009). The PRD can also bind to Src homology 3 domains of other proteins including the tyrosine (tyr) kinase, Fyn (Lee et al., 1998). The MTBD of tau together with the immediate flanking regions determines the

binding affinity of tau for microtubules, and the number of domains (3R or 4R) may also affect the speed of kinesin-driven axonal transport, with 3R tau allowing faster microtubule gliding (Peck et al., 2011). Phosphorylation in the MTBD decreases the affinity of tau for microtubules, enabling their detachment (Wang et al., 1995). Phosphorylation of tau in the C-terminal region may promote the self-aggregation of tau (Hanger and Wray, 2010), whilst dephosphorylation in this region may encourage caspase cleavage of tau and subsequent degradation by calpain to form C-terminal fragments of around 17-20 kDa which show greater propensity for aggregation (Gamblin et al., 2003).

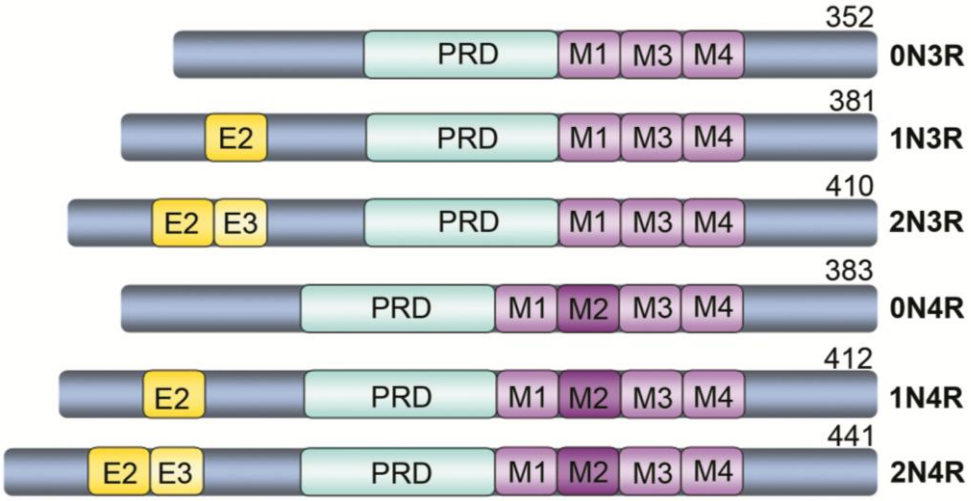

Figure 1.3: The six different tau isoforms in the adult human CNS and their main features

Alternative splicing leads to six different isoforms of tau in the adult human CNS. All isoforms contain a central proline rich domain (PRD) and vary in terms of their inclusion or exclusion of inserts resulting from the inclusion or exclusion of exon 2 and exon 3 at the N-terminus (E2 and E3); exon 3 is never included in the absence of exon 2, and either contain 3 or 4 microtubule-binding domains (M1-4). Numbers on the right refer to protein length in amino acids. From (Hanger et al., 2009).

1.3.2 Tau functions

A major function of tau is its ability to bind, assemble and stabilise microtubules, thus affecting cytoskeletal dynamics and neuronal stability (Noble et al., 2013). Interaction of the MTBDs of tau with tubulin enables the polymerisation of α- and β-tubulin dimers to assemble microtubules (Weingarten et al., 1975). Microtubules exist in a state of dynamic instability, constantly growing and shrinking depending on the needs of the cell and tau acts to regulate the stability of microtubules (Mitchison and Kirschner, 1984). Phosphorylation of tau reduces the affinity of tau for microtubules, allowing a dynamic regulation of microtubule stability (Wang et al., 1995). This dynamic instability supports and regulates cellular processes such as trafficking along the axon (Brandt and Lee, 1994), and tau is recognised to play a critical role in axonal transport of various proteins and cargoes (Dixit et al., 2008, Vossel et al., 2015). Tau can modulate anterograde and retrograde transport of vesicles and organelles to and from the synapse and cell body (Mandelkow et al., 2003). Perturbation from normal levels and species of tau causes it to compete with the motor proteins kinesin and dynein, affecting their ability to transport tau and other cargoes along the axon (Cuchillo-Ibanez et al., 2008). The normal functioning and localisation of tau is also important for the trafficking of mitochondria which is also affected in AD (Kopeikina et al., 2011).

Tau is also physiologically involved in maintaining neuronal polarity and promoting neurite outgrowth, which is particularly important during developmental processes. The dynamic nature of microtubules is differentially regulated in different parts of the neuron. Tau is normally found in the axon toward the distal end of the neuron,

particularly in the growth cone of developing neurons (Mandell and Banker, 1995, Liu et al., 1999).

The emerging role of tau in neuronal signalling is also important. The ability of tau to bind the SH3 domain of Src family tyr kinases including Fyn and to be targeted to the plasma membrane, is likely involved in membrane-associated signal transduction processes (Lee et al., 1998). The effects of tyr phosphorylation of tau on its localisation also suggests a role for tau in intracellular signalling, distinct from its role in microtubule assembly and stabilisation. Tyrosine phosphorylation of tau regulates its association with SH2 domain-containing proteins such as Fyn, to alter tau localisation with membrane microdomains such as lipid rafts (Usardi et al., 2011). In addition, tau interactions with Fyn are important for the dendritic localisation of tau and the resulting regulation of postsynaptic NMDAR-mediated signalling, as well as, NMDAR-Erk1/2 signalling (Ittner et al., 2010, Mondragón-Rodríguez et al., 2012).

1.3.3 Tau phosphorylation

Tau protein can undergo several post-translational modifications including glycosylation, phosphorylation, nitration, and acetylation. The phosphorylation of tau has been researched extensively and highlighted as particularly important in the pathology of AD and other tauopathies. Specifically, aberrant phosphorylation disrupts the microtubule network, hinders axonal transport and synaptic function (Buée et al., 2000) and can also drive neurotoxicity (Fath et al., 2002). In addition, highly phosphorylated tau species redistribute from the axon (where only low levels of physiologically phosphorylated tau

are found) to somatodendritic compartments (Zempel et al., 2010). In contrast, tau phosphorylation is physiologically important during embryonic development where it is thought to play an important role in allowing neurite outgrowth and restructuring. Phosphorylation is reduced in early postnatal stages and remains relatively low in normal adult brain, but aberrant phosphorylation is also a feature of tauopathy brain (Biernat and Mandelkow, 1999).

Tau exists in a dynamic balance between phosphorylated and dephosphorylated forms, largely regulated by kinase and phosphatase activity (Stoothoff and Johnson, 2005). Tau can be phosphorylated by a variety of protein kinases, namely proline-directed, non-proline directed and tyr kinases. Major tau kinases include the proline-directed ser/thr kinases, GSK-3 and cdk5 (Hanger et al., 1992, Lund et al., 2001). GSK-3 exists as two isoforms, α and β, that are encoded by different genes (Force and Woodgett, 2009). GSK-3 is constitutively active in the mammalian CNS (Beurel et al., 2015) where its activity is regulated via several pathways. Phosphorylation of ser 21 and 9 on GSK-3 α and β, respectively, inactivates GSK-3 by altering its conformation to reduce binding site availability (Sutherland et al., 1993), whilst phosphorylation of tyr 216 and 279 on GSK-3 increases the activity of GSK-3 and are thought to be responsible for its constitutive activity (Wang et al., 1994). GSK-3 activity is also highly dependent on intracellular concentrations of magnesium (Ryves and Harwood, 2001). Conditional overexpression of GSK-3 in mice results in progressive tau hyperphosphorylation, aggregation and neurodegeneration (Lucas et al., 2001) whereas inhibition of GSK-3β *in vivo* reduces tau phosphorylation, neurofibrillary tangle formation and associated axonal degeneration

(Noble et al., 2005). The activity of cdk5 is driven by its neuron-specific activators p39 and p35 (Lew et al., 1994, Tang et al., 1995). Calpain cleavage of p39 and p35 can form the proteolytic fragments of p29 and p25, respectively (Kusakawa et al., 2000, Patzke and Tsai, 2002) which also activate cdk5, but are not degraded as rapidly as their precursors (Patrick et al., 1999), resulting in prolonged pathogenic cdk5 activity. In particular, p25 is implicated in driving aberrant tau phosphorylation in AD, and is considered a more pathological activator of cdk5, in comparison to "physiological" p35-mediated activation of cdk5 (Patrick et al., 1999, Tsai et al., 2004). Constitutive or regulatable over-expression of p25 in mice leads to elevated tau phosphorylation, tangle formation and neurodegeneration (Noble et al., 2003, Cruz et al., 2003) and specific inhibition of p25/cdk5 with cdk5 inhibitory peptides reduces neurodegeneration *in vivo* (Sundaram et al., 2013). Furthermore, a growing body of evidence suggests a reciprocal regulation between cdk5 and GSK-3, particularly in ageing, and the importance of this relationship for tau phosphorylation in AD must not be ruled out (Engmann and Giese, 2009).

Phosphorylation of tau is also regulated by the activity of several protein phosphatases; the most dominant of these is protein phosphatase 2A (PP2A) (Wang et al., 2015). PP2A is responsible for approximately 71% of all tau phosphatase activity in the human brain, and its activity is severely reduced in AD brain where increased tau phosphorylation is observed (Gong et al., 1995). Inhibition of PP2A increases tau phosphorylation *in vivo,* and PP2A has also been deemed as the most effective phosphatase to dephosphorylate highly phosphorylated tau species isolated from AD brains (Wang et al., 1995). A

summary of major pathways of tau phosphorylation and dephosphorylation can be seen in **Figure 1.4**.

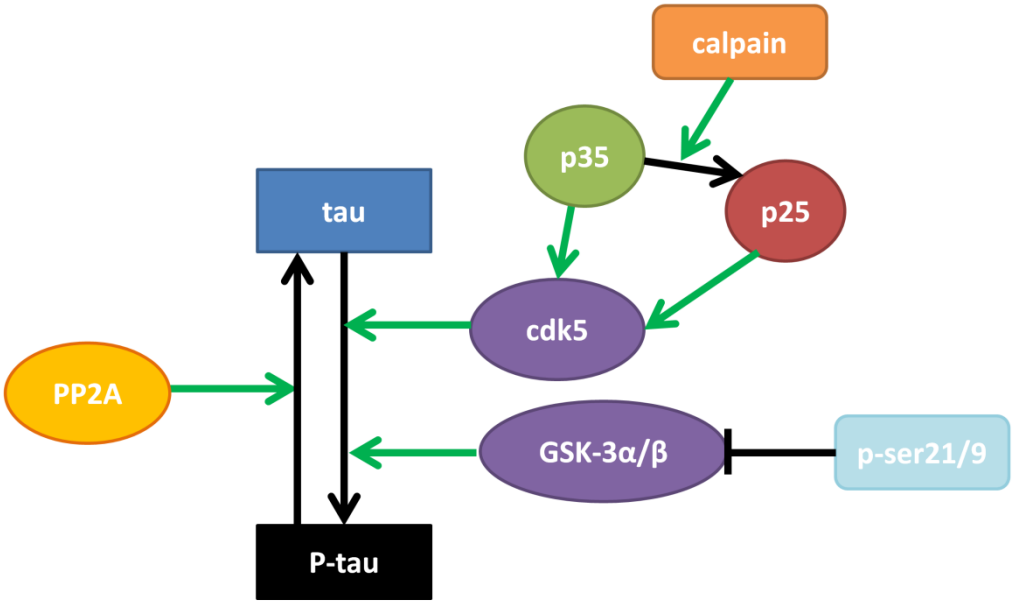

Figure 1.4: Schematic diagram showing the major pathways of tau phosphorylation and dephosphorylation.
Phosphorylation of tau can be driven by several kinases; the major tau kinases are known to be cdk5 and GSK-3. Cdk5 is activated by its activators p35 and p25. p25 is formed through the cleavage of p35 by calpain, and has a longer half-life than p35 causing it to drive prolonged cdk5 activity compared to p35. GSK-3 can be inactivated by several means, however phosphorylation of ser21/9 is a predominant pathway of its inactivation. Phosphorylated tau can be dephosphorylated by PP2A which is the major phosphatase known to reduce levels of tau phosphorylation.

In full-length 2N4R human tau approximately 80 residues can be phosphorylated (Stoothoff and Johnson, 2005). Phosphorylation of at least thirty of these known residues have been shown to alter tau physiological function (Hanger et al., 2009). In addition, normal, regulated phosphorylation of tau enables it to perform its physiological roles in the cell including neurite outgrowth and axonal transport (Biernat and Mandelkow, 1999). Under physiological conditions, 1 mole of tau should be

accompanied by 2-3 moles of phosphate (Kopke et al., 1993), and this ratio increases to 4-10 moles of phosphate per 1 mole of tau in disease (Alonso et al., 2004).

Abnormal phosphorylation of tau is implicated in the pathology of Alzheimer's disease and other tauopathies (Hanger et al., 2007). Indeed, tau found in PHFs and in NFTs can be abnormally phosphorylated at approximately 45 different residues (Grundke-Iqbal et al., 1986, Hanger et al., 2007) (see Figure 1.5), in comparison to phosphorylation at only approximately 8-10 sites in healthy brain (Hanger et al., 2007, Hanger et al., 2009). All six alternatively-spliced isoforms of tau can be aberrantly phosphorylated and incorporated into NFTs (Goedert et al., 1989). The increased phosphorylation of tau is in part driven by imbalances in kinase and phosphatase activity. Indeed, human AD brain shows signs of increased cdk5 and GSK-3 activity (Tseng et al., 2002, Leroy et al., 2007), and reduced PP2A activity (Gong et al., 1995). It remains unclear if phosphorylation at specific residues is critical for tau-associated neurodegeneration, although some residues are particularly important for normal tau function such as the association of tau with microtubules (Noble et al., 2013).

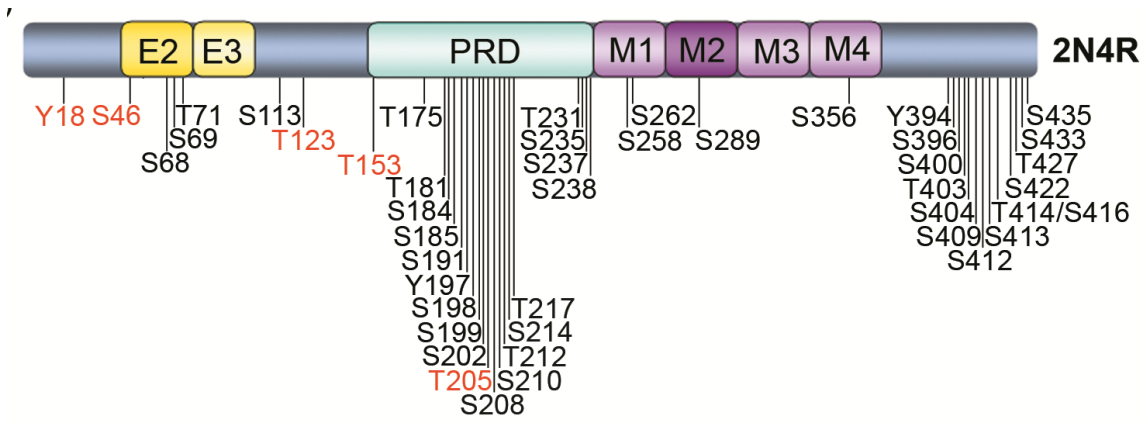

Figure 1.5: Known phosphorylation residues of tau in AD brain.
Tau is abnormally phosphorylated on at least 40 residues in AD brain, predominantly in the proline-rich domain and in the C-terminal region, with fewer residues found in the microtubule-binding domains or in the N-terminal region. Site numbering is based on the full length, 441 amino acid, human 2N4R tau. Sites in black were identified by mass spectrometry, and those in red by antibody labelling. Taken from (Hanger et al., 2009).

1.3.4 Tau cleavage

Truncation is another post-translational modification of tau, which, is implicated in AD. Tau cleaved at both the N- and C-termini is found in AD brain (Garcia-Sierra et al., 2008). The truncation of tau is catalysed predominantly by caspases, calpains and asparagine endopeptidases (Yang and Ksiezak-Reding, 1995, Rissman et al., 2004, Zhang et al., 2014) with the resulting cleavage products often showing properties that promote tau aggregation (Gamblin et al., 2003, Lee and Shea, 2012). Caspases can cleave tau at aspartate (asp) 22–25, asp 345–348 and asp 418–421 (Gamblin et al., 2003), with preferential cleavage occurring at asp 421 (Chung et al., 2001). In addition, N-terminal cleavage of tau by caspase-6 can occur at asp 13 (Horowitz et al., 2004). The calcium-activated cysteine proteases - calpain 1 and 2 - can also cleave tau *in vitro* (Johnson et al., 1989) and calpain-cleaved tau retains its N-terminus (Yang and Ksiezak-Reding,

1995). Furthermore, calpain activity is upregulated in AD brain, (Saito et al., 1993) whilst its endogenous inhibitor - calpastatin (CAST) is downregulated in AD brain (Rao et al., 2008). The elevated presence of a 17 kDa calpain-cleaved tau species has been reported in AD brain relative to controls (Ferreira and Bigio, 2011) although the pathogenicity of these tau fragments, especially in relation to Aβ, is somewhat controversial (Garg et al., 2011) as 35 and 45 kDa calpain- and caspase-cleaved tau has since been reported. The exact relationship of cleaved tau to tau phosphorylation remains poorly understood (Flores-Rodríguez et al., 2015) and likely varies according to truncation event. However, both phosphorylated and truncated tau species induce conformational changes in tau which are likely involved in tau aggregation and the pathogenesis of AD.

1.3.5 Tau aggregation

Tau is usually highly soluble in the brain; however, in AD and other tauopathies, tau becomes characteristically insoluble and aggregated, likely through changes in its secondary structure altering its conformation (Schweers et al., 1994). For aggregation to occur, tau must be dissociated from microtubules (Golde, 2006). Several post-translational modifications of tau are associated with tau aggregation and disassembly from the microtubules, including nitration, phosphorylation and truncation (Grundke-Iqbal et al., 1986, Hanger and Wray, 2010, Wang et al., 2014) and these can drive alterations in conformation (Binder et al., 2005). These conformational changes are proposed to trigger the formation of tau dimers, and the process of nucleation-elongation begins whereby further tau dimers are recruited and tau oligomers are generated (Friedhoff et al., 1998). Tau oligomers then form protomers which adopt the

β-sheet formation typical of amyloid aggregates before forming PHFs and NFTs (Meraz-Ríos et al., 2010, Cárdenas-Aguayo et al., 2014). It is unclear which of these species of tau are the most toxic in AD (Cárdenas-Aguayo et al., 2014, Flores-Rodríguez et al., 2015).

1.3.6 Extracellular tau and tau propagation

Traditionally, tau has been viewed as an intracellular protein. However, recent evidence has demonstrated that tau is found in extracellular spaces, and thought to be associated with the mechanisms involved in the spread of tau pathology across tauopathy brain.

Until recently, the presence of tau in extracellular spaces was thought to be the result of its release from dying neurons, since levels of both total and phosphorylated tau are elevated in the CSF of individuals with AD relative to controls (Blennow et al., 1995). However, tau was recently detected in the CSF of normal individuals (Hampel et al., 2010) as well as in the CSF of healthy mice (Barten et al., 2011, Yamada et al., 2011) suggesting that extracellular tau does not result solely from neurodegeneration. Tau has also been detected in the interstitial fluid (ISF) of mice, and its abundance is increased when neuronal activity is stimulated, indicating a possible physiological role of tau secretion or extracellular tau (Yamada et al., 2014). Indeed, the secretion of tau has also been demonstrated from primary cortical neurons and human induced pluripotent stem cells (iPSCs) at low but detectable steady state levels (Chai et al., 2012, Pooler et al., 2013). This release of endogenous tau has been shown to be a calcium-dependent

physiological process likely mediated by pre-synaptic mechanisms and neuronal activity (Pooler et al., 2013).

The importance of extracellular tau for disease is not well understood, however, several studies have shown that tau pathology can be seeded and transmitted across brain regions through anatomical connections or from cell to cell demonstrating a "prion-like" mechanism for the transmission and propagation of tau (Sanders et al., 2014). “Prion-like” in this sense, describes the self-propagation of tau across cells and tissues but does not imply that tau as a protein is infectious.

In vivo studies in mice, have shown that human FTD-causing mutant (P301L) tau expressed only in the entorhinal cortex under the control of the neuropsin promoter, leads to the progressive development of tangles in the entorhinal cortex, that progressively spreads, trans-synaptically, to regions downstream of the entorhinal cortex in a spatiotemporal manner (de Calignon et al., 2012). In addition, *in vivo* seeding experiments in mice, demonstrate that tau can be seeded and propagate through areas of the brain affected in AD. Injection of brain extracts from mice expressing FTD mutant human P301S mutant tau into brains of transgenic mice expressing wild-type (WT) tau caused tau pathology to develop at the site of injection and then spread to adjacent brain regions (Clavaguera et al., 2009). Furthermore, the pathological tau which can propagate *in vivo* retains characteristics of its tau seed (Clavaguera et al., 2013, Sanders et al., 2014), and this is thought to be a result of particular conformational properties of tau that are found in different conditions (Falcon et al., 2015).

The relationship between the extracellular spread of pathological tau and Aβ also needs to be considered. In mice where mutant P301L tau propagates through anatomically connected regions, the presence of Aβ dramatically increases the speed and distance of tau propagation and increases tau-induced neurotoxicity (Pooler et al., 2015). Aβ also increase tau release and affects which species of tau are released *in vitro* (Kanmert et al., 2015), suggesting an important relationship between the two.

The mechanisms underlying tau release from cells, tau propagation and tau uptake are incompletely understood. It is also not clear if "physiological" tau, that is tau in non-diseased brain, is released into extracellular spaces using the same mechanisms used for pathological tau propagation. It is also not clear if tau release and spread is phosphorylation-dependent, dependent on tau solubility, tau being truncated or full-length, misfolded beyond what is already known about tau conformation for the characteristic lesions that develop (Falcon et al., 2015), and/or its aggregation state.

Most evidence that exists shows that endogenous extracellular tau species are predominantly dephosphorylated compared to tau found intracellularly (Plouffe et al., 2012, Pooler et al., 2013) with exception to phosphorylation at thr 181 (Chai et al., 2012). Extracellular tau has also been demonstrated to contain both full-length and truncated tau species (Plouffe et al., 2012, Chai et al., 2012, Kanmert et al., 2015). It also seems that tau which propagates is soluble and oligomeric as PHFs will not propagate (Lasagna-Reeves et al., 2012, Iba et al., 2013). However, some studies have identified

propagation of small tau aggregates (Wu et al., 2013) and a highly phosphorylated high molecular weight tau species (Takeda et al., 2015).

How tau is released from and enters cells also needs further research. Evidence suggests that endogenously expressed tau is not contained within vesicles when it is released (Chai et al., 2012) whilst it is suggested that pathological forms of tau, particularly when exogenously expressed, is secreted within or in association with exosomes (Saman et al., 2012) and ectosomes (Dujardin et al., 2014). Exosomes are small membranous vesicles (40–100 nm) produced by the endocytosis of molecules which can be recycled to the plasma membrane or trafficked to multivesicular bodies which upon fusion with the plasma membrane are again released as exosomes. Ectosomes are larger extracellular vesicles (50–1000 nm) that are directly released from cells by plasma membrane budding (Dujardin et al., 2014). The physiological release of tau is thought to occur via a non-classical secretion pathway (Chai et al., 2012), that is stimulated by neuronal activity and is blocked when pre-synaptic vesicle release is inhibited (Pooler et al., 2013). Fewer data is available to explain tau uptake by neurons. Misfolded tau species have been shown to be taken up by neurons via endocytosis and subsequently transported along axons (Wu et al., 2013) but extracellular tau may also enter cells via other mechanisms. Additionally, a role for the microglial uptake of tau by phagocytosis and subsequent exosomal release of tau in AD has been demonstrated (Asai et al., 2015).

There remains a lot to be discovered about which tau species spread, the mechanisms involved, and differences between the release and spread of physiological and

pathological tau species. Elucidating the pathways involved are likely to be particularly important for the development of new therapies for AD since targeting extracellular tau and preventing its propagation will slow or halt disease progression.

1.4 The relationship between Aβ and tau pathologies in AD

The most widely accepted hypothesis describing the relationship between amyloid and tau and subsequent neurodegeneration in AD is known as the amyloid cascade hypothesis (Hardy and Higgins, 1992) as a result of the discoveries that mutations which cause FAD occur in PS1, PS2 and APP and alter the normal processing of APP resulting in the increased production of Aβ species (Goate et al., 1991, Sherrington et al., 1995, Levy-Lahad et al., 1995). The amyloid cascade hypothesis states that increased production and/or accumulation of Aβ influences the development of NFTs. Aβ triggers alterations in neuronal tau, alongside synaptic and neuronal dysfunction, thereby resulting in widespread neuronal death and inflammation which lead to the clinical symptoms of AD. As more and more evidence has emerged that the pathway from Aβ plaque deposition to the development of neurofibrillary tangles is not a linear process, the hypothesis has been revised (Hardy, 2009).

A multitude of evidence exists in support of the amyloid cascade hypothesis, including that from analysis of transgenic AD mouse models such as the 3xTg-AD line which expresses mutations in human *APP*, *PS1* and *MAPT* and progressively develop Aβ pathology prior to the development of tau alterations and the development of NFTs (Oddo et al., 2003a). Furthermore, reducing the amounts of Aβ genetically or via

immunotherapy in 3xTg-AD mice was found to reduce the development of tau pathologies, and when treatment was stopped Aβ pathology re-appeared prior to the appearance of new tau pathology (Oddo et al., 2008). Crossing transgenic mice that overexpress mutant human APP (Tg2576 line) with mice overexpressing the human tau harbouring the FTD-causing P301L mutation (JNPL3 line) also triggered accelerated tau pathology relative to single tau transgenics (Lewis et al., 2001). Similarly, injection of fibrillar Aβ species (Götz et al., 2001) or brain extracts from Aβ-producing mice (Bolmont et al., 2007) into tau transgenic mice enhances tau pathology. Interestingly, removal of endogenous tau in mice expressing mutant human APP that accumulate Aβ and develop plaques in the absence of tau pathology ameliorates synaptic dysfunctions, cognitive decline and excitotoxicity (Roberson et al., 2007, Ittner et al., 2010, Roberson et al., 2011), demonstrating the importance of tau for Aβ-mediated neurodegeneration.

The mechanisms by which Aβ affects tau to cause neurodegeneration has been an area of intensive research. Several studies have demonstrated that various Aβ species can drive both the phosphorylation, and cleavage of tau, which likely drive the oligomerisation or aggregation of tau to generate damaging tau species (Davis et al., 1995, Garg et al., 2011). As described earlier, the phosphorylation of tau is regulated by the activity of several kinases, predominantly GSK3β and cdk5. Both of these major tau kinases can be activated by Aβ (Lee et al., 2000, Hernández and Avila, 2008). Furthermore, tau is cleaved at several epitopes by caspases and calpains, which are also activated by Aβ through abnormal increases of intraneuronal calcium – another key pathogenic event in AD (O'Brien and Wong, 2011).

However, in recent years the amyloid cascade hypothesis has been challenged from several angles. Perhaps of most importance, many therapeutics aimed at altering the production or accumulation of Aβ have been largely unsuccessful in clinical trials as they did not alter cognition or amyloid burden. These treatments either directly targeted Aβ by active or passive immunisation or aimed to preclude the production of Aβ by the inhibition of β-secretases and γ-secretases (Morris et al., 2014). There are many reasons that these therapies may have shown limited, if any, success. However, in one of the first immunotherapy trials, immunotherapy with AN1792 effectively cleared Aβ from the brain, but did not substantially affect tau pathology and did not reduce cognitive deficits, suggesting that removing Aβ alone is not sufficient to treat AD. Reasons for the failure of amyloid therapies could also include insufficient stratification of patient groups, and the relatively late stage of disease in patients (Hardy, 2009).

It is evident that in human AD, Aβ and tau pathologies have a close relationship, but this relationship is not as linear and simplistic as the amyloid cascade hypothesis once proposed. An incomplete picture of the mechanisms underlying the mass loss of neurons and brain function that accompanies AD still remains and the interplay between Aβ and tau in AD needs to be further explored.

1.5 Synaptic changes in AD

Synaptic dysfunction and synaptic loss are major early features of AD, which precedes neuron loss. Synaptic dysfunction is evident in humans with MCI, well before the onset

of plaque or tangle pathologies (Scheff et al., 2007). Of most interest, synaptic loss correlates more robustly with cognitive dysfunction in AD than the build-up of Aβ plaques or neurofibrillary tangles containing tau (Terry et al., 1991, Masliah et al., 2001) implicating synaptic dysfunction and synaptic loss as a crucial early stage of disease. Since synapses are relatively plastic and recover well from damage, strategies to prevent synapse damage/loss in AD are likely to be very effective.

1.5.1 Effects of Aβ at the synapse

Physiological roles of Aβ at synapses have been described, including the demonstration that increasing concentrations of endogenous extracellular Aβ by inhibiting its degradation enhances activity-dependent synaptic vesicle release probability, boosting ongoing activity in the hippocampal network (Abramov et al., 2009). In AD, the synaptotoxic effects of Aβ are well recognised (Selkoe, 2002), but as with tau it remains unclear which species of Aβ is/are primarily responsible.

Several studies have shown both *in vitro* and *in vivo* that Aβ oligomers impair excitatory synaptic transmission, inhibit LTP, cause dendritic spine loss and impair spatial memory (Selkoe, 2002, Haass and Selkoe, 2007, Crews and Masliah, 2010). This disruption of synaptic function by Aβ, is likely in part through Aβ promoting the internalisation of postsynaptic glutamate receptors and associated dendritic spine loss, thus impairing glutamatergic synaptic transmission (Hsieh et al., 2006). Furthermore, it has been shown that soluble oligomeric Aβ associates with the post-synapse and contributes to the loss

of synapses and dendritic spines observed around Aβ plaques in human AD and in transgenic AD mice (Koffie et al., 2009).

The toxic effects of Aβ at the synapse is a complex mechanism, due to Aβ being able to trigger several synaptotoxic processes. Predominantly, Aβ can drive neurotoxic calcium dyshomeostasis, the activation of caspases and calcineurin, oxidative damage, alteration of synaptic receptor trafficking and anchoring, and other molecular events that culminate in synaptotoxicity and disrupted synaptic function (Lacor et al., 2007, Koffie et al., 2011).

It is clear that synaptic dysfunction and loss are critical early pathological features of AD that underlie disrupted neuron function and the clinical phenotypes of AD. It is also evident that Aβ can drive synaptotoxicity, but it is also important to recognise that loss of intact APP, which holds physiological roles at the synapse (Abramov et al., 2009), may also be critical to dysfunction in AD. In addition, the evidence that tau allows Aβ to exert its toxicity at synapses (Roberson et al., 2011) also needs further consideration.

1.5.2 Effects of tau at the synapse

Tau likely holds both physiological and pathological roles at the synapse dependent on its conformation, solubility, phosphorylation-state and whether it is the full length or truncated.

Tau has been found both pre- and post- synaptically in the human brain, albeit in much lower levels than it is present in the axon (Tai et al., 2012, Henkins et al., 2012) Amounts

of tau at the synapse have been shown to be similar in both control and AD patients. However, tau phosphorylated at ser 396/404 is only found in synapses in AD brain and tau phosphorylated at these sites was found in a greater number of postsynaptic than presynaptic sites (Tai et al., 2012). In synaptosomes prepared from human AD brains, phosphorylated tau species are found co-localised with Aβ (Fein et al., 2008, Henkins et al., 2012), and phosphorylated tau in synaptoneurosome preparations form human AD brain correlate strongly with dementia (Perez-Nievas et al., 2013). In addition, C-terminal truncated tau is released pre-synaptically from synaptosomes prepared from human AD brain (Sokolow et al., 2015). In mice expressing the mutant human P301L tau, tau phosphorylated at ser 396/404 was found to accumulate in the presynapse (Harris et al., 2012). However, an alternative study in P301L mice found that phosphorylated species of tau accumulated in dendritic spines at the post-synapse, unlike non-phosphorylated tau (Hoover et al., 2010)

Mutated tau and phosphorylated tau species drive impaired trafficking or anchoring of AMPARs and NMDARs in the post-synapse which precedes spine loss (Hoover et al., 2010, Kopeikina et al., 2013), and pre-synaptic injection of human tau in the giant squid axon completely abolishes synaptic transmission (Moreno et al., 2011). Tau also acts to traffic fyn to the synapse. Interaction between fyn and tau stabilise the NMDA receptor 2B (NR2B) and the post-synaptic density protein 95 (PSD-95) complex at the post-synapse (Ittner et al., 2010). Tau also plays a role in the trafficking of mitochondria along the axon to the synapse, which is essential for synaptic function (Kopeikina et al., 2011). In AD, it could be that the accumulation of pathological tau and the somatodendritic

accumulation of tau impairs its normal function to reduce this transport of mitochondria to the synapse, resulting in a local energy deficiency (Reddy, 2011). Together, these findings suggests that tau may exert toxicity both pre- and post-synaptically by interfering with normal synaptic function.

It is likely that Aβ or APP and tau interplay to drive synaptic dysfunction and synaptic loss in AD. *In vitro,* oligomeric Aβ can cause the translocation of tau from the axonal compartment to dendrites whilst concurrently increasing the phosphorylation of tau (Zempel et al., 2010). Similarly, other studies have shown that tau mislocalisation and the phosphorylation of tau at may be required to mediate Aβ-induced synaptotoxicity (Mairet-Coello et al., 2013, Miller et al., 2014). In APP transgenic mice, tau reduction as well as truncated tau, protect against Aβ-mediated toxicity to rescue premature death and memory deficits (Ittner et al., 2010). Similarly, tau reduction prevented cognitive decline, synaptic transmission deficits and plasticity deficits in APP transgenic mice (Roberson et al., 2011). Tau reduction also protects against excitotoxicity in both WT and transgenic APP mice (Roberson et al., 2007). This suggests a clear pathological function for tau mediating both Aβ-induced excitotoxicity and synaptic dysfunction.

Further work is required to determine which species or post-translational modification of tau is responsible for its toxicity at the synapse in AD. Additionally, the interplay between tau and Aβ or APP at the synapse in AD also requires further study to determine the best way in which to intervene therapeutically to reverse or slow neuronal loss and cognitive decline.

Taken together, the evidence described above indicates that interactions between specific forms of Aβ and tau, including their presence at (and downstream effects on) synapses play a critical role in mediating loss of synaptic function and neurodegeneration in AD. These events are summarised in Figure 1.6.

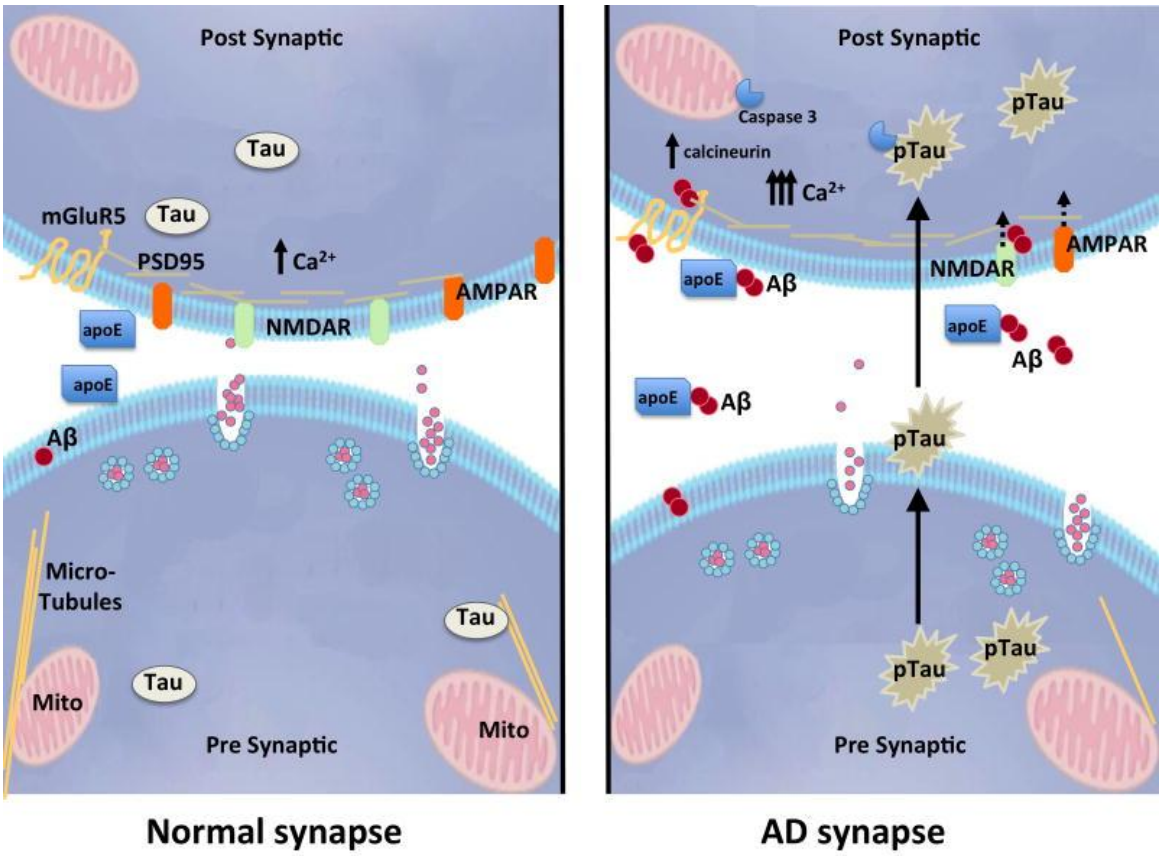

Figure 1.6: Effects of Aβ and tau at the synapse in AD
Schematic diagram summarising major effects of Aβ and tau at the synapse in AD. Aβ oligomers are implicated in causing synaptic dysfunction and loss in several models of AD. Aβ can bind to postsynaptic receptors initiating a cascade of events including increases in calcium, the activation of calcineurin and caspase 3, and the internalisation of the post-synaptic glutamate receptors - NMDA and AMPA. Tau at the synapse, including phosphorylated tau species can be mislocalised to dendritic spines driving increases in calcium and calcineurin activity, receptor internalisation and consequently disrupts neurotransmission. Tau has also been demonstrated to be transported trans-synaptically and the role of this in health and disease is unclear. Figure taken from (Spires-Jones and Hyman, 2014).

1.6 Animal models of AD

The use of animal models is necessary for us to understand the progressive neurodegeneration seen in AD since they share approximately 98% of their working DNA with humans (Waterston et al., 2002), are amenable to genetic modification, cognitive and behavioural testing, and their life-span allows tracking of progressive disease phenotypes with age. Furthermore, animal models are imperative for preclinical investigation of new potential therapies before human clinical trials can commence.

1.6.1 Mouse models of AD

Currently, none of the existing transgenic mouse models of AD fully recapitulate the wide spectrum of changes seen in human AD. Regardless, these "incomplete" animal models display some critical aspects of disease, thereby allowing us to identify mechanisms and pathways underling the development and progression of AD.

The majority of transgenic animal models of AD can be classified as follows:

- Mice expressing human *APP* and/or *PS1/PS2*: These mice generally show substantial Aβ pathology, synaptic dysfunction, behavioural changes, but no substantial neurodegeneration (Hsiao et al., 1996, Chapman et al., 1999). Additionally, these APP and/or PS mice show only some subtle increases in tau phosphorylation without any tangles or aggregates forming (Sturchler-Pierrat et al., 1997). The presence of mutations in *APP* and *PS1/2* usually drives the acceleration of disease progression compared to the expression of one transgene alone (Holcomb et al., 1998).

- Mice expressing human *MAPT*: Mice which express mutations in *MAPT* are typically used to understand changes in tau in tauopathies but are also useful to understand the development of AD-related changes in tau. For example, the P301S line shows the progressive development of hyperphosphorylated tau and the formation of intracellular NFTs similar to those in human AD and other tauopathies (Allen et al., 2002). Interestingly, mice which express non-mutant human tau also develop age-related changes in synaptic function and cognition associated with an increase in phosphorylated and aggregated tau (Andorfer et al., 2003, Polydoro et al., 2009).
- Mice expressing human *APP* or *APP+PS1/2* and *MAPT*: These mice which express multiple transgenes generally show the progressive development of changes in Aβ and the deposition of plaques, followed by changes in tau including increased phosphorylation and the development of NFTs. In addition, these mice show synaptic deficits and cognitive dysfunction and can show some neuronal loss (Oddo et al., 2003b, Oddo et al., 2003a, Saul et al., 2013). Again, increasing the number of transgenes present (e.g. in the 5XFADxPS19 model) also accelerates the disease phenotype (Saul et al., 2013).

We have been able to use these transgenic mouse models to gain insights into human AD, but it is important that more clinically relevant *in vivo* and *in vitro* models of AD are developed in order to uncover the mechanisms behind AD and allow better translation of therapeutic agents into the clinic.

1.6.2 The 3xTg-AD transgenic mouse model of AD

Mouse models which progressively develop human AD-like plaque and tangle pathology are multigenic. One of the best characterised and most successfully used lines is the 3xTg-AD mouse model, which co-expresses mutant human *PS1* (M146V), *APP* (Swe, K670N, M671L) and *tau* (P301L). 3xTg-AD mice (Oddo et al., 2003b) were generated by co-microinjection of two independent transgenes encoding human APP_{Swe} and human P301L tau (4R0N) (both under control of the mouse Thy1.2 regulatory element) into single-cell embryos harvested from homozygous mutant (M146V) PS1 knock-in (PS1-KI) mice (Guo et al., 1999). The presence of mutations in tau, APP and PS1 enables these mice to progressively accumulate Aβ plaques and intracellular NFTs with age.

At 3 months of age, 3xTg-AD mice accumulate intracellular Aβ in the cortex, but show no pathological alterations in tau. Levels of the astrocytic marker, glial fibrillary acidic protein (GFAP), are also comparable with WT controls at this age (Oddo et al., 2003a, Oddo et al., 2003b). By 4 months of age, 3xTg-AD mice display elevated levels of insoluble Aβ-42 in the cortex, but soluble levels of Aβ-40 and Aβ-42 are unchanged. This is further exacerbated at 6 months of age, a time when intracellular Aβ is reported to accumulate in the amygdala and hippocampus, and extracellular Aβ and small plaques are first detectable in the cortex (Billings et al., 2005, Oddo et al., 2003b). A reduction in the volume and surface area of astrocytes is also observed in the hippocampus of 6 month old 3xTg-AD mice (Olabarria et al., 2010). By 12 months of age, extracellular Aβ and plaques have developed in the hippocampus, in association with reactive astrocytes (Oddo et al., 2003b). Astrocytes distal to plaques show a reduced volume and surface

area indicative of atrophy at this age (Olabarria et al., 2010, Yeh et al., 2013). The first obvious tau changes are also observed in 12 month old mice, with increased phosphorylation of tau at thr 231 and ser 202/thr 205 detected in the cortex, amygdala and hippocampus alongside disease-associated conformational changes in tau. By 15 months of age, accumulations of tau with tangle-bearing features in the 3xTg-AD cortex, amygdala and hippocampus are detectable following histological staining (Oddo et al., 2003a, Oddo et al., 2003b). By 18 months of age tau phosphorylation at ser 396/404 is increased relative to WTs and reactive astrocytes colocalise with tau-reactive dystrophic neurites. Total levels of GFAP are also elevated at this age in 3xTg-AD mice, particularly in the cortex (Oddo et al., 2003a, Oddo et al., 2003b).

In line with the amyloid cascade hypothesis, these mice progressively develop synaptic dysfunction and neuronal death alongside tau and Aβ pathologies. Synaptic dysfunction as indicated by impaired LTP is reported at 6 months of age, and this is notably concomitant with the first detectable presence of intracellular Aβ in the hippocampus (Oddo et al., 2003b). Furthermore, spine density progressively reduces with age in the 3xTg-AD mice, indicating an age-dependent neurodegenerative phenotype similar to that of human AD (Bittner et al., 2010). 3xTg-AD mice also progressively develop other pathological features of human AD including upregulated microglial activity (Mastrangelo and Bowers, 2008), aberrant kinase activity (Sy et al., 2011), and substantial loss of noradrenergic (Manaye et al., 2013) and cholinergic (Girão da Cruz et al., 2012) neurons.

As well as developing several pathological and physiological features of AD, 3xTg-AD mice develop a range of cognitive and behavioural symptoms with age that are comparable to that seen in human AD. 3xTg-AD mice develop progressive cognitive impairments from a relatively young age; deficits in associative learning are first detected between 3 and 5 months of age, and deficits in spatial working memory (Morris water maze), associative learning/memory (contextual fear conditioning), and reference/working memory (Y-maze alternation) are apparent at 6 months of age. Recognition memory starts is impaired between 9 and 11 months of age, and reference memory, as measured in the Barnes maze, becomes notable impaired at 12 months of age (Webster et al., 2014). 3xTg-AD mice also develop other clinically relevant symptoms of human AD including circadian disturbances (Sterniczuk et al., 2010b), anxiety and restlessness (Sterniczuk et al., 2010a).

1.6.3 Pharmacological approaches to novel AD treatments using 3xTg-AD mice

Due to the molecular and behavioural AD-relevant phenotype of 3xTg-AD mice, many potential therapeutics targeted at alleviating the symptoms and pathology in AD have been investigated *in vivo* in this transgenic line. The main studies relevant for this project are briefly described below:

Lithium Chloride (LiCl)

Lithium is a widely prescribed drug for bipolar disorder. The exact mechanism of lithium in the brain is still speculated, but in terms of AD, the ability of lithium to deactivate GSK-3β may be important as GSK-3 is one of the most common kinases involved in tau

phosphorylation (Hanger et al., 1992). GSK-3α/β are inactivated when the inhibitory phosphorylation sites ser 21/9 are phosphorylated thereby activating GSK-3 and allowing this kinase to phosphorylate tau (Sutherland et al., 1993). The deactivation of GSK-3β results in decreased tau phosphorylation in primary neuronal cultures and *in vivo* (Muñoz-Montaño et al., 1997, Noble et al., 2005) and reduced production and deposition of APP (Phiel et al., 2003). In 3xTg-AD mice, lithium treatment reduced tau phosphorylation at thr 181, ser 202/thr 205, thr 231, and thr 212/ser 214 (all targets of GSK-3) to levels similar to those found in WT controls. Working memory, as determined by T maze assays, was not improved by lithium treatment and no reductions in the numbers of Aβ-positive plaques, insoluble and soluble Aβ-40 or Aβ-42 were resulted from lithium treatment (Caccamo et al., 2007).

NAPVSIPQ

NAPVSIPQ, also known as davunetide, is an octapeptide derived from activity-dependent neurotrophic factor (ADNF) which has broad neuroprotective properties in *in vitro* and *in vivo* neurodegenerative models. NAPVSIPQ protects against Aβ-induced neurotoxicity (Zemlyak et al., 2000), inhibits Aβ aggregation (Ashur-Fabian et al., 2003), and prevents disruption of microtubules and reduces tau phosphorylation *in vitro* (Gozes and Divinski, 2004). NAPVSIPQ treatment for 3 months in 9 month old 3xTg-AD mice lowered levels of Aβ–40 and Aβ–42 as well as reducing tau phosphorylation at ser 202/thr 205 and thr 231, but not ser 202 (Matsuoka et al., 2007). NAPVSIPQ treatment in older (12 month old) 3xTg-AD mice also yielded similar effects on AD-relevant phenotypes, namely reductions in levels of phosphorylated tau and insoluble tau, as well as improved

performance in spatial memory (Morris water maze) and non-associative memory (olfactory habituation/dishabituation test) (Matsuoka et al., 2008).

BTA-EG_4

BTA-EG_4 is an oligo (ethylene glycol) derivative of 6-methylbenzothiazole aniline which holds amyloid-binding properties to prevent interactions of amyloid fibrils with other amyloid-binding proteins (Inbar et al., 2006). Treatment with BTA-EG_4 is neuroprotective in cultures treated with Aβ preparations that lead to subsequent hydrogen peroxide release (Habib et al., 2010).

BTA-EG_4 treatment reduces the production of Aβ both *in vivo* in WT mice and *in vitro* in primary cortical neurons, as demonstrated in WT mice by an increased production of sAPPα and a reduced production of sAPPβ. This activity is likely due to the fact that BTA-EG_4 increases surface expression of APP, thereby enhancing preferential cleavage by α-secretase to preclude Aβ formation. Furthermore, BTA-EG_4 increases spine density, the number of functional synapses and overall synaptic function as measured by an increased frequency of mEPSCs in the cortex and hippocampus in WT mice. These synaptic improvements are also accompanied by improved cognitive performance (Megill et al., 2013).

In 6 to 10 month old 3xTg-AD mice which show mild synapse loss, 2-week treatment with BTA-EG_4 was found to increase spine density and spine size in the cortex and hippocampus, effects found to be mediated via upregulated Ras cell signalling activity

and increased GluA2 expression. In 13 to 16 month old 3xTg-AD mice, which show moderate synapse loss, treatment for 2-weeks with BTA-EG_4 increased spine density in the cortex but not in the hippocampus, and had no effect on spine size. Cognitive performance, as measured by the Morris water maze was improved in 2 to 3 month old BTA-EG_4 treated 3xTg-AD mice, which show no synaptic impairment, and to an extent in 6 to 10 month old 3xTg-AD mice, concurrent with increased markers of functional synapses. No improvement in cognition was seen in 13 to 16 month old 3xTg-AD mice (Song et al., 2014). No effects of BTA-EG_4 on tau have yet been reported.

1.7 Organotypic brain slice cultures

1.7.1 History

Culture of *ex vivo* organotypic brain slice cultures was first reported in the 1940s, but it was in 1981 when a roller-tube method of culturing *ex vivo* organotypic brain slices was fully established as a technique to model *in vivo* physiology and development in the brain (Gähwiler, 1981). The roller-tube culture method provided a more developed system compared to other *in vitro* methods available at the time, and was widely adopted. However, organotypic brain slices produced by this were found to dramatically thin once in culture, resulting in a monolayer of cells. Therefore, this method did not allow preservation of the cytoarchitecture of the tissues from which the cultures were prepared.

The most commonly used method to prepare organotypic brain slice cultures is the interface-slice culture method, which, was established by Stoppini and colleagues in

1991. This relatively simple method involves a tissue explant from neonatal mice/rats being cultured on a porous membrane interface between the humidified atmosphere and culture medium. The tissue explants are able to receive adequate nutrition through the membrane from the slice culture medium via capillary action (Stoppini et al., 1991). Organotypic brain slice cultures made by the interface-slice culture method only will be discussed from herein.

1.7.2 Advantages of *ex vivo* organotypic brain slice cultures

Organotypic brain slice cultures are a well-established model in which the three-dimensional organisation and architecture of the tissue is preserved, lending their application to developmental studies as well as electrophysiology, morphology and biochemical analyses (Gähwiler et al., 1997).

Since their establishment as a useful tool in neuroscience research, many uses and advantages of organotypic brain slice cultures have emerged. In particular, these long-term slice cultures provide a means to replace, refine and reduce some aspects of *in vivo* research (Humpel, 2015a). Slice cultures are generally produced from mice or rats at young ages – normally postnatal day 0 to postnatal day 12. Brain slices produced from these pups display high levels of plasticity, therefore show resistance to the mechanical trauma incurred during the slice culture procedure (Gähwiler et al., 1997). This allows viable healthy cultures to be maintained for several weeks/months in culture after explant (De Simoni and My Yu, 2006). Furthermore, neurodevelopment continues *ex vivo*; only immature synapses have been made in pups prior to culture preparation, but

these develop *ex vivo* as they do *in vivo*, maturing after 2-3 weeks in culture (De Simoni et al., 2003).

Several studies have shown that the development of brain slices *ex vivo* mimics the *in vivo* situation. Neurons in slice cultures grow to the same length and develop the same number of primary branches, show the same apical dendrite outgrowth and same spine density as they would *in vivo* as acute preparations (De Simoni et al., 2003). They also retain synaptic connectivity and function, show active synaptic vesicles and a similar capacity for LTP as intact brain (De Simoni et al., 2003). Furthermore, glia develop normally in organotypic cultures, in approximately the same proportions as observed in vivo (Hailer et al., 1996), and gene regulation and protein expression matches *in vivo* adult brain.

From a pharmaceutical or industrial perspective, slices can be utilised for medium throughput pre-clinical screening of compounds, and are a more readily tractable and considerably cheaper alternative to *in vivo* animal studies. In comparison to high-content screening, slice culture models enable a more robust selection of lead compounds to take forward to *in vivo* testing as slices are more biologically relevant than dissociated primary cells or cell lines, and if prepared from transgenic animals do not require any modification such as transfection of proteins of interest, to investigate mechanisms or targets, unlike more conventional methods of drug discovery (Sundstrom et al., 2005). In summary, organotypic slice culture models should be able to replicate human diseases

more robustly and effectively than other *in vitro* systems, which is likely to be advantageous to basic science as well as drug discovery and development.

1.7.3 Modelling disease in *ex vivo* organotypic brain slice cultures

The use of e*x vivo* organotypic brain slices has been widely exploited in order to model aspects of various diseases and disorders of the central nervous system for mechanistic and therapeutic investigations. Examples of a select few of such studies are listed below to demonstrate the breadth and variety of brain slice culture model systems.

- Ischaemia has been successfully modelled in rat hippocampal slice cultures (Pringle et al., 1997).
- Neurodegeneration characteristic of amyotrophic lateral sclerosis (ALS) has been modelled in spinal cord cultures from rats (Corse et al., 1999).
- The demyelination and remyelination typical of multiple sclerosis has been modelled in cerebellar, brainstem and spinal cord cultures from mice (Zhang et al., 2011a).

Organotypic brain slice cultures of AD have also been developed previously. Organotypic hippocampal cultures prepared from WT animals and maintained in culture for one week (immature – p14 equivalent) or for four weeks (mature – p35 equivalent) show significant cell death when treated with Aβ; mature cultures demonstrated more marked neurotoxicity modelling the susceptibility of aged brain to Aβ (Bruce et al., 1996). In addition, applying Aβ to acute hippocampal slices was found to prevent the

induction of LTP (Wang et al., 2004). Impaired LTP has also been reported in acute hippocampal slices prepared from several transgenic AD mouse lines including 3xTg-AD mice (Oddo et al., 2003b), and long-term organotypic brain slice cultures produced from mice expressing mutant human tau transgenes develop phosphorylated tau species and insoluble tau aggregates, and long-term cultures produced from mutant human APP transgenic mice develop small Aβ-containing plaque-like structures (Duff et al., 2002, Humpel, 2015b). Furthermore, the degeneration of cholinergic neurons in AD has also been recapitulated in organotypic cultures prepared from rats which are cultured without nerve growth factor (Humpel and Weis, 2002). However, no organotypic brain slice culture models that develop both tau and Aβ pathology have, to the best of our knowledge, yet been developed. Since, as outlined above, interactions between tau and Aβ are likely to be critical for neurodegeneration in AD, there is a considerable need to develop such a model since it will have widespread utility for investigations into the mechanisms underlying disease, and as a drug screening and/or development platform.

1.8 Aims and objectives of this thesis

This study was designed to develop a novel organotypic brain slice culture model of Alzheimer's disease that will progressively develop the main features of human AD including the progressive development of pathological tau and Aβ, and associated neurodegenerative pathways, and to use this model to elucidate mechanisms of disease and as a platform for small-scale discovery and testing of potential AD therapeutics. This project had the following specific aims:

1. Establish a novel organotypic brain slice culture model of AD from 3xTg-AD mice.

2. Fully assess the biochemical and physiological features of disease progression in 3xTg-AD brain slice cultures in comparison to WT cultures, *in vivo* 3xTg-AD brain and previously published work using post-mortem human AD brain.

3. Use slice cultures to investigate the molecular mechanisms underlying the development of Alzheimer's disease, with a particular focus on the release of tau from neurons and mechanisms of tau propagation and spread in AD.

4. Validate the utility of 3xTg-AD brain slice cultures as a sensitive model in which to investigate the effects of AD-relevant therapies by comparing the effects of treatments in slices to those previously published following *in vivo* treatment of 3xTg-AD mice.

5. Determine possible novel modes of action of previously tested therapeutic agents in 3xTg-AD brain slice cultures.

Chapter 2 : Materials and Methods

2.1 Materials

Unless otherwise stated, all molecular biology and cell culture reagents were purchased from Invitrogen Ltd., UK and all other chemicals were purchased from Sigma-Aldrich Company Ltd., UK. Stock solutions and buffers were prepared using ultrapure H_2O from an Elga® Maxima Purification System (Veolia Water Ltd., UK). When required, solutions were sterilised by autoclaving for 20 minutes at 15 lb/inch^2.

2.1.1 Cell culture materials

Primary neuron cultures

Poly-D-lysine	10 µg/mL Poly-D-lysine
Supplemented Neurobasal medium	Neurobasal™ medium without phenol red 1 % (v/v) B27 supplement 2 mM L-glutamine (PAA Laboratories GmbH, Austria) 60 units/mL penicillin (PAA Laboratories GmbH, Austria) 100 units/mL streptomycin (PAA Laboratories GmbH, Austria)

HBSS	Hank's balanced salt solution (HBSS), with Ca^{2+} and Mg^{2+}
HBSS without Ca^{2+} and Mg^{2+}	Hank's balanced salt solution without Ca^{2+} and Mg^{2+}
Trypsinising solution	0.05 % (w/v) trypsin 0.53 mM ethylenediaminetetraacetic acid (EDTA) in HBSS
DNase solution	Deoxyribonuclease (DNase) 1 (2000 kunitz units) in 0.9 % NaCl
Neutralising solution	Neurobasal™ medium without phenol red 10 % (v/v) Fetal calf serum (FCS) 0.1 % (v/v) DNase solution
Trypan blue	0.4 % (w/v) Trypan blue solution (Thermo Scientific Ltd., UK) in 50 mM phosphate-buffered saline (PBS)

Cell culture treatments

Lithium chloride	1, 5, 10, 20, 40 mM LiCl in ultrapure H_2O
Sodium chloride (NaCl)	20 mM NaCl in ultrapure H_2O
NAPVSIPQ	1 x 10^{-15}, 10^{-13}, 10^{-11}, 10^{-9}, 10^{-7} M NAPVSIPQ (Alpha Diagnostic International, USA) in ultrapure H_2O
Nocodazole	5 mg/ mL nocodazole in dimethyl sulfoxide (DMSO)
BTA-EG_4	20, 40, 60 µM BTA-EG_4 in DMSO

2.1.2 Slice culture materials

Slice culture preparation and culture

Dissection buffer	1.25 mM KH_2PO_4, pH 7.4 124 mM NaCl 3 mM KCl 8.19 mM $MgSO_4$ 2.65 mM $CaCl_2$ 3.5 mM $NaHCO_3$

	10 mM glucose
	2 mM ascorbic acid
	39.4 µM ATP
	in ultrapure H_2O, sterile filtered (0.2 µm)
Slice culture medium	Basal medium eagle (BME)
	26.6 mM HEPES, pH 7.1
	19.3 mM NaCl
	5 mM $NaHCO_3$
	511 µM ascorbic acid
	40 mM glucose
	2.7 mM $CaCl_2$
	2.5 mM $MgSO_4$
	1 % (v/v) GlutaMAX
	0.033 % (v/v) insulin
	0.5 % (v/v) penicillin/streptomycin
	25 % (v/v) heat inactivated horse serum
	in ultrapure H_2O, sterile filtered (0.2 µm)
Slice culture treatments	
Lithium chloride (LiCl)	20 mM LiCl in ultrapure H_2O

Sodium chloride	20 mM NaCl in ultrapure H_2O
NAPVSIPQ	1 x 10^{-15}, 10^{-13}, 10^{-11}, 10^{-9}, 10^{-7} M NAPVSIPQ (Alpha Diagnostic International, USA) in ultrapure H_2O
Nocodazole	5 mg/mL nocadazole in DMSO
BTA-EG_4	40, 60 µM BTA-EG_4 in DMSO
KCl	50 mM in ultrapure H_2O
Tetrodotoxin citrate	2 µM tetrodotoxin citrate (Abcam Plc., UK) in ultrapure H_2O

2.1.3 Materials for biochemical assays

Lactate dehydrogenase (LDH) assays

Cytotox 96® non-radioactive cytotoxicity assay (Promega, UK)

All reagents supplied complete by manufacturer.

LIVE/DEAD® assay

LIVE/DEAD® far red fixable dead cell stain kit (Invitrogen Ltd., UK)

	All reagents supplied complete by manufacturer.

General buffer solutions

50 mM PBS	4.3 mM Na_2HPO_4 1.47 mM KH_2PO_4 137 mM NaCl 2.7 mM KCl, pH 7.4 in ultrapure H_2O
50 mM Tris-buffered saline (TBS)	50 mM Tris-HCl, pH 7.6 150 mM NaCl in ultrapure H_2O

Bicinchoninic acid (BCA) protein assay

BCA® protein assay (Pierce™, USA)

	All reagents supplied complete by manufacturer.
Bovine serum albumin (BSA)	2 mg/mL BSA

Sample preparation

Extra strong lysis buffer	10 mM Tris-HCl, pH 7.5
	75 mM NaCl
	0.5 % (w/v) sodium dodecyl sulphate (SDS)
	20 mM sodium deoxycholate
	1 % (v/v) Triton X-100
	2 mM sodium orthovanadate
	1.25 mM NaF
	1 mM sodium pyrophosphate
	10 mM EDTA
	in ultrapure H_2O

1x Mini protease inhibitor cocktail tablet (Roche Diagnostics, UK) was added to 10 mL buffer prior to use to inhibit the action of serine, cysteine and metallo-proteases.

Synaptosome lysis buffer	10 mM Tris HCl, pH 7.4
	0.32 M Sucrose
	2 mM EGTA
	2 mM EDTA
	in ultrapure H_2O

1x Mini protease inhibitor cocktail tablet (Roche Diagnostics, UK) was added to each 10 mL buffer prior to use.

Microtubule-stabilising buffer	80 mM piperazine-N,N'-bis (2-ethane-sulfonic acid) (PIPES), pH 6.8
	1 mM GTP
	1 mM $MgCl_2$
	1 mM EGTA
	0.5 % (v/v) Triton X-100
	30 % (v/v) glycerol
	10 µM Taxol
	0.5 µM okadaic acid (Santa Cruz Biotechnology, USA)
	in ultrapure H_2O

1x Mini protease inhibitor cocktail tablet (Roche Diagnostics, UK) was added to each 10 mL buffer prior to use.

Hypotonic buffer for membrane fractionation

	10 mM $NaHCO_3$, pH 7.5
	25 µg/mL DNAse I
	1 mM sodium orthovanadate
	in ultrapure H_2O

1x Mini protease inhibitor cocktail tablet (Roche Diagnostics, UK) was added to each 10 mL hypotonic buffer prior to use.

Sarkosyl homogenisation buffer	50 mM TBS, pH 7.4

	2 mM EGTA
	10 mM NaF
	1 mM sodium orthovanadate
	in ultrapure H_2O

1x Mini protease inhibitor cocktail tablet (Roche Diagnostics, UK) was added to each 10 mL buffer prior to use.

2x Sample buffer	125 mM Tris-HCl, pH 6.8
	4 % (w/v) SDS
	100 mM dithiothreitol
	20 % (v/v) glycerol
	0.01 % (w/v) bromophenol blue
	in ultrapure H_2O

Sodium dodecyl sulphate-polyacrylamide gel electrophoresis (SDS-PAGE)

Gels for SDS-PAGE were prepared using stock solutions purchased from National Diagnostics, UK. Final gel compositions were:

12.5 % resolving gel, pH 8.8	12.5 % (v/v) acrylamide
	25 % (v/v) resolving buffer
	0.01 % (w/v) ammonium persulphate (APS)

	0.1 % (v/v) N,N,N’,N’, tetramethylethylenediamine (TEMED) in ultrapure H_2O
10 % resolving gel, pH 8.8	10 % (v/v) acrylamide 25 % (v/v) resolving buffer 0.01 % (w/v) APS 0.1 % (v/v) TEMED in ultrapure H_2O
7.5 % resolving gel, pH 8.8	7.5 % (v/v) acrylamide 25 % (v/v) resolving buffer 0.01 % (w/v) APS 0.1 % (v/v) TEMED in ultrapure H_2O
4 % stacking gel, pH 8.8	4 % (v/v) acrylamide 25 % (v/v) resolving buffer 0.075 % (w/v) APS 0.1 % (v/v) TEMED in ultrapure H_2O

Running buffer	Tris-glycine-SDS-PAGE buffer 10x (National Diagnostics, UK) diluted in ultrapure H_2O

Western blotting and immunodetection reagents

Immunoblotting transfer buffer	Tris-glycine buffer 10x (National Diagnostics, UK) diluted in ultrapure H_2O 20% (v/v) methanol
Washing buffer	50 mM TBS
Blocking solutions	5 % (w/v) skimmed milk powder in 50 mM TBS or 5 % (w/v) BSA in 50 mM TBS with 0.05 % (v/v) Tween-20 or Odyssey blocking solution (LI-COR Biosciences, UK)

Protein molecular weight marker

Precision Plus Protein™ All-Blue Standard (Bio-Rad Laboratories Inc., USA) consisting of 10 pre-stained bands with sizes 10 kDa, 15 kDa, 20 kDa, 25 kDa, 37 kDa, 50 kDa, 75 kDa, 100 kDa, 150 kDa, and 250 kDa when used with tris-glycine-SDS-PAGE running buffer.

Enzyme-Linked Immunosorbent Assay (ELISA) reagents for detection of Human Amyloid-β 40 and 42

Human Aβ-40 ELISA kit (Invitrogen Ltd., UK)

All reagents supplied complete by manufacturer.

Human Aβ-42 ELISA kit (Invitrogen Ltd., UK)

All reagents supplied complete by manufacturer.

Standard reconstitution buffer	55 mM $NaHCO_3$, pH 9.0
Standard diluent buffer	50 mM TBS 0.13 mM Tris-HCl, pH 7.5 1 mM NaCl 0.006 % (w/v) SDS 0.26 mM sodium deoxycholate 0.013 % (v/v) Triton X-100 26 µM sodium orthovanadate 17 µM NaF 13 µM sodium pyrophosphate 0.13 mM EDTA in ultrapure H_2O

1x Mini protease inhibitor cocktail tablet (Roche Diagnostics, UK) was added to each 10 mL buffer prior to use.

ELISA reagents for detection of extracellular tau

ELISA coating buffer, pH 7.2	15.6 mM K_2HPO_4
	25.6 mM KH_2PO_4
	136.9 mM NaCl
	1.3 mM EDTA
	7.7 mM NaN_3
	in ultrapure H_2O
Washing buffer	50 mM TBS
	0.05 % (v/v) Tween-20
Blocking solutions	
Starting block solution	50% (v/v) StartingBlock™ blocking buffer
	(Thermo Scientific Ltd., UK)
	in 50 mM TBS
Primary antibody blocking solution	20% (v/v) SuperBlock™ blocking buffer
	(Thermo Scientific Ltd., UK)
	in 50mM TBS

Secondary antibody blocking solution	5 % (w/v) skimmed milk powder in 50 mM TBS
Stabilised chromogen substrate solution	Tetramethylbenzidine (TMB)-ultra reagent (Thermo Scientific Ltd., UK)
Stop solution	1M HCl
Immunocytochemistry	
4 % paraformaldehyde (PFA)	4 % (w/v) PFA in 50 mM PBS
Permeabilisation solution	0.1 % (v/v) Triton X-100 in 50 mM PBS
Blocking solution	5 % (w/v) BSA in 50 mM PBS 0.05 % (v/v) Tween-20
Washing solution	50 mM PBS 0.05 % (v/v) Tween-20
Hoechst 33258	2 µg/mL bis-Benzimide H33258 pentahydrate (Invitrogen Ltd., UK) in 50 mM PBS

Immunohistochemistry reagents for labelling of organotypic brain slice cultures

4 % paraformaldehyde (PFA)	4 % (w/v) PFA in 50 mM PBS
Permeabilisation solution	0.1 % (v/v) Triton X-100 in 50 mM PBS
Blocking solution	20 % (w/v) BSA in 50 mM PBS
Antibody solution	5 % (w/v) BSA in 50 mM PBS
Washing solution	50 mM PBS
Hoechst 33258	2 µg/mL bis-Benzimide H33258 pentahydrate in 50 mM PBS

Immunohistochemistry reagents for labelling of mouse brains

50 mM TBS	50 mM Tris, pH 7.6 150 mM NaCl in ultrapure H_2O
Cryoprotectant solution	30 % (w/v) sucrose in 50 mM TBS
TBS-anti freeze (TBS-AF)	30 % (v/v) ethylene glycol 15 % (w/v) sucrose

	0.05 % (w/v) sodium azide in 50 mM TBS
Peroxidase blocking solution	1 % (v/v) Hydrogen peroxide (H_2O_2) in 50 mM TBS
Blocking solution	15 % (v/v) normal goat serum (Vector Laboratories Ltd., UK) in 50 mM TBS-T or 15 % (v/v) normal rabbit serum (Vector Laboratories Ltd., UK) in 50 mM TBS-T
IHC antibody incubation solution	10 % (v/v) normal goat serum (Vector Laboratories Ltd., UK) in 50 mM TBS-T or 10 % (v/v) normal rabbit serum (Vector Laboratories Ltd., UK) in 50 mM TBS-T
Avidin-biotin peroxidase complex	Vectastain Elite ABC Kit (Vector Laboratories Ltd., UK) in 50mM TBS
DAB solution	0.05 % (w/v) 3.3'-diaminobenzidine tetrahydrochloride (DAB) 0.001 % H_2O_2 in 50 mM TBS

2.1.4 Antibodies

Antibody	Specificity	Species	Source/Primary reference	Dilution
DAKO tau	Total tau (phosphorylated and non-phosphorylated)	Rabbit polyclonal	DAKO Ltd., UK	1/10000
Tg5	Amino acids 220-240 of tau. Total tau (phosphorylated and non-phosphorylated)	Mouse monoclonal	Kind gift from P. Davies (Duff et al., 2000)	1/500
CP27	Amino acids 130-150 of human tau (phosphorylated and non-phosphorylated)	Mouse monoclonal	Kind gift from P. Davies (Duff et al., 2000).	1/400
β-actin	N-terminal end of the β-isoform of actin, clone AC-74	Mouse monoclonal	Sigma-Aldrich Company Ltd., UK	1/10000
β-actin	N-terminal end of the β-isoform of actin	Rabbit polyclonal	Abcam Plc., UK	1/5000
Tau-1	Tau dephosphorylated at ser 195, 198, 199, 202 and thr205	Mouse monoclonal	Merck Millipore Ltd., UK	1/5000
PHF-1	Tau phosphorylated at ser 396 and 404	Mouse monoclonal	Kind gift from P. Davies (Wolozin et al., 1986).	1/400
CP13	Tau phosphorylated at ser 202	Mouse monoclonal	Kind gift from P. Davies	1/200
Tg3	Abnormal conformation around tau phosphorylated at thr 231.	Mouse monoclonal	Kind gift from P. Davies (Dickson et al., 1995).	1/10
TP007	Amino acids 1-16 of tau (N-terminus)	Rabbit polyclonal	(Davis et al., 1995)	1/2000
TP70	Amino acids 428-441 of tau (C-terminus)	Rabbit polyclonal	(Brion et al., 1993)	1/2000
GFAP	Glial fibrillary acidic protein (GFAP)	Rabbit polyclonal	DAKO Ltd., UK	1/1000
GSK-3α/β	Glycogen synthase kinase 3 (GSK-3) (phosphorylated and non-phosphorylated)	Mouse monoclonal	Enzo Life Sciences Ltd., UK	1/1000

GSK-3α/β pser21/9	Glycogen synthase kinase 3 phosphorylated at ser 21/9	Rabbit polyclonal	Cell Signaling, USA	1/1000
cdk5	Clone J-3 to amino acids 1-291 of cdk5	Mouse monoclonal	Santa Cruz Biotechnologies Inc., USA	1/25
p35	Clone C-19 to C-terminus of p35	Rabbit polyclonal	Santa Cruz Biotechnologies Inc. USA	1/25
APP A4	Amino acids 66-81 of Amyloid precursor protein (APP) (N-terminus)	Mouse monoclonal	Merck Millipore Ltd., UK	1/1000
APP 6E10	Amino acids 1-16 of β-amyloid (C-terminus APP)	Mouse monoclonal	Covance Inc., USA	1/1000
Synaptophysin	Synaptophysin	Mouse monoclonal	Enzo Life Sciences Ltd., UK	1/1000
PSD-95	Total post-synaptic density protein 95 (PSD-95)	Rabbit Monoclonal	Cell Signaling, USA	1/1000
α-Tubulin	Clone DM1A α-Tubulin	Mouse Monoclonal	Sigma-Aldrich Company Ltd., UK	1/5000
acetylated α-Tubulin	Clone 6-11B-1 Acetylated α-Tubulin	Rabbit Polyclonal	Abcam Plc., UK	1/5000

Table 2.1: Primary antibodies used for Western blotting in this study.
Antibody name, specificity, species, dilution, and source/reference are shown. For tau antibodies, epitopes are numbered according to the longest isoform of CNS human tau, 2N4R.

Antibody	Species	Source	Dilution
Alexa Fluor® 680 goat anti-mouse IgG	Goat	Molecular Probes, Invitrogen Ltd., UK	1/10000
IRDyeTM 800 conjugated goat anti-rabbit IgG	Goat	Rockland Inc., USA	1/10000
Horseradish peroxidase (HRP)-linked goat anti-mouse IgG	Goat	GE Healthcare UK Ltd., UK	1/1000
HRP-linked goat anti-rabbit IgG	Goat	GE Healthcare UK Ltd., UK	1/1000

Table 2.2: Secondary antibodies used for Western blotting in this study.
Antibody reactivity, species, dilution and source are shown. Antibodies were compatible with the Li-Cor Odyssey Infrared Imaging system or enhanced chemiluminescence.

Antibody	Specificity	Species	Source	Dilution
DAKO tau	Tau (phosphorylated and non-phosphorylated)	Rabbit Polyclonal	DAKO Ltd., UK	1/1000
GFAP	Glial fibrillary acidic protein (GFAP)	Rabbit Polyclonal	DAKO Ltd., UK	1/1000

Table 2.3: Primary antibodies used for immunocytochemistry.
Antibody name, specificity, species, dilution, and source are shown.

Antibody	Species	Source	Dilution
Alexa Fluor® 568 goat anti-mouse IgG	Goat	Molecular Probes, Invitrogen Ltd., UK	1/500
Alexa Fluor® 488 goat anti-rabbit IgG	Goat	Molecular Probes, Invitrogen Ltd., UK	1/500

Table 2.4: Secondary antibodies used for immunocytochemistry.
Antibody reactivity, species, dilution, and company are shown.

Antibody	Specificity	Species	Source/Primary reference	Dilution
DAKO tau	Tau (phosphorylated and non-phosphorylated)	Rabbit Polyclonal	DAKO Ltd., UK	1/1000
CP13	Tau phosphorylated at ser 202	Mouse Monoclonal	Kind gift from P. Davies	1/200
GFAP	Glial fibrillary acidic protein (GFAP)	Mouse Monoclonal	Vector Laboratories Ltd., UK	1/1000
PHF-1	Tau phosphorylated at ser 396 and 404	Mouse Monoclonal	Kind gift from P. Davies (Wolozin et al., 1986)	1/200

Table 2.5: Primary antibodies used for organotypic brain slice culture immunohistochemistry.
Antibody name, specificity, species, dilution, and source/reference are shown.

Antibody	Species	Source	Dilution
Alexa Fluor® 568 goat anti-mouse IgG	Goat	Molecular Probes, Invitrogen Ltd., UK	1/500
Alexa Fluor® 488 goat anti-rabbit IgG	Goat	Molecular Probes, Invitrogen Ltd., UK	1/500

Table 2.6: Secondary antibodies used for organotypic brain slice culture immunohistochemistry.
Antibody reactivity, species, dilution, and company are shown.

Antibody	Specificity	Species	Source/Primary reference	Dilution
DAKO tau	Tau (phosphorylated and non-phosphorylated)	Rabbit Polyclonal	DAKO Ltd., UK	1/10000
MC1	Conformational change around residues 5-15 and 312-322 of tau	Mouse Monoclonal	Kind gift from P. Davies (Jicha et al., 1997)	1/100
PHF-1	Tau phosphorylated at ser 396 and 404	Mouse Monoclonal	Kind gift from P. Davies (Wolozin et al., 1986)	1/100

Table 2.5: Primary antibodies used in free-floating immunohistochemistry of mouse brains.
Antibody reactivity, species, dilution, and company are shown.

Antibody	Species	Source	Dilution
Biotinylated anti-rat IgG (H+L)	Rabbit	Vector Laboratories Ltd., UK	1/1000
Biotinylated anti-rabbit IgG (H+L)	Goat	Vector Laboratories Ltd., UK	1/1000
Biotinylated anti-mouse IgG (H+L)	Rabbit	Vector Laboratories Ltd., UK	1/1000

Table 2.6: Secondary antibodies used for free-floating immunohistochemistry for mouse brains.
Antibody reactivity, species, dilution, and source are shown.

2.1.5 3xTg-AD mice

3xTg-AD mice were obtained under a material transfer agreement from Professor Frank LaFerla (University of California Irvine, USA). A colony of breeding mice was established at the Institute. 3xTg-AD mice express mutant human PS1 (M146V), APP (Swe, K670N, M671L) and tau (P301L) transgenes. 3xTg-AD mice (Oddo et al., 2003b) were generated by co-microinjection of two independent transgenes encoding human APP_{Swe} and human tau_{P301L} (4R0N) (both under control of the mouse Thy1.2 regulatory element) into single-cell embryos harvested from homozygous mutant $PS1_{M146V}$ knock-in (PS1-KI) mice (Guo et al., 1999). Wild-type (WT) mice of an identical background strain (F2 hybrid: C57BL/6J and 129S1/SvImJ) were maintained as background controls. In this study, pups of both WT and 3xTg-AD were taken from breeding pairs to produce organotypic brain slice cultures at postnatal day 8 or 9. All procedures carried out were in accordance with the UK Animals in Scientific Procedures Act (1986).

2.1.6 3xTg-AD genotyping materials

REDExtract-N-Amp™ Tissue PCR Kit

All reagents supplied complete by manufacturer (Sigma-Aldrich Company Ltd., UK.)

Primer Pairs (Eurofins Genomics, Germany)

PS1	5’-CACACGCAACTCTGACATGCACAGGC-3’
	5’-AGGCAGGAAGATCACGTGTTCAAGTAC-3’
MAPT	5’-GAGGTATTAGTCATGTGCT-3’
	5’-TTCAAAGTTCACCTGATAGT-3’
APP	5’-GCTTGCACCAGTTCTGGATGG-3’
	5’-GAGGTATTCAGTCATGTGCT-3’

PCR (polymerase chain reaction) reaction mixture

20 % (v/v) extracted template DNA

10 µM forward primer

10 µM reverse primer

10 µL REDExtract-N-Amp™ PCR Reaction Mix (containing buffer, salts, dNTPs, Taq

	polymerase, REDTaq dye, and JumpStart Taq antibody) 20 % (v/v) nuclease-free H_2O (Thermo Scientific Ltd., UK)
PS1 Digestion	5 % (v/v) BstEII-HF® (New England Biolabs, USA) 50 % (v/v) extracted DNA 10 % (v/v) CutSmart™ Buffer (New England Biolabs, USA) 0.1 mg/ml BSA 30 % (v/v) nuclease-free H_2O (Thermo Scientific Ltd., UK)
1.5% Agarose Gel	1.5% (w/v) agarose 40 mM Tris 20 mM acetic acid 1 mM EDTA in ultrapure H_2O
TAE Running Buffer	40 mM Tris 20 mM acetic acid 1 mM EDTA in ultrapure H_2O

DNA molecular weight marker

Quick-Load® 100 bp DNA Ladder (New England Biolabs, USA) consisting of 12 pre-stained bands with sizes 100 bp, 200 bp, 300 bp, 400 bp, 500/517 bp, 600 bp, 700 bp, 800 bp, 900 bp, 1000 bp, 1200 bp, 1500/1517 bp when visualised with ethidium bromide on 1.5% agarose gels.

2.2 Methods

2.2.1 Cell culture

Primary culture of rat cortical neurons

Cortical neurons were prepared from embryonic day 18 Sprague Dawley rat embryos (Charles River Laboratories, UK) as previously described (Ackerley et al., 2000). In brief, the rat was sacrificed by cervical dislocation, the abdominal wall was cut through and the foetuses (on average, 9-12 per rat) were removed and dissected individually in HBSS without Ca^{2+} or Mg^{2+}. Brains were removed from the skull; the brainstem and cerebellum were removed under a dissecting microscope, as well as the meninges to prevent contamination of the cultures with fibroblasts. The cortex was dissected and processed separately.

Isolated cortices were washed with HBSS without Ca^{2+} or Mg^{2+}, and were dissociated by incubation in trypsinising solution for 30 minutes at 37 ^{o}C. Trypsinisation was stopped by removal of the trypsinising solution and three washes with neutralising solution. The final resuspension in 5 mL neutralisation solution produced a single cell suspension that was passed through a 70 µm cell strainer prior to centrifugation at 1000 $g_{(av)}$ for 2

minutes. Pelleted cells were resuspended in Complete Neurobasal medium and a sample was removed, stained with Trypan blue and cell density determined using a haemocytometer.

Where cells were to be harvested for SDS-PAGE, cells were plated at $1x10^6$ cells/well of a poly-D-lysine coated 6-well plate (Nunclon, Thermo Scientific Ltd., UK). For immunocytochemistry, cells were cultured on poly-D-lysine coated glass coverslips at a density of 2.5 x 10^5 cells/well of a 12-well plate. For microtubule binding assays, cells were cultured in poly-D-lysine coated 10 cm dishes at a density of 4 x 10^6 cells/plate. Neurons were maintained in supplemented Neurobasal medium at 37 ^oC in a humidified atmosphere of 95% air/5% CO_2.

Treatment protocol for primary cortical neurons

For LiCl treatments, 10 days *in vitro* (*div*) primary cortical neurons were treated for 4 hours with 1, 5, 10, 20, 40 mM LiCl before harvesting for immunoblot and immunocytochemical analysis. 20 mM NaCl was used as vehicle. Cell viability was measured 4 hours after treatment by live/dead assay.

For NAPVSIPQ treatments, 7 *div* primary cortical neurons were treated for 24 hours with 1 x 10^{-15}, 10^{-13}, 10^{-11}, 10^{-9}, 10^{-7} M NAPVSIPQ or vehicle (ultrapure H_2O) before harvesting for immunoblot or immunocytochemical analysis. Cell viability was measured 24 hours after treatment by live/dead assay.

For microtubule binding assays, 7 *div* primary cortical neurons were pre-treated for 21 hours with vehicle (ultrapure H_2O) or 1 x 10^{-7} M NAPVSIPQ before treatment for a further 3 hours with the microtubule destabilising agent, nocodazole (5mg/mL diluted in DMSO) or with vehicle (DMSO). Cell viability in both instances was measured 24 hours after treatment by live/dead assay.

For BTA-EG_4 treatments, 7 *div* or 14 *div* primary cortical neurons were treated for 24 hours with 20, 40, 60 µM BTA-EG_4 or vehicle (DMSO) before harvesting for preparation of synaptosomes, immunoblot or immunocytochemical analysis. Cell viability was measured 24 hours after treatment by live/dead assay.

Preparation of cell lysates for immunoblotting

Cell culture medium was aspirated from primary neurons; cells were then washed once in ice-cold PBS and collected via vigorous scraping into ice-cold PBS. Cells were pelleted by centrifugation at 7,000 $g_{(av)}$ for 30 seconds at ambient temperature. The supernatant was discarded and the pelleted cells were then lysed in 100 µL ice-cold extra strong lysis buffer. The cell suspension was then sonicated briefly (10 seconds) using a Vibra-Cell™ (Sonics and Materials Inc., USA) probe sonicator to improve sample handling. Cell lysates were centrifuged at 23,000 $g_{(av)}$ for 20 minutes at 4 ^{o}C and the supernatant collected. The protein content of cell lysates was determined by a BCA assay (section 2.2.4) and protein concentrations standardised prior to immunoblotting. Cell lysates were mixed with an equal volume of 2x sample buffer before immunoblotting.

Preparation of cell lysates for synaptosomes

Cell culture medium was aspirated from primary neurons; cells were then washed once in ice-cold PBS and collected via vigorous scraping into ice-cold PBS. Cells were pelleted by centrifugation at 7,000 $g_{(av)}$ for 30 seconds at ambient temperature. Cells were then homogenised by hand in synaptosome lysis buffer at a concentration of 200 mg lysates per mL of synaptosomes lysis buffer before differential centrifugation for preparation of synaptosomes (section 2.2.4).

Preparation of cell lysates for microtubule binding assay

Cell culture medium was aspirated from primary neurons in 10 cm dishes; cells were then washed once in pre-warmed PBS and collected via vigorous scraping into 600 µL pre-warmed microtubule-stabilising buffer before differential centrifugation to separate microtubule-bound and unbound proteins (section 2.2.4).

2.2.2 Slice Culture

Preparation of organotypic brain slice cultures

Organotypic brain slice cultures were prepared from WT and 3xTg-AD pups. Postnatal day 8 and 9 pups were culled by decapitation in accordance with the UK Animals in Scientific Procedures Act (1986). Brains from pups were bisected into hemi-brains by a single cut along the midline. The cerebellum, thalamus and brainstem were removed and discarded to leave the cortex, hippocampus and connecting areas. These were kept in ice-cold dissection buffer with constant oxygenation throughout the preparation procedure. 350 µm coronal slices were cut using a McIlwain Tissue Chopper (Stoelting

Co., USA). Eighteen slices from each hemi-brain were collected and 3 consecutive slices per well were positioned on interface-style Millicell culture inserts (Merck Millipore Ltd., UK) in 6 well culture plates (Nunclon, Thermo Scientific Ltd., UK) containing 1 mL of sterile slice culture medium. Three hours after plating, the culture medium was removed by aspiration and replaced with 1 mL of pre-warmed fresh sterile culture medium. Brain slices were incubated at 37 ^{o}C and the culture medium was changed from the bottom of each well every 2 to 3 days. Cultured slices initially appear white in colour, but within 2 weeks they become translucent, which indicates that they are healthy, viable slices. After this time any colour change to white signifies tissue death, and slices which showed significant regions of white were not analysed in this work. Organotypic brain slices were maintained in culture for up to 1 month. The process of making slice cultures can be visualised in Figure 2.1.

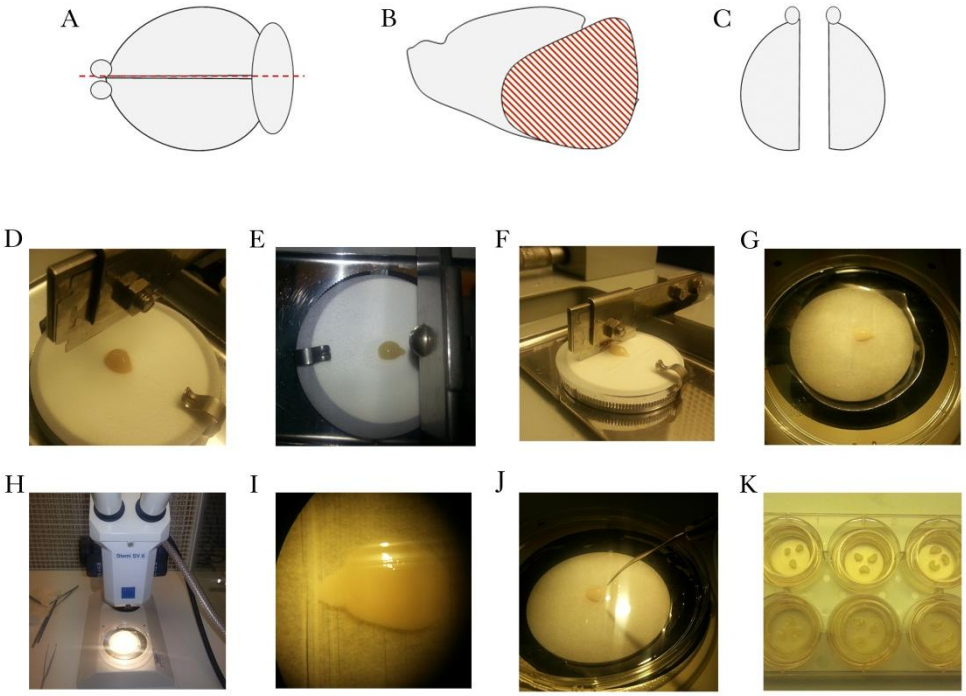

Figure 2.1: Preparation of Organotypic Brain Slice Cultures
(A) After dissection from the skull; brains are bisected along the midline. (B) The thalamus, cerebellum and brain stem are removed leaving the cortex, hippocampus and connected brain regions. (C) Two hemi-brains are kept in oxygenated dissection buffer throughout the procedure; one hemi-brain is stored whilst the other is processed. (D) Hemi-brains are placed on filter paper dampened with dissection buffer on the cutting surface of a McIlwain tissue chopper (E-F) 350 µm coronal slices are cut by an automated razor. (G-J) Sliced hemi-brains are sequentially separated under a dissection microscope. (K) Three consecutive slices are plated per well on Millipore membrane inserts. Slices are plated in order, with frontal slices in the first well etc. Initially slices are white in colour but after 1-2 weeks in culture they become translucent. Any white tissue at this time or after signifies tissue death.

Treatment protocol for slice cultures

For LiCl treatments, 28 *div* slice cultures were treated for 4 hours with 20 mM LiCl or NaCl (as control) before harvesting for immunoblot and immunohistochemical analysis. Slice viability was measured 4 hours after treatment by LDH assay.

For NAPVSIPQ treatments, 28 *div* slice cultures were treated for 24 hours with 1 x 10^{-7} M NAPVSIPQ or vehicle (ultrapure H_2O) before harvesting for immunoblot analysis. For microtubule binding assays, 28 days *in vitro* slice cultures were pre-treated with 1 x 10^{-7} M NAPVSIPQ or vehicle (ultrapure H_2O) before treatment for a further 3 hours with the microtubule destabilising agent nocodazole (5 mg/mL diluted in DMSO) or with vehicle (DMSO). Slice viability was measured 24 hours after application of NAPVSIPQ by LDH assay.

For BTA-EG_4 treatments, 28 *div* slice cultures were treated for 48 hours with 40 or 60 µM BTA-EG_4 or vehicle (ultrapure H_2O), before harvesting for preparation of synaptosomes, immunoblot or immunohistochemical analysis. Slice viability was measured 48 hours after treatment by LDH assay.

For extracellular tau release/neuronal stimulation experiments, slice cultures were treated after 28 days *in vitro.* The serum-containing slice culture medium was removed and replaced with 600 µL of HBSS containing Ca^{2+} and Mg^{2+}. Slice cultures were stimulated with 50 mM KCl or vehicle (ultrapure H_2O) for 30 minutes before harvesting for preparation of membrane and cytosol fractions and immunoblot analysis. Some slice cultures were pre-treated for 1 hour with 2 µM tetrodotoxin or equivalent volume of vehicle (ultrapure H_2O) and then stimulated with 50 mM KCl or vehicle (ultrapure H_2O) for 30 minutes before harvesting for immunoblot analysis. HBSS from treated slice cultures was kept and stored at -80 ^{o}C and used to measure extracellular amounts of tau. Slice viability was measured after treatment by LDH assay.

Preparation of slice lysates for immunoblotting and Aβ ELISA

Slice culture medium was aspirated from slice cultures. Slices were then washed once in ice-cold PBS and collected via vigorous scraping into ice-cold PBS. Tissue was pelleted by centrifugation at 7,000 $g_{(av)}$ for 30 seconds at ambient temperature. The supernatant was discarded and the pelleted slices were then lysed in 100 µL ice-cold extra strong lysis buffer. The suspension was then sonicated briefly (10 seconds) using a Vibra-Cell™ probe sonicator to improve sample handling. Slice lysates were centrifuged at 23,000 $g_{(av)}$ for 20 minutes at 4 ^{o}C and the supernatant collected. The protein content of the slice lysates was determined by a BCA assay (section 2.2.4) and standardised before immunoblotting or measurement of human Aβ-40 or Aβ-42 content by ELISA. Slice lysates were mixed with an equal volume of 2x sample buffer before immunoblotting.

Preparation of slice lysates for synaptosomes

Slice culture medium was aspirated from slice cultures. Slices were then washed once in ice-cold PBS and collected via vigorous scraping into ice-cold PBS. Tissue was pelleted by centrifugation at 7,000 $g_{(av)}$ for 30 seconds at RT. Slices were homogenised by hand at 200 mg tissue /mL synaptosome lysis buffer before differential centrifugation for preparation of synaptosomes (section 2.2.4).

Preparation of slice lysates for microtubule binding assay

Slice culture medium was aspirated from organotypic brain slice cultures. Slices were then washed once in pre-warmed PBS and collected via vigorous scraping into pre-warmed microtubule-stabilising buffer (300 µL microtubule-stabilising buffer/well). Two

wells of slices were pooled. Tissue was homogenised in microtubule stabilising buffer by hand before differential centrifugation for preparation of unbound and bound fractions of microtubules (section 2.2.4).

Preparation of slice lysates for membrane fractionation

HBSS was harvested from slice cultures. Slices were then washed once in ice-cold PBS and collected via vigorous scraping into ice-cold PBS. Tissue was pelleted by centrifugation at 7,000 $g_{(av)}$ for 30 seconds at ambient temperature. The supernatant was discarded and the pelleted slices were then lysed in 100 µL hypotonic buffer. The suspension was then sonicated briefly (10 seconds) using a Vibra-Cell™ probe sonicator to improve sample handling. Slice lysates were centrifuged at 800 $g_{(av)}$ for 10 minutes at 4 ^{o}C to remove cell nuclei and cell debris and the supernatant collected prior to further subcellular fractionation (section 2.2.4).

2.2.3 Analysis of Protein from Mouse Brains

Dissection and removal of brains

WT and 3xTg-AD male and female mice at 1, 2, 4, 9 and 12 months of age (n=3 per group) were culled by cervical dislocation in accordance with the UK Animals in Scientific Procedures Act (1986). Brains were rapidly removed and bisected into hemi-brains. Hemi brains were crudely dissected into a region containing the frontal cortex, hippocampus and associated cortex, and an amygdala-containing region. These regions are all affected in AD where both Aβ-containing plaques and neurofibrillary tau tangles

are found as the disease progresses (Braak and Braak, 1991, Braak and Braak, 1995). Tissue was frozen at -80 ^{o}C until required.

Preparation of mouse brains for immunoblotting and Aβ-40 and Aβ-42 ELISAs

The frontal cortex region was homogenised in extra strong lysis buffer at a concentration of 100 mg brain/mL extra strong lysis buffer using a Tissue Master-125 mechanical homogeniser (Omni International, USA) for approximately 20 seconds until a homogenous solution was obtained. The protein concentration of the samples was determined using a BCA assay and the protein concentration of samples standardised before ELISA and immunoblotting. Tissue samples were mixed with an equal volume of 2x sample buffer prior to immunoblotting.

Preparation of crude synaptosomes from mouse brains

The hippocampus-containing region was homogenised in synaptosome lysis buffer at a concentration of 200 mg tissue/mL synaptosome lysis buffer with a mechanical homogeniser for approximately 20 seconds until a homogenous solution was obtained. The homogenate was then processed by differential centrifugation to prepare crude synaptosomes (section 2.2.4).

Preparation of mouse brains for sarkosyl extraction of insoluble tau

The amygdala-containing region was homogenised in sarkosyl homogenisation buffer at a concentration of 100 mg tissue/ml sarkosyl homogenisation buffer with a mechanical homogeniser for approximately 20 seconds until a homogenous solution was obtained.

The tissue was then processed to isolate sarkosyl-insoluble (aggregated) tau (section 2.2.4).

Perfusion of mice and tissue sectioning

Two 4-month-old and two 12-month-old 3xTg-AD mice were sacrificed by terminal anaesthesia and transcardial perfusion with PBS followed by 4% (w/v) PFA in PBS. Hemi-brains were dissected from which the cerebellum was removed and discarded and the remaining tissues post-fixed in 4% (w/v) PFA overnight before washing in PBS for 24 hours at 4 ^{o}C. The tissue samples were then cryoprotected for 24 hours in 30 % (w/v) sucrose in PBS to prevent fracturing of the tissue during sectioning. Tissue was washed with PBS prior to being frozen for 30 seconds in isopentane chilled to -90°C with dry ice. Frozen tissue was stored at -80°C until required.

Hemi-brains were sectioned using a Leica CM1860 cryostat (Leica Microsystems, Germany). Samples were mounted onto a specimen disk using OCT mounting medium and sectioned coronally at 30 µm. Sections were collected and stored free floating in TBS-AF in a 96-well plate at 4 °C prior to histological processing (section 2.2.9).

2.2.4 Biochemical Analysis

Determination of protein concentration

Protein concentrations of cell, slice or mouse brain lysates were determined using a BCA protein assay according to the manufacturer's instructions (Pierce™, USA). This method combines the biuret reaction (reduction of Cu^{2+} to Cu by protein in an alkaline medium)

with the sensitive and selective colorimetric detection of the cuprous cation (Cu) using a BCA-containing reagent. The purple reaction product is formed by chelation of two molecules of BCA to Cu and this water soluble complex exhibits a strong absorbance at 562 nm. A set of BSA standards in extra strong lysis buffer were freshly prepared at concentrations ranging from 0-2 mg/mL for each assay.

Absorbance was measured at 562 nm using a Wallac 1420 Victor3™ plate reader (PerkinElmer, USA), and values were compared to a standard curve to determine protein concentration in µg/ml. Samples were then diluted with the appropriate volume of extra strong lysis buffer to ensure equal protein concentrations in all samples. For immunoblotting, 5-10 µg of protein were loaded per well.

Preparation of synaptosomes

Cell, slice and mouse brain lysates homogenised in synaptosome lysis buffer as described above were centrifuged at 1,000 $g_{(av)}$ for 10 minutes at 4^{o}C to remove cell nuclei and debris, and an aliquot of supernatant was kept as the total fraction. The remaining supernatant was then centrifuged at 10,000 $g_{(av)}$ for 20 minutes at 4 ^{o}C to obtain a crude synaptosomal pellet. The supernatant resulting from this centrifugation was retained as the non-synaptosomal fraction and the pellet which contains a high concentration of synaptic proteins is referred to as the synaptosomal pellet. The pellet was washed briefly in synaptosome lysis buffer to remove traces of non-synaptosome proteins. Equal volumes of total, non-synaptosome and synaptosome fractions were mixed with 2x sample buffer and proteins of interest detected by immunoblotting

Microtubule binding assay

Cell and slice lysates scraped into pre-warmed microtubule-stabilising buffer were centrifuged at 5,000 $g_{(av)}$ for 10 minutes at RT to remove cell nuclei and debris. An aliquot of supernatant (1/12th of the starting volume) was taken as the total fraction and the remaining supernatant was centrifuged at 100,000 $g_{(av)}$ for 1 hour at RT. The supernatant was kept as the unbound protein fraction. The pellet of microtubule-bound proteins was washed twice by the addition of microtubule-stabilising buffer and further centrifugation at 100,000 $g_{(av)}$ for 10 minutes at RT, and was then resuspended in a microtubule-stabilising buffer. All fractions were mixed with an equal volume of 2x sample buffer and immunoblotted with an antibody for total tau.

Sarkosyl extraction of insoluble tau

Sarkosyl insoluble tau was extracted from mouse brain using a method adapted from (Greenberg and Davies, 1990) as described in (Kelleher et al., 2007). Mouse brain homogenates in sarkosyl homogenisation buffer were centrifuged at 14,000 $g_{(av)}$ for 20 minutes at 4 °C to remove cell nuclei and debris. An aliquot of the resulting low speed supernatant was kept as the total fraction and this was mixed with 2x sample buffer for immunoblotting. The remaining supernatant was incubated with 1% sarkosyl for 30 minutes at RT and then centrifuged at 100,000 $g_{(av)}$ for 1 hour at RT. The high speed supernatant resulting from this centrifugation contains sarkosyl soluble tau and was mixed with an equal volume of 2x sample buffer for immunoblotting. The pellet contains sarkosyl insoluble (aggregated tau) and was washed by the addition of 1 % sarkosyl in

sarkosyl homogenisation buffer and centrifuged at 100,000 $g_{(av)}$ for 10 minutes. The pellet was then resuspended in 2x sample buffer.

Membrane fractionation

An aliquot of supernatant from slice lysates homogenised in hypotonic buffer and centrifuged at 800 $g_{(av)}$ for 10 minutes at 4 ^{o}C to remove unbroken cells and cell debris was kept as the total protein fraction prior to further subcellular fractionation. The remaining supernatant was centrifuged at 100,000 $g_{(av)}$ for 1 hour at 4 ^{o}C and the supernatant was kept as the cytosolic fraction and the pellet containing the membrane fraction was resuspended in 2x sample buffer. Total and cytosolic fractions were mixed with equal volumes of 2x sample buffer before immunoblotting.

SDS-polyacrylamide gel electrophoresis (SDS-PAGE)

Prior to electrophoresis, cell, slice and mouse brain lysates prepared for immunoblotting or through differential fractionation were mixed with an equal volume of 2x sample buffer. Samples were heated at 95 ^{o}C for 5 minutes before centrifugation at 10,000 $g_{(av)}$ for 20 seconds. Molecular weight protein standards and proteins were loaded onto the first lane of 7.5%, 10%, or 12.5% (w/v) polyacrylamide gels, prepared as detailed in section 2.1.3 and cast in Invitrogen Ltd., UK, 1.0mm plastic cassettes. If samples were run across more than one gel, one reference sample was loaded onto each gel to allow standardisation of the data when taking into account inter-gel variability. Gels were inserted into the Invitrogen XCell SureLock™ Mini-Cell electrophoresis system and were

electrophoresed at 150 V in running buffer with a Bio-Rad PowerPac™ 300, until the dye front reached the bottom of the gel.

Immunoblotting

Gels were placed onto Protran® 0.45 µm pore size nitrocellulose membranes (Whatman Ltd., UK), sandwiched between Grade 1A filter papers (Whatman Ltd., UK) and sponges in an XCell II Blot Module (Invitrogen Ltd., UK), immersed in transfer buffer. Proteins were transferred onto membranes at 40 V for 120 minutes and kept at approximately 4 ^{o}C using ice. Non-specific binding of primary antibodies was blocked by incubating membranes in appropriate blocking solution for 1 hour at ambient temperature. Membranes were then incubated overnight at 4 ^{o}C with appropriate primary antibodies in blocking solution.

After incubation with primary antibodies, membranes were washed three times in TBS for 5 minutes with rocking prior to the addition of species-specific fluorophore- or HRP-conjugated secondary antibodies diluted in blocking solution for 1 hour at ambient temperature. Proteins were detected by scanning at 700 nm and 800 nm using the Odyssey® infra-red detection system (LI-COR Biosciences, UK), which allows simultaneous detection of two target antigens, and thus two proteins of interest. If necessary, scanning intensity was adjusted according to signal strength following the initial scan at the default intensity (5.0). Densitometric analysis was performed for semi-quantitative analysis of each detected immunogen. Bands were manually selected and

background readings for each lane were subtracted automatically using proprietary Odyssey® software.

Alternatively, immunogens were detected using enhanced chemiluminescence (ECL) detection reagents (Pierce™, USA). The HRP-conjugate causes catalysis of luminol in alkaline conditions. This results in the excitation of luminol which decays in a chemiluminescent reaction. The two ECL detection reagents were mixed together 1:1 and applied to the membrane for 3 minutes before transfer of the membrane to an autoradiography cassette containing Amersham ECL film (GE Healthcare Ltd., UK) and automatic development of the film in a Konica Minolta SRX-101A film processor (Konica Minolta UK Ltd., UK). Films were scanned using an Epson V700 scanner and densitometric analysis was performed by manually selecting bands for each lane for semi-quantitative analysis of each detected immunogen using ImageJ and manually subtracting an average background reading.

Enzyme-linked immunosorbent assay for detection of human Amyloid-Beta 40 and 42

Slice lysates and mouse brain homogenates of crude cortical sections were prepared as described earlier. The human Aβ-40 and Aβ-42 ELISAs were run in parallel according to the manufacturer's protocol (Invitrogen Ltd, UK) albeit with samples and standards prepared in extra strong lysis buffer and TBS rather than the provided standard diluent buffer. Samples were diluted to a concentration of 5 mg tissue/mL buffer. The human Aβ-40 and Aβ-42 standards were reconstituted in 55 mM sodium bicarbonate, pH 9.0. The reconstituted standards were then diluted to provide standards for the assay

containing 0, 15.63, 31.25, 62.5, 125, 250, 500 and 1000 pg/mL of human Aβ-40 and Aβ-42. 50 µL of standards and samples were loaded in duplicate onto the provided ELISA plates pre-coated with a primary antibody either to the N-terminus of Aβ-40 or Aβ-42. 50 µL of rabbit primary antibody to the C terminus of Aβ-40 or Aβ-42 was added and incubated for 3 hours at ambient temperature. Wells were washed 4 times with the provided wash solution to remove unbound primary antibody. 100 µL of an HRP-linked secondary anti-rabbit IgG antibody was added to each well for 30 minutes at ambient temperature to detect the bound rabbit antibody. Wells were washed again 4 times, to remove any unbound secondary antibody before the addition of the stabilised chromogen substrate solution for 30 minutes which reacted with the HRP-tagged bound secondary antibody to produce a blue colour. The reaction was then stopped using the provided stop solution, which resulted in a yellow sample colour and absorbance was detected at 450 nm with a Wallac 1420 Victor3™ plate reader (PerkinElmer, USA). The absorbance values of Aβ-40 or Aβ-42 of known concentration were used to generate a standard curve from which the Aβ concentration of samples could be calculated in pg/ml. Average absorbance values for blank wells containing diluted extra strong lysis buffer were subtracted from the absorbance values obtained for treated samples.

Enzyme-linked immunosorbent assay for detection of extracellular tau

A sandwich ELISA for detection of low concentrations of extracellular total tau amounts was developed in-house (unpublished).

The coating antibody (BT2, Thermo Scientific Ltd., UK) raised against the tau epitope 194-198 was diluted at a concentration of 2 µg/mL in ELISA coating buffer. 100 µL of the diluted coating antibody solution was added to the required number of wells of 96-well Nunc Maxi-Sorp plate (Thermo Scientific Ltd., UK), the plate sealed and the antibody allowed to adsorb to the plastic for 8 days at 4^{o}C on a shaker. The plates were washed three times with ELISA washing buffer to remove any unadsorbed coating antibody and 200 µL of the starting block solution was added per well for 4 hours at ambient temperature with the plate sealed on a shaker to block non-specific binding. After 4 hours, the starting block solution was removed and the plate was washed 3 times with washing buffer, as before. Samples of HBSS from treated slice cultures were centrifuged for 5 minutes at 7,200 *g* at 4 ^{o}C to remove any cell debris. 50µL of undiluted HBSS from treated slice cultures was added in triplicate to the plate, and the samples incubated overnight at 37 ^{o}C, sealed, without rocking.

The HBSS was removed and the plate washed 3 times with washing buffer. The capture antibody, which also detects total tau (DAKO tau) raised against residues 243 to 441 towards the C-terminus of tau, was diluted in primary antibody blocking solution. 50 µL of the diluted antibody was added per well and the sealed plate was incubated, overnight, at ambient temperature on a shaker. The antibody was removed and the plate was washed 3 times with washing buffer, to remove any excess capture antibody. The HRP-tagged anti-rabbit IgG secondary antibody was diluted in secondary antibody blocking solution and 50 µL was added to each well of the plate and incubated, sealed, for 1 hour at ambient temperature on a shaker. Unbound antibody was removed by

washing 5 times with washing buffer. 100 µL per well of stabilised chromogen substrate solution (TMB) was added to each well of the plate and allowed to react with the bound HRP-tagged secondary antibody. When left at ambient temperature this develops a characteristic blue colour. The reaction was stopped by the addition of 100 µL per well of stop solution and absorbance was detected at 450 nm with a Wallac 1420 Victor3™ plate reader (PerkinElmer, USA). Average absorbance values for blank wells containing HBSS were subtracted from the absorbance values obtained for HBSS from treated samples.

2.2.5 Cell Death Assays

LIVE/DEAD® cell assay

The viability of primary neurons was assessed using a LIVE/DEAD® far red fixable dead cell assay stain kit (Invitrogen Ltd., UK) according to the manufacturer's protocol. The amine-reactive stain in the kit reacts with free amines in the cell interior and cell surface in cells with compromised membranes yielding a signal detectable at 700 nm. In brief, one vial of stain was dissolved in 50 µL DMSO prior to use. The medium was removed from the neurons and cells were washed in pre-warmed PBS (37 ^{o}C). The stock solution of far red stain was diluted 500-fold in PBS before incubation with the cells for 30 minutes at 37 ^{o}C in a humidified atmosphere of 95 % air/5 % CO_2. The stain was removed and cells were washed with pre-warmed PBS. The fluorescent signal produced from the far red stain incorporated into cells with compromised membranes was detected at 700 nm using the Odyssey® infra-red detection system. The difference in fluorescent intensity in treated cells was then calculated as a proportion of fluorescence

in control wells using Odyssey® software. Coverslips were then fixed in 4 % (w/v) PFA in PBS for 5 minutes at 37 ^{o}C, and washed 3 times in PBS prior to immunocytochemistry.

Lactate dehydrogenase assays

Cell death was measured from slice cultures by measuring LDH release into the slice culture medium. LDH was measured according to the manufacturer's protocol (Promega, UK). In brief, one vial of substrate mix was reconstituted in 12 mL of assay buffer. 50 µL of slice culture medium or HBSS from treated slices, or slice lysates in extra strong lysis buffer or hypotonic buffer, diluted in untreated slice culture medium or HBSS, were loaded in triplicate on a 96 well plate. 50 µL of reconstituted substrate mix was added to each well and incubated for 30 minutes at ambient temperature, protected from light. The reaction was stopped with stop solution and absorbance at 490 nm, a direct measure of LDH, was measured immediately using a Wallac 1420 Victor3™ plate reader (PerkinElmer, USA). The percentage of LDH in the medium was calculated as a proportion of the total amount of LDH (LDH in the lysates plus LDH in the medium).

2.2.6 3xTg-AD Genotyping

DNA extraction

Genomic DNA was extracted from mice ear clips digested in 125 µL extraction and tissue preparation solution mixture provided with the REDExtract-N-Amp™ Tissue PCR Kit for 30 minutes at ambient temperature. Samples were then heated to 95 ^{o}C for 3 minutes and then 125 µL provided neutralisation B solution was added for 10 minutes. Samples were stored at 4 ^{o}C until PCR.

Polymerase chain reaction

PCR was used to amplify genomic DNA. PCR amplification was carried out in reaction volumes of 20 µL of PCR mixture containing 4µl of template DNA, final concentrations of 10µM of each of the forward and reverse primers, 10 µL of the REDExtract-N-Amp™ PCR Reaction Mix containing buffer, salts, dNTPs, Taq polymerase, REDTaq dye, and JumpStart Taq antibody and 4 µL of nuclease-free H_2O (Thermo Scientific Ltd., UK). PCR was performed using a G-Storm GS1 thermal cycler (G-Storm, UK). Reaction conditions were as follows:

- *PS1*: initially denatured at 94 °C for 2.5 minutes and then subjected to 35 cycles of 94 °C for 40 seconds (denaturation), 62 °C for 40 seconds (annealing) and 72 °C for 1 minute (extension), with a final extension step of 3 minutes at 72 °C.

- *APP*: initially denatured at 94 °C for 5 minutes and then subjected to 20 cycles of 94 °C for 30 seconds (denaturation), 53 °C for 30 seconds (annealing) and 72 °C for 1 minute (extension), with a final extension step of 3 minutes at 72 °C.

- *MAPT*: initially denatured at 94 °C for 5 minutes and then subjected to 25 cycles of 94 °C for 30 seconds (denaturation), 52 °C for 30 seconds (annealing) and 72 °C for 1 minute (extension), with a final extension step of 3 minutes at 72 °C.

Digestion of PS1 Products

PS1 PCR products were digested in a BstEII restriction mixture as detailed in section 2.1.6. This was performed as the primers used amplify the endogenous PS1 gene. The products were incubated in the reaction mixture at 37 ^{o}C for approximately 90 minutes before electrophoresis.

Electrophoresis of PCR products

PCR fragments and restriction digests were resolved on 1.5 % agarose gels microwaved for ~ 90 seconds until the agarose was fully melted. The gel mixture was allowed to cool down and 0.7 mg/ml of ethidium bromide was added to the gel mixture to enable visualisation of DNA bands. The gel mixture was poured into the gel tray, combs added and left to set for ~30 minutes before being placed in the electrophoresis tank filled with TAE running buffer. Gels were run for 45 minutes at 120 V before DNA was visualised under UV illumination and images captured.

Expected product sizes

A 100 bp ladder molecular marker was electrophoresed next to the amplified/digested samples. *APP* was detected at 450 bp, *MAPT* at 400 bp, *PS1* at 300 bp and 250 bp, and endogenous *PS1* at 550 bp.

2.2.7 Immunocytochemistry

Immunocytochemical staining

Cells were washed once with PBS pre-warmed to 37 ^{o}C followed by fixation in 4 % (w/v) PFA in PBS for 5 minutes at 37 ^{o}C. Following fixation, cells were washed three times in ice-cold PBS and then permeabilised in permeabilisation solution for 3 minutes. Non-specific binding was blocked for 1 hour with ICC blocking solution prior to incubation with the relevant primary antibody diluted in ICC blocking solution for 2 hours at ambient temperature. Coverslips were washed three times with PBS and then incubated with the appropriate secondary antibodies diluted in ICC blocking solution for 1 hour, followed by a further three PBS washes. Nuclei were stained with Hoechst 33258 (2 µg/mL bis-Benzimide H33258 pentahydrate in PBS), before mounting coverslips on to slides using fluorescent mounting medium (Dako Ltd., UK).

Imaging of immunocytochemical staining

All images were captured on a CTR5000 camera (Leica Microsystems, Germany) using AIF lite software (Leica Microsystems, Germany) from a Leica DM5000B fluorescence microscope (Leica Microsystems, Germany) using the appropriate filter sets and 10X, 20X and 40X objective lenses and were stored as JPEG files. All parameters including lamp intensity, video camera setup and calibration were constant through image capturing.

2.2.8 Slice immunohistochemistry

Tissue preparation

Slice culture medium was aspirated from slice cultures of 350 µm thickness; slices were then washed once in ice-cold PBS and were fixed with 4 % PFA for 1 hour at ambient temperature whilst still attached to the membrane inserts. PFA was removed by washing twice in PBS and then for long term storage before staining, slices were kept in PBS containing 0.01 % sodium azide. Individual slices were cut out, whilst still attached to the membrane, from the insert prior to staining.

Immunohistochemical staining

Slices cultured for 1 month old were immunohistochemically stained for phosphorylated tau and total tau, as well as neuron- and astrocyte- specific markers. Slices were stained using a protocol adapted from (Gogolla et al., 2006). In brief, slices were permeabilised with permeabilisation solution for approximately 18 hours at 4 ^{o}C. Slices were then blocked in a 20 % BSA blocking solution overnight at 4 ^{o}C prior to incubation with primary antibodies overnight on a shaker at 4 ^{o}C. Slices were washed 3 times in 5 % BSA to remove traces of unbound primary antibodies prior to incubation with the appropriate fluorescently-tagged secondary antibodies for 4 hours at ambient temperature. Slices were then washed a further 3 times in PBS before counterstaining cell nuclei with Hoechst 33258 (2 µg/mL bis-Benzimide H33258 pentahydrate in PBS), and mounting under glass coverslips in fluorescent mounting medium (Dako Ltd., UK).

Spinning disk confocal microscopy

Slices were examined using an Eclipse Ti-E Inverted (Nikon Instruments, UK) microscope and images were collected via a CSU-X1 Spinning Disk Confocal and Andor Ixon3 EM-CCD camera imaging system setup using a 60 Plan Apo VC N2 objective lens (Nikon Instruments, UK) and were stored as TIFF files. All parameters including laser settings, video camera setup and calibration were constant through image capturing. 488/562 nm lasers were used for excitation and emitted fluorescence detected at 520/562 nm. 12 image 'Z' stacks using a 1x confocal zoom, a closed pinhole and a 560 MHz frame rate were acquired. The stack covered a total Z depth of 12 µm and images were recorded at 1024 x 1024 pixels. A maximum intensity projection was produced from collapsing the Z stacks in NIS-Elements AR software (Nikon Instruments, UK).

2.2.9 Mouse Brain Immunohistochemistry

Immunohistochemical staining

A one in six series of sections from young and aged 3xTg-AD mice was immunohistochemically stained for phosphorylated tau, abnormal conformations of tau and total tau. The 30 µm sections were washed twice in TBS before quenching of endogenous peroxidase activity with methanol containing 0.5 % H_2O_2. Sections were washed twice in TBS prior to incubation in TBS containing 2 % normal goat serum for 30 minutes to block non-specific antibody binding. Sections were then incubated with primary antibody overnight with shaking at 4 ^{o}C. Unbound primary antibody was removed by washing 3 times for 15 minutes with TBS. Sections were then incubated with appropriate secondary antibody in TBS containing 1 % normal goat serum for 1

hour. Unbound secondary antibody was removed by 3 washes in TBS for 15 minutes. Sections were then incubated for 60 minutes in the avidin-biotin peroxidase complex (Vectastain Elite ABC Kit, Vector Laboratories Ltd., UK). Sections were washed 3 times in TBS for 15 minutes and then incubated in DAB reagent made up according to the manufacturer's instructions (Vector Laboratories Ltd., UK). DAB was applied for 2-10 minutes until a strong purple colour developed. To stop the reaction, sections were washed in TBS twice for 5 minutes and then mounted onto gelatin-chrome alum coated Superfrost microscope slides, air dried overnight, cleared in 98/99 % (v/v) industrial methylated spirit and xylene and then coverslipped with DPX mountant.

Imaging of immunohistochemical staining

All images were captured via a live video camera (JVC, 3CCD, KY-FFB), mounted onto a Zeiss Axioplan (Carl Zeiss, Inc.) microscope using 10, 20 and 40X objective lenses and were stored as JPEG files. All parameters including lamp intensity, video camera setup and calibration were constant through image capturing.

2.3 Statistical Analysis

All data were statistically analysed using Graphpad Prism 6.0 software (La Jolla, USA). Data from immunoblots, ELISAs, cell death and LDH assays were analysed for homogeneous variances in each sample group using a Brown-Forsythe test.

Data were then analysed using Student's unpaired t-test when comparing two unrelated groups, by ordinary one-way analysis of variance (ANOVA) with Dunnett's post-hoc

analysis when comparing three or more groups defined by one factor or by using a two-way ANOVA with Sidak's post-hoc analysis when comparing three or more groups defined by two factors. Differences were considered statistically significant when $p<0.05$.

Chapter 3 : Organotypic brain slice cultures from AD mice faithfully recapitulate some hallmark features of AD

3.1 Introduction

The main neuropathological features of AD are extracellular deposits of Aβ in senile plaques (Braak and Braak, 1991), which result from aberrant processing of APP to generate aggregation-prone Aβ (O'Brien and Wong, 2011), as well as the presence of NFTs mainly composed of hyperphosphorylated tau aggregates (Braak and Braak, 1995). Alongside this, there is a notable increase in kinase activation, calcium dyshomeostasis, microglial and astrocytic activation and neuroinflammation, synaptic loss and dysfunction - all of which converge to culminate in mass neuronal loss, associated cognitive decline and the progression of other dementia-related symptoms (Selkoe, 2002, Hardy, 2009).

The 3xTg-AD model of AD harbours mutations in human *APP*, *PS1* and *MAPT* and progressively develops several prominent features of human AD, including Aβ plaques, phosphorylated tau, NFTs, increased neuroinflammation, microglial activation, increased kinase activity, noradrenergic and cholinergic dysfunction, synaptic loss and dysfunction, and associated cognitive and memory decline (Oddo et al., 2003a, Oddo et al., 2003b, Mastrangelo and Bowers, 2008, Sy et al., 2011, Girão da Cruz et al., 2012, Manaye et al., 2013). These mice also show other behavioural symptoms of human AD including anxiety, circadian dysfunction and sleep disruption (Sterniczuk et al., 2010b, Sterniczuk

et al., 2010a). The concomitant and progressive development of multiple features of human AD makes this model of considerable interest for studying the mechanisms underlying AD and for pre-clinical development of novel therapeutics.

A principle aim of this thesis was to establish a novel organotypic brain slice culture model of AD, using 3xTg-AD mice, which could be used as a sensitive and human disease-relevant alternative to *in vivo* AD research. Organotypic brain slice cultures are considered an excellent alternative to *in vivo* research (Gähwiler et al., 1997, Humpel, 2015a) since they are readily tractable, and can be used as medium to high throughput platforms for rapid pre-clinical screening of compounds in a much more biologically relevant system than would be achieved using dissociated primary neural cell cultures or cell lines. It is also possible to study more than one time point or parameter in brain slices produced from the same mouse pup, reducing experimental variation. Organotypic brain slice cultures are also easily applied to other techniques which can be more technically difficult to execute *in vivo* such as transfection, live imaging, and electrophysiology (Sundstrom et al., 2005).

Perhaps more importantly, gene regulation and protein expression in long-term slice cultures matches that observed in *in vivo* adult brain (Gähwiler et al., 1997, Humpel, 2015a), demonstrating the biological relevance of slice culture models. Additionally, of particular interest to this project, long-term organotypic brain slice cultures produced from transgenic mice expressing human mutant (P301L) tau and APP (Swedish K670N/M671L, Dutch E693Q, and Iowa D694N mutations) progressively develop

phosphorylated tau and insoluble tau aggregates, and Aβ-containing plaques, respectively (Duff et al., 2002, Humpel, 2015b), thereby suggesting that *in vivo* AD-relevant neurodegenerative mechanisms are retained *ex vivo*. However, to date, no brain slice culture models of AD have been developed which display both AD-relevant changes in tau and the development of Aβ, as would be expected in slice cultures prepared from 3xTg-AD mice. This is a particularly important goal since interactions between Aβ and tau are believed to underlie many neurodegenerative processes in AD (Ittner et al., 2010, Crimins et al., 2013, Pooler et al., 2015, Nisbet et al., 2015).

3.2 Aims and objectives

The primary objective of the studies presented in this chapter was to fully characterise the progressive development of AD-relevant features in organotypic brain slice cultures prepared from 3xTg-AD mice in comparison to WT slice cultures and aged 3xTg-AD mice. The specific aims of this chapter were to:

- Use biochemical and histological techniques to examine the progressive development of AD-relevant features in the brain of 3xTg-AD mice with respect to WT controls.

- Optimise methods that allow long-term culture of brain slices from 3xTg-AD and WT mice.

- Characterise the progressive development of AD-relevant biochemical and histological changes in cultured 3xTg-AD brain slices with respect to WT slice cultures.

- Compare the development of AD-relevant phenotypes *in vivo* to those observed in long-term slice cultures from 3xTg-AD mice.

The results of this work will provide key information regarding the suitability of 3xTg-AD slices as a model which faithfully recapitulates hallmark features of human AD that can be used for further study into the identification of candidate AD drugs (Chapter 4) and the mechanisms underlying AD development (Chapter 5).

3.3 Methods

The methods used for this work are described in detail in Chapter 2. In brief, brains were collected from WT and 3xTg-AD mice at 1, 2, 4, 9 and 12 months of age. One hemi-brain was processed for immunohistochemistry. Cortical-, hippocampal- and amygdala-containing brain regions were dissected from the other hemi-brain for assessment of biochemical and histological changes relevant to AD. The cortex was used to prepare a total homogenate for analysis of disease-related biochemical protein changes, the amygdala was used to isolate sarkosyl insoluble tau, and the hippocampus to prepare synaptosomes. Organotypic brain slice cultures were prepared from postnatal day 8/9 WT and 3xTg-AD mice and cultured for up to 28 days. Slice cultures were harvested at 14, 21, and 28 days *in vitro* for assessment.

3.4 Results

3.4.1 3xTg-AD mice express human mutant APP, PS1 and tau

Human mutant *APP, PS1* and *MAPT* are expressed in 3xTg-AD mice (Oddo et al., 2003a). To confirm the presence of the mutant transgenes in our colony, DNA was extracted, amplified by PCR and visualised on agarose gels. As expected, mutant human *PS1, APP* and tau were detected in 3xTg-AD mice, but not WT controls (Figure 3.1).

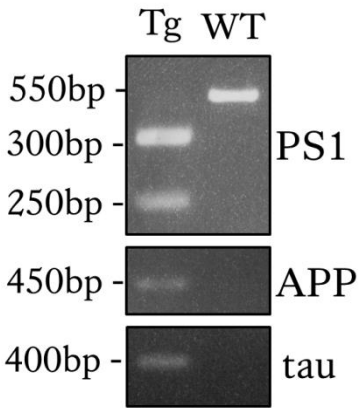

Figure 3.1: 3xTg-AD mice express human mutant PS1, APP and tau
DNA from WT and 3xTg-AD was extracted, amplified by PCR and the transcripts detected on agarose gels. Human PS1 (at 300 bp and at 250 bp), APP (450 bp) and tau (400 bp) were detected in 3xTg-AD, but not WT. Endogenous mouse PS1 (550 bp) was detected in WTs.

3.4.2 Tau protein is overexpressed in 3xTg-AD cortex

Recent unpublished communications from other laboratories have reported an absence of protein overexpression of APP, tau and human tau in the 3xTg-AD mice despite the detection and presence of mutant transgenes in their colonies. It was therefore important to examine our colony for these features. Levels of total tau (phosphorylated and non-phosphorylated) were detected in cortical homogenates from 1, 2, 4, 9, and 12 month old WT and 3xTg-AD mice by immunoblotting with a DAKO pan-tau antibody

which detects both mouse and human tau. Bands of approximately 50-64 kDa were detected, corresponding to the expected molecular weight of tau. The higher molecular weight bands (approximately 64 kDa) were more prominent in 3xTg-AD cortical homogenates than in WT controls. At all ages examined, the amount of tau detected in 3xTg-AD mice was increased by approximately two-fold when compared to age-matched WT mice; however, these differences in total tau amounts between genotypes were not statistically significant at any of the ages examined (Figure 3.2). In addition, an increase in amounts of total tau over time for 3xTg-AD mice can be observed, and when comparing to 1 month old mice, total tau levels are significantly higher in 4 month old mice (Figure 3.2, $p<0.05$). It is apparent that total tau amounts are increasing with age from this graph and the blots, and these increases are likely due to an accumulation of both endogenous tau and human tau.

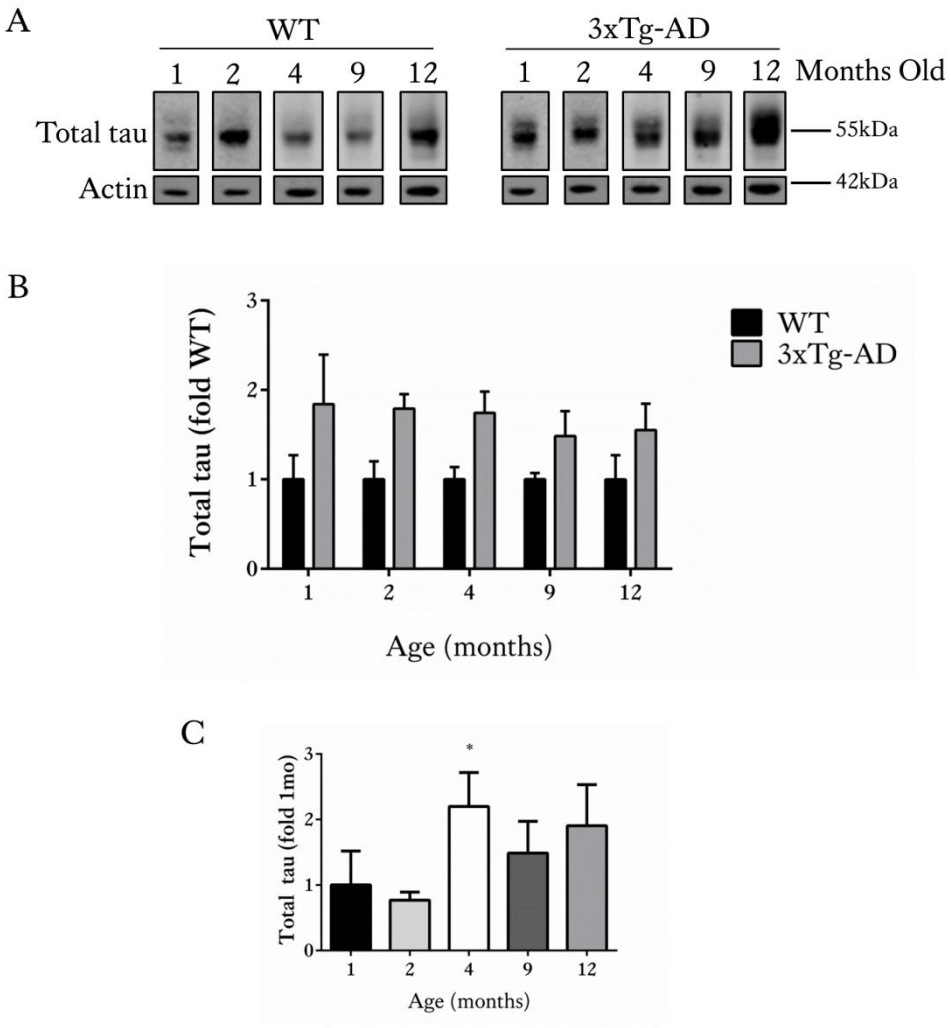

Figure 3.2: Total tau amounts are increased in 3xTg-AD cortex.
(A) Representative western blots of total (phosphorylated and non-phosphorylated) tau (50-64 kDa) in cortical homogenates of WT and 3xTg-AD mouse brain taken at 1, 2, 4, 9 and 12 months of age. An antibody against β-actin was used as a loading control (42 kDa). Bar charts show amounts of total tau following normalisation to β-actin amounts in each sample. (B) Data are shown as fold change from WT at each time point. (C) Data are shown as fold change from 1 month old for 3xTg-AD mice only. Data is mean ± SEM, (n=3 mice per group, $p<0.05$).

Amounts of human tau were next detected by immunoblotting with an antibody specific to human tau (CP27), which does not cross-react with endogenous mouse tau (Duff et al., 2000). Immunoblots identified the presence of human tau protein only in cortical homogenates from 3xTg-AD mice (Figure 3.3A). Moreover, the amounts of human tau in

3xTg-AD mice appeared to increase in an age-dependent manner, although these increases were found not to be statistically significant (Figure 3.3B).

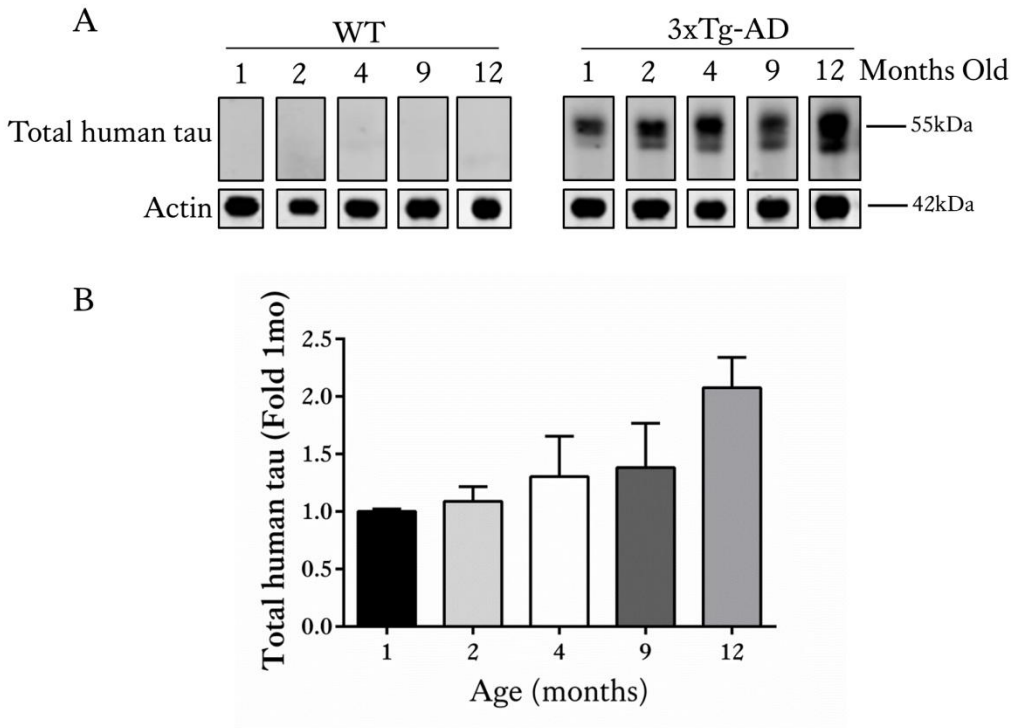

Figure 3.3: 3xTg-AD mice express human tau protein.
(A) Representative western blots of total human tau (CP27) (50-64 kDa) in cortical homogenates of WT and 3xTg-AD mouse brain taken at 1, 2, 4, 9 and 12 months of age. An antibody against β-actin was used as a loading control (42 kDa). (B) Bar chart shows amounts of human tau following normalisation to β-actin amounts in each sample. Data are shown as fold change from 1 month of age. Data is mean ± SEM, (n=3 mice per group).

3.4.3 APP amounts are increased in the cortex of 3xTg-AD mice

APP protein amounts were assessed in 3xTg-AD cortex by immunoblotting with an antibody specific to the N-terminus of APP. APP of 90-120 kDa was detected, corresponding to the expected sizes of immature and mature mammalian APP. Total APP holoprotein amounts in the cortex of 3xTg-AD mice were unchanged from WT at 1,

2, 4 and 9 months of age, but were significantly increased at 12 months of age (Figure 3.4, $p<0.01$).

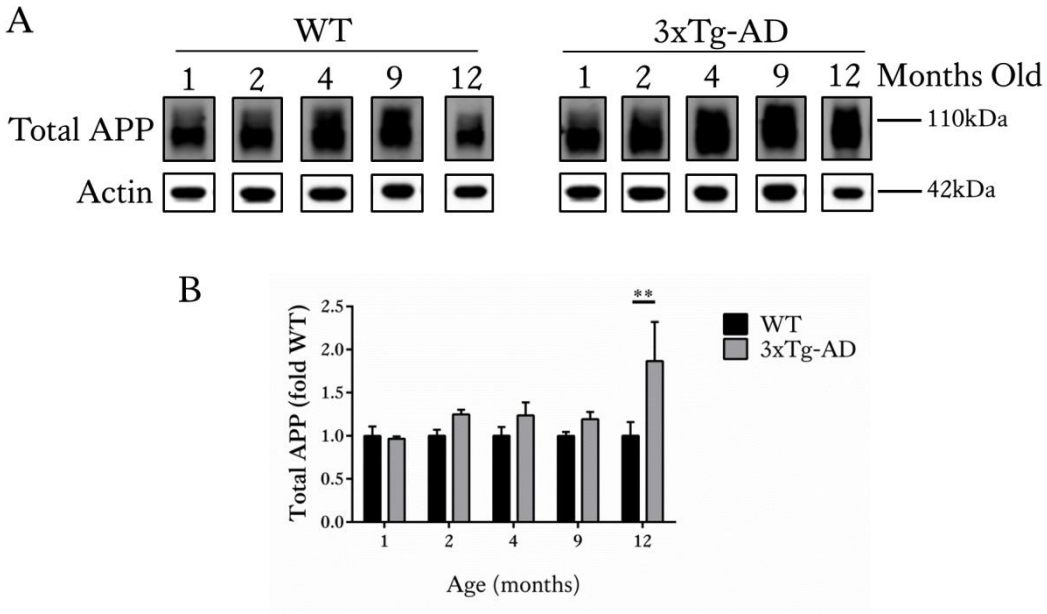

Figure 3.4: Total amounts of APP are increased in the cortex of 12 month old 3xTg-AD mice
(A) Representative western blots of APP (90-120 kDa) in cortical homogenates of WT and 3xTg-AD mouse brain taken at 1, 2, 4, 9 and 12 months of age. An antibody against β-actin was used as a loading control (42 kDa). (B) Bar chart shows amounts of APP following normalisation to β-actin amounts in each sample. Data are shown as fold change from WT at each time point. Data is mean ± SEM, (n=3 mice per group, **p<0.01).

3.4.4 Aβ-42 amounts increase with age in 3xTg-AD cortex

Progressive increases in levels of Aβ-40 and Aβ-42, as well as in the ratio of Aβ-42 to Aβ-40 are widely reported in 3xTg-AD mice and human AD brain (Oddo et al., 2003a, O'Brien and Wong, 2011). Cortex homogenates from 4 and 12 month old WT and 3xTg-AD mice from our colony were therefore assessed for levels of human Aβ-40 and Aβ-42 by ELISA (Section 2.2.4). 12 month old 3xTg-AD mice exhibited significantly higher levels of Aβ-42 compared to 12 month old WT mice (Figure 3.5, $p<0.05$), and also showed a

non-significant increase in this measure when compared to 4 month old 3xTg-AD mice. The amounts of Aβ-42 detected in the cortex did not differ between 4 month old WT and 3xTg-AD mice. Levels of Aβ-40 showed a trend towards increase in the 3xTg-AD cortex at both 4 and 12 months relative to WTs, but these differences did not reach significance. The ratio of Aβ-42 to Aβ-40 is thought to be important in AD pathogenesis since many APP and PS1/PS2 mutations do not increase Aβ amounts, but alter this ration (Fernandez et al., 2014), therefore the Aβ-42 to Aβ-40 ratio was also determined. However, although there was a trend towards a switch in the Aβ-42 to Aβ-40 ratio in 12 month old 3xTg-AD mice relative to age-matched WTs and 4 month old 3xTg-AD mice, these differences were not significant (Figure 3.5).

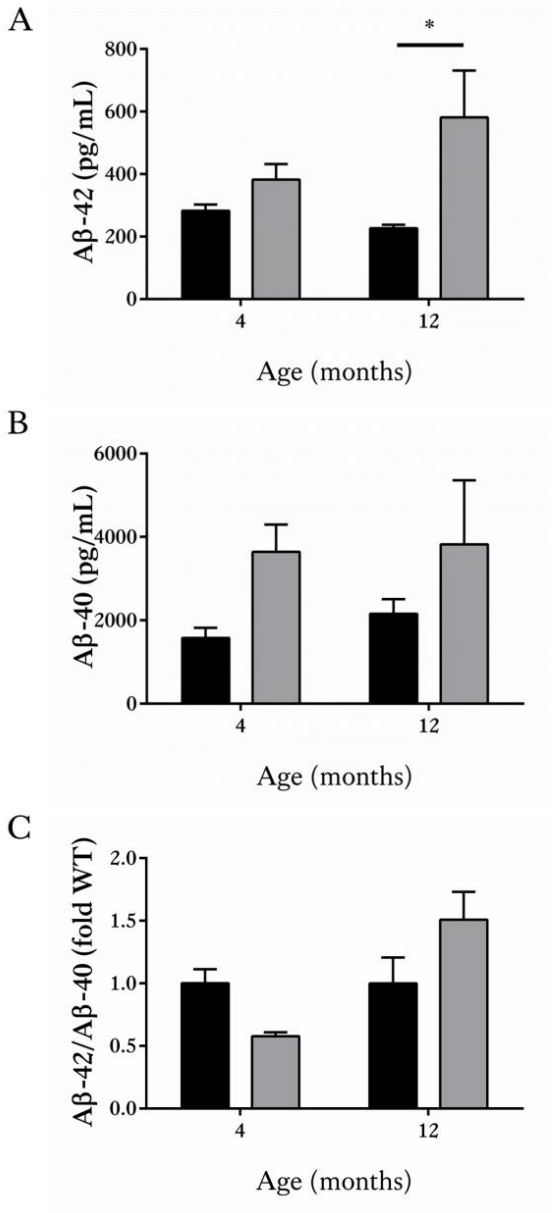

Figure 3.5: Levels of Aβ-42 are significantly increased in the cortex of 12 month old 3xTg-AD mice.

Amounts of Aβ-40 and Aβ-42 were measured in cortical homogenates from 4 and 12 month old WT and 3xTg-AD mice containing equivalent amounts of total protein by Aβ-40 and Aβ-42 ELISAs. Bar charts show (A) amounts of Aβ-42 and (B) Aβ-40 in pg/mL, and (C) Aβ-42 to Aβ-40 ratio in the cortex of both WT and 3xTg-AD mice at 4 and 12 months of age. Data are shown as fold change from WT at each time point. Data is mean ± SEM (n=3 mice per group, *$p<0.05$).

3.4.5 No changes in tau phosphorylation or conformation are observed in 3xTg-AD cortex

Progressive increases in tau phosphorylation have previously been reported in 3xTg-AD mice relative to WT controls (Oddo et al., 2003a), which are similar to the altered pattern of tau phosphorylation observed in post-mortem human AD brain (Iqbal et al., 2005, Hanger et al., 2009). Therefore, phosphorylation-specific antibodies to AD-relevant tau epitopes were used in western blotting to examine changes in tau phosphorylation in the cortex of 3xTg-AD and WT mice. The antibodies used were specific to tau phosphorylated at ser 202 (CP13), and ser 396/404 (PHF-1), and tau dephosphorylated at ser 199/202/thr 205 (Tau-1). In all cases, the levels of phosphorylated tau were normalised to levels of total tau in each sample prior to statistical analysis. The results of this work revealed no changes in the phosphorylation of tau at any of the epitopes studied with aging of 3xTg-AD mice or in comparison to age-matched controls, although a non-significant increase in phosphorylation of tau at ser 202 could be observed in 12 month old 3xTg-AD mice (Figure 3.6). The tau bands detected were typically 50-55 kDa, and an approximately 64 kDa tau band, which appeared to be preferentially labelled with the ser 202 antibody, was observed in 12 month old 3xTg-AD mice. Tau bands of 64 kDa have been previously reported in other tau transgenic lines as hyperphosphorylated tau species (Lewis et al., 2000, Lewis et al., 2001, Noble et al., 2003).

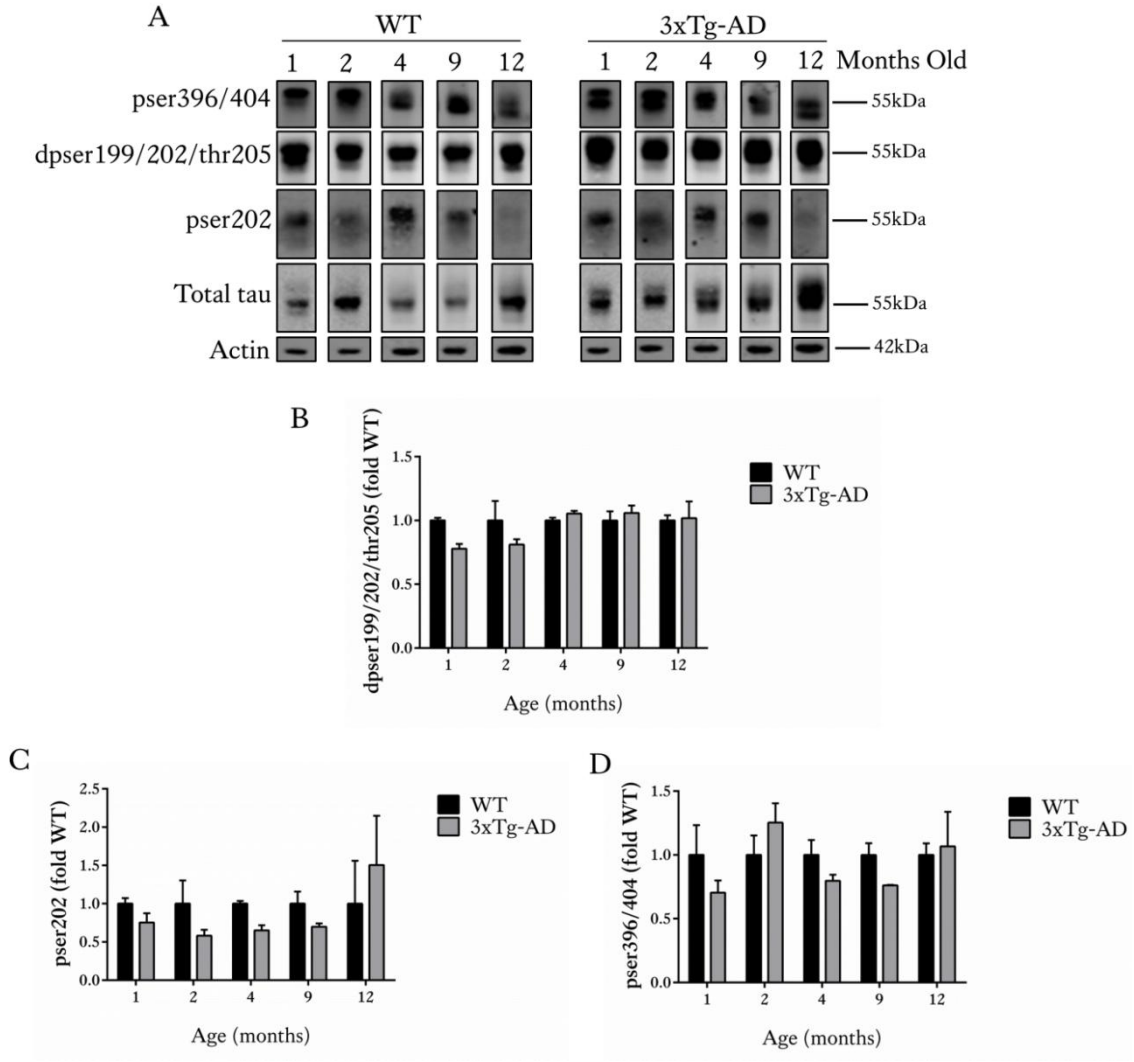

Figure 3.6: Phosphorylation of tau at several AD-relevant sites is unchanged in the cortex of 3xTg-AD mice.

(A) Representative western blots of total tau (phosphorylated and dephosphorylated), tau phosphorylated at ser 202, ser 396/404, and tau dephosphorylated at ser 199/202 and thr 205 (all ~50-64 kDa) in cortical homogenates of WT and 3xTg-AD mouse brain taken at 1, 2, 4, 9 and 12 months of age. An antibody against β-actin was used as a loading control (42 kDa). Bar charts show amounts of (B) tau dephosphorylated at ser 199/202 and thr 205 (C) tau phosphorylated at ser 202 and (D) tau phosphorylated at ser 396/404, all normalised to amounts of total tau in each sample. Data are shown as fold change from WT at each time point. Data is mean ± SEM, (n=3 mice per group).

To further investigate tau phosphorylation, sections of 3xTg-AD cortex from 4 and 12 month old mice were fixed and then immunohistochemically stained for tau phosphorylated at ser 396/404 (PHF-1). In addition, the presence of abnormal

conformations of tau were investigated using a conformation-specific antibody, MC1, which recognises a discontinuous tau epitope (residues 5-15 and 312-322 of 2N4R tau), reported to be one of the earliest pathological changes to tau in AD brain (Jicha et al., 1997) and in tau transgenic mice (Terwel et al., 2005) (Figure 3.7). These analyses showed increased background labelling of 3xTg-AD tissues, but there were no clearly defined neuronal accumulations of phosphorylated or abnormal conformations of tau. Therefore, these data further confirm the absence of any changes in tau phosphorylation, at least at ser 396/404, in aged 3xTg-AD cortex and also suggest that no conformational changes in tau have occurred at this age.

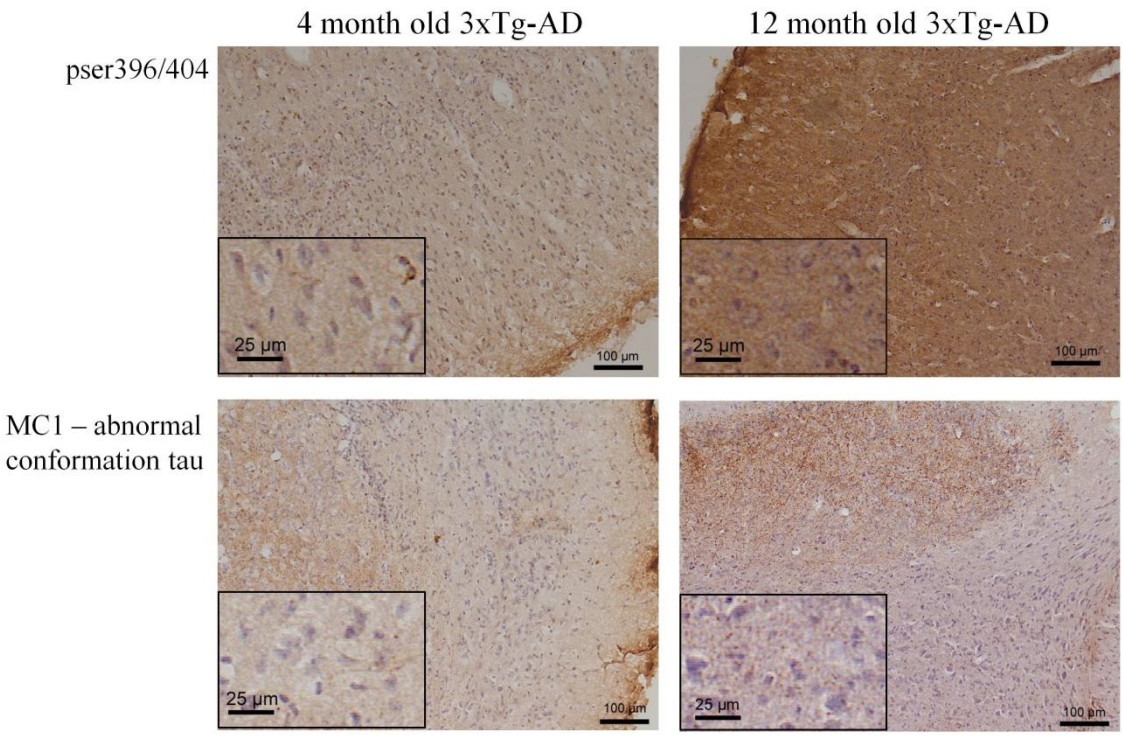

Figure 3.7: Tau phosphorylation and conformation is unaltered in the cortex of 4 and 12 month old 3xTg-AD mice.
30 µm sections of 4 and 12 month old 3xTg-AD cortex were immunostained with antibodies against tau phosphorylated at ser 396/404 (PHF-1) and abnormal conformations of tau (MC1). Sections were counterstained with haematoxylin. Representative images are shown. Scale bar 100 µm, inset scale bar 25 µm.

3.4.6 Tau undergoes changes in phosphorylation and conformation by 12 months of age in 3xTg-AD hippocampus

Tau pathology spreads from the entorhinal cortex to the hippocampus and connected regions before being detectable in association areas of the neocortex in human AD brain (Braak and Braak, 1995). Therefore, changes in tau phosphorylation at ser 396/404 and abnormal (MC1) tau conformation were examined in the hippocampi of 3xTg-AD mice using immunohistochemistry, as described above. The results of this experiment showed the presence of discrete populations of neurons containing tau phosphorylated at ser 396/404 (PHF-1) in the CA3 region of the hippocampus and dentate gyrus, as well as abnormal (MC1) conformations of tau in the CA1 region of the hippocampus by 12 months (Figure 3.8). Prominent cell body staining was apparent with both PHF-1 and MC1 antibodies, whilst MC1 also labelled tau in the axons of CA1 neurons. This staining was absent in the hippocampus of 4 month old 3xTg-AD mice, and both ages of WT mice. These findings demonstrate that localised alterations in tau phosphorylation and conformation, similar to those observed in human AD brain, have occurred in 12 month old 3xTg-AD mice, at least in the hippocampus. Unfortunately, it was not possible to examine hippocampal tissue biochemically since the hippocampus from these mice was processed separately to prepare synaptosomes (section 3.4.8).

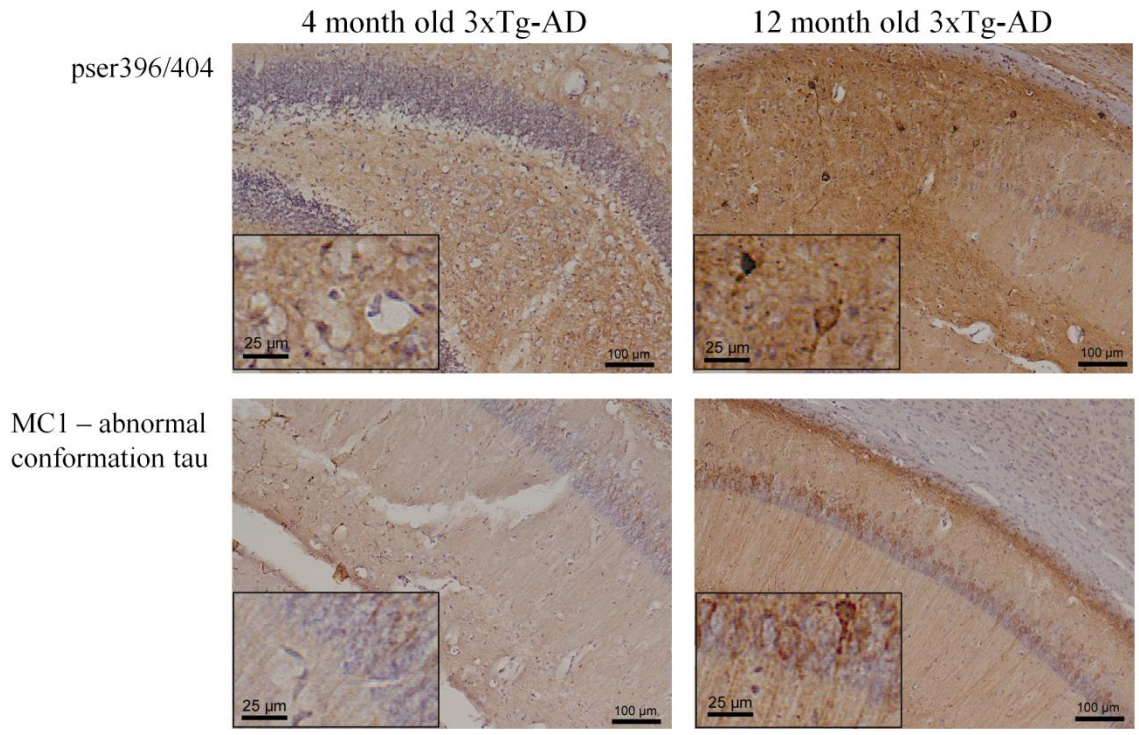

Figure 3.8: **Tau phosphorylation and conformation are altered in the hippocampus of 12 month old 3xTg-AD mice.**
30 µm sections of 4 and 12 month old 3xTg-AD hippocampus were immunostained for tau phosphorylated at ser 396/404 (PHF-1) and abnormal conformations of tau (MC1). Sections were counterstained with haematoxylin. Representative images are shown. Scale bar 100 µm, inset scale bar 25 µm.

3.4.7 Amounts of insoluble tau are increased in the amygdala of 3xTg-AD mice

3xTg-AD mice progressively develop neurofibrillary tangles containing aggregates of tau, a prominent feature of human AD (Oddo et al., 2003a). To determine if 3xTg-AD mice progressively accumulate aggregated, tangle-like tau, sarkosyl-insoluble tau was isolated from the amygdala of 4 and 12 month old WT and 3xTg-AD mice. Sarkosyl-insoluble tau is synonymous with the tau filaments that accumulate in NFTs (Noble et al., 2003). The method used generates three fractions: a low-speed supernatant (LSS), which contains both sarkosyl-soluble and sarkosyl-insoluble tau, a high speed supernatant containing sarkosyl-soluble tau, and a high speed pellet containing sarkosyl-insoluble, aggregated,

tau. In both the LSS and sarkosyl-insoluble tau fraction, tau was detected at approximately 50-64 kDa, with the 64 kDa tau species again found to be prominent in 3xTg-AD samples. Levels of sarkosyl-insoluble tau were clearly increased in the amygdala of 3xTg-AD mice at 12 months compared to WT mice at the same age and 4 month old 3xTg-AD mice (Figure 3.9A), however, following normalisation to tau amounts in the LSS, this difference was not significant (Figure 3.9B, p=0.08 and p=0.07, respectively). Levels of sarkosyl-insoluble tau did not differ between genotypes at 4 months of age (Figure 3.9). These results suggest that aggregated tau is beginning to accumulate in 12 month old 3xTg-AD brain.

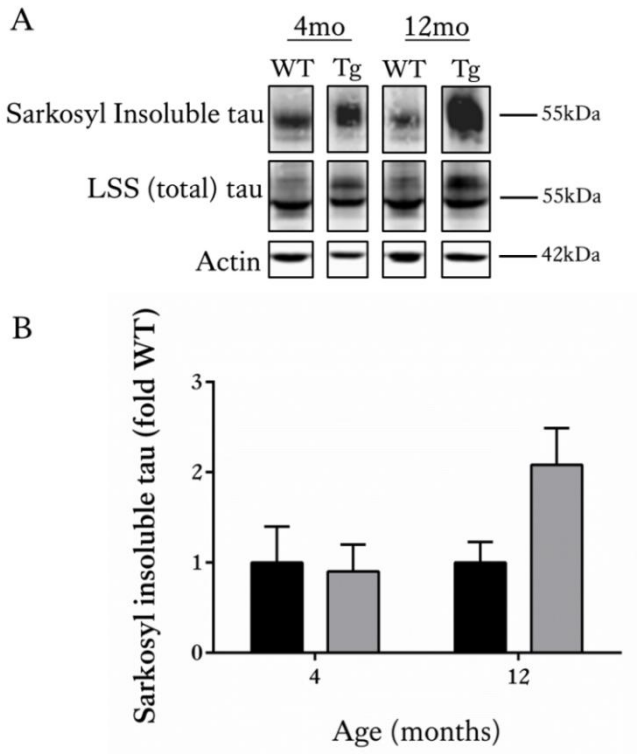

Figure 3.9: Sarkosyl insoluble tau is increased in 3xTg-AD amygdala
(A) Representative western blots of low speed supernatant and the sarkosyl-insoluble fraction prepared from the amygdala of 4 and 12 month old WT and 3xTg-AD mice immunoblotted for total tau (phosphorylated and non-phosphorylated, 50-64 kDa). An antibody against β-actin was used as a loading control (42 kDa). (B) Bar chart shows amounts of aggregated, insoluble tau following normalisation to amounts of total tau in the LSS in the same sample. Data are shown as fold change from WT at each time point. Data is mean ± SEM, (n=3 mice per group).

3.4.8 Pre- and post-synaptic markers are unchanged in the hippocampus of 3xTg-AD mice

Synaptic dysfunction and degeneration are a major feature of human AD (Selkoe, 2002), and synapse loss is believed to be the most clinically relevant biological correlate of cognitive decline in AD (Terry et al., 1991, Masliah et al., 2001). Synaptic dysfunction and loss has also been reported in the 3xTg-AD mice (Oddo et al., 2003b, Bittner et al., 2010). Levels of the pre- and post-synaptic markers, synaptophysin and PSD-95, respectively, have been reported to closely correlate with the numbers of functional synapses and a loss of these markers can be indicative of early AD (Masliah et al., 2001). To begin to understand if synapse health is affected in our colony of 3xTg-AD mice, synaptosomal fractions, enriched in synaptic proteins, were prepared from the hippocampus of WT and 3xTg-AD mice at 1, 2, 4, 9, and 12 months of age (section 2.2.4). These fractions were immunoblotted with antibodies against the pre-synaptic marker synaptophysin and the post-synaptic marker, PSD-95. Quantification of band densities showed that the amounts of synaptophysin did not differ between genotypes at any of the ages studied (Figure 3.10), although a non-significant loss of synaptophysin was apparent in 12 month old 3xTg-AD hippocampus relative to WT controls. Similarly, there were no significant changes in PSD-95 between 3xTg-AD and WT mice, or with increasing age (Figure 3.10). These data suggest that synapses remain functional in 12 month old 3xTg-AD mice.

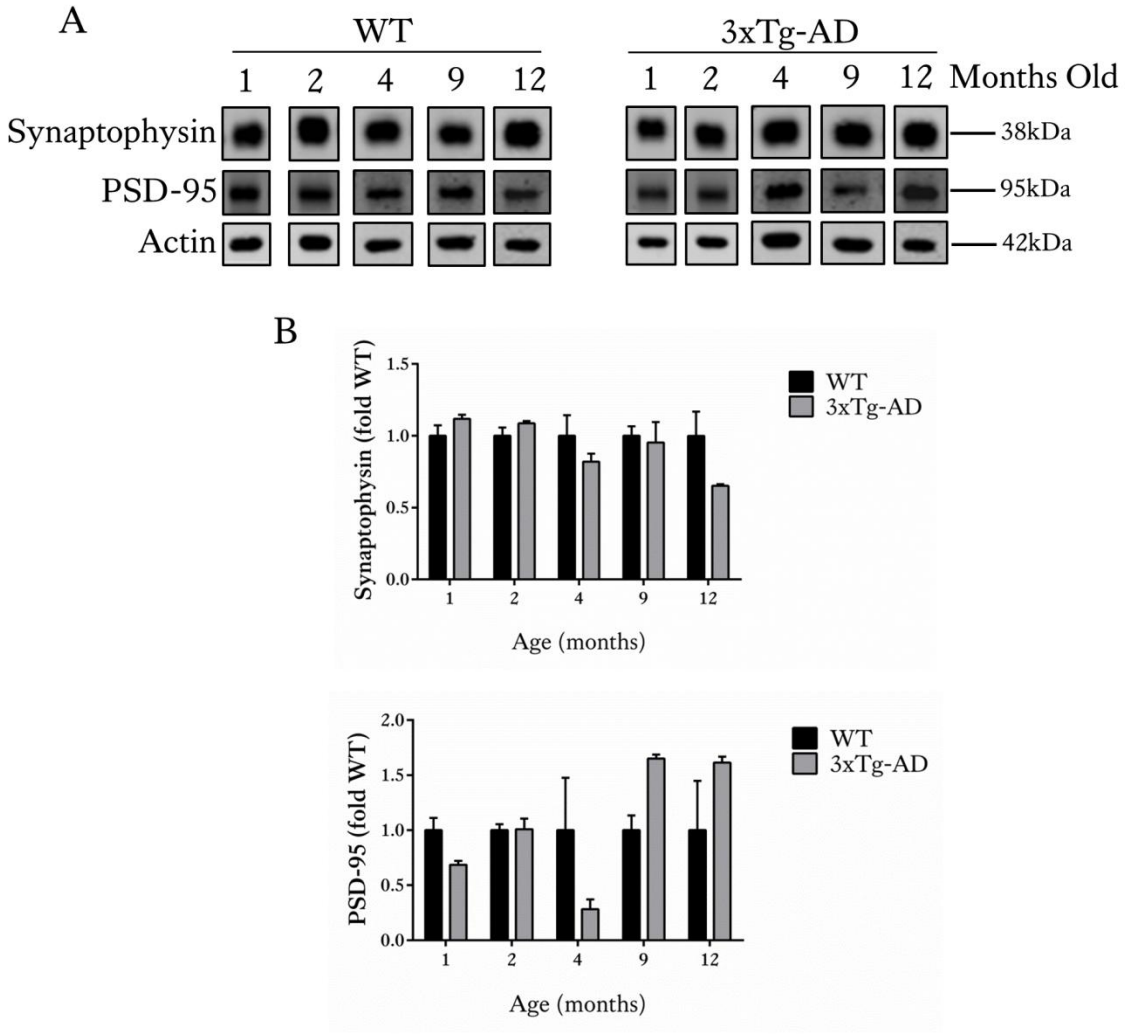

Figure 3.10: Levels of pre- and post- synaptic markers are unaltered in hippocampi of 3xTg-AD mice.
(A) Representative Western blots of synaptosomal fractions prepared from the hippocampus and associated cortex of WT and 3xTg-AD mice at 1, 2, 4, 9, and 12 months of age, and immunoblotted with antibodies against synaptophysin (38 kDa) and PSD-95 (95 kDa). An antibody against β-actin was used as a loading control (42 kDa). Bar charts show amounts of (B) synaptophysin and (C) PSD-95, both standardised to amounts of β-actin in the same sample. Data are shown as fold change from WT at each time point. Data is mean ± SEM, (n=3 mice per group).

3.4.9 3xTg-AD mice show changes in synaptic APP and tau amounts

The hippocampal synaptosome preparations were next used to examine total amounts of APP and tau at the synapse. The physiological and pathological role of APP and tau at the synapse still remains unclear but it is likely that both exert physiological and

pathological effects which may be relevant to the progression of AD (Spires-Jones and Hyman, 2014). Synaptosomal fractions were immunoblotted for amounts of total APP, total tau and actin, as described above. Synaptosomes from the hippocampus of 3xTg-AD mice showed significantly increased amounts of tau at both 1 and 2 months of age compared to synaptosomes prepared from age-matched WT hippocampus (Figure 3.11, $p<0.01$ and $p<0.001$, respectively). There were no differences in tau amounts in the synaptosomal fraction prepared from older animals. In addition, significantly higher levels of APP were detected in synaptosomes of 1, 2 and 9 month old 3xTg-AD mice compared to WT controls (Figure 3.11, $p<0.01$). These results appear to suggest a relocalisation of tau and APP from synaptosomes of 3xTg-AD mice, which might reflect a loss of their function in synapses as disease progresses.

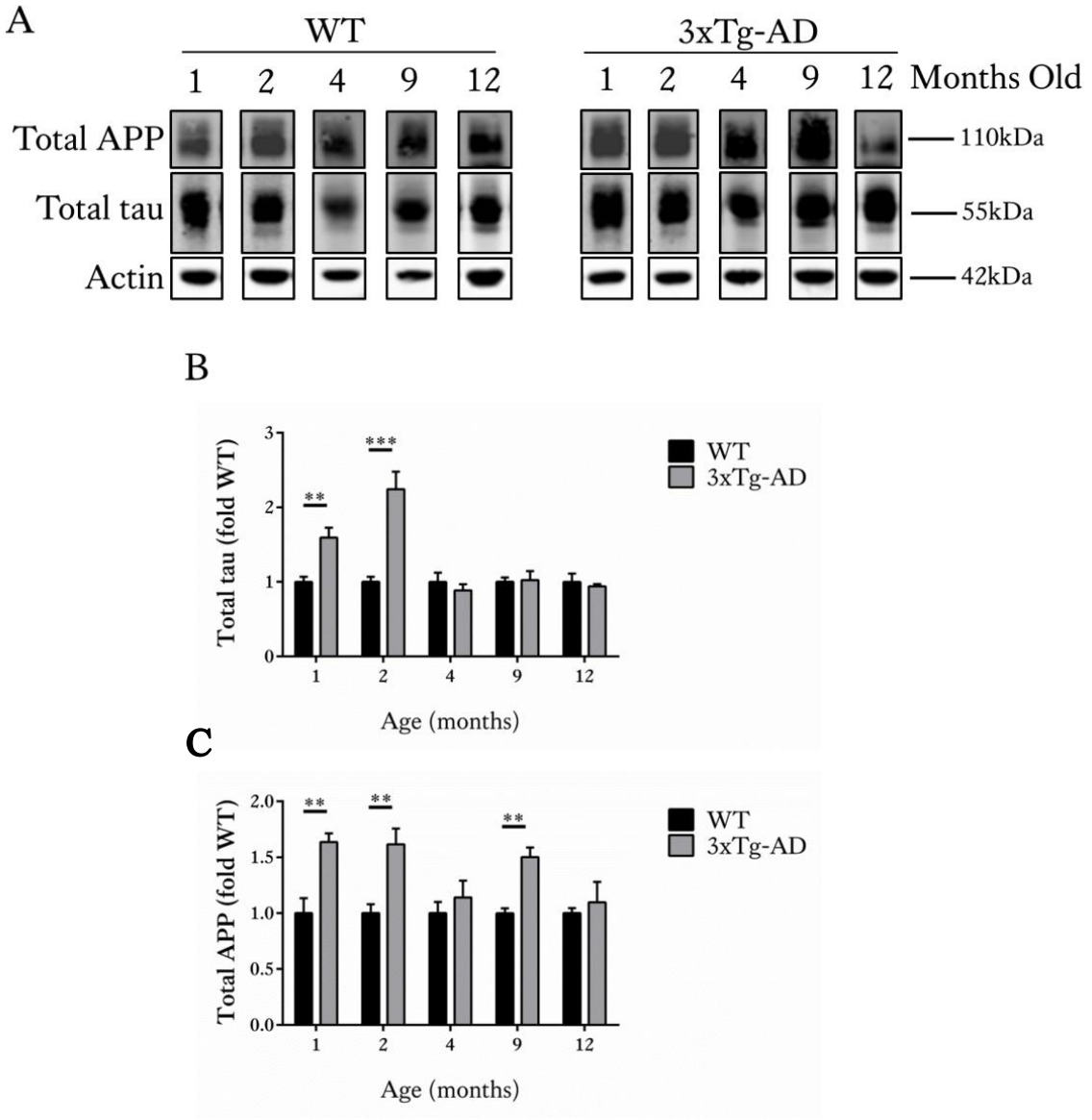

Figure 3.11: Tau and APP are increased at the synapse in the hippocampus of young 3xTg-AD mice.

(A) Representative Western blots of synaptosomal fractions prepared from hippocampus of WT and 3xTg-AD mice at 1, 2, 4, 9, and 12 months of age, and immunoblotted with antibodies specific to total tau (phosphorylated and non-phosphorylated, ~50-64 kDa) and APP (~90-120 kDa). An antibody against β-actin was used as a loading control (42 kDa). Bar charts show amounts of (B) total tau and (C) total APP both standardised to amounts of β-actin in the same sample. Data are shown as fold change from WT at each time point. Data is mean ± SEM, (n=3 mice per group, **p<0.01, ***p<0.01).

3.4.10 Slice cultures from WT and 3xTg-AD mice can be prepared and maintained for at least 28 days in culture

Methods to establish and maintain organotypic brain slice cultures using the membrane-cell interface method are well established in neuroscience research (Stoppini et al., 1991, Gähwiler et al., 1997). In particular, conditions have been described where long-term cultures from mice expressing human mutant *APP* or *MAPT* transgenes can be maintained for up to 6 months in culture which allows slices to develop pathologies similar to those found *in vivo* (Duff et al., 2002). These conditions were used as a starting point for producing organotypic brain slice cultures from WT and 3xTg-AD mice. The dissection and production of cortical and hippocampal containing brain slice cultures can be technically challenging, but it was found that dissecting brains for culturing in the same manner as previously described (Duff et al., 2002) was possible, although when prepared from postnatal day 11 to 12 mouse pups, as suggested by this group, slices showed poor survival rates (Figure 3.12). By 14 *div* healthy slice cultures are transparent, whereas unhealthy or dead cultures have a cloudy white appearance. These visual assessments were used to gain an initial impression of culture health when slices were prepared from postnatal day 8-12 pups and the results of this assessment are shown in Figure 3.12. Due to the better survival of slice cultures prepared from postnatal day 8 and 9 pups, slice cultures were prepared from this age for the rest of the work described in this thesis. All other parameters including slice media composition, incubator conditions, and media change frequency were as described in (Duff et al., 2002) and in section 2.2.2. Following these methods, slices from WT and 3xTg-AD brain survived for at least 28 *div.*

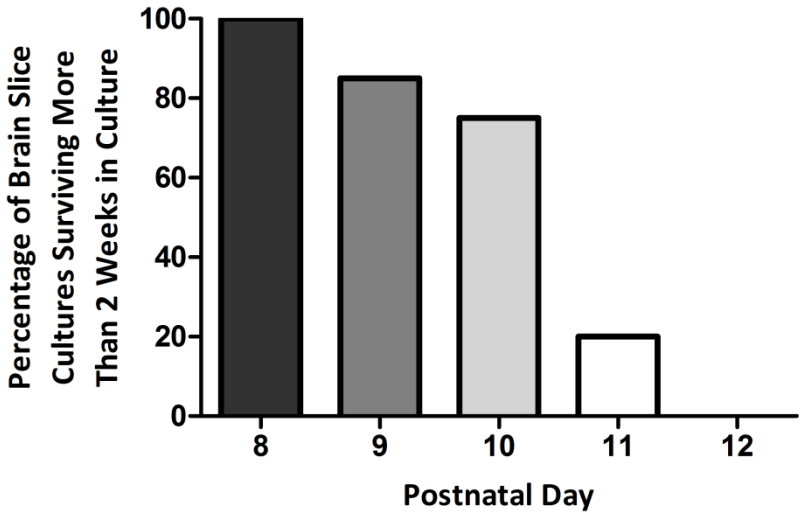

Figure 3.12: Organotypic brain slices cultured from postnatal day 8 or 9 pups are most viable.
Bar chart shows the percentage of cultures that survive when prepared from mouse pups of postnatal day 8-12. (n=36 wells from three independent experiments).

3.4.11 Organotypic brain slice cultures from 3xTg-AD mice contain increased amounts of tau protein

Organotypic brain slice cultures from WT and 3xTg-AD mouse pups were cultured in order to characterise development of AD-relevant features over time. Slice cultures were harvested at 14, 21 and 28 *div* in order to understand whether the overexpression of the P301L mutation in the *MAPT* gene would cause translation and the overproduction of total mouse and human tau protein in the culture model as seen *in vivo* in our colony as described in section 3.4.2, and in other 3xTg-AD colonies (Oddo et al., 2003a).

Slice culture lysates from both WT and 3xTg-AD were first immunoblotted with an antibody against total tau (phosphorylated and non-phosphorylated, mouse and

human). Similar to findings in homogenates from WT and 3xTg-AD mice, tau was detected at 50-64 kDa, with the 64 kDa tau band being particularly prominent in aged slices from 3xTg-AD mice. At 21 and 28 *div* 3xTg-AD slice cultures showed significantly higher total tau protein amounts than WT slice cultures of the same *div* (Figure 3.13, $p<0.01$, $p<0.05$). No significant changes were found in total tau amounts when 21 and 28 *div* 3xTg-AD slice cultures were compared to those at 14 *div*. In contrast, in WT slice cultures, amounts of tau protein were significantly reduced by 28 *div* compared to 14 *div* (Figure 3.13). This might suggest an upregulation of tau in newly prepared WT slices that normalises after extended periods of time in culture.

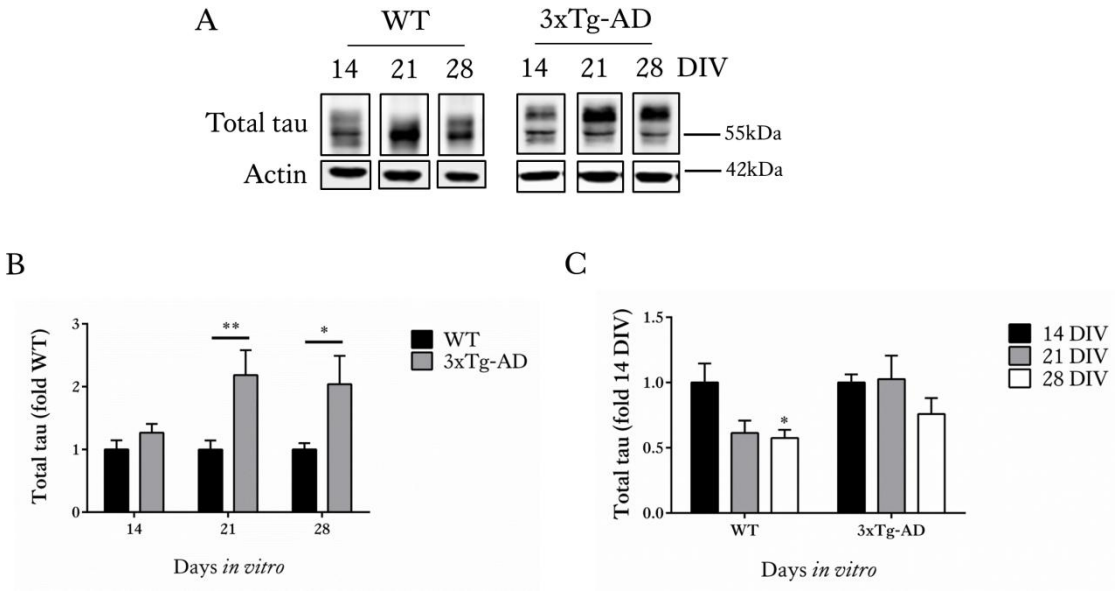

Figure 3.13: Organotypic brain slice cultures from 3xTg-AD mice show overexpression of total tau protein at 21 and 28 *div*

(A) Representative western blots of total (phosphorylated and non-phosphorylated) tau (~50-64 kDa) in lysates prepared from WT and 3xTg-AD slice cultures harvested at 14, 21 and 28 *div*. An antibody against β-actin was used as a loading control (42 kDa). Bar charts show (B) amounts of total tau normalised to β-actin content in each sample, presented as fold change from WT at each time point, and (C) amounts of total tau normalised to β-actin content in each sample, presented as fold change from 14 *div* for each genotype. Data is mean ± SEM, (n=12 wells from two independent experiments, *p<0.05, **p<0.01).

Immunoblots were also probed with CP27, an antibody specific to only human forms of tau (phosphorylated and non-phosphorylated). 3xTg-AD slice cultures expressed human tau protein as detected by CP27, whereas slice cultures from WT mice did not express any human tau protein (Figure 3.14). Over time in culture, 3xTg-AD slice cultures at 21 and 28 *div* did not express significantly higher amounts of human tau compared to cultures at 14 *div,* however there was an observed elevation in human tau in 28 *div* 3xTg-AD slices relative to those at 14 and 21 *div* (Figure 3.14).

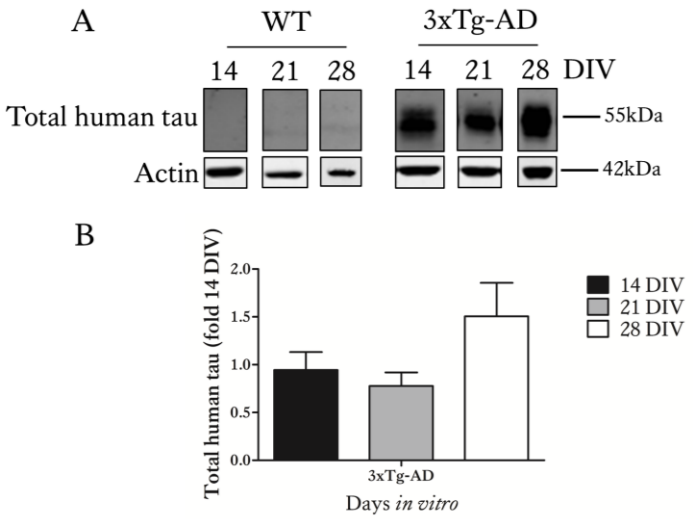

Figure 3.14: Human tau is expressed in 3xTg-AD organotypic brain slice cultures
(A) Representative western blots of total human tau (phosphorylated and non-phosphorylated) (CP27) (~50-64 kDa) in lysates prepared from WT and 3xTg-AD slice cultures harvested at 14, 21 and 28 *div*. An antibody against β-actin was used as a loading control (42 kDa). (B) Bar chart shows amounts of total human tau normalised to β-actin content in each sample, presented as fold change from 14 *div* for 3xTg-AD slice cultures only. Data is mean ± SEM, (n=12 wells from two independent experiments).

Tau protein was also examined in 28 *div* WT and 3xTg-AD slices by immunohistochemical staining using an antibody against total tau. An antibody specific to GFAP was also used to show activated astrocytes. An increased abundance of total tau was observed in 28 *div* 3xTg-AD slice cultures in comparison to slice cultures from 28 *div*-matched WT slice cultures (Figure 3.15), confirming the results of immunoblotting. Tau in slice cultures was restricted mainly to neurons, although some colocalisation between tau and GFAP can be observed; small amounts of tau have been identified by others in astrocytes, previously (Papasozomenos and Binder, 1987). Neuronal staining of tau was mainly somatic although some staining of axons and dendrites could also be observed.

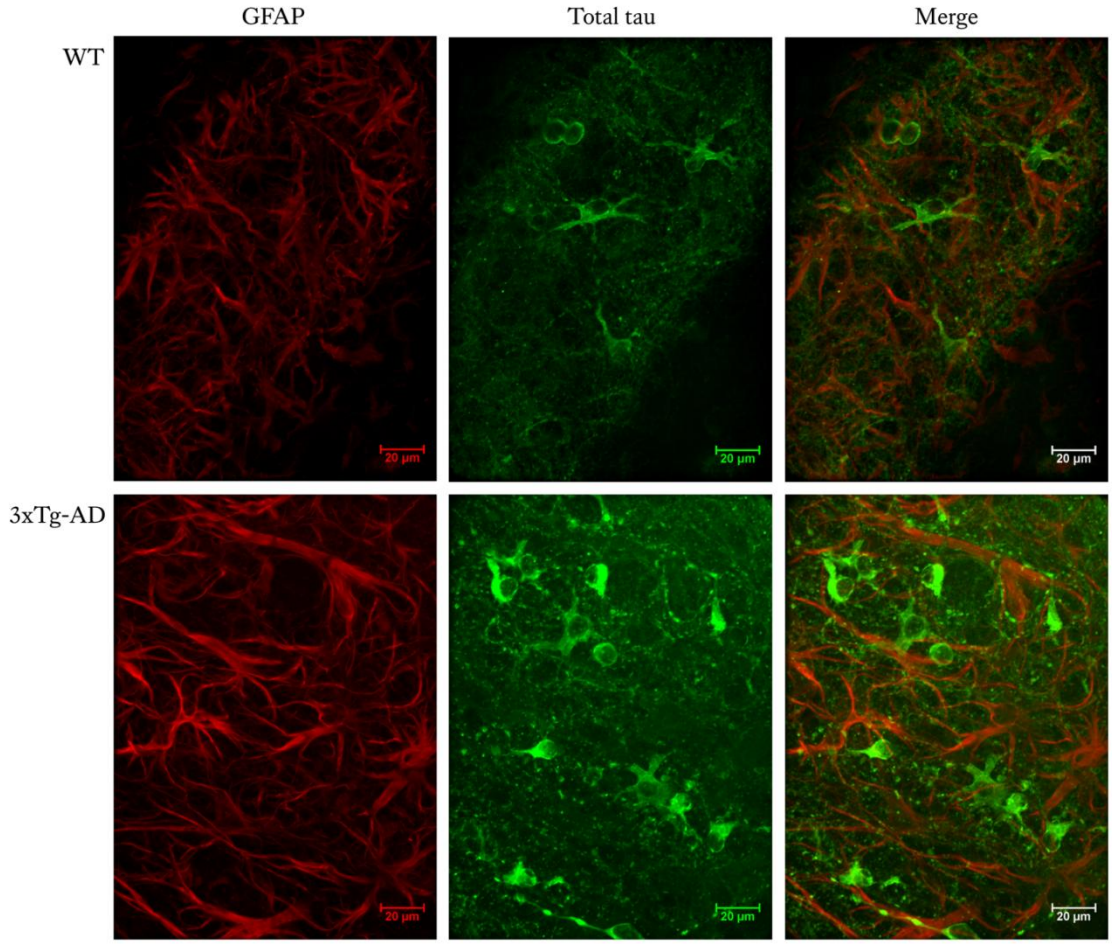

Figure 3.15: Total tau amounts are increased in 3xTg-AD slice cultures
Organotypic brain slice cultures prepared from WT and 3xTg-AD mice and cultured for 28 *div* were fixed and immunolabelled with antibodies against tau (green) and GFAP, an astrocytic marker (red). Representative images are shown. Scale bar is 20 µm.

3.4.12 3xTg-AD organotypic brain slice cultures develop increased amounts of higher molecular weight tau

There is much speculation as to which forms of tau are the most detrimental in AD. It is well established that higher molecular weight tau, and in particular, phosphorylated forms of tau, show an increased propensity to aggregate and form paired helical filaments which accumulate in NFTs. However, whether it is the NFTs or pre-fibrillar forms of tau that are responsible for neuron and synapse loss remains a matter of

debate (Iqbal et al., 2005, Wang et al., 2014). High molecular weight tau that is detected on immunoblots at 64 kDa, is believed to be an intermediate tau species of highly phosphorylated tau that is, or will become insoluble, and that contributes to disruption of microtubules in neurons (Barghorn et al., 2000, Lewis et al., 2000).

Since high molecular weight tau is considered an important pathological tau species, and it is shown here that this form of tau is detected in 12 month old 3xTg-AD mice (section 3.4.2), it was important to determine if 64 kDa tau is also present in brain slice cultures from 3xTg-AD mice. Therefore, slice culture lysates from WT and 3xTg-AD slices were immunoblotted with antibodies specific to total (phosphorylated and non-phosphorylated) tau, and high molecular weight tau detected at ~64 kDa was quantified as a proportion of total tau. In 3xTg-AD slices cultured for 21 and 28 *div*, a significantly higher proportion of the tau detected was the 64 kDa species when compared to tau in matched WT slice cultures ($p<0.05$, Figure 3.16B). Although not reaching statistical significance, 21 and 28 *div* cultures also showed higher amounts of 64 kDa tau than 14 *div* 3xTg-AD cultures, suggesting that this potential pathogenic tau species may progressively accumulate over time *(*Figure 3.16C). These results showing a classical shift of tau towards higher molecular weight species is typical of models in which hyperphosphorylated aggregated tau species accumulate (Lewis et al., 2000, Lewis et al., 2001, Kelleher et al., 2007) and therefore suggests that cultured 3xTg-AD brain slices are developing characteristic tau pathology *ex vivo*.

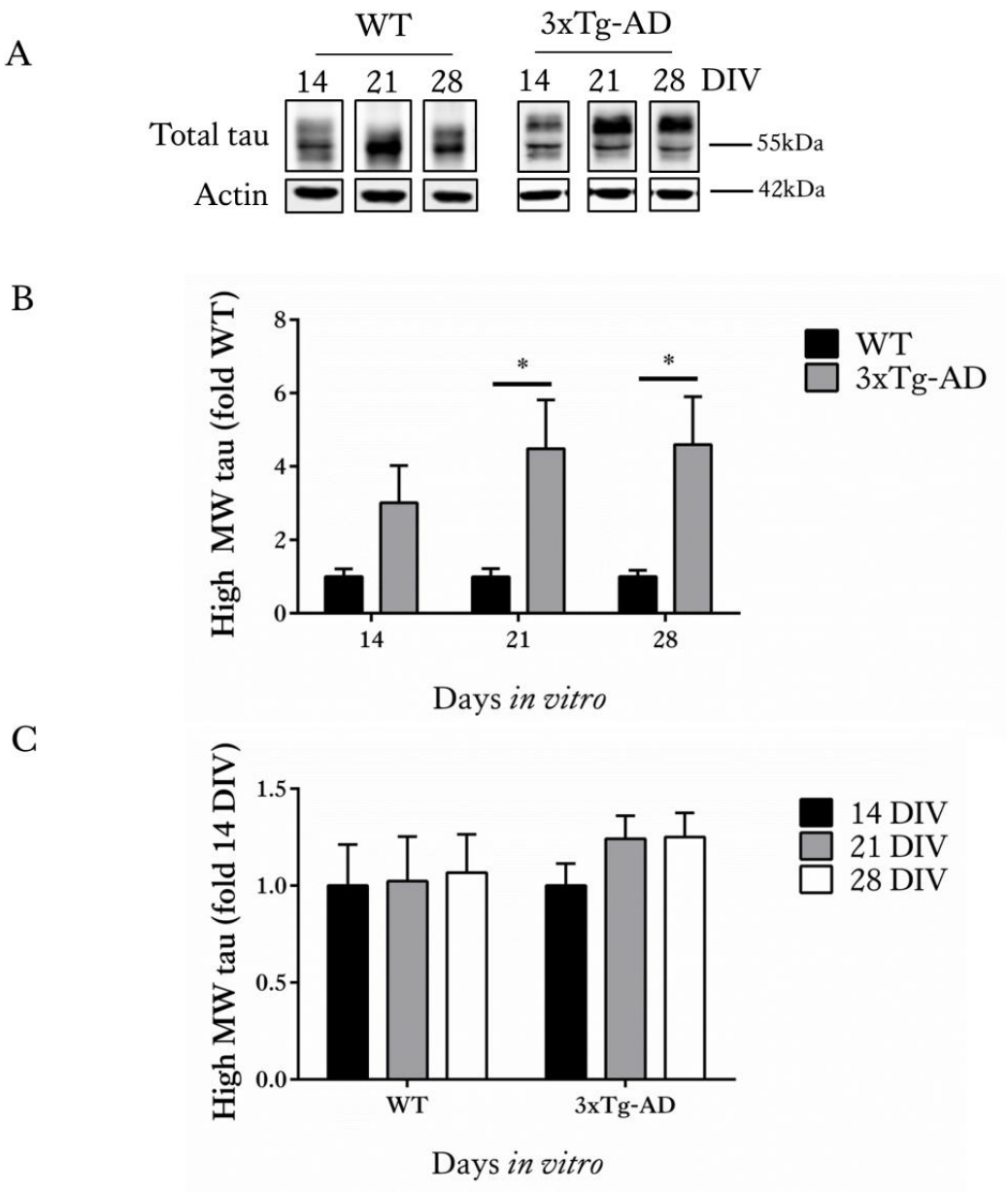

Figure 3.16: Organotypic brain slice cultures from 3xTg-AD mice develop higher molecular weight tau protein at 21 and 28 *div*

(A) Representative western blots of total (phosphorylated and non-phosphorylated) tau (~50-64 kDa) in lysates prepared from WT and 3xTg-AD slice cultures harvested at 14, 21 and 28 *div*. An antibody against β-actin was used as a loading control (42 kDa). Bar charts show amounts of high molecular weight tau (64 kDa) normalised to total tau amounts in each sample, presented as (B) fold change from WT at each time point, and (C) fold change from 14 *div* for each genotype. Data is mean ± SEM, (n=12 wells from two independent experiments, *p<0.05).

3.4.13 Tau in 3xTg-AD organotypic brain slice cultures rapidly becomes phosphorylated at several AD-relevant sites.

The accumulation of phosphorylated tau was characterised in WT and 3xTg-AD organotypic brain slice cultures. The progressive accumulation of hyperphosphorylated tau is a major feature of Alzheimer's disease and other tauopathy brain (Iqbal et al., 2005). In addition, there is some evidence that tau phosphorylation at specific sites corresponds with Braak staging. For example, phosphorylation of tau at ser 396/404 is characteristic of late stage AD (Wolozin et al., 1986), whilst phosphorylation of tau at ser 202 is more representative of early stage AD (Su et al., 1994). Similar findings have been reported in transgenic mouse models of tauopathy (Lewis et al., 2000, Noble et al., 2005). In our 3xTg-AD mouse colony, no increases in tau phosphorylation at ser 202, ser 396/404 or ser 199/202 and thr205 were found in the cortex of 3xTg-AD mice compared to WT mice (section 3.4.5), however increased phosphorylation of tau at ser 396/404 and abnormal conformations of tau were detected in the hippocampus of 3xTg-AD mice at 12 months of age (section 3.4.6). Increases in the amounts of tau phosphorylated at ser 202 and other AD-relevant tau phosphorylation sites has previously been reported in 12 month old 3xTg-AD mice in other colonies (Oddo et al., 2003a).

Immunoblotting with an antibody specific to tau phosphorylated at ser 202 (CP13) revealed significantly increased amounts of tau phosphorylated at this site in 21 *div* 3xTg-AD slice cultures compared to WT slice cultures (Figure 3.17B, $p<0.001$). Tau phosphorylated at ser 202 was also clearly increased at 28 *div* in 3xTg-AD slices relative to those from *div*-matched WTs, but this did not reach significance. Tau at 64 kDa is

clearly labelled with CP13 (Figure 3.17A), characteristic of previous reports of an intermediate tau species of highly phosphorylated tau that is, or will become insoluble leading to the dysfunction of tau (Barghorn et al., 2000, Lewis et al., 2000). There were no significant increases in the levels of CP13 reactive tau with increasing *div* in either WT or 3xTg-AD slice cultures (Figure 3.17C).

Tau phosphorylated at ser 396/404 was also examined in brain slice cultures from WT and 3xTg-AD mice. Tau phosphorylated at ser 396/404 is characteristic of late-stage AD, and is typically found in mature NFTs (Wolozin et al., 1986). Immunoblots were probed with an antibody specific to tau phosphorylated at ser 396/404 (PHF-1) and the amount of PHF-1-positive tau was normalised to total tau amounts in each sample. At 14, 21 and 28 *div* 3xTg-AD slice cultures showed significantly higher amounts of PHF-1-positive tau when compared to age-matched WT slice cultures (Figure 3.17B, $p<0.01$, $p<0.001$, $p<0.01$, respectively). There were no significant increases in the levels of PHF-1 reactive tau with increasing *div* in either WT or 3xTg-AD slices (Figure 3.17C).

Levels of tau dephosphorylated at ser 199/202/thr 205 were also examined in both WT and 3xTg-AD slice cultures which had been cultured for 14, 21 and 28 *div*. An antibody specific to tau dephosphorylated at the above sites was used (Tau-1) and amounts of Tau-1-positive tau were normalised to total amounts of tau in each sample. Slice cultures from both WT and 3xTg-AD slice cultures showed similar levels of Tau-1 immunoreactivity at 14, 21 and 28 *div* (Figure 3.17B). In addition, there were no changes in amounts of Tau-1-positive tau over time in culture in either genotype (Figure 3.17C).

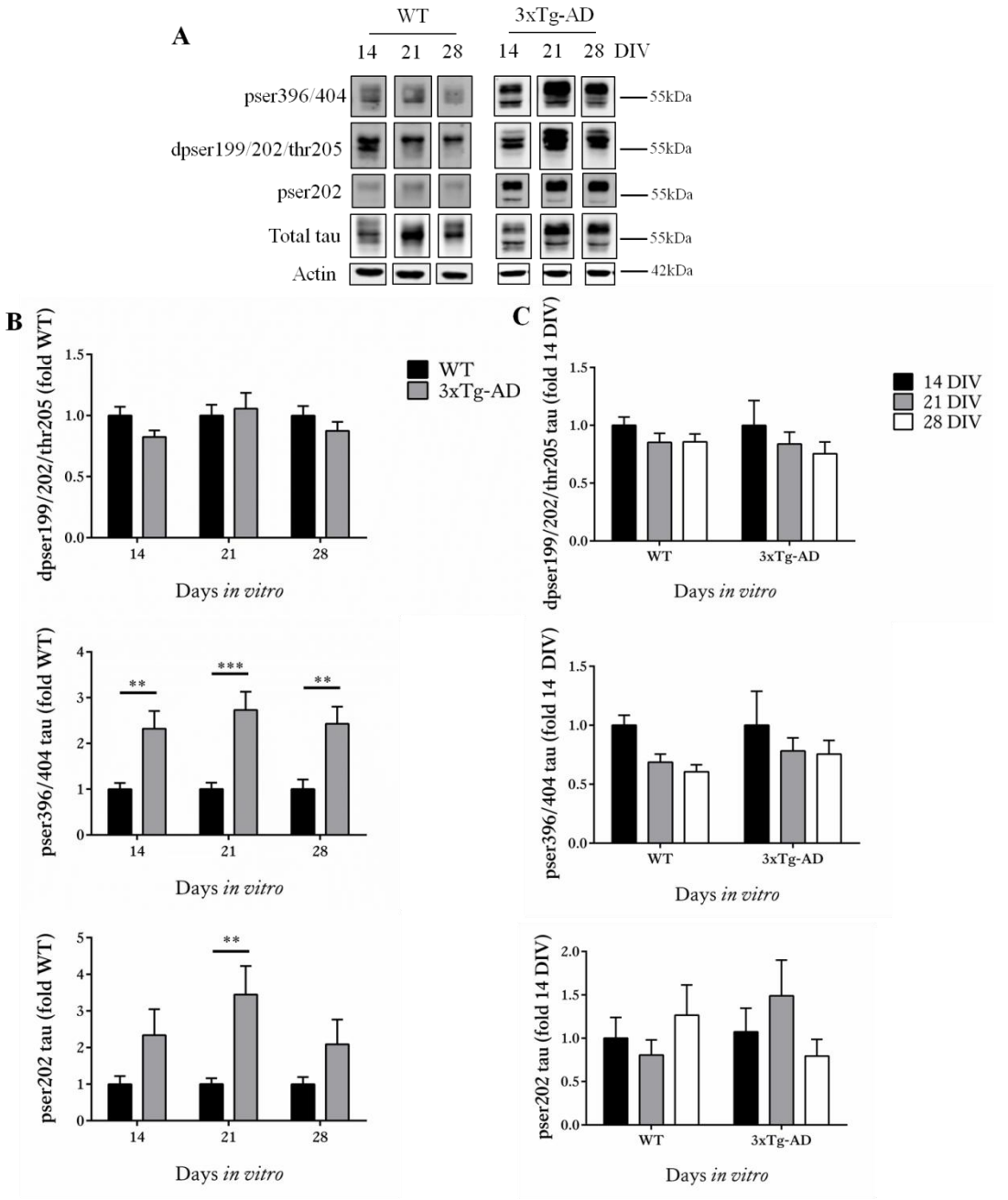

Figure 3.17: Slice cultures from 3xTg-AD mice show increased amounts of phosphorylated tau compared to WT slice cultures.

(A) Representative western blots of lysates from 14, 21 and 28 *div* WT and 3xTg-AD slice cultures showing total tau, tau phosphorylated at ser 202 (CP13), ser 396/404 (PHF-1) and dephosphorylated at ser 199/202 and thr 205 (Tau-1), all at ~50-64 kDa. An antibody against β-actin was used as a loading control (42 kDa). Bar charts show amounts of tau dephosphorylated at ser 199/202 and thr 205, tau phosphorylated at ser 202, and tau phosphorylated at ser 396/404, all normalised to total tau amounts in the same sample. (B) Data is shown as fold change from WT at each time point. (C) Data is shown as fold change from 14 *div* for each genotype. Data is mean ± SEM, (n=12 wells from two independent experiments, *p<0.05, **p<0.01, ***p<0.001).

Phosphorylation of tau at ser 202 and ser 396/404 was also detected in slice cultures that were fixed at 28 *div* and immunohistochemically stained with the CP13 (Figure 3.18) and PHF-1 (Figure 3.19) antibodies, respectively. Increased CP13- and PHF-1-immunoreactive tau is clearly apparent in cell soma of 3xTg-AD slice cultures when compared to slice cultures prepared from WT mice (Figure 3.18, Figure 3.19). Taken together, these findings further indicate that slice cultures prepared from 3xTg-AD mice show accelerated development of human tauopathy-like tau abnormalities over time.

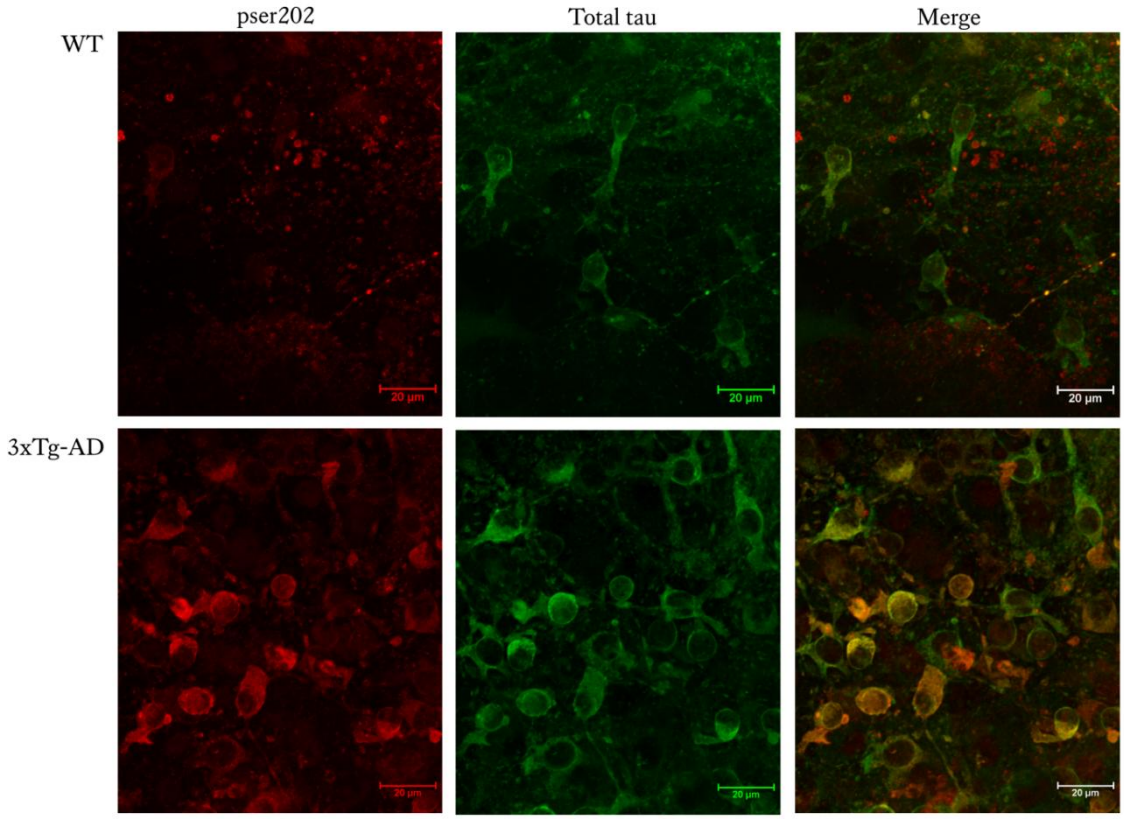

Figure 3.18: Organotypic brain slice cultures from 3xTg-AD mice show increased amounts of tau phosphorylated at ser 202.
Organotypic brain slice cultures prepared from WT and 3xTg-AD mice and cultured for 28 *div* were fixed, and immunolabelled with antibodies against total tau (green) and tau phosphorylated at ser 202 (red). Scale bar is 20 µm.

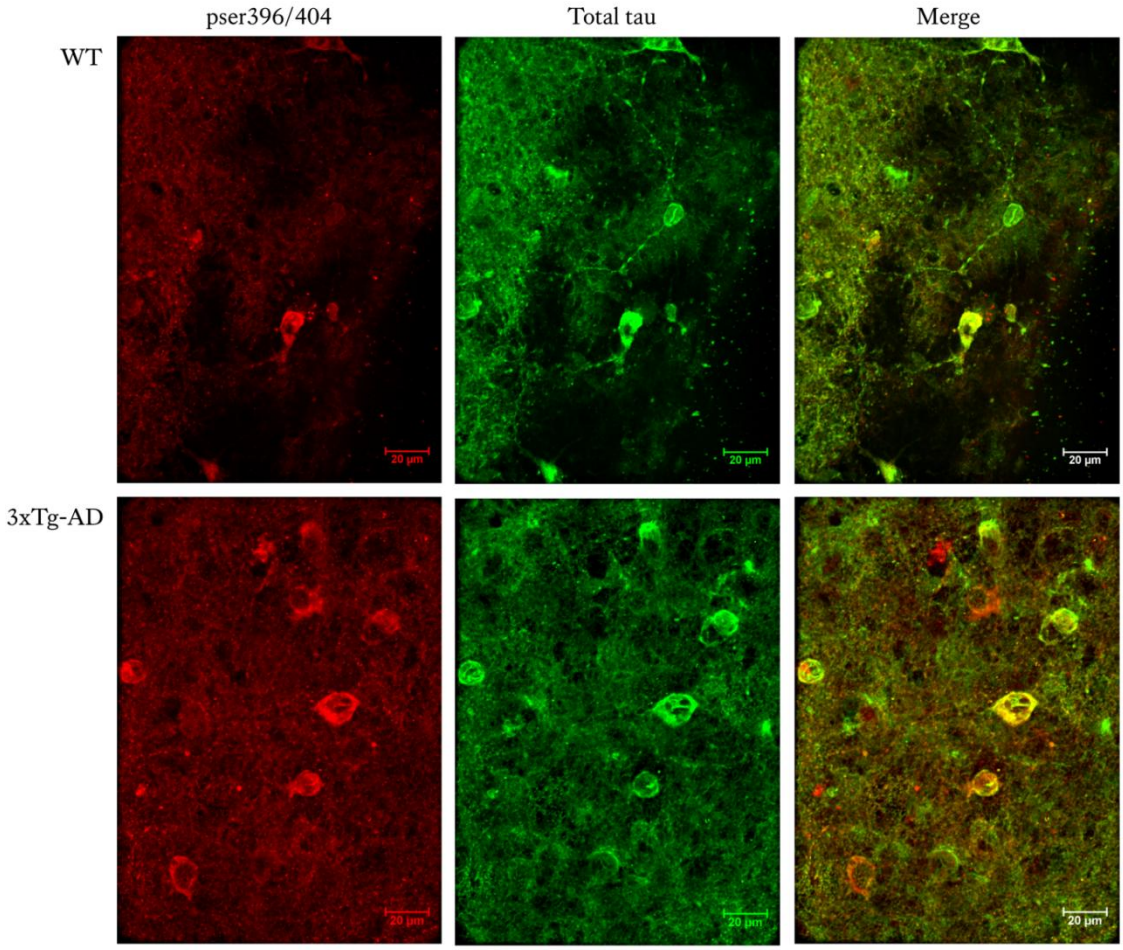

Figure 3.19: Organotypic brain slice cultures from 3xTg-AD mice show increased amounts of tau phosphorylated at ser 396 and 404
Organotypic brain slice cultures prepared from WT and 3xTg-AD mice and cultured for 28 *div* were fixed, and immunolabelled with antibodies against total tau (green) and tau phosphorylated at ser 396/404 (red). Scale bar is 20 µm.

3.4.14 Organotypic brain slice cultures from 3xTg-AD mice produce increased amounts of APP

Significant increases in the amounts of APP holoprotein and Aβ-42 were detected in the cortex of 12 month old 3xTg-AD mice compared to their WT counterparts (Figure 3.4, Figure 3.5).

To determine if cultured slices from these mice recapitulate these features, slice culture lysates from WT and 3xTg-AD mice cultured for 14, 21, and 28 *div* were immunoblotted with antibodies that detect total levels of APP (one N-terminal, one C-terminal) and the total amounts of APP detected were then standardised to β-actin levels in each sample. 3xTg-AD slice cultures at 14 *div* were found to have significantly higher amounts of APP with an intact N-terminus when compared to WT slice cultures at this time point (Figure 3.20, $p<0.01$). There were no significant differences in amounts of N-terminal APP at 21 or 28 *div* between genotypes. Using an antibody which recognises C-terminal APP, amounts of APP with an intact C-terminus were significantly higher at 28 *div* in 3xTg-AD slice cultures than their WT counterparts (Figure 3.20, $p<0.05$), and no differences in amounts of C-terminal APP were found at 14 or 21 *div* between genotypes.

3xTg-AD slice cultures did not show any increases in the amounts of N-terminal or C-terminal APP with increasing time in culture. However, in WT slices there were significantly higher amounts of N-terminal APP (Figure 3.20, $p<0.001$) and significantly decreased amounts of C-terminal APP (Figure 3.20, $p<0.05$) at 28 *div* than at 14 *div*, suggesting an altered regulation of APP processing with increasing time in culture in WT slices, a feature not apparent in slices from 3xTg-AD mice.

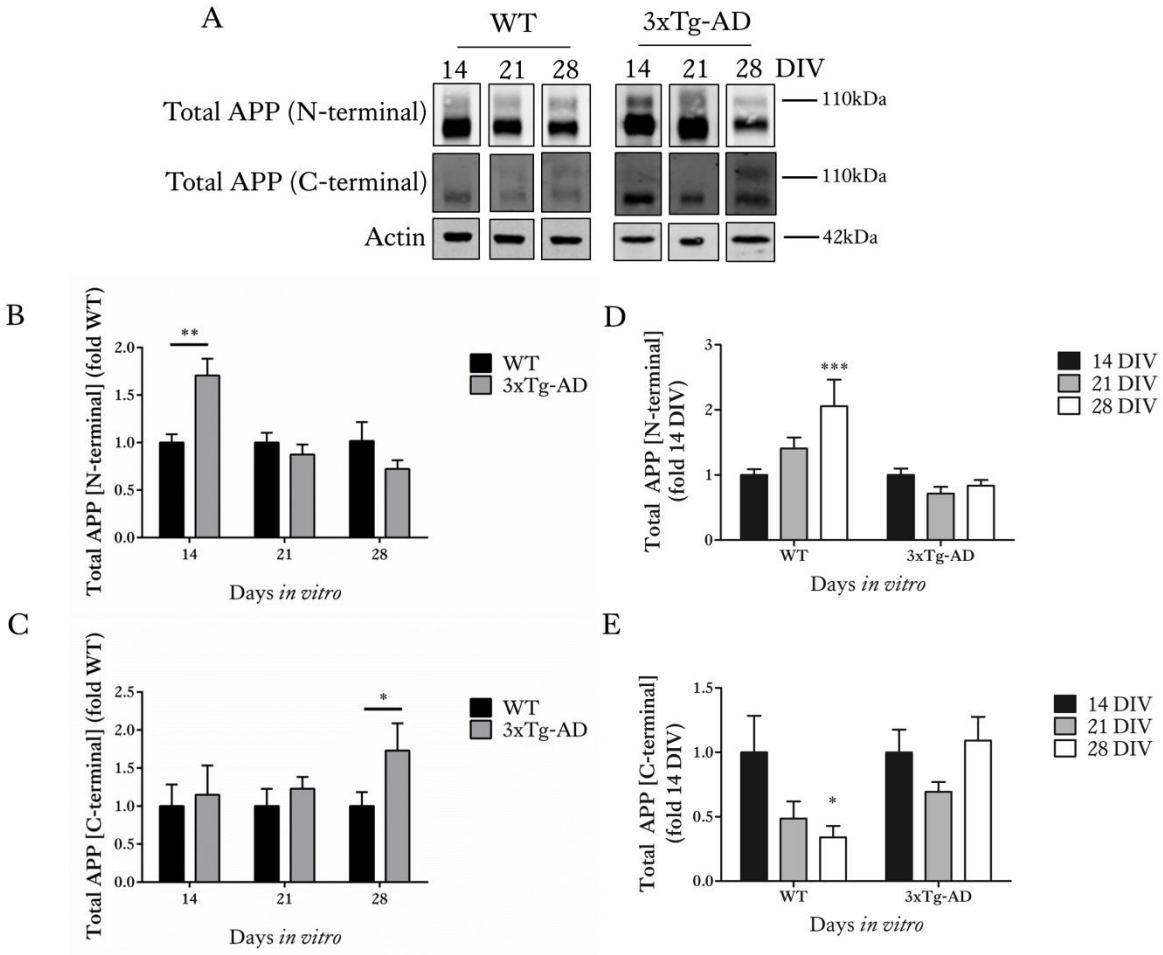

Figure 3.20: Organotypic Brain slice cultures from 3xTg-AD mice have higher levels of APP

(A) Representative western blots of lysates from 14, 21 and 28 *div* WT and 3xTg-AD slice cultures showing total APP (N-terminal) and total APP (C-terminal), both ~90-120 kDa. An antibody against β-actin was used as a loading control (42 kDa). Bar charts shows amounts of (B) total APP (N-terminal) and (C) total APP (C-terminal) normalised to β-actin amounts in the same sample, presented as fold change from WT at each time point and (D) total APP (N-terminal) and (E) total APP (C-terminal) normalised to β-actin amounts in the same sample, presented as fold change from 14 *div* for each genotype. Data is mean ± SEM, (n=12 wells from two independent experiments, *p<0.05, ***p<0.001).

3.4.15 Significantly increased levels of Aβ-42 are detected in organotypic brain slice cultures from 3xTg-AD mice

The amounts of Aβ-40 and Aβ-42 in lysates containing equal amounts of protein from WT and 3xTg-AD slices cultured for 14, 21 and 28 *div* were detected using commercial

human specific Aβ-40 and Aβ-42 ELISA kits, as described above. 3xTg-AD slices cultured for 14, 21, and 28 *div* showed significantly increased amounts of Aβ-42 compared to *div*-matched WT slice cultures (Figure 3.21, $p<0.001$, $p<0.05$, $p<0.05$, respectively). No significant differences between genotypes were found in amounts of Aβ-40 at any time point (Figure 3.21). Finally, the ratio of Aβ-42 to Aβ-40 was significantly increased at 14 *div* in 3xTg-AD slice cultures (Figure 3.21, $p<0.05$), and although increases in this ratio were apparent when 3xTg-AD slices were cultured for longer periods of time, these later changes were not significant when compared to matched WT slice cultures.

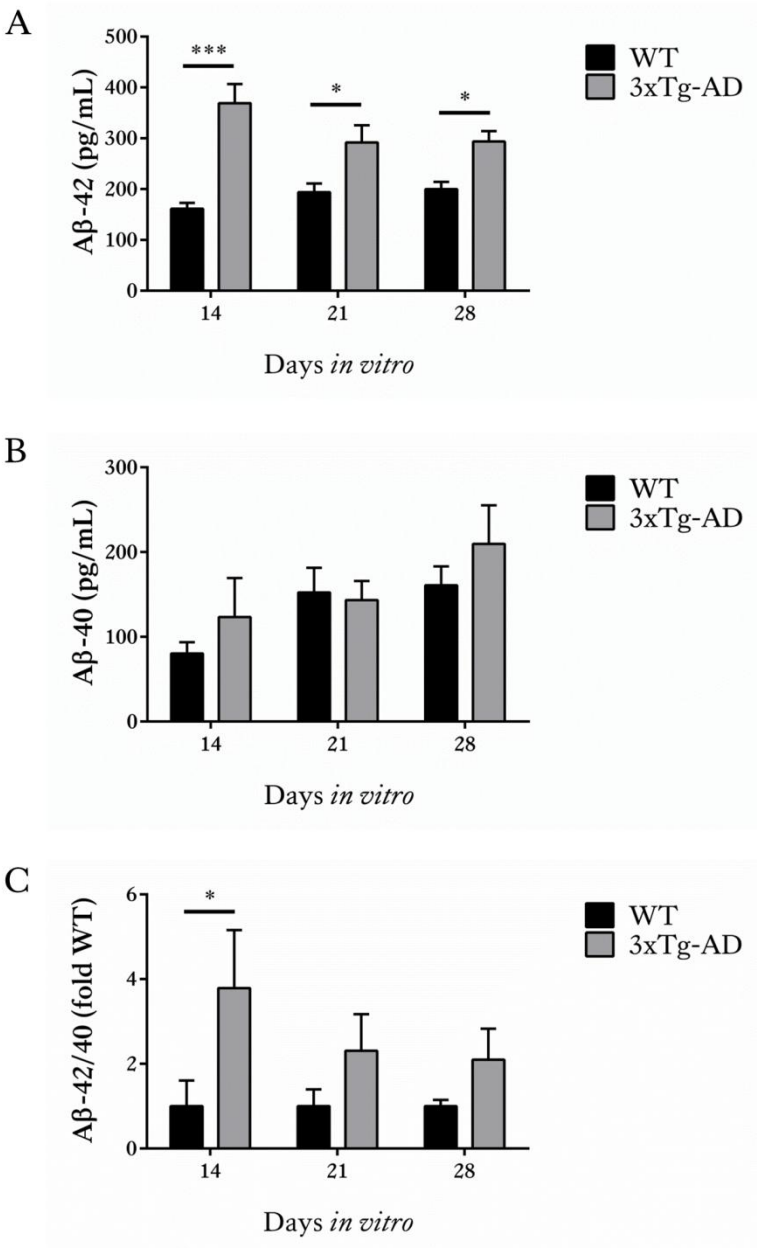

Figure 3.21: Amounts of Aβ-42 are increased in slice cultures from 3xTg-AD mice.
Amounts of Aβ-40 and Aβ-42 were measured in slice culture lysates prepared from WT and 3xTg-AD mice harvested at 14, 21, and 28 *div*. Bar charts show (A) amounts of Aβ-42 and (B) Aβ-40 in cortical lysates from 14, 21 and 28 *div* WT and 3xTg-AD slice cultures. Data are shown in pg/mL. (C) Bar chart shows amounts of Aβ-42 relative to Aβ-40. Data are shown as fold WT at each time point. Data is mean ± SEM (n=9 wells from three independent experiments, *p<0.05, ***p<0.001).

3.4.16 GSK-3 activity is not altered in 3xTg-AD organotypic brain slice cultures

GSK-3 is a ser/thr proline-directed kinase which is implicated in tau phosphorylation at numerous AD-relevant sites and is recognised as a major tau kinase (Hanger et al., 1992). Increased GSK-3 activity is found in post-mortem brain from AD patients, as well as in several animal models of AD (Noble et al., 2005, Leroy et al., 2007). Activity of GSK-3 is regulated in several ways, predominantly through phosphorylation of the inhibitory site ser 9 in GSK-3β or ser 21 in GSK-3α, which significantly decreases active site availability thereby reducing kinase activity (Sutherland et al., 1993).

Lysates from WT and 3xTg-AD slice cultures harvested at 14, 21 and 28 *div* were immunoblotted with an antibody which detects total amounts of GSK-3α and GSK-3β, and the amount of protein detected was standardised to β-actin amounts in the same sample. Levels of total GSK-3 were unchanged at 14, 21 and 28 *div* in both WT and 3xTg-AD slice cultures (Figure 3.22).

Levels of inactive GSK-3 were next quantified by probing immunoblots with an antibody which detects GSK-3α phosphorylated at ser 21 and GSK-3β phosphorylated at ser 9 (pser21/9). The amounts of phosphorylated GSK-3 detected were normalised to total amounts of GSK-3 in the same sample. No significant changes in the amounts of phosphorylated GSK-3 were detected with increasing time in culture in either WT or 3xTg-AD slice cultures (Figure 3.22).

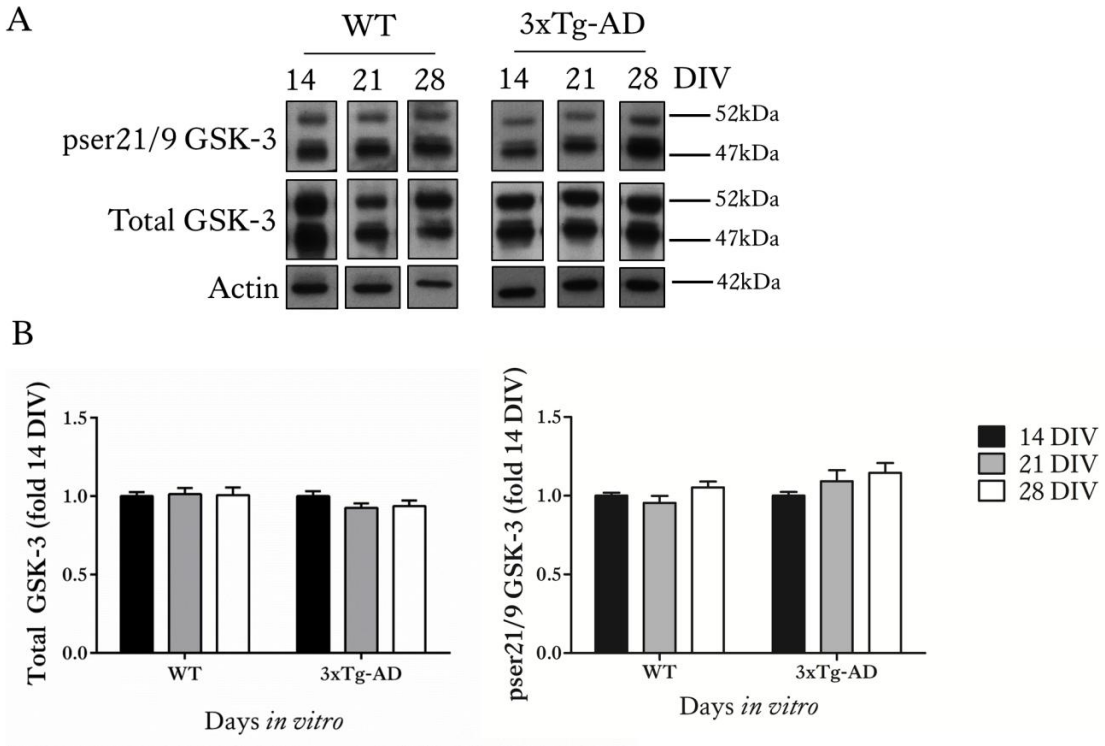

Figure 3.22: GSK-3 activity is not altered with increasing time in culture in WT and 3xTg-AD organotypic brain slice cultures.
(A) Representative western blots of total GSK-3α/β (47, 52 kDa), and pser21/9 GSK-3 in lysates prepared from WT and 3xTg-AD slice cultures harvested at 14, 21 and 28 *div*. An antibody against β-actin was used as a loading control (42 kDa). (B) Bar charts show amounts of total GSK-3α/β standardised to β-actin amounts in each sample, and amounts of pser21/9 GSK-3 normalised to total GSK-3α/β in each sample. Data are shown as fold change from 14 *div* for each genotype. Data is mean ± SEM, (n=12 wells from two independent experiments).

3.4.17 Increased p25/cdk5 is apparent with increasing time in culture in 3xTg-AD brain slice cultures

Cdk5 is another proline-directed tau kinase which, when activated by the neuron-specific activators p35, p39, p29 and p25 can drive pathological tau phosphorylation prior to, or independently of, tau aggregation (Tsai et al., 2004). Cdk5 is normally activated by p35, and this activation is often to be seen as more physiological due to its necessity for important roles in neuron outgrowth, development, stability and neuronal

transport (Tang et al., 1995). The calcium-activated cysteine protease calpain can cleave p35 to create the more stable proteolytic p25 fragment, which drives higher levels of cdk5 activity and increased amounts of p25 are found in pathological and neurotoxic conditions (Patrick et al., 1999, Lee et al., 2000). In addition, increased amounts of p25 are significantly increased in post-mortem AD brain and in transgenic animal models of AD, thereby resulting in upregulated cdk5 activity and tau phosphorylation (Tseng et al., 2002, Noble et al., 2003, Sy et al., 2011), although this is somewhat controversial in human brain studies (Tandon et al., 2003). It was important to examine cdk5 activation in WT and 3xTg-AD slice cultures to determine if cdk5 is important for the increased tau phosphorylation found in 3xTg-AD slice cultures (section 3.4.13).

Lysates of WT and 3xTg-AD slice cultures harvested at 14, 21 and 28 div were immunoblotted with an antibody against cdk5. Following normalisation to β-actin in the same sample, cdk5 levels were found to be unchanged with increasing time in culture in both WT and 3xTg-AD organotypic brain slice cultures (Figure 3.23).

The amounts of p35 and p25 were quantified by immunoblotting slice culture lysates from WT and 3xTg-AD mice with an antibody which recognises p35 and its proteolytic cleavage product, p25. The p35 and p25 bands detected were normalised to cdk5 amounts in each sample. There were no changes in p35/cdk5 or p25/cdk5 amounts with increasing time in culture in WT slices, and although not significant there was a trend towards increased p35/cdk5 in 3xTg-AD organotypic brain slice cultures at 21 and 28 *div* in 14 *div* cultures (Figure 3.23). In contrast, significant increases in p25/cdk5 were

apparent in 28 *div* 3xTg-AD slices in comparison to those at 14 *div* (Figure 3.23, $p<0.01$). An increase in p25/cdk5 was also noted in 21 *div* relative to 14 *div* 3xTg-AD slice cultures but this did not reach significance. These findings suggest that cdk5 activity may be, at least in part, responsible for the increased tau phosphorylation observed in 3xTg-AD brain slice cultures.

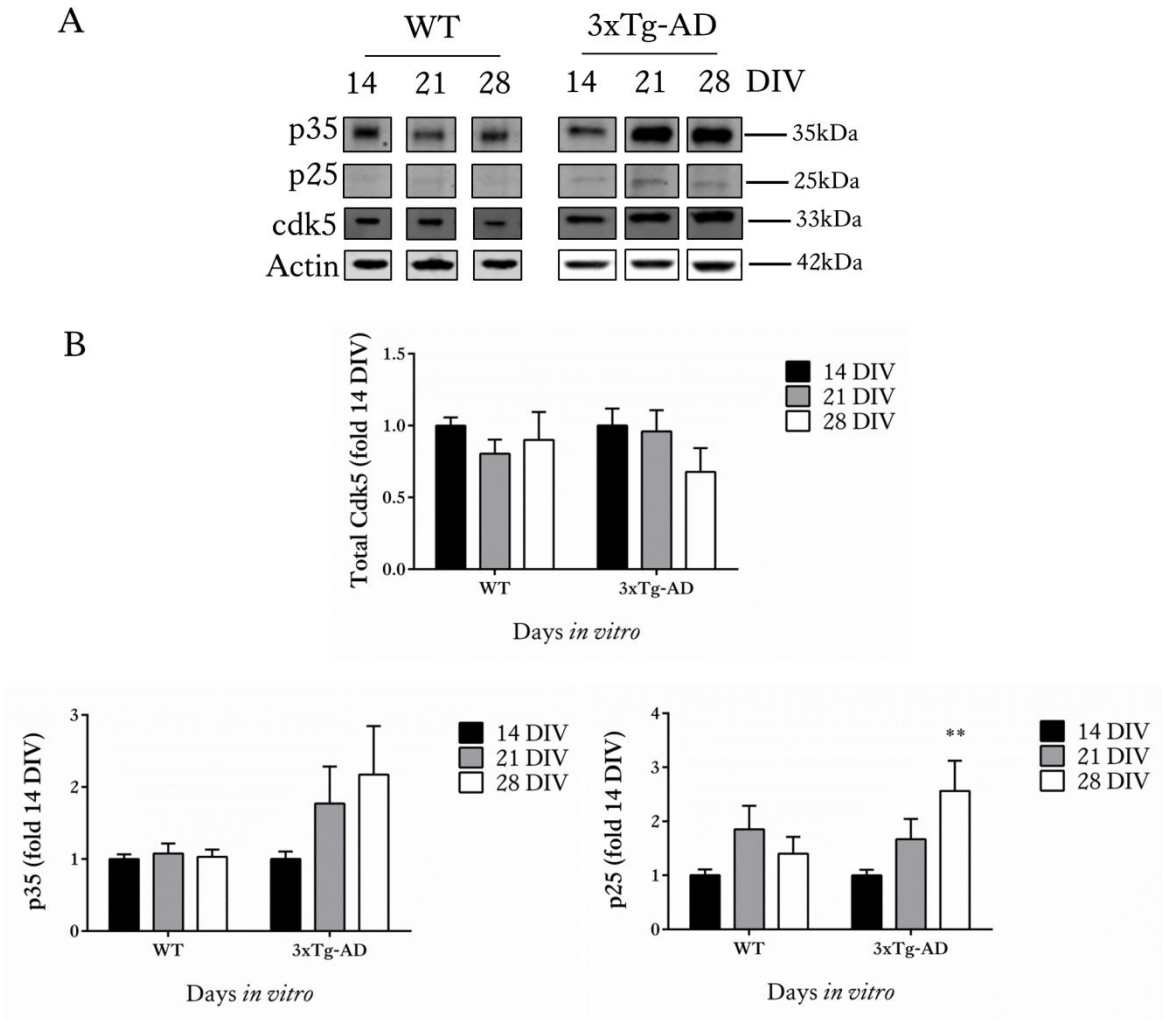

Figure 3.23: Increased p25/cdk5 is apparent with increasing time in culture in 3xTg-AD brain slice cultures.

(A) Representative western blots of total cdk5 (33 kDa), and p35/p25 (35 and 25kDa) in lysates prepared from WT and 3xTg-AD slice cultures harvested at 14, 21 and 28 div. An antibody against β-actin was used as a loading control (42 kDa). (B) Bar charts shows amounts of total cdk5 normalised to β-actin amounts in each sample, amounts of p35 relative to cdk5 in each sample, and amounts of p25 relative to cdk5 in each sample. Data are shown as fold change from 14 *div* for each genotype. Data is mean ± SEM, (n=12 wells from two independent experiments, **p<0.01).

3.4.18 Slice cultures from 3xTg-AD mice show no alterations in synaptic markers

In our colony of 3xTg-AD mice, amounts of the pre- and post-synaptic markers synaptophysin and PSD-95 were unaltered in the hippocampus compared to WT mice (section 3.4.8), despite previous reports of synaptic dysfunction and loss in this AD mouse model (Oddo et al., 2003b, Bittner et al., 2010).

To determine if there were any changes in synaptic markers in slice cultures, synaptosomes, enriched in synaptic proteins, were isolated from homogenised WT and 3xTg-AD slice cultures that were harvested at 14, 21, and 28 *div.* Levels of the pre-synaptic marker synaptophysin and the post-synaptic marker PSD-95 in the synaptosomes were detected by immunoblotting. This is thought to be an indicator of the number of functional synapses (Masliah et al., 2001).

Following normalisation to β-actin, the amounts of synaptophysin and PSD-95 did not significantly differ between WT and 3xTg-AD slice cultures at 14, 21 or 28 *div* (Figure 3.24). In addition, no significant changes in amounts of synaptophysin or PSD-95 were seen in WT slices with increasing time in culture. A slight trend towards increased amounts of synaptophysin and PSD-95 was found in 3xTg-AD slices maintained for 21 and 28 *div* but these changes were not significant (Figure 3.24). This finding indicates that there is no loss of functional synapses in 3xTg-AD slices maintained for up to 28 *div.*

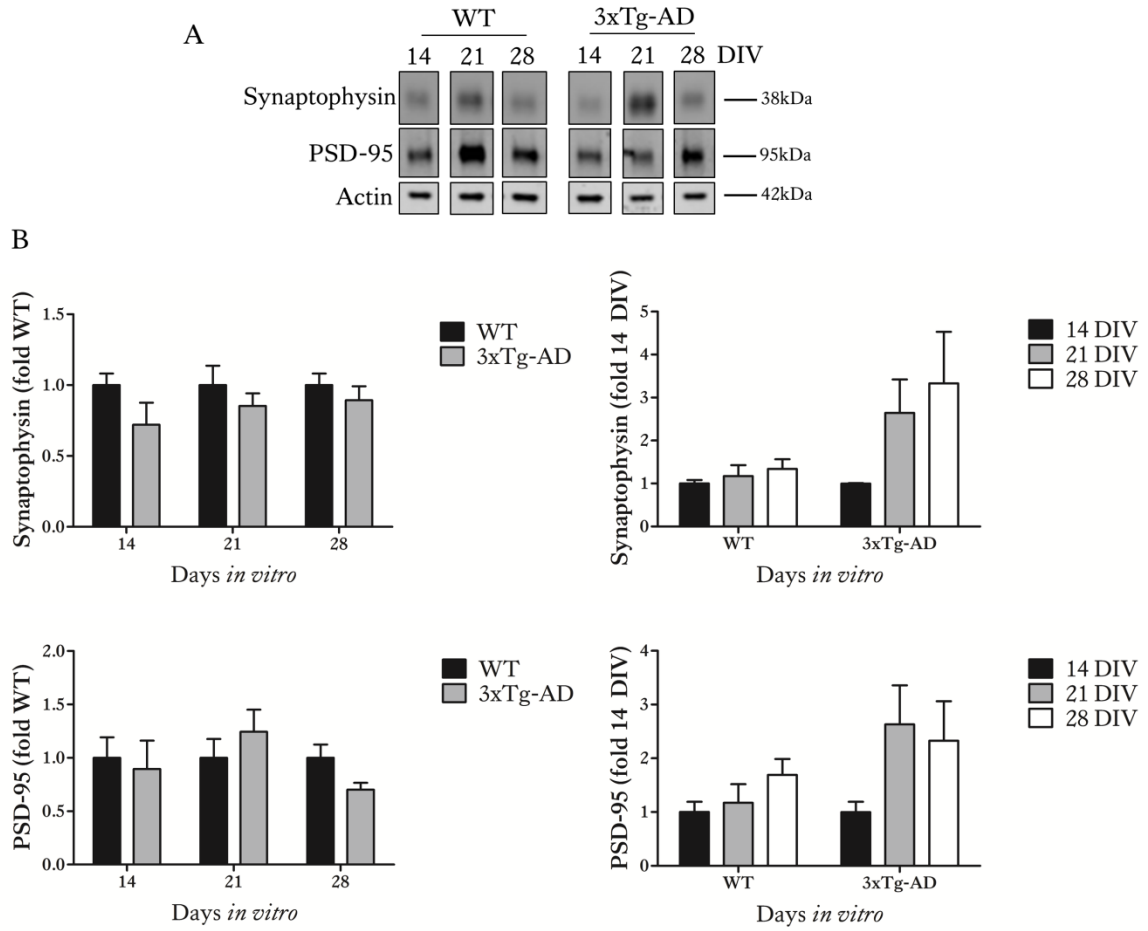

Figure 3.24: Levels of pre- and post- synaptic markers are unaltered in WT and 3xTg-AD slice cultures.

(A) Representative western blots of synaptosome fractions prepared from 14, 21, and 28 *div* WT and 3xTg-AD slice cultures, probed with antibodies against synaptophysin (38 kDa) and PSD-95 (95 kDa). An antibody against β-actin was used as a loading control (42 kDa). (B) Bar charts show amounts of PSD-95 and synaptophysin following normalisation to β-actin in each sample. Data on the left are shown as fold change from WT slices at each time point. Data on the right are shown as fold change from 14 *div* for each genotype. Data is mean ± SEM, (n=9 wells from three independent experiments).

3.4.19 Tau, but not APP, is increased at the synapse in 3xTg-AD slice cultures

In our 3xTg-AD colony, we found early increases in amounts of tau and APP in enriched synaptosomes prepared from hippocampal-containing brain regions of 3xTg-AD mice relative to WTs (Figure 3.11). To examine these features in slice cultures, synaptosomes prepared from 14, 21 and 28 *div* WT and 3xTg-AD slice cultures were immunoblotted for total (phosphorylated and non-phosphorylated) tau, and total APP (N-terminal).

Following normalisation to β-actin, synaptosomes from 3xTg-AD slice cultures were found to contain significantly higher amounts of tau at 14 *div* compared to WT slice cultures (Figure 3.25, $p<0.01$), and non-significant increases in synaptic tau were also apparent at 21 and 28 *div*. There were no significant changes in the amounts of APP in synaptosomes between WT and 3xTg-AD slices at any age. Neither were there any changes in synaptic tau or APP amounts with increasing time in culture in WT or 3xTg-AD slices (Figure 3.25).

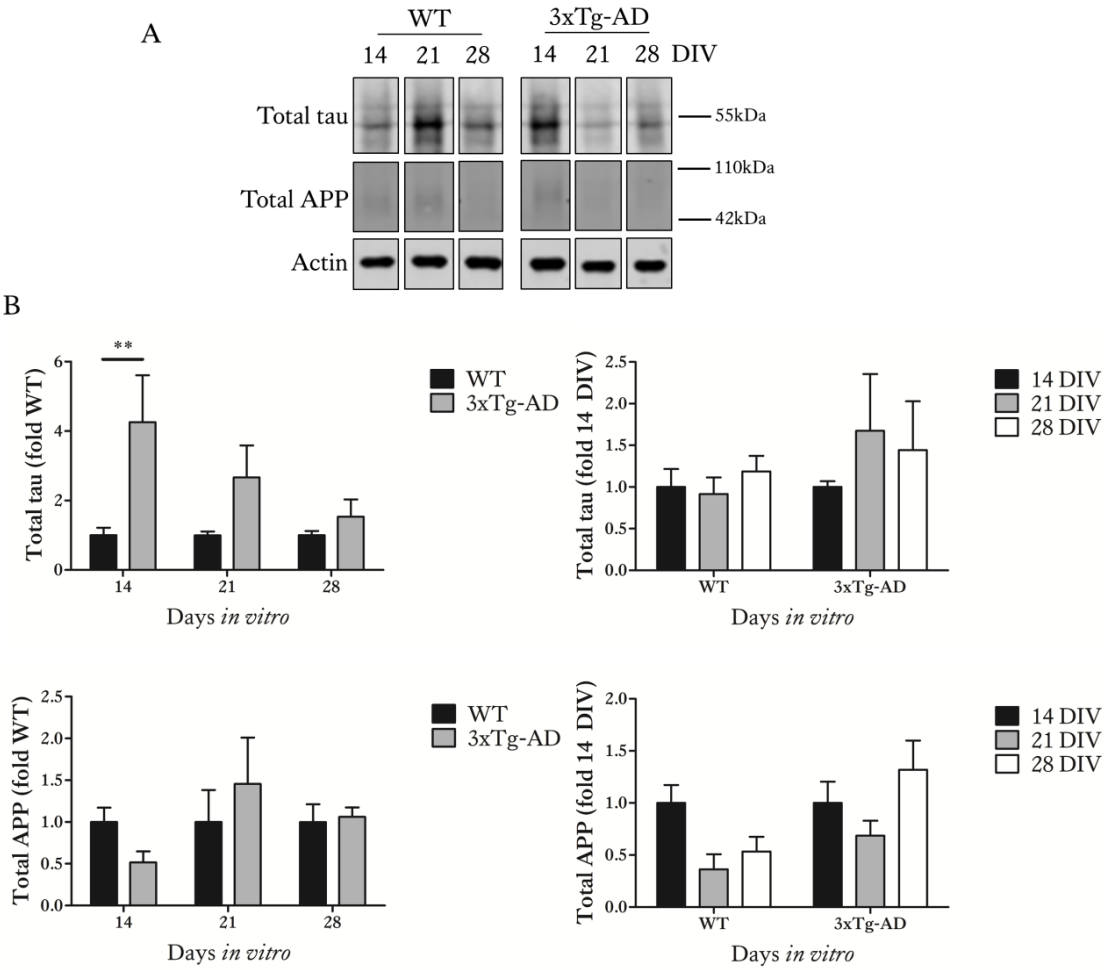

Figure 3.25: Tau is increased at the synapse in 3xTg-AD slice cultures
(A) Representative western blots of synaptosome fractions prepared from 14, 21, and 28 *div* WT and 3xTg-AD slice cultures blotted with antibodies against total APP (90-120 kDa) and total tau (50-64 kDa). An antibody against β-actin was used as a loading control (42 kDa). (B) Bar charts show amounts of total APP and total tau, both normalised to β-actin amounts in each sample. Data on the left are shown as fold change from WT slice cultures at each time point. Data on the right are shown as fold change from 14 *div* for each genotype. Data is mean ± SEM, (n=9 wells from three independent experiments, **p<0.01).

3.5 Summary

The main findings presented in this chapter are that 3xTg-AD organotypic brain slice cultures maintained for up to 28 *div* display some key features of human AD that are also observed in 3xTg-AD mice *in vivo* (Table 3.1). Particularly, it was apparent that the development of some disease features, most notably pathological changes in tau, are accelerated *ex vivo*.

Table 3.1: Summary of AD-like features that develop in 3xTg-AD slice cultures, in comparison to those observed *in vivo* and in human AD brain.

Pathology	Human AD	3xTg-AD *In Vivo*	3xTg-AD *Ex Vivo*
Total tau	Increased total tau protein in human AD (Khatoon et al., 1994, Sjogren et al., 2001).	Tau is transgenically over-expressed - section 3.4.2 and (Oddo et al., 2003a).	Tau over-expression is apparent in slices cultured for 21 and 28 *div* (Section 3.4.11).
Phosphorylated tau	Tau phosphorylation is increased at several epitopes in human AD brain, including ser 202 and ser 396/404 (Wolozin et al., 1986, Su et al., 1994, Iqbal et al., 2005).	Tau phosphorylation was previously reported to be increased in 12 to 15 month old mice (Oddo et al., 2003a). In the colony examined here, increased tau phosphorylation at ser 396/404 was observed in the hippocampus, but not the cortex, of 12 month old mice (sections 3.4.5 and 3.4.6).	Tau phosphorylation at ser 202 and ser 396/404 is significantly increased (section 3.4.13).
High molecular weight tau/ tau aggregates	Characteristic high molecular weight tau, tau aggregates and NFTs in human AD (Grundke-Iqbal et al., 1986).	High molecular weight tau and sarkosyl-insoluble aggregated tau detected in 12 month old mice here (section 3.4.7), and, together with tau aggregates and NFTs, in 18 month old mice (Oddo et al., 2003a).	High molecular weight tau (64 kDa) is found at 21 and 28 *div* (section 3.4.12).

APP	Total amounts of APP are unaltered (Nordstedt et al., 1991), however, altered APP processing is apparent (O'Brien and Wong, 2011).	APP is transgenically over-expressed - section 3.4.3 and (Oddo et al., 2003a).	APP is transgenically over-expressed (section 3.4.14).
Aβ-40 and Aβ-42	Increased amounts of Aβ-40 and Aβ-42 are deposited in senile plaques (Glenner and Wong, 1984, O'Brien and Wong, 2011).	Significantly increased levels of Aβ-42 at 12 months of age in our colony (section 3.4.4.), and increased Aβ and plaque deposition reported from 6 months of age by others (Oddo et al., 2003a, Oddo et al., 2003b).	Significantly increased levels of Aβ-42 by 14 *div* (section 3.4.15).
GSK-3 activity	Disparities in the literature. Increased GSK-3 activity detected by some (Leroy et al., 2007) but not others (Pei et al., 1997).	Not examined here. Others report that GSK-3 activity is increased by 15 months of age (Sy et al., 2011, Kazim et al., 2014).	No change in GSK-3 activity (section 3.4.16).
Cdk5 activity	Increased cdk5 activity (Tseng et al., 2002). Increased p25 amounts (Patrick et al., 1999), but this is controversial (Tandon et al., 2003).	Not examined here. Cdk5 activity reported by others as increased by 12 months of age (Sy et al., 2011).	Increased p25/cdk5 in 28 *div* slices (section 3.4.17).
Synaptic dysfunction	Levels of synaptophysin and PSD-95 are reduced (Masliah et al., 2001, Proctor et al., 2010).	No changes in PSD-95 or synaptophysin (section 3.4.8). Decreases in PSD-95 and synaptophysin reported at 13 months of age (Revilla et al., 2014).	No changes in amounts of PSD-95 and synaptophysin (section 3.4.18).
Tau at the synapse	Tau is found at the synapse in both control and AD patients, however, phosphorylated tau species are only found in AD synapses (Tai et al., 2012).	Levels of total tau at the synapse increased in 1 and 2 month old mice, reducing to WT levels at 4, 9 and 12 months of age (section 3.4.9).	Increased tau at the synapse in 14, but not 21 or 28 *div* slice cultures (section 3.4.19).
APP at the synapse	APP is not increased in AD synapses (Gylys et al., 2004).	Increased presence of APP at the synapse at 1, 2 and 9 months of age (section 3.4.9).	No change in APP amounts at the synapse (section 3.4.19).

3.6 Discussion

The work described in this chapter was conducted to characterise disease-associated changes in Aβ, tau and synapses over time *in vivo* in our colonies of WT and 3xTg-AD mice, in comparison to organotypic brain slice culture models produced from these mice.

3.6.1 The disease phenotype in our 3xTg-AD colony is similar to that previously reported

Our 3xTg-AD colony displayed a progressive development of relevant, and previously reported AD-like changes, which recapitulate features of human AD. The majority of this data corroborates others' findings; however a few disparities were apparent.

Firstly, although it is evident from genotyping and immunoblots that our 3xTg-AD colony overexpress tau and APP, the changes in the expression of these proteins was quite mild and was deemed only to be significantly different from WTs rarely. This likely reflects variations between animals in each group when taking into account the small group size available for this work (n=3). Our 3xTg-AD colony show significantly higher levels of Aβ-42 in the cortex by 12 months of age, as reported previously in 3xTg-AD mice (Oddo et al., 2003b, Oddo et al., 2003a). At 4 months of age in our 3xTg-AD colony, no changes in levels of Aβ-42, Aβ-40 or Aβ-42/40 in the cortex were detected, as predicted from previous findings (Oddo et al., 2003b). Similarly, Aβ-40 and Aβ-42/40 were not elevated in the cortex in our 3xTg-AD colony at 12 months of age, which agrees with previous

reports that the increases in these parameters are first apparent at 13 months of age (Oddo et al., 2003b).

Furthermore, tau pathology in our 3xTg-AD colony follows a similar spatiotemporal progression as reported in previous literature. Indeed, tau in an abnormal (MC1) conformation, one of the early changes observed in tau in AD brain (Weaver et al., 2000), and increased tau phosphorylation at ser 396/404 were detected in the hippocampus of our 3xTg-AD mice at 12 months of age, at the same time, increased levels of sarkosyl-insoluble tau were detected in the amygdala. No changes in tau phosphorylation were detected in the cortex at this age, which again corroborates previous reports of tau pathology developing in the hippocampus prior to the neocortex (Oddo et al., 2003b), similar to in human AD (Braak and Braak, 1995).

Lastly, no loss of amounts of the synaptic markers, synaptophysin and PSD-95 in the hippocampus was detected at any age of 3xTg-AD brain studied here. This is in agreement with some previous reports which describe no reductions in synaptophysin or PSD-95 in whole brain 3xTg-AD lysates at 9 months of age (Chen et al., 2014). However, synaptic dysfunction in the hippocampus is clearly apparent in other 3xTg-AD colonies at 6 months of age (Oddo et al., 2003b) including reports that synaptophysin is reduced in the cortex, but not in the hippocampus at 6 to 7 months of age (Hedberg et al., 2010), and that PSD-95 and synaptophysin are subtly but significantly reduced in the hippocampus by 13 months of age (Revilla et al., 2014). Thus, there is clearly some variation between individual colonies of these mice, which may explain the results

obtained in this work. It is not possible to exclude the possibility that there could be synaptic changes in our colony of 3xTg-AD mice since synaptic dysfunction does not necessarily result in a rapid loss of functional synapses, and an associated loss of synaptic markers, but could instead arise from subtle changes in the size and distribution of synaptic coupling (Barnes, 1999).

In summary, these findings suggest that our colony of 3xTg-AD mice show progressive development of AD-like Aβ and tau abnormalities by 12 months of age, as would be expected from previous reports.

3.6.2 *Ex vivo* 3xTg-AD organotypic brain slice cultures can survive at least 28 *div* and faithfully recapitulate key features of AD pathology

Slice cultures from 3xTg-AD mice were successfully cultured for up to 28 *div* for the first time and these developed similar AD-like abnormalities as the 3xTg-AD mice from which they are derived. In particular, the over-production of Aβ-42 and the progressive accumulation of phosphorylated and aggregated tau are recapitulated in 3xTg-AD slice cultures. The presence of these features was associated with alterations in kinase activity and an early accumulation of tau at the synapse.

Slice cultures from 3xTg-AD mice show significantly increased levels of Aβ-42, another feature of human AD brain (O'Brien and Wong, 2011), which is also found in 3xTg-AD mice *in vivo* from 6 months of age (Oddo et al., 2003a). Since pro-aggregatory Aβ-42 is considered to be the most toxic species of Aβ (Zhang et al., 2011b), the rapid

accumulation of Aβ-42 in 3xTg-AD slice cultures may suggest that they are a particularly relevant method for assessing Aβ-directed therapies for AD.

In addition, slice cultures from 3xTg-AD mice aged in culture for up to 28 days show significantly increased amounts of high molecular weight tau and tau phosphorylated at ser 202 and ser 396/404 compared to slice cultures produced from WT mice. These human AD-like changes (Wolozin et al., 1986, Su et al., 1994, Barghorn et al., 2000, Sjogren et al., 2001, Iqbal et al., 2005) are all found *in vivo* in this transgenic mouse line but not until the mice are considerably older (Oddo et al., 2003a, Oddo et al., 2003b).

GSK-3 is a prominent tau kinase, recognised to phosphorylate many of the residues of tau that are abnormally phosphorylated in AD (Hanger et al., 1992). *In vivo,* 3xTg-AD mice show significantly decreased phosphorylation of ser 21/9 GSK-3, and therefore increased GSK-3 activity, at 15 months of age compared to younger transgenics and age-matched WT controls (Sy et al., 2011). Increased GSK-3 activity indicated by the inhibitory phosphorylation of ser 21/9 GSK-3 (Sutherland et al., 1993) was unaltered in 3xTg-AD slice cultures, suggesting that GSK-3 may not contribute to tau phosphorylation in these slice cultures. However, there are several mechanisms leading to GSK-3 activation (Wang et al., 1994, Ryves and Harwood, 2001), not all of which were studied here, so a contribution of GSK-3 to tau phosphorylation in 3xTg-AD slice cultures cannot be completely discounted.

Significantly increased amounts of the cdk5 activator p25, but not p35, relative to cdk5 were found in 3xTg-AD slice cultures. This recapitulates *in vivo* findings in this AD transgenic line where significantly increased p25 is found in 12 month old mice compared to 3 month old mice (Sy et al., 2011). Again, this finding recapitulates the increased cdk5 activation by p25 reported in human AD brain (Tseng et al., 2002), although the human brain findings are highly controversial (Tandon et al., 2003). This data suggests that the 3xTg-AD slice culture model may also be useful for investigating therapeutic strategies based on p25/cdk5 inhibitors, such as the cdk5 inhibitory peptide, CIP (Sundaram et al., 2013).

Levels of the synaptic markers, synaptophysin and PSD-95, were not significantly different between WT and 3xTg-AD slice cultures, or over time in culture. This is not unexpected, as no differences in synaptic marker amounts were detected between genotypes *in vivo* in our colony, and only subtle but significant reductions have been shown in 13 month old 3xTg-AD mice (Revilla et al., 2014). Loss of synapses is the most accurate neuropathological correlate of loss of cognition in AD (Terry et al., 1991), however measurement of synaptic markers is not the most sensitive method of detecting synapse loss, and synaptotoxicity may have been better studied using alternative methods, for example, quantification of spine size and number (Rochefort and Konnerth, 2012).

Overall, disease features in slice cultures from 3xTg-AD mice develop much more rapidly than those observed *in vivo* in our colony and those reported *in vivo* previously. It is

plausible to suggest that the disease features observed in 14, 21 and 28 *div* slice cultures recapitulate those found *in vivo* at approximately 6, 9 and 12 months of age. These estimates are provided on the basis that Aβ-42 levels are increased at 14 *div* in slice cultures and at 6 months *in vivo* (Oddo et al., 2003a), whilst increased tau phosphorylation is found at 28 *div* in slice cultures and at 12 months *in vivo* (Oddo et al., 2003a), in the absence of any changes in levels of synaptic markers (section 3.4.8). The reasons for this rapid development of AD-like features in slice cultures remain unclear, however one may speculate that the culture environment may promote oxidative stress and encourage the acceleration of this disease phenotype (Sundstrom et al., 2005, Butterfield et al., 2002).

3.6.3 Increased APP and tau at synapses may be early disease features in 3xTg-AD mice

The results presented here show for the first time that total amounts of APP and tau are significantly increased in the synapse at an early age. Significantly increased amounts of APP and tau were found at early ages (1, 2 and 9 months, 1 and 2 months, respectively) in enriched synaptosomes of the hippocampus of 3xTg-AD mice in comparison to age-matched WT controls. In addition, significantly increased tau amounts were found in enriched synaptosomes of 3xTg-AD slice cultures at 14 *div* but not at 21 or 28 *div*.

In human AD, total tau (Tai et al., 2012, Tai et al., 2014) and APP (Gylys et al., 2004) amounts at the synapse do not differ from controls. However, tau at the synapse is phosphorylated and misfolded in human AD (Tai et al., 2014) and Aβ is also found at the

synapse in human AD (Fein et al., 2008). Similarly, in mice expressing mutant FTD-linked P301L tau, phosphorylated tau is found at the synapse (Harris et al., 2012, Kopeikina et al., 2013), and only P301L tau, but not WT tau, is targeted to spines (Xia et al., 2015).

It is plausible that during the course of AD, increased phosphorylation of tau and misfolding of tau occur at the synapse, potentially as a result of mislocalisation of tau that has detached from microtubules upon increased phosphorylation. Synaptic tau may be synaptotoxic and prevent physiological functions of tau at the synapse, mechanisms that are presently poorly understood (Crimins et al., 2013).

Increased amounts of APP were also found in synaptosomes prepared from the hippocampus of 3xTg-AD mice at 1, 2 and 9 months, but no changes were found in 3xTg-AD slice cultures at 14-28 *div*. In human AD brain, APP amounts at the synapse are similar to control levels (Gylys et al., 2004), however increased amounts of Aβ are found at the synapse in human AD brain (Fein et al., 2008). Taken together, this might suggest that early increases in APP amounts at synapses in AD may precede APP processing via the amyloidogenic pathway (Zhang et al., 2011b) to generate increased amounts of Aβ which are retained at the synapses throughout AD. This build-up of Aβ at the synapse is likely detrimental to synapse health and function in AD (Sheng et al., 2012).

3.6.4 Limitations of this work

Although overall disease progression was similar in our colony to that reported by others (Oddo et al., 2003a, Oddo et al., 2003b) some of the results failed to reach statistical

significance, despite clear changes being apparent on immunoblots. This is likely a reflection of the small sample size available for this analysis (n=3), and variation between samples within groups, typical of transgenic colonies.

At the outset of the project, the intention was to culture slices for much longer periods of time, since successful culture up to 6 months had previously been reported (Duff et al., 2002). However, slices cultured beyond 28 *div* showed a rapid death rate with the majority suddenly dying at around 30 *div*, and only a few slice cultures were able to survive up to 2/3 months *in vitro.* It is difficult to ascertain exactly why slice health was compromised after 30 *div.* Previous studies in the laboratory group routinely maintained slices for 5-6 months (Dawn Lau, 2014; PhD thesis). The slices in this previous study were prepared in exactly the same way as in this project, so the problems were unlikely to have been due to the methodology used. However, it is possible that one of the reagents used could have been a factor. The slice culture inserts used in this project were sourced from Millipore. These were very reliable in the past, and preliminary work undertaken as part of this project showed that PET membrane alternatives from BD Falcon Ltd. were not as efficient in promoting the health of slice cultures. Notably, at around the time the project started the description of this product on the Millipore website first included the information that "The Biopore™ (PTFE) membrane provides high viability - for as long as 40 days - and excellent trans-membrane oxygen transport", the text "- for as long as 40 days -" was not previously a part of the product overview. The laboratory queried this addition, but we were not able to determine whether or not the composition of the inserts had been altered such that they were no longer able to

support slice culture up to 6 months. In addition, there were issues with the tissue culture facilities being used for the culture of slices. These included problems with the manifolds used to automatically switch from one CO_2 cylinder to another when one emptied. Such an event occurs on a regular basis, and it is possible that manifold failure resulted in insufficient CO_2 levels for a period of time which affected slice health. There were also several occasions on which fans that control air-flow through the tissue culture hoods malfunctioned and this would have affected the sterility of the tissue culture hoods. Since slice culture medium is changed every 2-3 days, it is possible that infections were obtained whilst in the tissue culture hoods which also affected slice health. Finally, several of the incubators used for this work, although carefully monitored, developed issues with humidity. It was believed that this might have contributed to slice death, but this was not formally assessed.

Additionally, several antibodies to detect PS1, sAPPα, sAPPβ, C83 and C89 were used in order to further characterise our 3xTg-AD colony and the 3xTg-AD slice cultures compared to their WT counterparts and over time; however for reasons beyond our control, the proteins of interest were not detected in the time-scale of the project.

3.6.5 Conclusions

In conclusion, the results presented in this chapter suggest that organotypic brain slice cultures prepared from 3xTg-AD mice provide a novel *ex vivo* alternative to *in vivo* experiments aimed at investigating the mechanisms underlying AD, and for testing potential new therapies. 3xTg-AD slice cultures faithfully recapitulate several AD-like

features, and they demonstrate a rapid progression of the disease phenotype compared to their *in vivo* counterparts. The following chapter extends these results by investigating the utility of 3xTg-AD slice cultures as a platform for pre-clinical testing of AD treatments.

Chapter 4 : Organotypic brain slice cultures as a tool for AD drug discovery

4.1 Introduction

Organotypic 3xTg-AD brain slice cultures show conservation of some of the key AD-like features that develop over time *in vivo* (Chapter 3). It was next important to determine if this brain slice culture model has utility for AD drug screening and pre-clinical development.

3xTg-AD mice have been used to test the efficacy of several candidate AD drugs. For example:

- Tau-directed therapies: Treatment of 12 month old 3xTg-AD mice for 3 months with the GSK-3 inhibitor, LiCl, was shown to reduce phosphorylation of tau at several sites; thr 181, ser 202 and thr 205, thr 231, and thr 212 and ser 214, but not ser 396/404. Levels of soluble and insoluble Aβ-40 and Aβ-42, and Aβ-positive plaque load were not reduced by LiCl (Caccamo et al., 2007), in contrast to previous publications (Su et al., 2004), nor did LiCl recover working memory in 3xTg-AD mice (Caccamo et al., 2007).
- Microtubule-stabilising drugs/neuroprotective agents: neuroprotective effects of the peptide NAPVSIPQ, previously reported to maintain microtubule stabilisation in mutant tau (P301S; K257T) over-expressing transgenic mice (Shiryaev et al., 2009), were investigated over a 3 month treatment period in 12 month old 3xTg-

AD mice. NAPVSIPQ lowered levels of Aβ-40 and Aβ-42 and also reduced phosphorylation of tau at ser 202/thr 205 and thr 231, but not at ser 202 alone. As well as these changes in pathological protein accumulations, improvements in memory were also observed following NAPVSIPQ treatment (Matsuoka et al., 2007).

- Aβ-targeted therapies: BTA-EG_4 is an amyloid-binding drug which reduces Aβ-induced toxicity *in vitro* (Habib et al., 2010). BTA-EG_4 can cross the blood brain barrier and reduce production of Aβ-40, whilst also increasing synaptic density and function in WT mice *in vivo* (Megill et al., 2013). A 2 week treatment of 6 to 10 month old 3xTg-AD mice with BTA-EG_4 was found to decrease increase spine density, drive other alterations in spine morphology and improve cognitive performance (Song et al., 2014). Effects of this compound on tau and kinase activity have not yet been reported.

4.2 Aims and objectives

The aims of the studies presented in this chapter were to investigate the effects of the therapeutic strategies described above (LiCl, NAPVSIPQ, and BTA-EG_4) in 3xTg-AD organotypic brain slice cultures. These studies should elucidate whether or not 3xTg-AD slice cultures are a useful tool for AD drug discovery and development. The primary aims of this chapter were to:

- Use primary cortical neurons to identify effective and non-toxic treatment conditions for LiCl, NAPVSIPQ and BTA-EG_4, for subsequent use in organotypic brain slice culture experiments.

- Treat 3xTg-AD brain slice cultures with LiCl, NAPVSIPQ and BTA-EG_4 to assess the effectiveness of these treatments on relevant AD-like phenotypes, and to further explore their modes of action.

- Determine whether the effects of drug administration to 3xTg-AD organotypic brain slice cultures recapitulates the published effects of the same treatments *in vivo,* providing data in support of the use of 3xTg-AD brain slice cultures as a relevant and sensitive model for pre-clinical AD drug testing.

4.3 Methods

The methods used in this work are detailed in Chapter 2. In brief, embryonic day 18 rat primary cortical neurons were cultured for between 7 and 14 *div* and treated with LiCl, NAPVSIPQ and BTA-EG_4 for 4, 24, and 24 hours, respectively. At 7 *div,* primary cortical neuron cultures contain approximately 4% astrocytes and 0.01% microglia, at 14 *div*, cultures contain approximately 15% astrocytes and 0.01% microglia (Garwood et al., 2011). Cell viability was determined using live/dead cell assays (section 2.2.5), and biochemical analysis of AD-relevant protein and synaptic changes were also investigated (section 2.2.4). Organotypic brain slice cultures containing the cortex, hippocampus and

connecting regions were prepared from p8/9 3xTg-AD mice and cultured for 28 days. Slice cultures were then treated with LiCl, NAPVSIPQ and BTA-EG_4, for 4, 24 and 48 hours, respectively. The effects of treatments were assessed by measuring LDH release from slices as an indicator of cell viability (Section 2.2.5) and biochemical changes, as described above.

4.4 Results

4.4.1 LiCl is not toxic to primary cortical neurons

A live/dead cell assay was performed to assess any toxicity resulting from treatment of 10 *div* primary cortical cultures for 4 hours with 1-40 mM LiCl. In this assay, the fluorescent dead cell dye is taken up by cells with compromised membranes, and the levels of fluorescent dye remaining after washing can be visualised and quantified as a measure of cell death. The results of these experiments showed no increases in cell death after application of 1-40mM LiCl in comparison to vehicle (20mM NaCl)-treated control cultures (Figure 4.1).

Immunolabelling of fixed cells identified basal levels of cell death in these cultures as being largely neuronal, as indicated by a lack of colocalisation between the dead cell dye and GFAP-labelled astrocytes. In addition, there were no apparent increases in GFAP immunoreactivity indicating that LiCl has not activated astrocytes in these cultures (Figure 4.1).

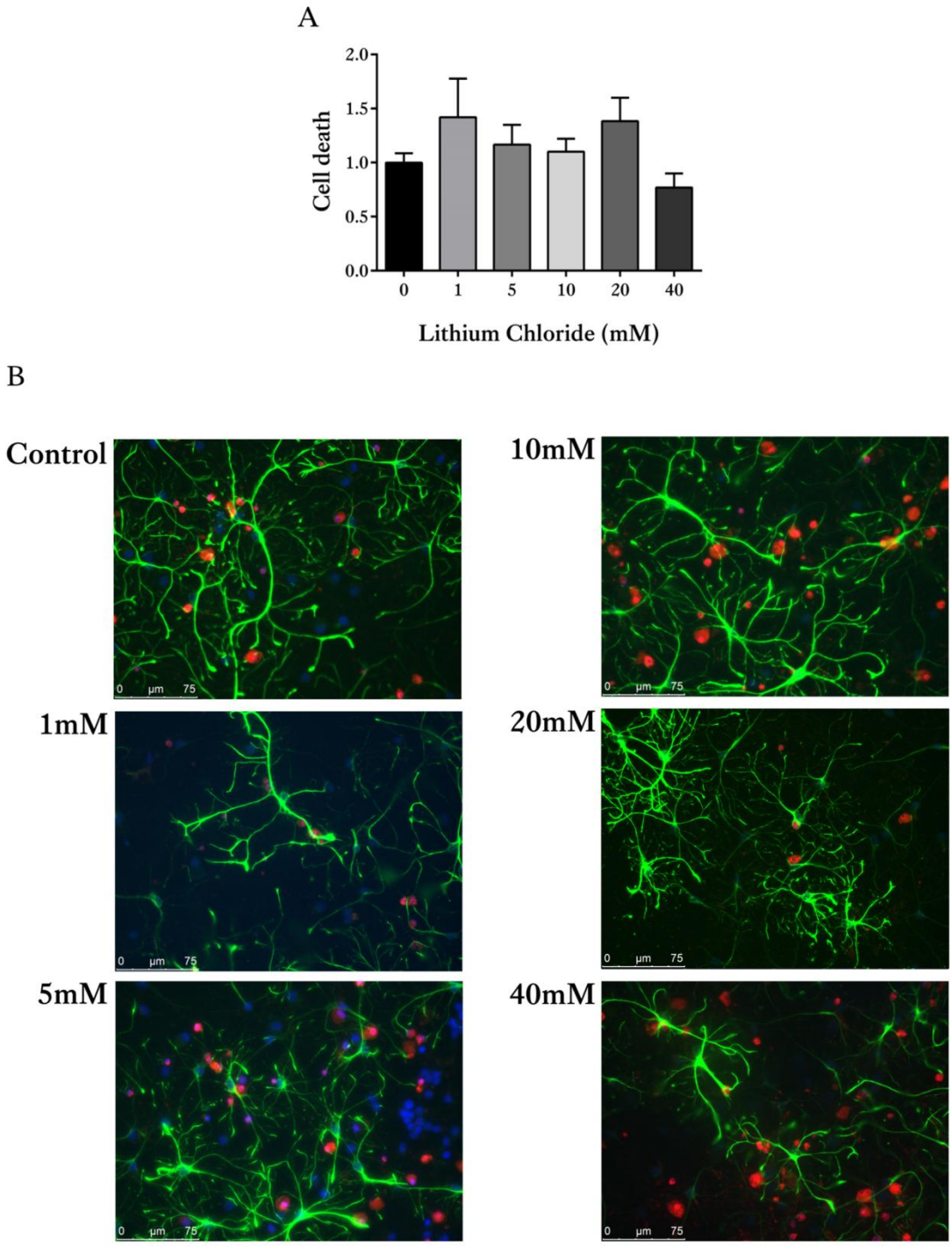

Figure 4.1: Lithium treatment is not toxic in primary cortical cultures.
(A) Bar chart shows levels of cell death, measured by incorporation of dead cell dye, following treatment of 10 div primary cortical cultures with 1-40mM LiCl or control (20mM NaCl) for 4 hours. Data is shown as fold change from control. Data is mean ± SEM, (n=9 wells from three independent experiments). (B) Representative images from these analyses showing incorporation of the dead cell dye (red), astrocytes immunolabelled using an antibody against GFAP (green) and Hoechst 33342 staining of cell nuclei (blue). Scale bar: 75µm.

4.4.2 LiCl inactivates GSK-3 in primary cortical neurons

LiCl is a known inhibitor of GSK-3 (Noble et al., 2005) and GSK-3 is a major tau kinase that is implicated in AD pathogenesis (Hanger et al., 1992). To demonstrate that LiCl inhibits GSK-3 activity in the primary cortical cultures, lysates from treated cells were immunoblotted with antibodies specific to total (phosphorylated and non-phosphorylated) GSK-3α/β and GSK-3α/β phosphorylated at ser 21/9, respectively. These are sites of inhibitory phosphorylation on GSK-3 (Sutherland et al., 1993); therefore increased phosphorylation of GSK-3 at ser 21/9 indicates inhibition of kinase activity. Immunoblotting with these antibodies revealed bands of approximately 47 and 52 kDa corresponding to the expected sizes of GSK-3β and α, respectively. Treatment of primary cultures with LiCl did not affect total GSK-3 levels relative to that detected in vehicle-treated cell lysates (data not shown). However, 20 mM and 40 mM LiCl significantly increased GSK-3 phosphorylation at ser 21/9 when normalised to levels of total GSK-3 in the same sample, thereby indicating that 20 and 40 mM LiCl is sufficient to significantly inhibit GSK-3 activity in primary cortical cultures (Figure 4.2, $p<0.05$, $p<0.001$).

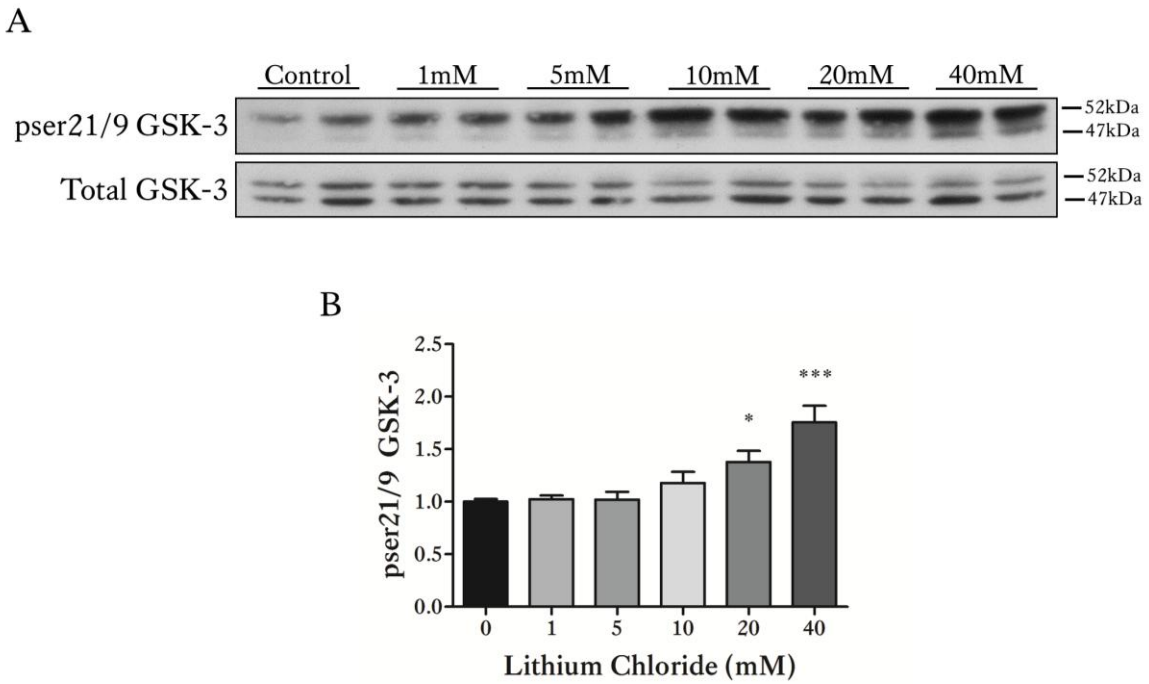

Figure 4.2: Lithium chloride treatment inactivates GSK-3 in primary cortical neurons. (A) Representative western blots of lysates from LiCl- or control (NaCl, 20mM)-treated primary cortical neurons showing total (phosphorylated and non-phosphorylated) GSK-3α/β and GSK-3α/β phosphorylated at ser 21/9 (47 and 52 kDa). (B) Bar chart shows amounts of GSK-3α/β phosphorylated at ser 21/9 following normalisation to total GSK-3 in each sample. Data are shown as fold change from control. Data is mean ± SEM, (n=6 wells from two independent experiments, *p<0.05, ***p<0.001).

4.4.3 LiCl decreases tau phosphorylation in primary cortical neurons

The effect of LiCl on amounts of total and phosphorylated tau was assessed. Total tau (phosphorylated and non-phosphorylated) and tau phosphorylation-dependent primary antibodies were used to immunoblot lysates from LiCl and control treated primary cortical cultures. LiCl was found not to affect total tau amounts, as assessed by quantification of tau amounts relative to β-actin amounts in each sample (Figure 4.3). However, treatment of cultured cells with 5-40 mM LiCl, but not 1 mM LiCl, significantly reduced phosphorylation of tau at ser 396/404 (Figure 4.3, p<0.01, p<0.001), a known GSK-3 phosphorylation site on tau (Hanger et al., 2009). Taken together, these

experiments indicate that a 4 hour treatment of primary cortical neurons with 20 mM LiCl leads to a marked reduction of tau phosphorylation and GSK-3 activity whilst avoiding any cell death. Therefore, these conditions were selected for experiments using 3xTg-AD brain slice cultures.

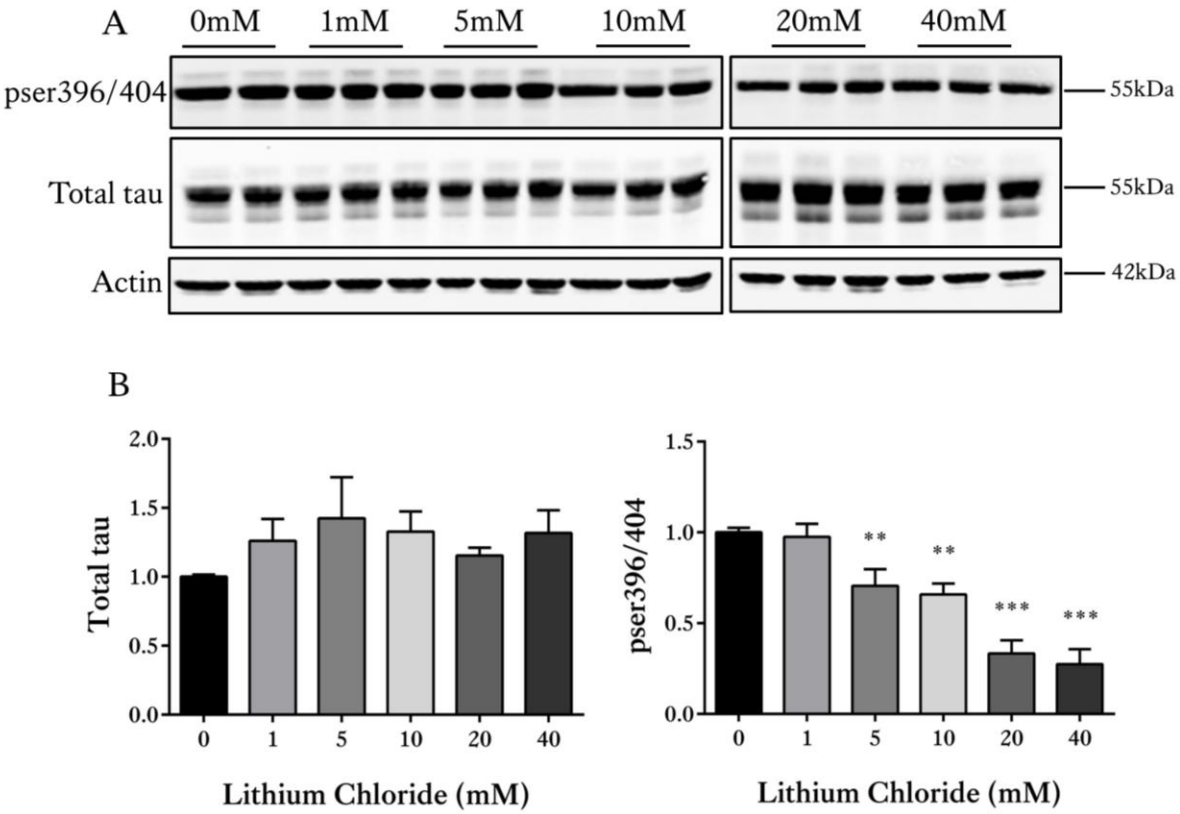

Figure 4.3: Lithium chloride treatment reduced tau phosphorylation at ser 396/404 in primary cortical neurons.
(A) Representative western blots of lysates from LiCl- and control (NaCl, 20mM)-treated primary cortical cultures probed with antibodies against total (phosphorylated and non-phosphorylated) tau and tau phosphorylated at ser 396/404 (both 50-55 kDa). An antibody against β-actin (42 kDa) was used as a loading control. (B) Bar charts show amounts of total tau following normalisation to actin amounts in each sample, and amounts of tau phosphorylated at ser 396/404 following normalisation to total tau levels in each sample. Data are shown as fold change from control. Data is mean ± SEM, (n=9 wells from three independent experiments, **p<0.01, ***p<0.001).

4.4.4 LiCl is not toxic to 3xTg-AD slice cultures

An LDH assay (section 2.2.5) was used to quantify any toxicity resulting from a 4 hour treatment of 28 *div* 3xTg-AD slice cultures with 20 mM LiCl. LDH is released into culture medium when cell membranes are compromised, and therefore an indirect measure of cell death can be gained by quantifying LDH content in medium as a proportion of the total LDH content in the slice culture lysates and medium. Treatment of slice cultures with 20 mM LiCl for 4 hours did not cause any significant change in the proportion of LDH in medium, when compared to control (20 mM NaCl)-treated cultures, indicating that 20 mM LiCl treatments are not toxic to brain slice cultures (Figure 4.4).

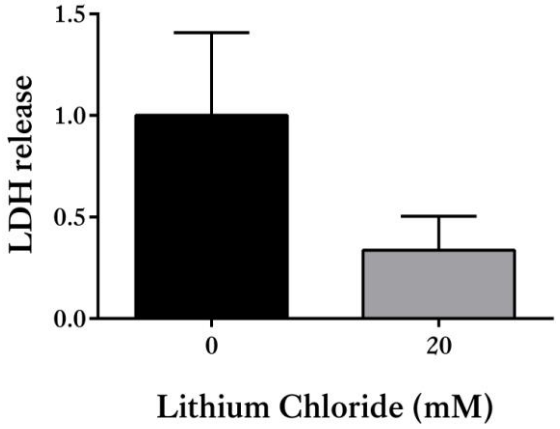

Figure 4.4: 20 mM LiCl does not significantly affect viability of 3xTg-AD organotypic brain slice cultures.
LDH assays were used to measure the effects of LiCl and NaCl (control) on slice viability. LDH in culture medium was determined as a proportion of total LDH (LDH in lysates plus that in culture medium). Bar chart shows medium/total LDH as fold change from control (20mM NaCl). Data is mean ± SEM, (n=9 wells from three independent experiments).

4.4.5 LiCl does not significantly inactivate GSK-3 in 3xTg-AD slice cultures

LiCl treatment of 3xTg-AD mice inactivates GSK-3α/β through the inhibitory phosphorylation of GSK-3α/β at ser 21/9 (Caccamo et al., 2007). To determine if LiCl application for 4 hours led to inactivation of GSK-3 in 28 *div* 3xTg-AD slice cultures, lysates were immunoblotted with total GSK-3α/β and pser21/9 GSK-3 α/β antibodies, as described above. Total GSK-3 amounts were normalised to β-actin amounts in each sample and this quantification showed no change in total GSK-3 amounts in treated cultures compared to controls (Figure 4.5). Surprisingly, treatment of the slice cultures with LiCl led to a small, but significant decrease in the amounts of GSK-3 phosphorylated at ser 21/9 when this was quantified as a proportion of total GSK-3 in each sample (Figure 4.5, $p<0.05$), thereby suggesting that LiCl treatment increases GSK-3 activity in 3xTg-AD slice cultures. To further investigate this, lysates were also immunoblotted using an antibody against β-catenin. β-catenin is targeted for degradation upon its phosphorylation by GSK-3, and therefore if GSK-3 activity is increased, a reduction in β-catenin amounts would be predicted (MacDonald et al., 2009), and vice versa. Analysis of β-catenin amounts as a proportion of β-actin in each sample showed no significant differences between LiCl and NaCl-treated slices (Figure 4.5). Therefore, from these analyses it is not possible to conclude that GSK-3 activity has been significantly modified by LiCl treatment of slice cultures.

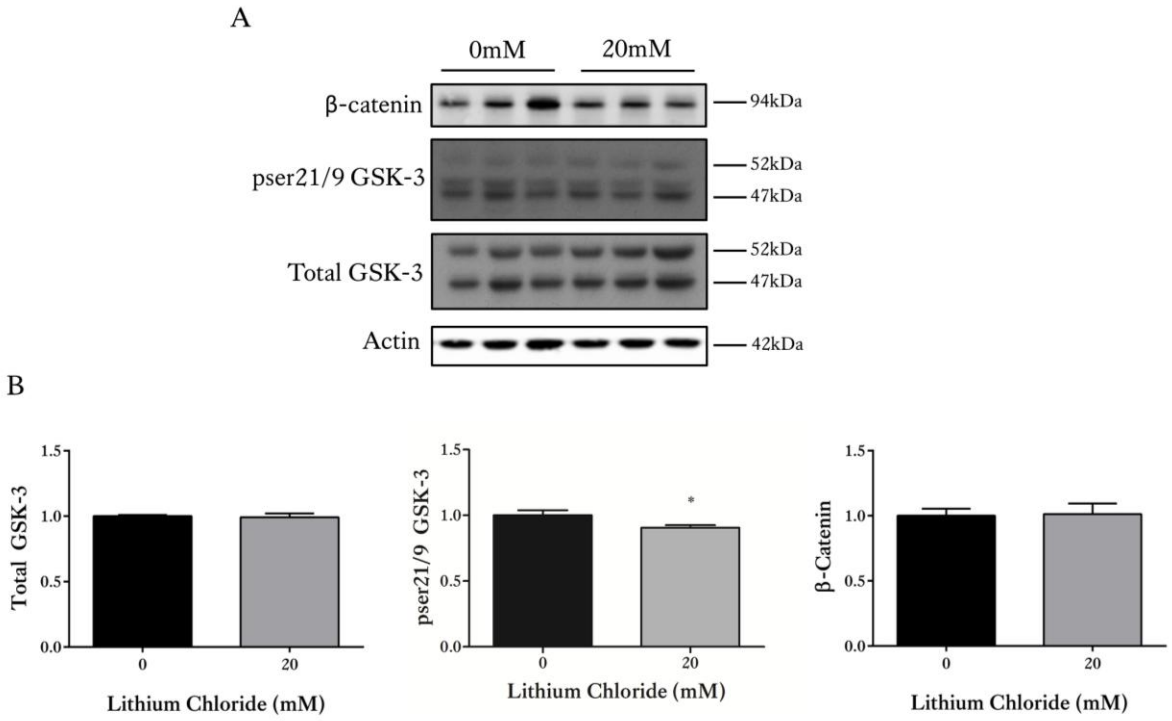

Figure 4.5: Lithium chloride treatment increases activity of GSK-3 in organotypic brain slice cultures from 3xTg-AD mice
(A) Representative western blots of lysates from LiCl- or control (NaCl, 20mM)-treated 3xTg-AD slice cultures showing total (phosphorylated and non-phosphorylated) GSK-3α/β, GSK-3α/β phosphorylated at ser 21/9 (47 and 52 kDa) and β-catenin (94 kDa). β-actin was used as a loading control (42 kDa). (B) Bar charts shows amounts of total GSK-3 normalised to β-actin, GSK-3α/β phosphorylated at ser 21/9 normalised to total GSK-3 and β-catenin normalised to β-actin in each sample. Data are shown as fold change from control. Data is mean ± SEM, (n=9 wells from three independent experiments, *p<0.05).

4.4.6 LiCl decreases phosphorylated tau load and levels of total tau in 3xTg-AD slice cultures

As described above, tau can be phosphorylated by GSK-3; therefore the effects of a 4 hour treatment with 20 mM LiCl on levels of phosphorylated tau was assessed in 28 *div* 3xTg-AD slice cultures. Slice culture lysates were immunoblotted with antibodies specific to tau phosphorylated at different sites that are known to be aberrantly phosphorylated in AD (Hanger et al., 2007). Total tau amounts were normalised to β-actin content in each sample, whereas the amounts of phosphorylated tau detected were standardised

to total tau levels in each sample. Treatment of 3xTg-AD slices with LiCl caused a significant decrease in the levels of total (phosphorylated and non-phosphorylated) tau when compared to control cultures (Figure 4.6, $p<0.05$). There was also a notable shift in tau molecular mass in lysates from LiCl treated cultures; this increased motility of tau on blots being characteristic of reduced tau phosphorylation (Pooler et al., 2012). Phosphorylation at ser 396/404 was also significantly reduced by LiCl treatment (Figure 4.6, $p<0.01$), and a concomitant increase in amounts of tau dephosphorylated at ser 199/202 and thr 205 was also detected in LiCl-treated cultures compared to NaCl-treated controls (Figure 4.6, $p<0.01$). These data indicate that tau phosphorylation has been reduced by LiCl treatment of 3xTg-AD slices, despite inhibition of GSK-3 activity by LiCl not being detected in these slice culture lysates.

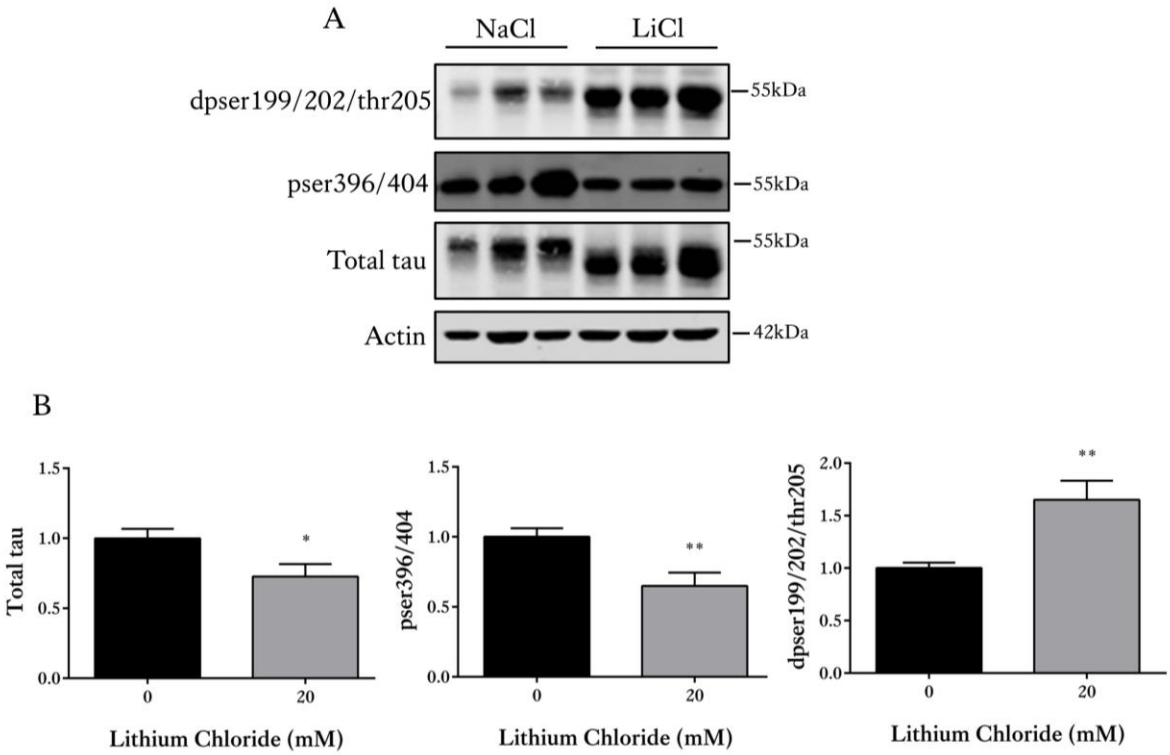

Figure 4.6: LiCl reduces total tau amounts and tau phosphorylation in organotypic brain slice cultures from 3xTg-AD mice.
(A) Representative western blots of lysates from LiCl- and control (NaCl, 20mM)-treated 3xTg-AD slice cultures probed with antibodies against total (phosphorylated and non-phosphorylated) tau, tau phosphorylated at ser 396/404, and tau dephosphorylated at ser 199/202 and thr 205 (all 50-55 kDa). An antibody against β-actin (42 kDa) was used as a loading control. (B) Bar charts show amounts of total tau following normalisation to β-actin amounts in each sample, amounts of tau phosphorylated at ser 396/404 and amounts of tau dephosphorylated at ser 199/202 and thr 205 following normalisation to total tau levels in each sample. Data are shown as fold change from control (NaCl). Data is mean ± SEM, (n=9 wells from three independent experiments, *p<0.05, **p<0.01).

4.4.7 LiCl decreases APP phosphorylated at thr 668 but does not affect levels of total APP in 3xTg-AD slice cultures

The effect of LiCl treatment on levels of APP phosphorylated at thr 668 *in vivo* in 3xTg-AD mice has previously not been reported. Phosphorylation of APP at thr 668 has been implicated in increasing the propensity of APP to be cleaved by β-secretase and γ-secretase via the amyloidogenic pathway to produce Aβ-42 which can then lead to the

build-up of amyloid plaques and associated neuronal loss (Lee et al., 2003). GSK-3 has previously been shown to contribute to phosphorylation of APP at thr 668 (Standen et al., 2001, Acevedo et al., 2014) and inhibition of GSK-3α with LiCl has been shown *in vivo* to reduce amyloidogenic APP processing (Phiel et al., 2003). The effect of LiCl treatment of 3xTg-AD slice cultures on levels of phosphorylation of APP at thr 668 was explored by probing immunoblots with an antibody specific to phosphorylation at this APP site, and the phosphorylated APP amounts were then normalised to levels of total (phosphorylated and non-phosphorylated) APP. Levels of total APP were established by probing immunoblots with an antibody to amino acids 61-88 at the N-terminus of APP and the amounts of total APP were normalised to levels of β-actin. The results of this analysis showed that levels of total APP were unaffected by LiCl treatment when compared to controls (Figure 4.7). However, treatment with LiCl resulted in a significant reduction in phosphorylation of APP at thr 668 when compared to control-treated 3xTg-AD slice cultures (Figure 4.7, $p<0.05$). These data provide further evidence that LiCl treatment of 3xTg-AD slices inhibits GSK-3 activity to lower tau and APP phosphorylation.

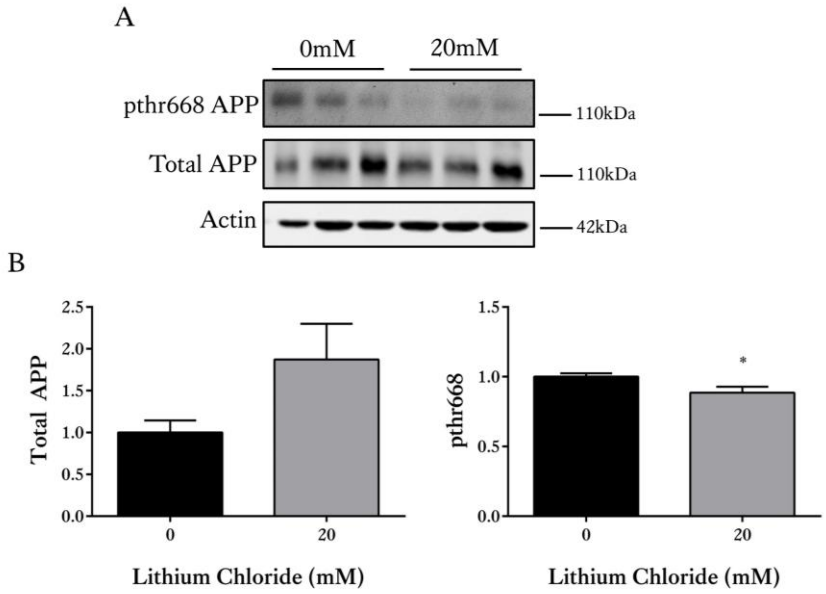

Figure 4.7 LiCl reduces phosphorylation of APP at thr 668 in 3xTg-AD organotypic brain slice cultures.
(A) Representative western blots of lysates from LiCl- and control (NaCl, 20mM)-treated 3xTg-AD slice cultures probed with antibodies against total (phosphorylated and non-phosphorylated) APP and APP phosphorylated at thr 668 (both 90-120 kDa). An antibody against β-actin (42 kDa) was used as a loading control. (B) Bar charts show amounts of total APP following normalisation to actin, and APP phosphorylated at thr 668 following normalisation to total APP levels in each sample. Data is shown as fold change from control (NaCl). Data is mean ± SEM, (n=9 wells from three independent experiments, *p<0.05).

4.4.8 LiCl treatment does not affect astrocyte activation in 3xTg-AD cultures

The role of inflammation and astrocytic activation in AD are the subject of much current research in the field (Phillips et al., 2014). Of relevance to this work are findings showing that GSK-3β regulates activity of the inflammatory transcription factor NF-κB, an interaction important for astrocyte survival (Sanchez et al., 2003). To determine if LiCl treatment of 3xTg-AD slice cultures affects levels of astrocyte activation, immunoblots were probed with an antibody against GFAP, a key marker of activated astrocytes. LiCl treatment was found not to alter levels of GFAP in 3xTg-AD cultures (Figure 4.8), indicating that LiCl does not alter astrocyte activation, at least in this model.

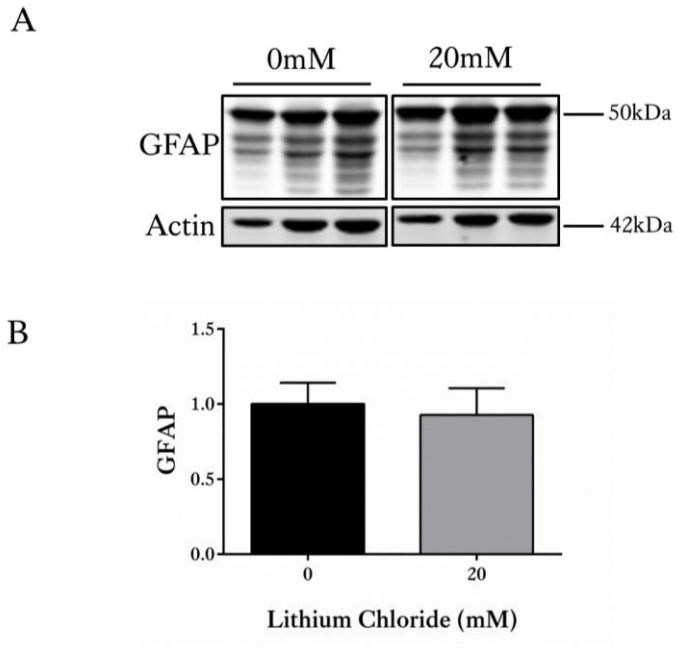

Figure 4.8: LiCl does not alter GFAP levels in 3xTg-AD slice cultures
Representative western blots of lysates from LiCl- and control (NaCl)- treated 3xTg-AD slice cultures probed with antibodies against GFAP (50 kDa). An antibody against β-actin (42 kDa) was used as a loading control. (B) Bar chart shows amounts of total GFAP following normalisation to β-actin amounts in the same sample. Data is shown as fold change from control (NaCl). Data is mean ± SEM, (n=9 wells from three independent experiments).

4.4.9 NAPVSIPQ is not toxic to primary cortical neurons.

NAPVSIPQ has previously been shown to be neuroprotective at low concentrations *in vitro* (Habib et al., 2010), and in 3xTg-AD mice *in vivo* (Matsuoka et al., 2007). Prior to treating 3xTg-AD slice cultures with NAPVSIPQ, the potential toxicity, effects on tau, and microtubule-stabilising properties of a range of concentrations of the octapeptide were explored.

7 *div* primary cortical neurons were treated for 24 hours with 1 x 10^{-15}, 10^{-13}, 10^{-11}, 10^{-9} and 10^{-7} M NAPVSIPQ to first identify a suitable non-toxic, but effective dose. No toxicity

was observed with any of the above concentrations of NAPVSIPQ when compared to vehicle-treated control cultures (Figure 4.9).

Immunolabelling of fixed cultures identified basal levels of cell death as largely neuronal, as there was no colocalisation between the dead cell dye and astrocytes. Furthermore, there were no increases in GFAP immunofluorescence indicating that NAPVSIPQ application did not activate astrocytes in these cultures (Figure 4.9).

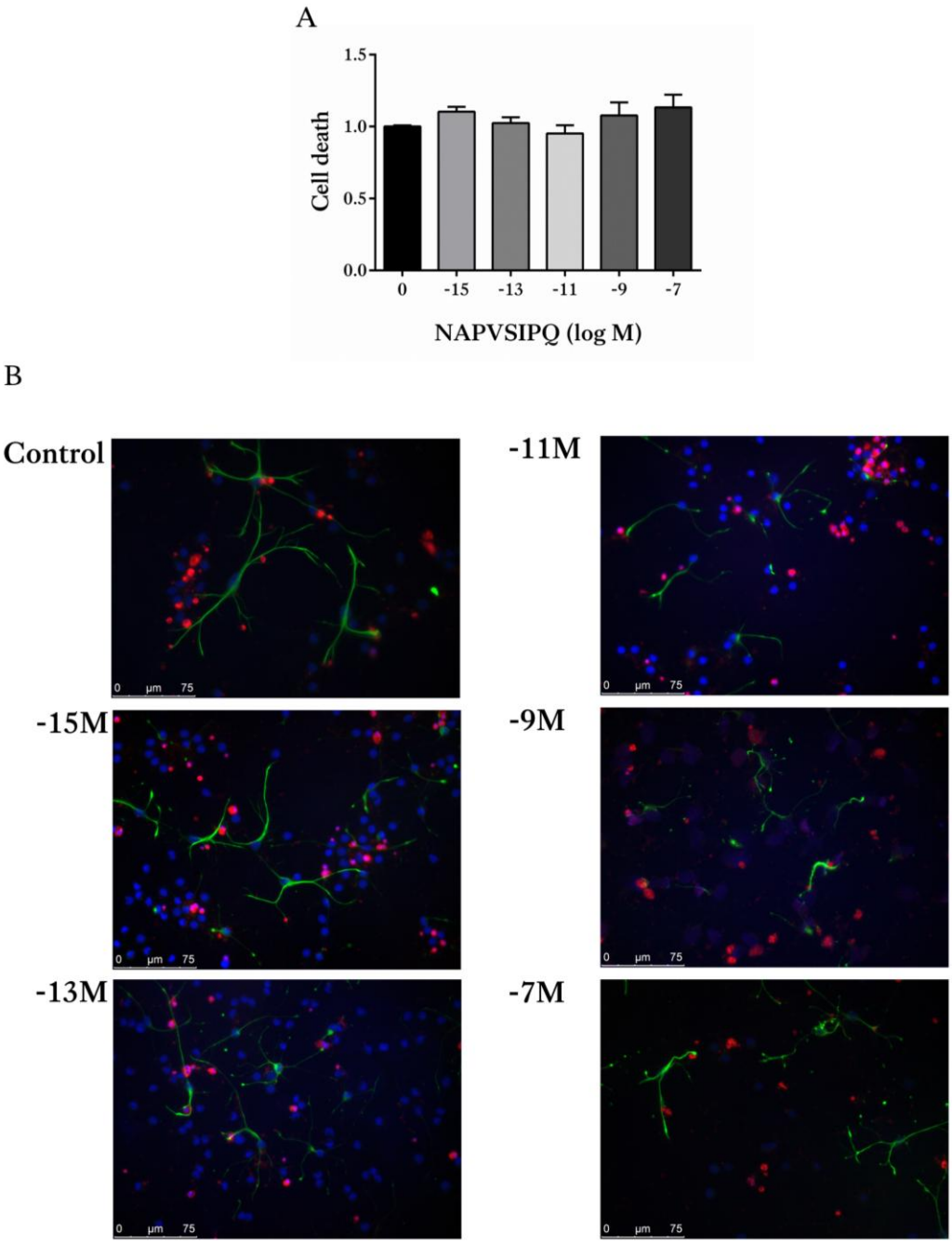

Figure 4.9: NAPVSIPQ is not toxic in primary cortical cultures.
(A) Bar chart shows levels of cell death, measured by incorporation of dead cell dye, following treatment of 7 *div* primary cortical cultures with 1 x 10^{-15} – 1 x 10^{-7}M NAPVSIPQ treatment or control (H_2O, 0M). Data is shown as fold change from control. Data is mean ± SEM, (n=9 wells from three independent experiments). (B) Representative images from these analyses showing incorporation of the dead cell dye (red), astrocytes immunolabelled using an antibody against GFAP (green) and Hoechst 33342 staining of cell nuclei (blue). Scale bar: 75 µm.

4.4.10 NAPVSIPQ reduces tau phosphorylation at specific sites without affecting total tau levels in primary cortical neurons

NAPVSIPQ has previously been shown to reduce tau phosphorylation *in vitro* and *in vivo* (Gozes and Divinski, 2004, Matsuoka et al., 2007, Matsuoka et al., 2008, Shiryaev et al., 2009). The effects of 24 hour treatments of 7 *div* primary cortical neurons with NAPVSIPQ on tau were therefore assessed by immunoblotting with a panel of antibodies specific to sites of tau phosphorylation identified in these previously published studies. Levels of total (phosphorylated and non-phosphorylated) tau in each sample were normalised to β-actin, and these analyses showed no effect of any concentration of NAPVSIPQ on amounts of total tau relative to control (H_2O)-treated cultures (Figure 4.10). Levels of phosphorylated tau were quantified as a proportion of total tau. Treatment for 24 hours with 10^{-13}, 10^{-11} , 10^{-9} and 10^{-7} M NAPVSIPQ significantly reduced levels of tau phosphorylation at thr 231 (Figure 4.10, $p<0.05$), a putative GSK-3, cdk5 and PKA phosphorylation site. Tau phosphorylated at ser 202 was unaffected by any dose of NAPVSIPQ when compared to vehicle-treated controls (Figure 4.10).

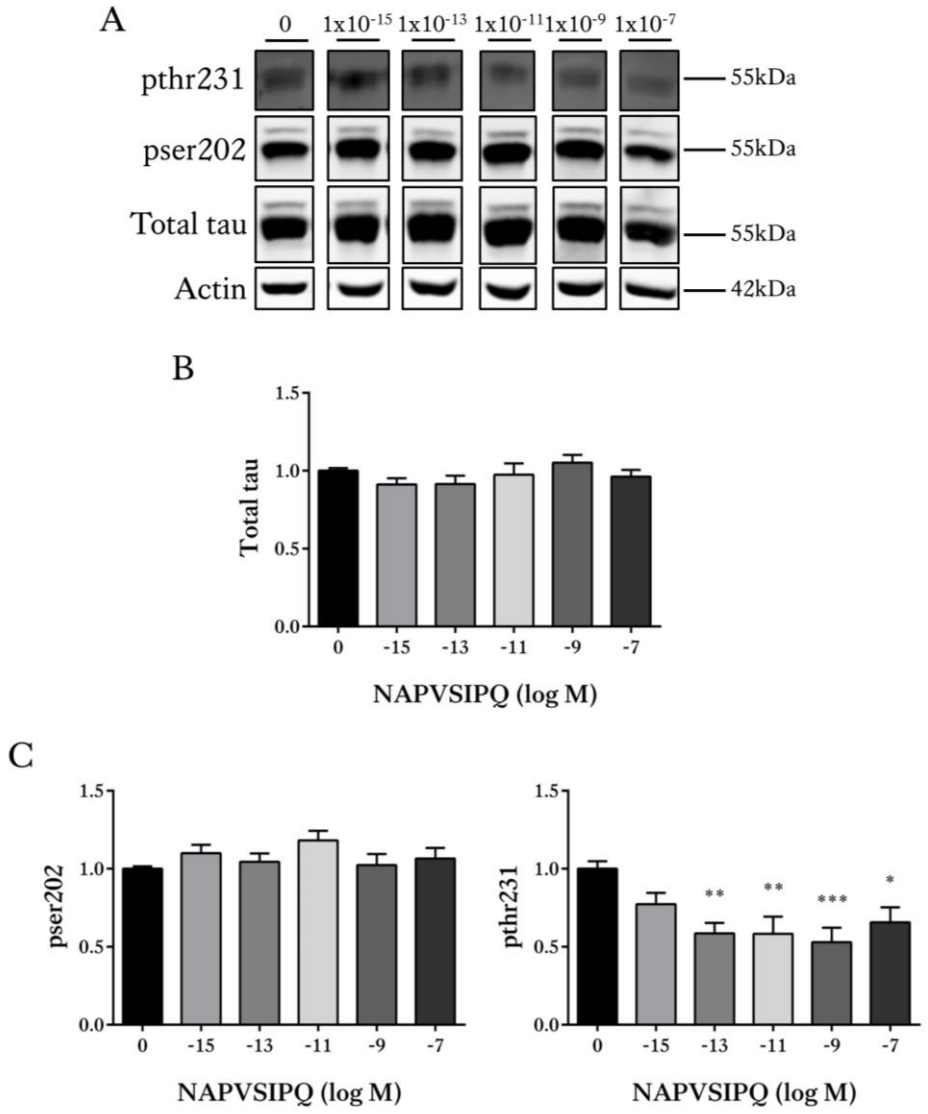

Figure 4.10: NAPVSIPQ reduces tau phosphorylation at thr 231 without affecting total tau amounts in primary cortical neurons

(A) Representative western blots of lysates from NAPVSIPQ-treated and control (H_2O, 0M)-treated primary cortical cultures probed with antibodies against total (phosphorylated and non-phosphorylated) tau, tau phosphorylated at ser 202 and tau phosphorylated at thr 231 (all at ~50-55 kDa). An antibody against β-actin (42 kDa) was used as a loading control. Bar charts show (B) amounts of total tau following normalisation to actin amounts in each sample, and (C) amounts of tau phosphorylated at ser 202 and tau phosphorylated at thr 231 following normalisation to total tau levels in each sample. Data are shown as fold change from control. Data is mean ± SEM, (n=9 wells from three independent experiments, *p<0.05, **p<0.01, ***p<0.001).

4.4.11 NAPVSIPQ does not affect binding of tau to microtubules nor does it rescue nocodazole-induced microtubule destabilisation in primary cortical neurons

NAPVSIPQ is reported to interact with microtubules, and this is commonly reported to be related to its neuroprotective effects (Shiryaev et al., 2009). In addition, phosphorylation of tau at thr 231 is known to affect the binding of tau to microtubules and affect microtubule stability (Sengupta et al., 1998). Therefore, a microtubule binding assay was carried out to assess whether a 24 hour treatment with NAPVSIPQ alters the binding of tau to microtubules. The assay uses differential centrifugation to pellet bound microtubules and any associated proteins such as tau, and these can be detected by immunoblotting. Lysates from primary cortical neurons treated with different doses of NAPVSIPQ were processed through this assay and the microtubule-unbound and bound fractions were immunoblotted with an antibody against total tau. Treatment of primary cortical neurons with 10^{-15}, 10^{-11}, 10^{-7} M NAPVSIPQ did not alter the proportion of microtubule-bound tau when compared to vehicle-treated controls (Figure 4.11).

In addition, to determine if NAPVSIPQ can protect neurons from chemically-induced microtubule destabilisation, primary cortical neurons were treated with control or 10^{-7} M NAPVSIPQ for 21 hours, followed by a 3 hour treatment with the microtubule destabilising agent nocodazole (5 mg/ mL). Nocodazole destabilises microtubules by blocking the self-assembly of tubulin (Samson et al., 1979). As before, microtubule-unbound and -bound fractions were prepared and these were immunoblotted with an antibody against total tau. Treatment with nocodazole was found to significantly reduce the proportion of tau bound to microtubules (Figure 4.12, $p<0.001$), and pre-treatment

of cells with NAPVSIPQ did not prevent this destabilisation (Figure 4.12, $p<0.05$), when compared to vehicle-treated controls. As shown above, treatment with NAPVSIPQ alone did not alter the proportion of microtubule-bound tau when compared to vehicle-treated controls (Figure 4.12).

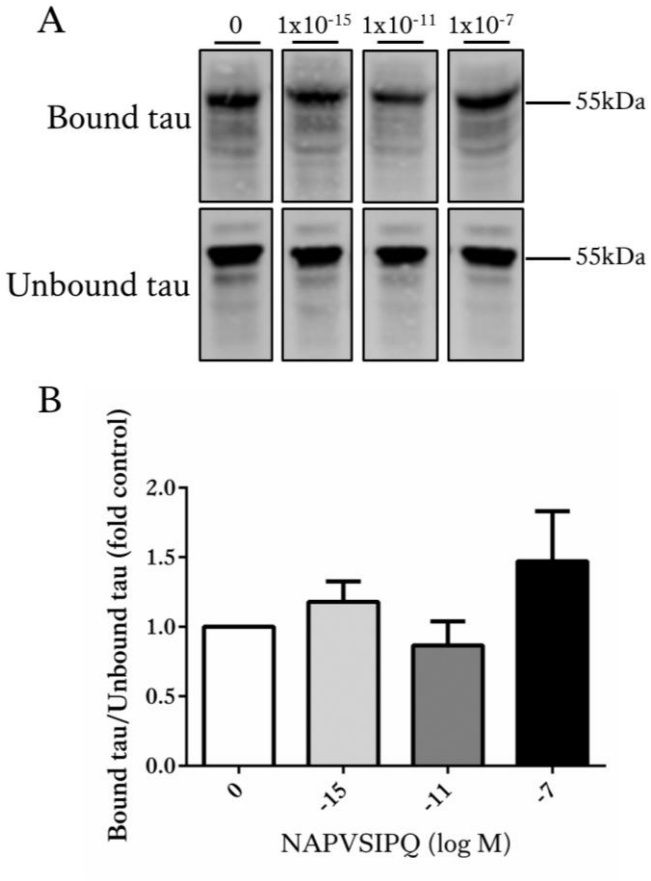

Figure 4.11: NAPVSIPQ treatment of primary cortical neurons does not increase the proportion of tau that is bound to microtubules.
(A) Representative western blots of microtubule-bound and -unbound fractions prepared from primary cortical cultures treated with 10^{-15}, 10^{-11}, 10^{-7} M NAPVSIPQ or control (H_20, 0M) immunoblotted with an antibody to total (phosphorylated and non-phosphorylated) tau (50-55 kDa). (B) Bar chart shows amounts of microtubule-bound relative to unbound tau. Data are shown as fold change from control. Data is mean ± SEM, (n=6 wells from two independent experiments).

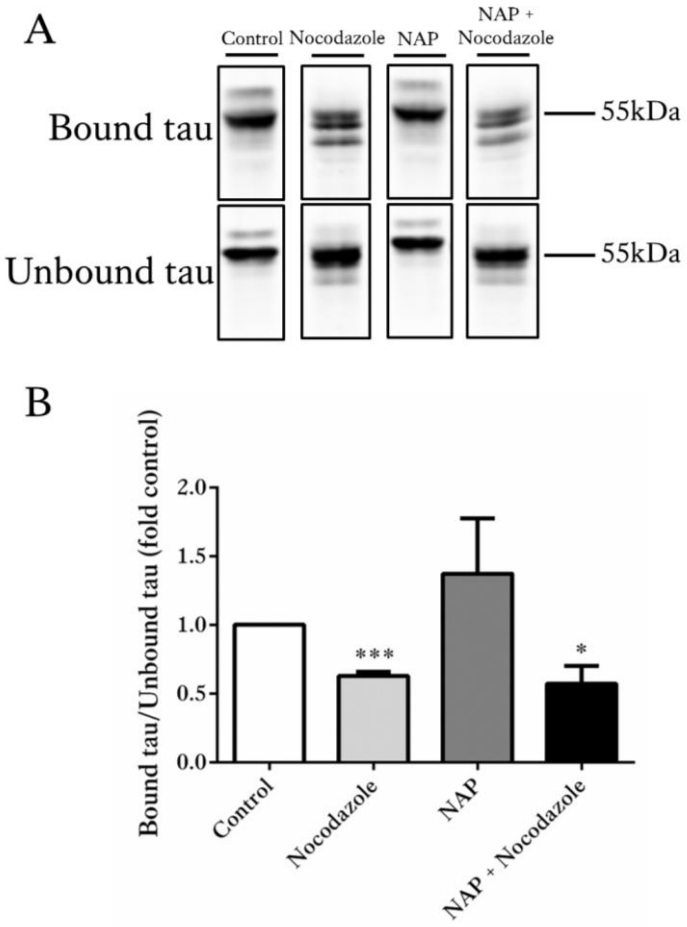

Figure 4.12: NAPVSIPQ treatment does not rescue nocodazole-induced tau dissociation from microtubules in primary cortical cultures.
(A) Representative western blots of microtubule-bound and -unbound fractions prepared from primary cortical cultures treated for 3 hours with 5mg/mL nocodazole or control, +/- a 21 hour pre-treatment with 10^{-7} M NAPVSIPQ. Blots were probed with an antibody to total (phosphorylated and non-phosphorylated) tau (50-55 kDa). (B) Bar chart shows amounts of microtubule-bound relative to unbound tau. Data are shown as fold change from control. Data is mean ± SEM, (n=4 wells from four independent experiments, *p<0.05, ***p<0.001).

4.4.12 NAPVSIPQ treatment does not affect viability of 3xTg-AD slice cultures

NAPVSIPQ treatment of primary cortical neurons identified a 24 hour dose of 10^{-7} M as effective, but not toxic to cells in primary cortical cultures, therefore this concentration of NAPVSIPQ was chosen for investigations in 3xTg-AD slice cultures. An LDH assay was used to quantify any toxicity resulting from a 24 hour application of 10^{-7} M NAPVSIPQ to

28 *div* 3xTg-AD slice cultures. Release of LDH into the media was calculated as a proportion of the total LDH, as described before. 10^{-7} M NAPVSIPQ did not cause any significant change in the proportion of LDH in culture medium relative to vehicle-treated control cultures, indicating that this treatment is not toxic to 3xTg-AD slice cultures (Figure 4.13).

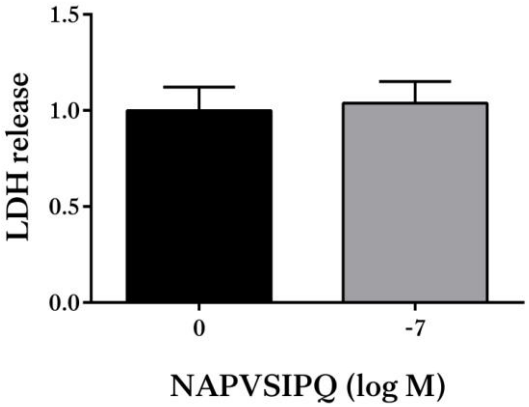

Figure 4.13: NAPVSIPQ does not significantly affect the viability of 3xTg-AD organotypic brain slice cultures.
LDH assays were used to determine the effects on cell viability of 1 x 10^{-7} M NAPVSIPQ and control (vehicle) treatments in 28 *div* 3xTg-AD brain slices. Bar chart shows LDH content in medium as a proportion of total LDH (LDH in lysates plus that in culture medium) represented as fold change from control (vehicle). Data is mean ± SEM, (n=12 wells from two independent experiments).

4.4.13 NAPVSIPQ decreases tau phosphorylation at thr 231 without affecting total tau levels in 3xTg-AD slice cultures

NAPVSIPQ has previously been shown to reduce tau phosphorylation in 3xTg-AD mice *in vivo* (Matsuoka et al., 2007). Therefore, effects of a 24 hour treatment of 10^{-7} M NAPVSIPQ on tau were next explored in the 28 *div* 3xTg-AD slice cultures. Slice culture lysates were immunoblotted with antibodies to several tau phosphorylation sites, and the resulting signals were normalised to total tau levels in the same sample. Levels of

total (phosphorylated and non-phosphorylated) tau were unchanged by treatment with NAPVSIPQ following normalisation of tau signals to those of β-actin in the same sample (Figure 4.14). Phosphorylation of tau at thr 231, calculated as a proportion of total tau, was significantly reduced in 3xTg-AD slice cultures following treatment with 10^{-7} M NAPVSIPQ (Figure 4.14, $p<0.05$). Phosphorylation of tau at ser 202 and at ser 396/404 was unaffected by 10^{-7} M NAPVSIPQ treatment (Figure 4.14). Similarly, dephosphorylation of tau at ser 199/202 and thr 205 was also unaffected in 3xTg-AD slice cultures after 10^{-7} M NAPVSIPQ treatment relative to control cultures (Figure 4.14). These findings substantiate those from primary cultures and indicate that NAPSVIPQ can significantly reduce tau phosphorylation at specific sites that are known to be aberrantly phosphorylated in AD (Hanger et al., 2009).

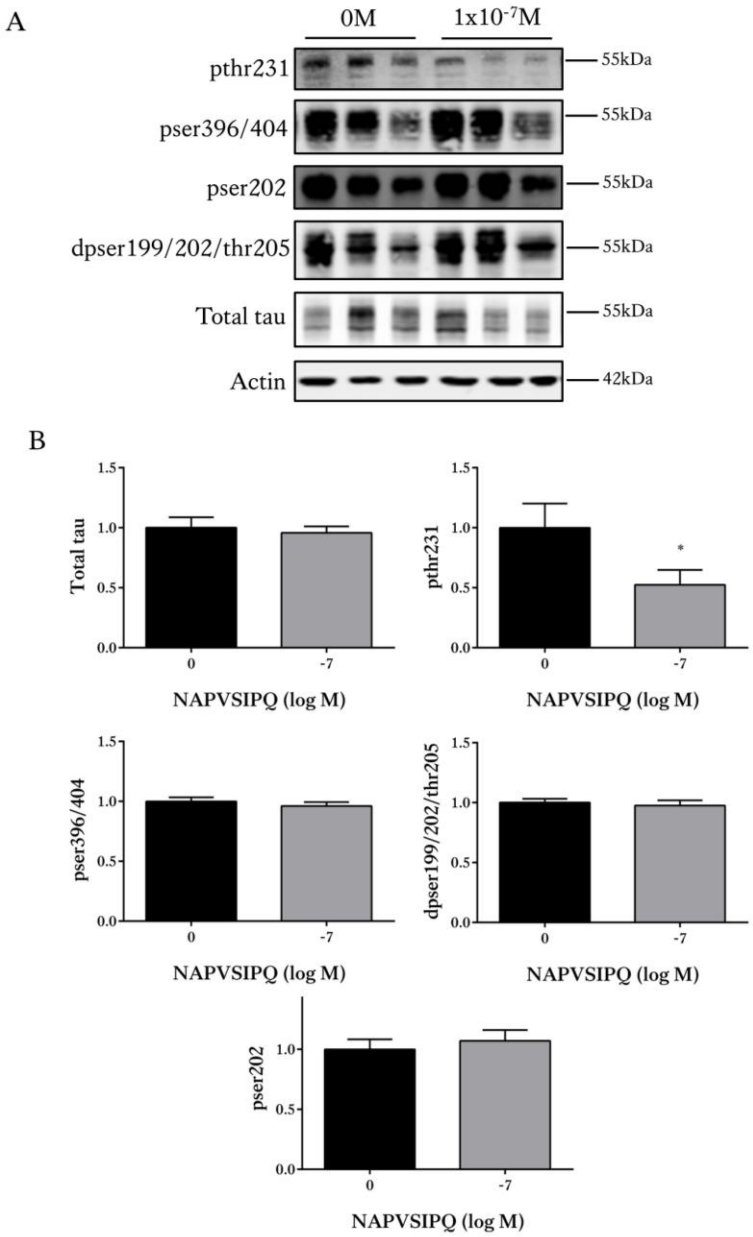

Figure 4.14: NAPVSIPQ reduces tau phosphorylation at thr 231 without affecting total tau amounts in 3xTg-AD slice cultures

(A) Representative western blots of lysates from NAPVSIPQ-treated and control (H_2O, 0M)-treated 3xTg-AD slice cultures probed with antibodies against total (phosphorylated and non-phosphorylated) tau, tau phosphorylated at ser 202, thr 231, ser 396/404 and tau dephosphorylated at ser 199/202 and thr 205 (all at ~50-55 kDa). An antibody against β-actin (42 kDa) was used as a loading control. (B) Bar charts show amounts of total tau normalised to actin amounts in each sample and amounts of tau phosphorylated at thr 231, ser 202, ser 396/404 and tau dephosphorylated at ser 199/202 and thr 205 following normalisation to total tau levels in each sample. Data are shown as fold change from control. Data is mean ± SEM, (n=12 wells from two independent experiments, *p<0.05).

4.4.14 NAPVSIPQ does not affect microtubule stabilisation in 3xTg-AD slice cultures

Although NAPVSIPQ was shown above not to affect the microtubule binding of tau in primary cells, it was also important to check this in a disease model. Therefore, 3xTg-AD slice cultures were pre-treated with control or 10^{-7} M NAPVSIPQ for 21 hours, followed by a 3 hour application of nocodazole treatment (5 mg/ mL), and microtubule-bound and unbound fractions prepared as described above. In 3xTg-AD slices, treatment with nocodazole was not found to reduce the proportion of tau bound to the microtubules relative to unbound tau, despite a marked reduction in the amount of tau in the microtubule-bound fraction being apparent on blots. Pre-treatment of nocodazole-treated slices with NAPVSIPQ also did not affect the amounts of microtubule-bound tau when compared to vehicle-treated controls (Figure 4.15). As seen with primary cortical neurons, NAPVSIPQ treatment alone also did not increase amounts of tau bound to the microtubules when compared to vehicle-treated controls in 3xTg-AD slice cultures (Figure 4.15). The reason for the discrepancy in the effects on microtubule-binding of tau following nocodazole treatment in primary neurons and 3xTg-AD slices is not clear, but may reflect the higher phosphorylation status of tau in slice cultures leading to lower proportion of tau being microtubule-bound. Under these conditions, any effect of microtubule destabilisation may be difficult to detect. Nevertheless, when taken together these findings indicate that NAPVSIPQ reduces tau phosphorylation via a mechanism not related to the microtubule-binding capacity of tau. Any microtubule-stabilising properties of NAPVSIPQ were also assessed by measuring amounts of acetylated α-tubulin in control and NAPVSIPQ-treated 3xTg-AD slice cultures. Acetylated α-tubulin has previously been demonstrated to be a marker of long-lived stable

microtubules (Hubbert et al., 2002, Fukushima et al., 2009), although this is somewhat contentious as others have shown that the acetylation of α-tubulin does not affect microtubule stability, and increased amounts of acetylated α-tubulin have actually been found in AD brain (Palazzo et al., 2003, Zhang et al., 2015a). Nonetheless, amounts of acetylated α-tubulin were measured in lysates from 24 hour NAPVSIPQ and control-treated 3xTg-AD slice cultures by immunoblotting and standardised to total amounts of α-tubulin. Acetylated α-tubulin was significantly reduced with NAPVSIPQ treatment (Figure 4.16, $p<0.01$), again suggesting that NAPVSIPQ does not reduce tau phosphorylation by affecting microtubule stability.

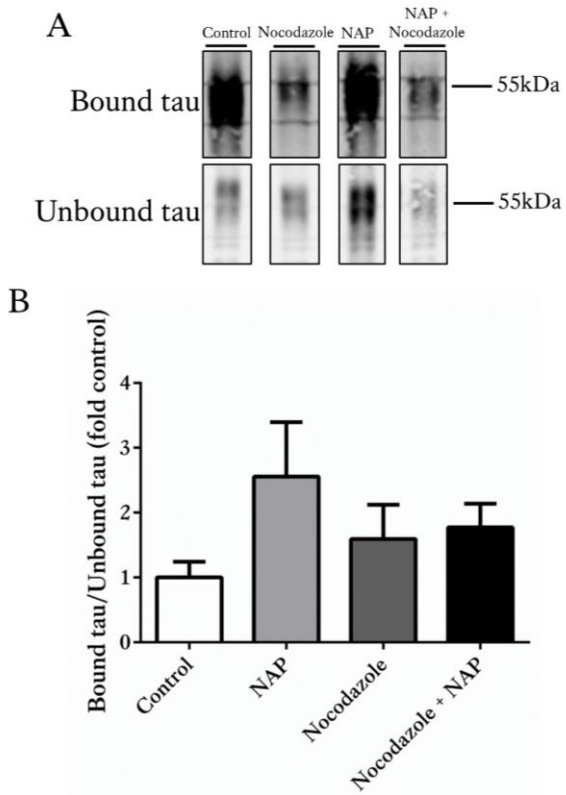

Figure 4.15: NAPVSIPQ does not affect the proportion of tau that is microtubule-bound in 3xTg-AD slice cultures.

(A) Representative western blots of microtubule-bound and -unbound fractions prepared from 3xTg-AD slice cultures treated for 3 hours with 5mg/mL nocodazole or control, +/- a 21 hour pre-treatment with 10^{-7} M NAPVSIPQ. Blots were probed with an antibody to total (phosphorylated and non-phosphorylated) tau (50-55 kDa). (B) Bar chart shows amounts of microtubule-bound relative to unbound tau. Data are shown as fold change from control. Data is mean ± SEM, (n=6 wells from two independent experiments).

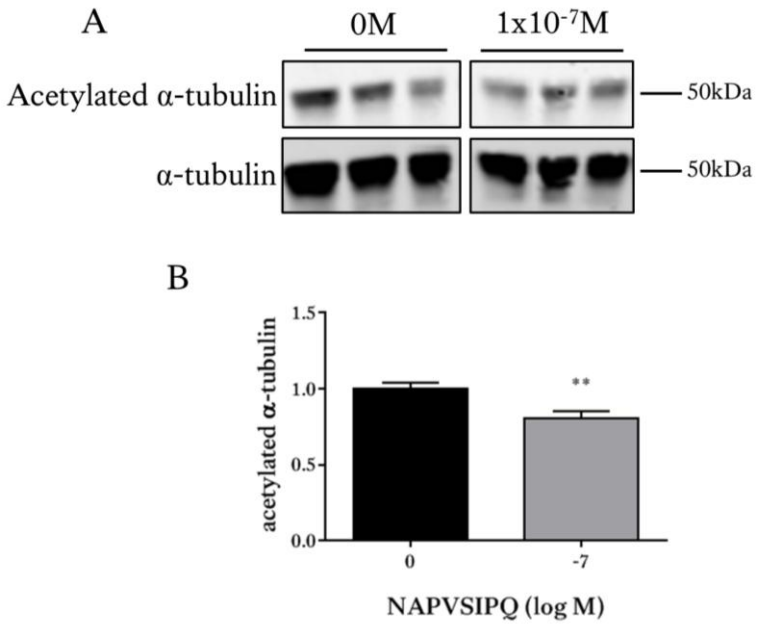

Figure 4.16: NAPVSIPQ reduces amounts of acetylated α-tubulin in 3xTg-AD slice cultures.
(A) Representative western blots of lysates from NAPVSIPQ-treated and control (H_2O, 0M)-treated 3xTg-AD slice cultures probed with antibodies against total α-tubulin and acetylated α-tubulin (both at ~50 kDa). (B) Bar chart shows amounts of acetylated α-tubulin following normalisation to total α-tubulin levels in each sample. Data are shown as fold change from control. Data is mean ± SEM, (n=12 wells from two independent experiments, **p<0.01).

4.4.15 BTA-EG_4 is not toxic to primary cortical neurons

The amyloid-binding drug, BTA-EG_4 was identified as a compound of interest to treat 3xTg-AD slice cultures due to its neuroprotective effects against Aβ *in vitro* (Habib et al., 2010) and *in vivo* in WT mice (Megill et al., 2013), as well as its ability to maintain synapse health and improve cognitive performance in 3xTg-AD mice (Song et al., 2014). The effects of this compound on tau and kinase activity are currently unknown. As with the studies described above, preliminary experiments were conducted in primary cortical cultures to determine an effective sub-toxic dose of BTA-EG_4 for further investigation in 3xTg-AD slice cultures.

In the first instance, primary cortical neurons were cultured for 7 *div* and then treated with control (vehicle, DMSO), 20, 40 or 60 μM BTA-EG_4 for 24 hours, and the effects on cell viability determined using a quantitative live/dead cell assay. No changes in cell viability were apparent following treatment of primary cortical neurons with any concentration of BTA-EG_4 when compared to vehicle-treated control neurons (Figure 4.17). Since potential effects of BTA-EG_4 on synapse health became of interest for this work, 14 *div* primary cortical neurons, which have developed, functional synapses, were used for most BTA-EG_4 studies; therefore the non-toxic effect of a 24 hour, 40 μM BTA-EG_4 treatment was confirmed in these older neurons using the same methods (Figure 4.18).

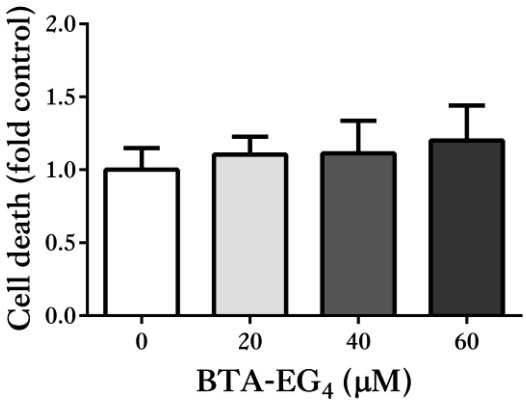

Figure 4.17: BTA-EG_4 is not toxic to 7 *div* primary cortical neurons.
Bar chart shows levels of cell death measured by incorporation of dead cell dye following treatment of 7 *div* primary cortical cultures with control (DMSO, 0μM), 20, 40 or 60 μM BTA-EG_4. Data is shown as fold change from control. Data is mean ± SEM, (n=9 wells from three independent experiments).

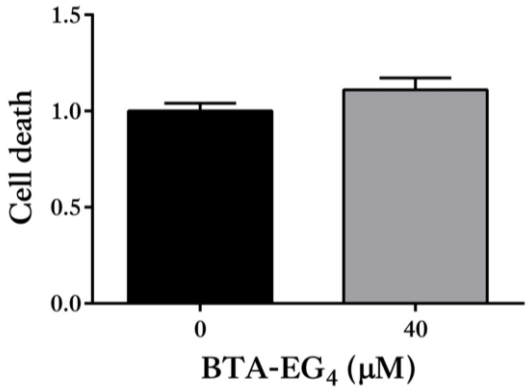

Figure 4.18: 40 μM BTA-EG_4 is not toxic to 14 *div* primary cortical neurons.
Bar chart shows levels of cell death measured by incorporation of dead cell dye following treatment of primary cortical cultures with control (vehicle, 0μM) or 40 μM BTA-EG_4. Data is shown as fold change from control. Data is mean ± SEM, (n=12 wells from two independent experiments).

4.4.16 BTA-EG_4 treatment does not affect levels of total APP in primary cortical neurons

BTA-EG_4 has previously been shown to bind amyloid *in vitro* (Habib et al., 2010) and also act *in vivo* in WT mice to alter APP processing (Megill et al., 2013). Treatment of WT mice with BTA-EG_4 results in increased levels of sAPPα and reduces levels of sAPPβ, thereby likely precluding formation of Aβ. This is without altering total amounts of APP (Megill et al., 2013). Therefore, the effects of BTA-EG_4 on amounts of total APP were determined in primary cortical cultures. Lysates from 24 hour control and BTA-EG_4 treated 14 *div* primary cortical neurons were immunoblotted with antibodies against total APP, and β-actin as a loading control. Treatment with BTA-EG_4 did not affect levels of total APP in the BTA-EG_4-treated neurons compared to vehicle-treated controls (Figure 4.19). Unfortunately, in the time of the project it was not possible to detect and examine amounts of sAPPα and sAPPβ in these cultures with the antibodies available. Additionally, it was not possible to measure any effects of BTA-EG_4 on Aβ levels in the

medium of these cultures, since assays for detecting endogenous rat Aβ are not sufficiently sensitive.

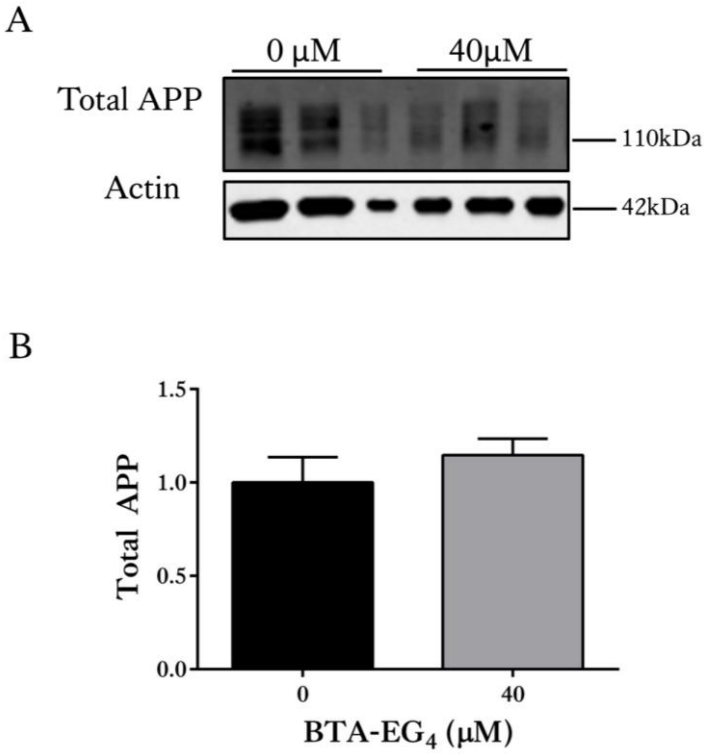

Figure 4.19: Treatment with BTA-EG$_4$ does not affect levels of total APP in primary cortical neurons
Representative western blots of lysates prepared from 14 *div* primary cortical neuron treated with BTA-EG$_4$ and control (DMSO, 0μM) probed with an antibody against total APP (90-120 kDa). Blots were also probed with an antibody against β-actin (42 kDa) as a loading control. (B) Bar chart shows amounts of total APP following normalisation to β-actin amounts in the same sample. Data are shown as fold change from control. Data is mean ± SEM, (n=9 wells from three independent experiments).

4.4.17 BTA-EG$_4$ decreases total tau amounts and tau phosphorylation in primary cortical neurons

The effects of BTA-EG$_4$ on cognition, synaptic enhancement and Aβ have previously been explored *in vivo* in 3xTg-AD mice (Song et al., 2014); however, the effect of BTA-EG$_4$ on tau *in vitro* or *in vivo* has not been studied. Therefore, levels of total (phosphorylated

and non-phosphorylated) tau and phosphorylated tau were measured in lysates from primary cortical cultures treated for 24 hours with 40 μM BTA-EG_4. A BTA-EG_4 treatment significantly reduced total tau levels in 14 *div* primary cortical neurons (Figure 4.20, $p<0.05$). In addition, the amount of tau phosphorylated at ser 396/404 and also at ser 202 relative to total tau was significantly reduced in primary cortical neurons by 40 μM BTA-EG_4 when compared to vehicle-treated controls (Figure 4.20, both $p<0.001$). Furthermore, the amount of tau dephosphorylated at ser 199/202 and thr 205 was found to be significantly increased in BTA-EG_4 treated primary cortical cultures when compared to vehicle-treated controls (Figure 4.20, both $p<0.001$). This novel data indicates that BTA-EG_4 has the capacity to significantly reduce tau phosphorylation at several AD-relevant epitopes, at least in primary culture.

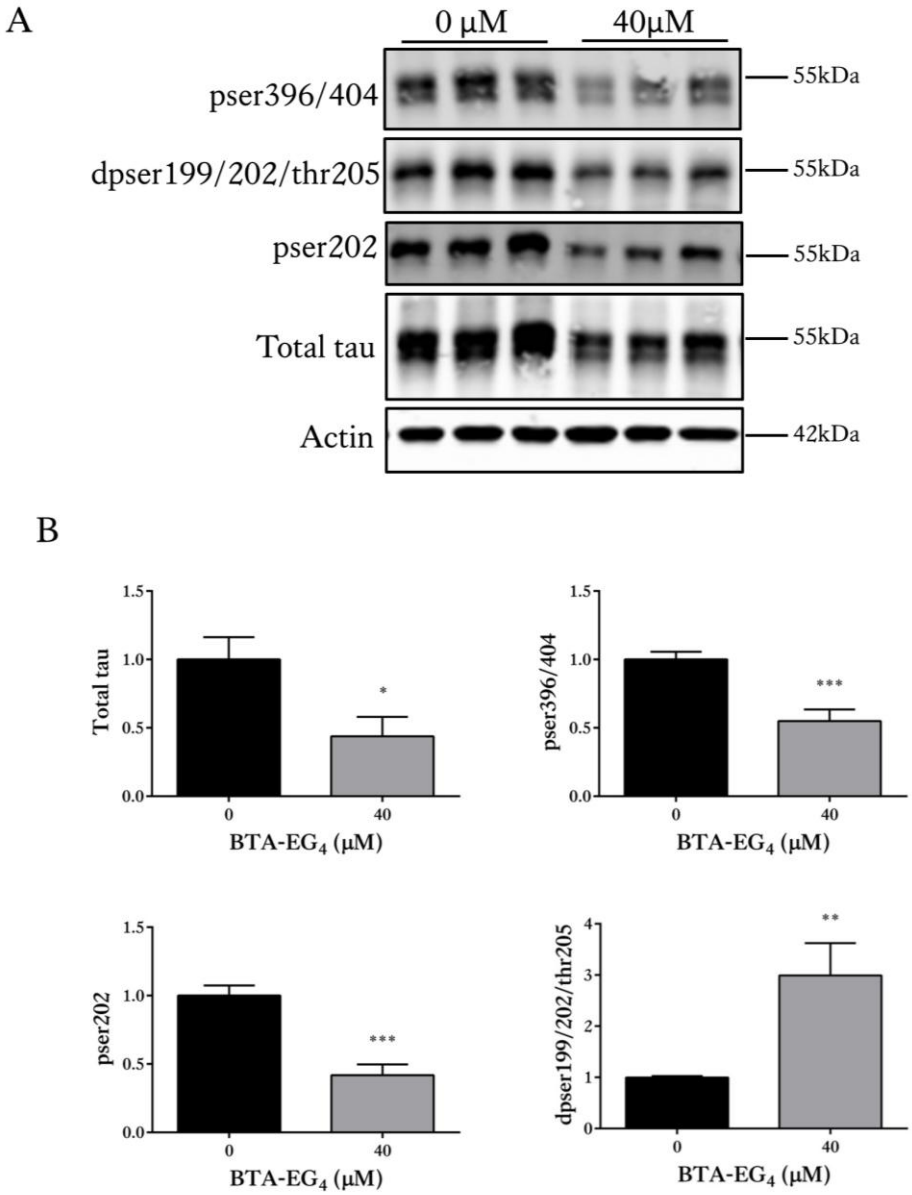

Figure 4.20: 40 µM BTA-EG$_4$ significantly reduces total and phosphorylated tau amounts in primary cortical cultures.

(A) Representative western blots of lysates from BTA-EG$_4$-treated and control (vehicle, DMSO)-treated primary cortical cultures probed with antibodies against total (phosphorylated and non-phosphorylated) tau, tau phosphorylated at ser 202 and ser 396/404 and tau dephosphorylated at ser 199/202 and thr 205 (all at ~50-55 kDa). An antibody against β-actin (42 kDa) was used as a loading control. (B) Bar charts show amounts of total tau normalised to actin amounts in each sample and amounts of tau phosphorylated at ser 396/404 and ser 202 and tau dephosphorylated at ser 199/202 and thr 205 following normalisation to total tau levels in each sample. Data are shown as fold change from control. Data is mean ± SEM, (n=9 wells from three independent experiments, *p<0.05, **p<0.01, ***p<0.001).

4.4.18 BTA-EG_4 increases GSK-3 activity in primary cortical neurons

The mechanism by which BTA-EG_4 affects tau phosphorylation has not previously been explored. BTA-EG_4 was shown above to reduce tau phosphorylation at epitopes known to be substrates for the prominent tau kinases GSK-3 and cdk5 (Hanger et al., 2009); therefore the activity of these kinases was determined in lysates from treated cells by western blotting. As described above, GSK-3 activity was investigated by immunoblotting with antibodies against total GSK-3α/β and GSK-3α/β phosphorylated at ser 21/9. Total amounts of GSK-3 were unaffected by treatment with BTA-EG_4 in primary cortical neurons (Figure 4.21). However, when amounts of GSK-3 phosphorylated at ser 21/9 were quantified as a proportion of total GSK-3, a small but significant decrease was observed following BTA-EG_4 treatment, suggesting that increased activation of GSK-3 results from treatment of primary neurons with this compound (Figure 4.21, $p<0.001$).

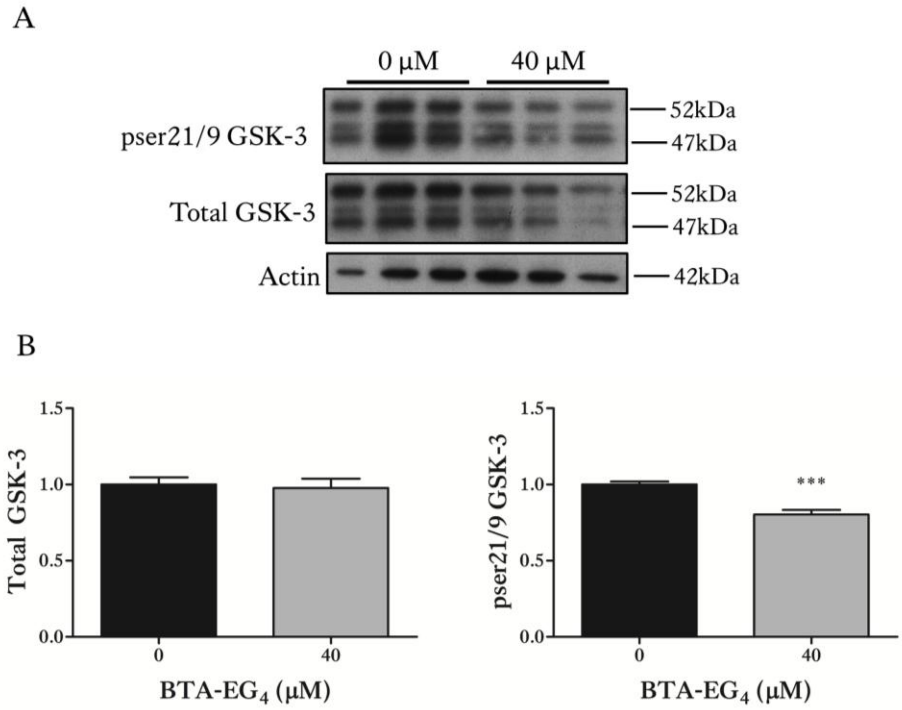

Figure 4.21: BTA-EG$_4$ increases activation of GSK-3 in 14 *div* primary cortical neurons. (A) Representative western blots of lysates from BTA-EG$_4$-treated and control (vehicle, DMSO)-treated primary cortical cultures probed with antibodies against total (phosphorylated and non-phosphorylated) GSK-3α/β and GSK-3 α/β phosphorylated at ser 21/9 (both at 47 and 52 kDa). An antibody against β-actin (42 kDa) was used as a loading control. (B) Bar charts show amounts of total GSK-3 normalised to actin amounts in each sample and amounts of phosphorylated GSK-3 at ser 21/9 following normalisation to total GSK-3 levels in each sample. Data are shown as fold change from control. Data is mean ± SEM, (n=9 wells from three independent experiments, ***p<0.001).

4.4.19 BTA-EG$_4$ inactivates cdk5 to reduce tau phosphorylation in primary cortical neurons

The results presented above show that BTA-EG$_4$ is able to reduce levels of phosphorylated tau at several AD-relevant sites in primary cortical neurons (section 4.4.16), despite increasing GSK-3 activity (section 4.4.18). Cdk5 is another major tau kinase which is shown to phosphorylate tau at many of the same sites as GSK-3 (Tsai et al., 2004). Moreover, inhibition of cdk5 has previously been shown to result in increased

GSK-3 activity (Engmann and Giese, 2009). Therefore, lysates from BTA-EG_4 treated primary cortical cultures were immunoblotted with antibodies against cdk5 and its neuronal activators, p35 and p25, as described previously (section 3.4.17). Total levels of cdk5 were found to be unaffected by treatment with BTA-EG_4 (Figure 4.22). In contrast, amounts of p35, but not p25, were significantly decreased in primary cortical neurons following BTA-EG_4 treatment relative to control cultures (Figure 4.22, $p<0.001$), indicating reduced cdk5 activity in these cultures. This finding may explain the observed decrease in tau phosphorylation observed in the presence of increased GSK-3 activity in these studies.

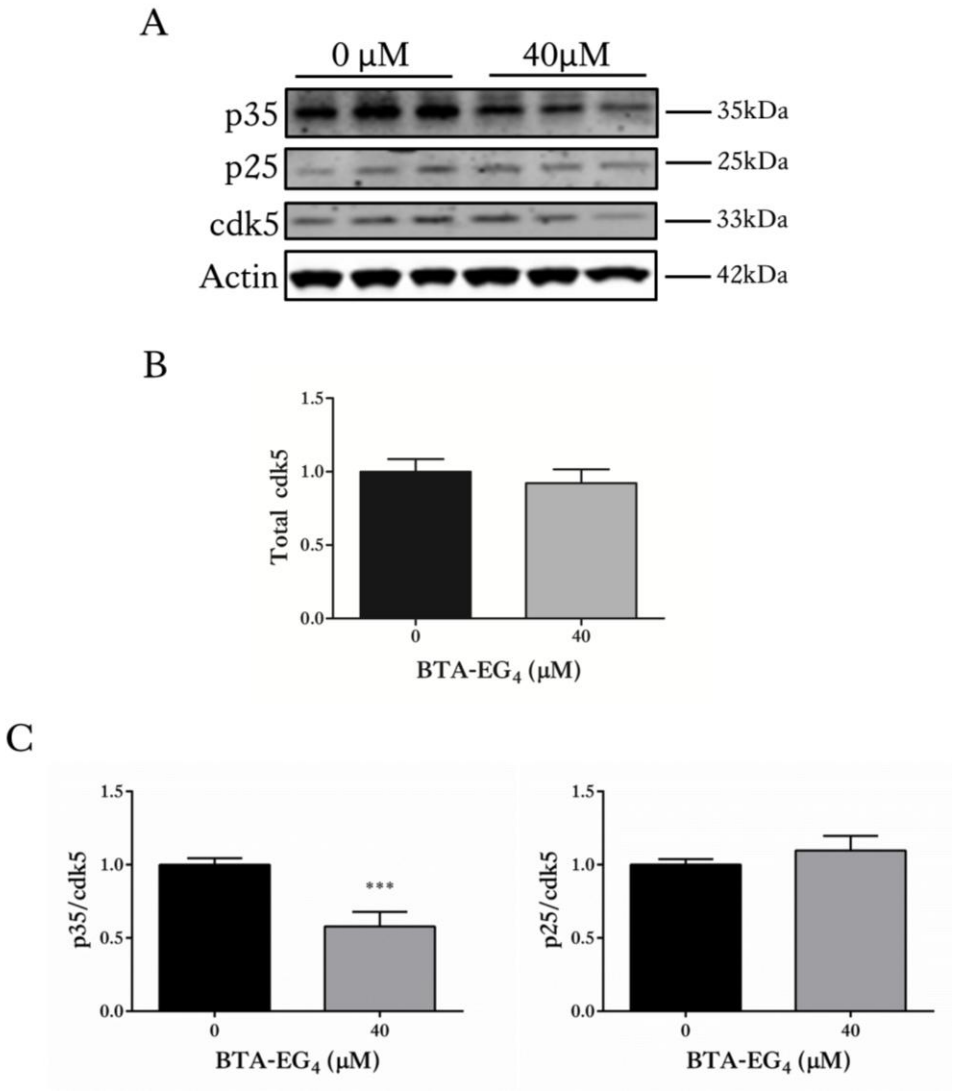

Figure 4.22: BTA-EG_4 reduces p35/cdk5 in 14 *div* primary cortical neurons
(A) Representative western blots of lysates from BTA-EG_4- and control-treated primary cortical cultures probed with antibodies against cdk5 (33 kDa), p35 (35 kDa) and p25 (25 kDa). An antibody against β-actin (42 kDa) was used as a loading control. Bar charts show (B) amounts of total cdk5 following normalisation to β-actin amounts in each sample, and (C) amounts of p35 and p25 following normalisation to total cdk5 in each sample. Data are shown as fold change from control. Data is mean ± SEM, (n=9 wells from three independent experiments, ***p<0.001).

4.4.20 BTA-EG_4 reduces levels of pre- and post-synaptic markers in primary cortical neurons

BTA-EG_4 has previously been shown to increase synaptic density and levels of synaptic markers *in vivo* in both WT and 3xTg-AD mice (Megill et al., 2013, Song et al., 2014). To corroborate this, synaptosome fractions enriched in synaptic proteins were prepared from 24 hour BTA-EG_4-treated and control-treated 14 *div* primary cortical neurons, and levels of synaptophysin and PSD-95 were quantified as described above. Surprisingly, treatment of primary cortical cultures with BTA-EG_4 caused a significant reduction in amounts of both PSD-95 and synaptophysin relative to β-actin in synaptosomal fractions when compared to vehicle-treated controls (Figure 4.23, $p<0.01$, $p<0.05$, respectively). This finding suggests that despite reducing tau phosphorylation, BTA-EG_4 may be synaptotoxic in primary cultured cells.

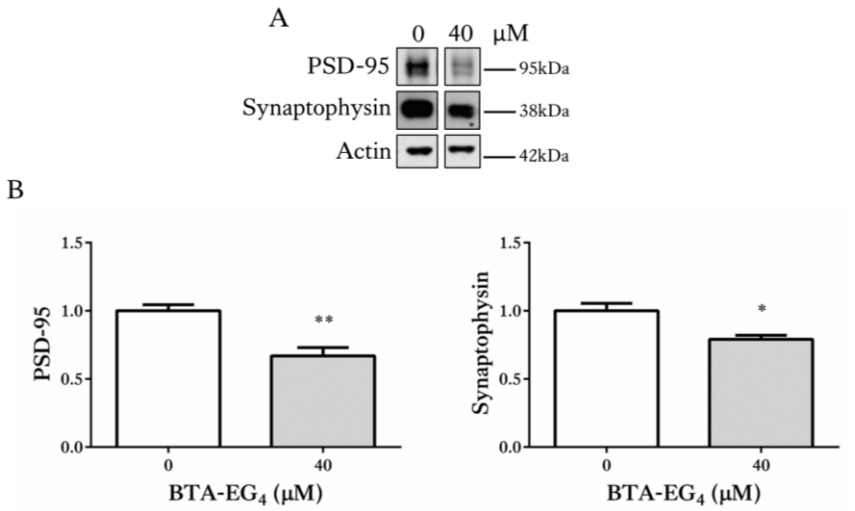

Figure 4.23: Treatment of primary cortical neurons with BTA-EG_4 significantly reduces levels of the pre- and post-synaptic markers, synaptophysin and PSD-95
(A) Representative western blots of synaptosome fractions isolated from BTA-EG_4 and control (DMSO) treated primary cortical neurons probed with antibodies against synaptophysin (38 kDa) and PSD-95 (95 kDa). Blots were also probed with an antibody against β-actin (42 kDa) as a loading control. (B) Bar charts show amounts of PSD-95 and synaptophysin, following normalisation to β-actin levels in each sample. Data are shown

as fold change from control. Data is mean ± SEM, (n=6 wells from two independent experiments, *p<0.05, **p<0.01).

4.4.21 BTA-EG_4 reduces levels of total APP and tau in synaptosomes from primary cortical neurons

As BTA-EG_4 has previously been shown to have actions at the synapse *in vivo* (Megill et al., 2013, Song et al., 2014), it was important to determine if levels of APP and/or tau may be altered at the synapse following BTA-EG_4 treatment, since both tau and APP may hold physiological and pathological roles at the synapse (Spires-Jones and Hyman, 2014). Therefore, synaptosome fractions were immunoblotted with antibodies against total (phosphorylated and non-phosphorylated) tau, APP and β-actin. Treatment with BTA-EG_4 was found to cause a significant reduction in the amounts of both tau and APP in synaptosomes relative to vehicle-treated controls, when the amounts of these proteins was normalised to β-actin (Figure 4.24, $p<0.01$, $p<0.05$, respectively). This finding suggests relocalisation of tau and APP following BTA-EG_4 treatment - events that might be related to the apparent synaptotoxicity observed here upon BTA-EG_4 treatment.

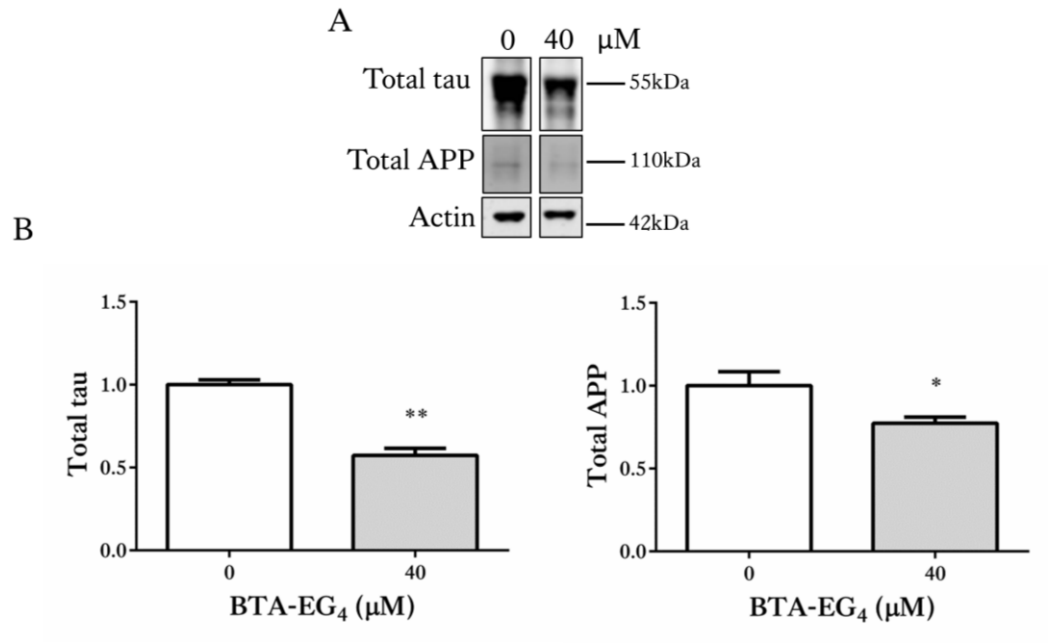

Figure 4.24: Treatment of primary cortical neurons with BTA-EG$_4$ significantly reduces levels of total tau and APP in synaptosome preparations
(A) Representative western blots of synaptosome fractions isolated from BTA-EG$_4$-and control (DMSO)-treated primary cortical neurons probed with antibodies against APP (90-120 kDa) and tau (50-55 kDa). Blots were also probed with an antibody against β-actin (42 kDa) as a loading control. (B) Bar charts show amounts of total tau and total APP following normalisation to β-actin amounts in each sample. Data are shown as fold change from control. Data is mean ± SEM, (n=6 wells from two independent experiments, *p<0.05, **p<0.01).

4.4.22 BTA-EG$_4$ does not affect viability of 3xTg-AD slice cultures

Based on the findings described above, the effect of 40 and 60 μM BTA-EG$_4$ was further investigated in 28 *div* organotypic brain slice cultures from 3xTg-AD mice. An LDH assay was used to first quantify any toxicity resulting from BTA-EG$_4$ treatments of 3xTg-AD slice cultures. Release of LDH into the media was calculated as a proportion of the total LDH in the slice culture lysates and media. Treatment with 40 μM and 60 μM BTA-EG$_4$ over 48 hours did not significantly affect the amount of LDH in culture medium, indicating no change in slice viability when compared to vehicle-treated control cultures (Figure 4.25).

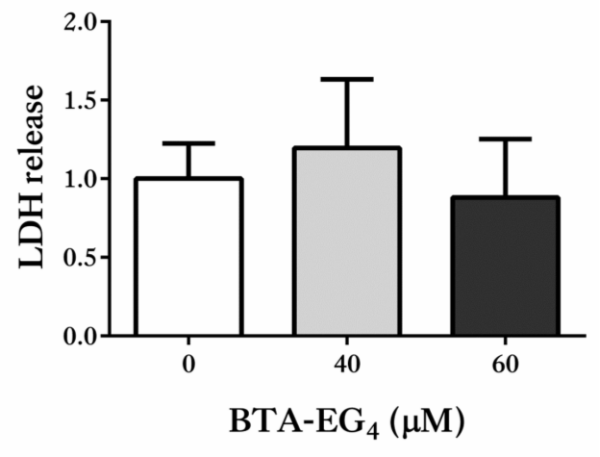

Figure 4.25: Treatment of 3xTg-AD organotypic brain slice cultures with BTA-EG_4 does not affect slice culture viability.
Bar chart shows levels of cell death measured by incorporation of dead cell dye following treatment of 3xTg-AD slice cultures with control (vehicle, 0μM), 40 μM or 60μM BTA-EG_4. Data is shown as fold change from control. Data is mean ± SEM, (n=12 wells from two independent experiments).

4.4.23 BTA-EG_4 treatment does not affect levels of total APP in 3xTg-AD slice cultures

It was next important to determine if BTA-EG_4 treatment of 3xTg-AD slice cultures affected levels of total APP since this model shows altered APP processing and increased Aβ production. Lysates from 3xTg-AD slice cultures treated for 48 hours with control (DMSO), 40 or 60 μM BTA-EG_4 were therefore immunoblotted for total APP and β-actin. Treatment with 40 and 60 μM BTA-EG_4 did not affect levels of total APP, quantified relative to β-actin amounts in the same sample, when compared to vehicle-treated controls (Figure 4.26). Unfortunately, as before, in the time of the project it was not possible to detect and examine amounts of sAPPα and sAPPβ in these cultures with the antibodies available.

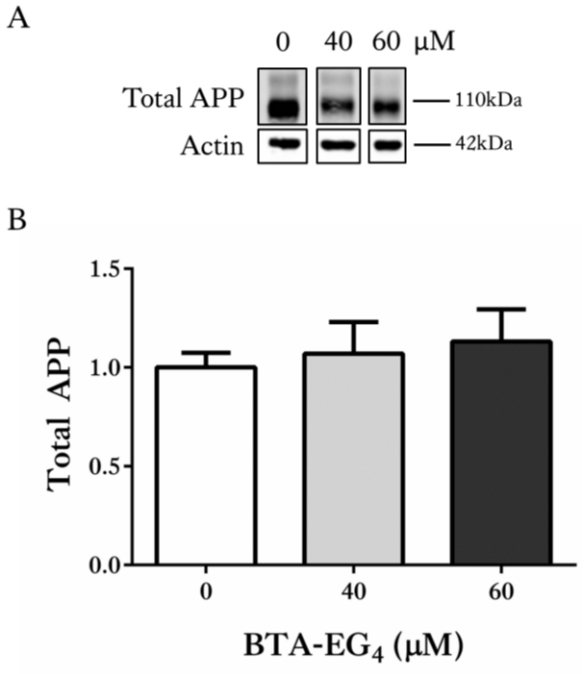

Figure 4.26: BTA-EG$_4$ treatment does not affect levels of total APP in 3xTg-AD slice cultures.
(A) Representative western blots of lysates prepared from 3xTg-AD slice cultures treated with BTA-EG$_4$ and control (DMSO, 0 μM) probed with an antibody against total APP (90-120 kDa). Blots were also probed with an antibody against β-actin (42 kDa) as a loading control. (B) Bar chart shows amounts of total APP following normalisation to β-actin amounts in the same sample. Data are shown as fold change from control. Data is mean ± SEM, (n=12 wells from two independent experiments).

4.4.24 BTA-EG$_4$ does not reduce Aβ amounts in 3xTg-AD slice cultures

Treatment with BTA-EG$_4$ increases amounts of sAPPα and reduces levels of sAPPβ in WT mice, suggesting an ability of BTA-EG$_4$ to alter APP processing, whilst also reducing Aβ-40 amounts *in vivo* (Megill et al., 2013). BTA-EG$_4$ also protects against Aβ and prevents the interaction of amyloid fibrils with amyloid binding proteins *in vitro* (Inbar et al., 2006, Habib et al., 2010). Results from chapter 3 demonstrated that 3xTg-AD slice cultures produce increased amounts of Aβ-42 and Aβ-42/40 compared to WT slice cultures. Therefore the effects of BTA-EG$_4$ on Aβ production in 3xTg-AD mice cultured for 28 *div* and treated for 48 hours with control, 40 or 60 μM BTA-EG$_4$ was determined using

commercial ELISA kits specific for human Aβ-40 and Aβ-42. BTA-EG_4 treatment had no effect compared to control on amounts of Aβ-42, Aβ-40 or the Aβ-42/40 ratio in 3xTg-AD brain slice cultures (Figure 4.27), suggesting a lack of amyloid-binding capacity of this compound in the slice culture model.

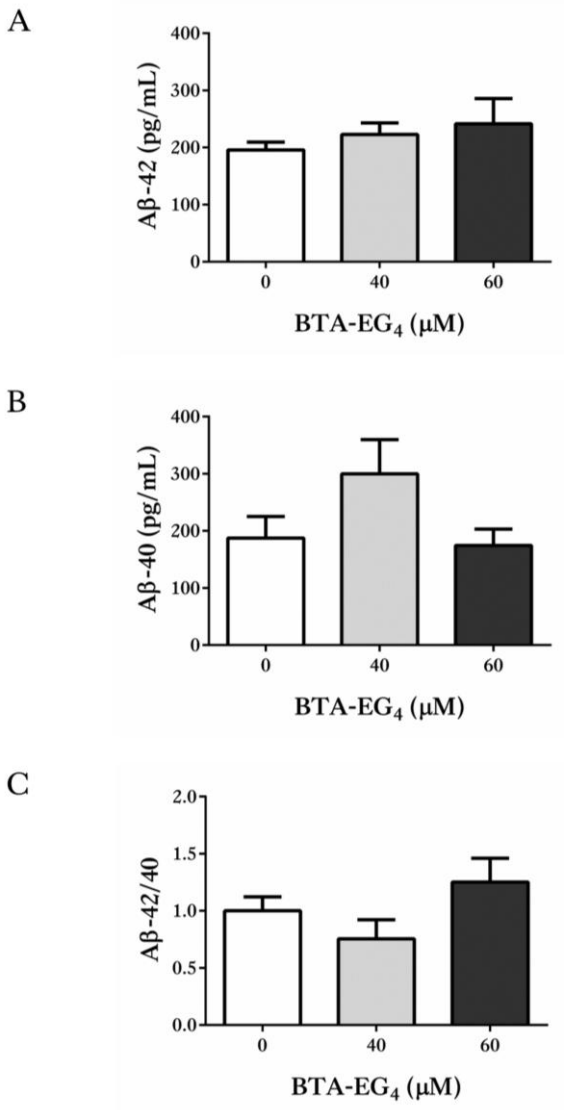

Figure 4.27: Levels of Aβ are unchanged in 3xTg-AD slice cultures following BTA-EG_4 treatment

Amounts of Aβ-40 and Aβ-42 were measured in lysates prepared from 28 *div* 3xTg-AD slice cultures treated for 48 hours with control (DMSO), 40 or 60 μM BTA-EG_4 by specific Aβ-40 and Aβ-42 ELISAs. Lysates contained equivalent amounts of total protein. Bar charts show amounts of (A) Aβ-42 and (B) Aβ-40. Data are shown in pg/mL. (C) Bar chart shows ratio of Aβ-42 relative to Aβ-40. Data are shown as fold control. Data is mean ± SEM, (n=4 wells from two independent experiments).

4.4.25 BTA-EG_4 decreases phosphorylation of tau at ser 202 in 3xTg-AD slice cultures

It was then investigated whether or not BTA-EG_4 can alter tau phosphorylation in 28 *div* 3xTg-AD slice cultures treated with vehicle, 40 μM or 60 μM BTA-EG_4 for 48 hours. Slice culture lysates were immunoblotted with tau antibodies and quantified as described above (section 4.4.17). A 48 hour treatment with 40 and 60 μM BTA-EG_4 did not affect levels of total tau, tau dephosphorylated at ser 199/202, or tau phosphorylated at ser 396/404 in 3xTg-AD slices relative to controls (Figure 4.28). In contrast, the amounts of tau phosphorylated at ser 202 were significantly reduced by 60 μM BTA-EG_4 treatment of 3xTg-AD slice cultures compared to vehicle-treated controls (Figure 4.28, $p<0.05$). This significant reduction in tau phosphorylated at ser 202 in 3xTg-AD slice cultures with 60 μM BTA-EG_4 treatment is also seen following immunolabelling of fixed slices with the antibody against tau phosphorylated at ser 202 (Figure 4.29). It is also apparent from immunolabelling that tau is redistributed from cell soma into axons upon BTA-EG_4 treatment (Figure 4.29).

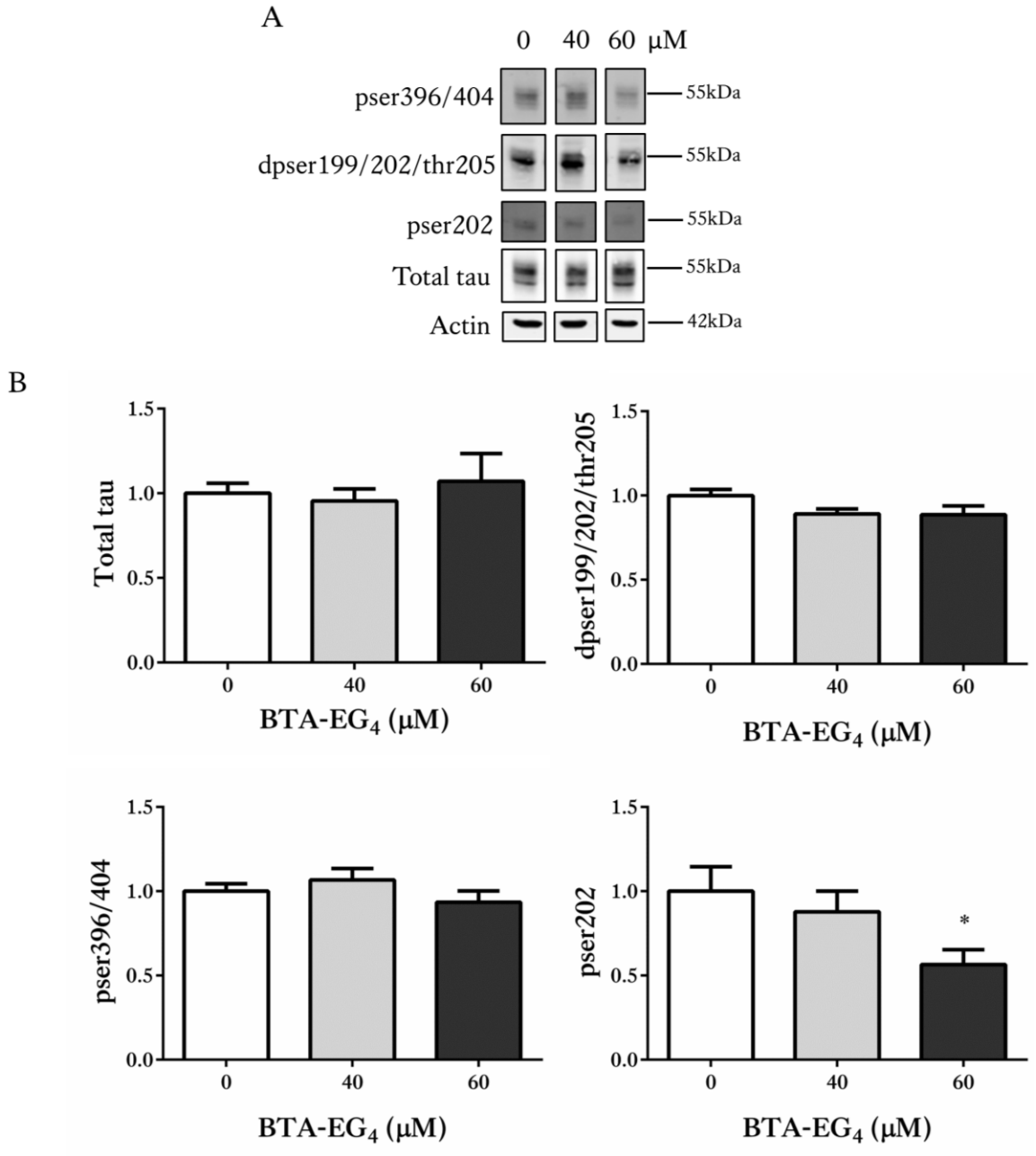

Figure 4.28: BTA-EG$_4$ decreases phosphorylation of tau at ser 202 in 3xTg-AD slice cultures.

(A) Representative western blots of lysates from BTA-EG$_4$-treated and control (vehicle, DMSO)-treated 3xTg-AD slice cultures probed with antibodies against total (phosphorylated and non-phosphorylated) tau, tau phosphorylated at ser 202 and ser 396/404 and tau dephosphorylated at ser 199/202 and thr 205 (all at ~50-55 kDa). An antibody against β-actin (42 kDa) was used as a loading control. (B) Bar charts show amounts of total tau normalised to actin amounts in each sample and amounts of tau dephosphorylated at ser 199/202 and thr 205, tau phosphorylated at ser 396/404 and at ser 202 following normalisation to total tau levels in each sample. Data are shown as fold change from control. Data is mean ± SEM, (n=12 wells from two independent experiments, *p<0.05).

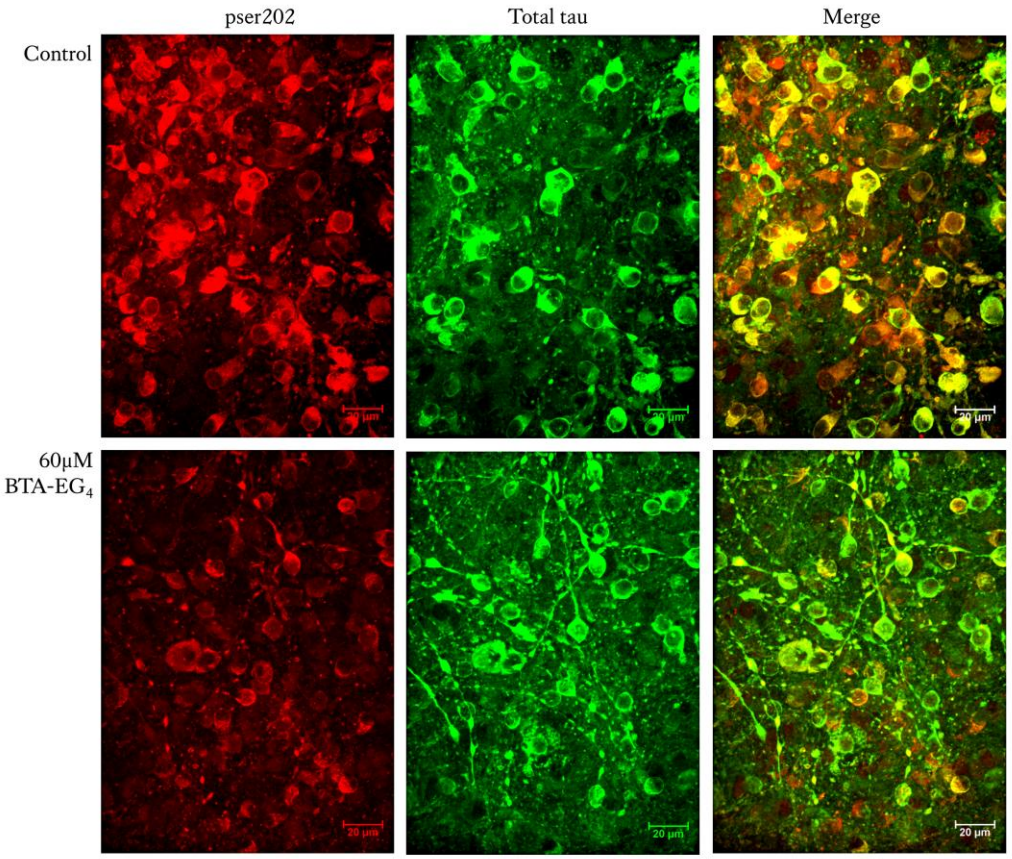

Figure 4.29: BTA-EG$_4$ reduces tau phosphorylation at ser 202 in 3xTg-AD slice cultures
Representative images from fixed 3xTg-AD organotypic brain slice cultures cultured for 28 *div* and treated with control (DMSO) or 60 µM BTA-EG$_4$, immunolabelled with antibodies against total tau (green) and tau phosphorylated at ser 202 (red). Scale bar is 20 µm.

4.4.26 BTA-EG$_4$ significantly reduces GSK-3 activity in 3xTg-AD slice cultures

Treatment of primary cortical neurons with BTA-EG$_4$ significantly increased GSK-3 activity but decreased cdk5 activation by p35 resulting in significant reductions in tau phosphorylation at several AD relevant sites. The activity of GSK-3 and cdk5 was therefore determined in 28 *div* 3xTg-AD slice cultures BTA-EG$_4$ since significant reductions in tau phosphorylated at ser 202 were observed in this model upon BTA-EG$_4$

treatment. Immunoblotting with antibodies against total GSK-3 and phosphorylated ser 21/9 GSK-3 showed that total amounts of GSK-3 were unaffected by treatment with BTA-EG_4 (Figure 4.30), however, phosphorylation of GSK-3 at ser 21/9 was significantly increased following 60 µM BTA-EG_4 treatment relative to controls (Figure 4.30, $p<0.05$), suggesting decreased activation of GSK-3.

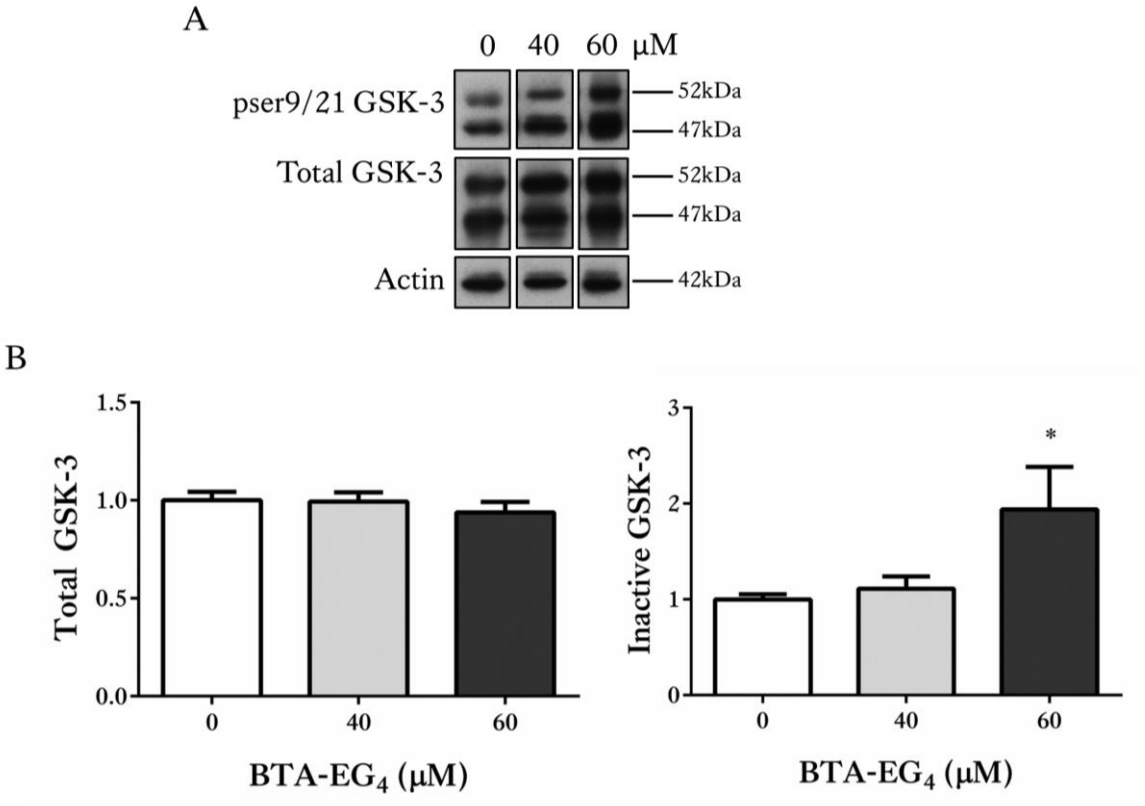

Figure 4.30: BTA-EG_4 significantly decreases inhibitory phosphorylation of GSK-3 in 3xTg-AD slice cultures

(A) Representative western blots of lysates from BTA-EG_4-treated and control (vehicle, DMSO)-treated 3xTg-AD slice cultures probed with antibodies against total (phosphorylated and non-phosphorylated) GSK-3α/β and GSK-3α/β phosphorylated at ser 21/9 (both at 47 and 52 kDa). An antibody against β-actin (42 kDa) was used as a loading control. (B) Bar charts show amounts of total GSK-3 normalised to actin amounts in each sample and amounts of phosphorylated GSK-3 at ser 21/9 following normalisation to total GSK-3 levels in each sample. Data are shown as fold change from control. Data is mean ± SEM, (n=12 wells from two independent experiments, *$p<0.05$).

4.4.27 BTA-EG_4 does not affect cdk5 activity in 3xTg-AD slice cultures

Treatment of primary cortical neurons with BTA-EG_4 decreased cdk5 activity (section 4.4.19). Levels of cdk5, p35 and p25 were detected in lysates from 3xTg-AD slice cultures treated for 48 hours with control, 40 or 60 μM BTA-EG_4 by immunoblotting. Levels of total cdk5 were standardised to actin and amounts of p35 and p25 were normalised to total amounts of cdk5. Total levels of cdk5, and its activators p35 and p25 were unaffected by treatment with BTA-EG_4 (Figure 4.31) suggesting that inhibition of cdk5 activity does not mediate the reduction in tau phosphorylation at ser 202 detected following BTA-EG_4 treatment of 3xTg-AD slice cultures. The reason for the discrepancy in the effect of BTA-EG_4 on cdk5 and GSK-3 activities in primary cortical cultures and 3xTg-AD brain slice cultures is not clear; however, this might be related to alterations in interactions between cdk5 and GSK-3 during the progression of AD in various model systems (Engmann and Giese, 2009).

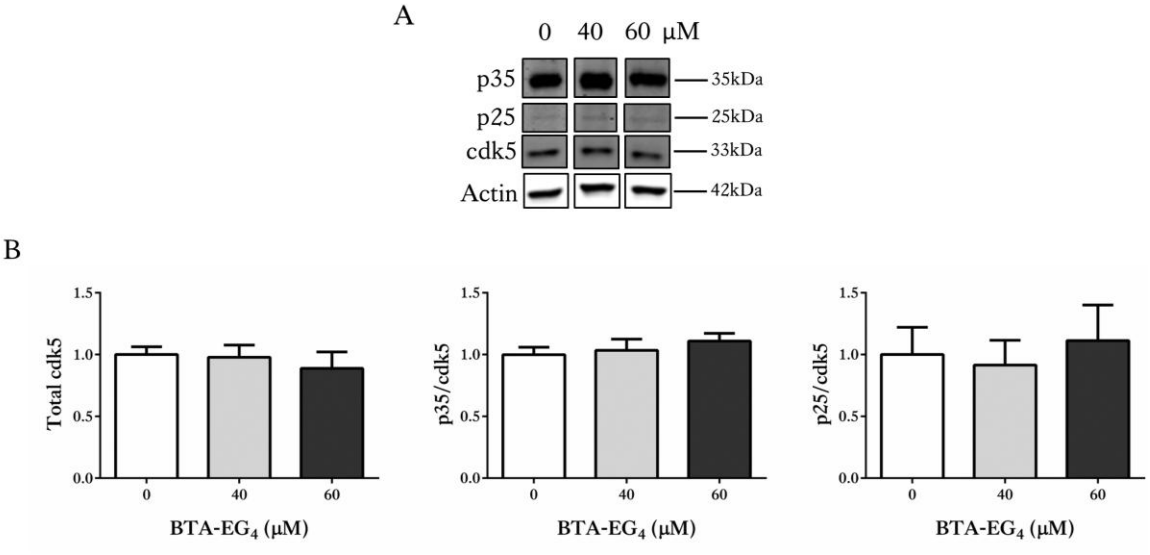

Figure 4.31: BTA-EG$_4$ does not affect cdk5 activity in 3xTg-AD slice cultures
(A) Representative western blots of lysates from BTA-EG$_4$- and control-treated 3xTg-AD slice cultures probed with antibodies against cdk5 (33 kDa), p35 (35 kDa) and p25 (25 kDa). An antibody against β-actin (42 kDa) was used as a loading control. (B) Bar charts show amounts of total cdk5 following normalisation to β-actin amounts in each sample, and amounts of p35 and p25 following normalisation to total cdk5 in each sample. Data are shown as fold change from control. Data is mean ± SEM, (n=12 wells from two independent experiments).

4.4.28 BTA-EG$_4$ does not affect levels of pre- and post- synaptic markers in 3xTg-AD slice cultures

To begin to determine the effect of BTA-EG$_4$ treatment on synapse health in the 3xTg-AD slice culture model, synaptosome fractions were isolated from 28 *div* 3xTg-AD slice cultures after treatment for 48 hours with control, 40 or 60 µM BTA-EG$_4$. The synaptosomal fraction was immunoblotted for synaptophysin, PSD-95 and actin. Treatment with BTA-EG$_4$ did not significantly affect amounts of PSD-95 nor synaptophysin, relative to actin in the synaptosome fraction, when compared to vehicle-treated controls (Figure 4.32).

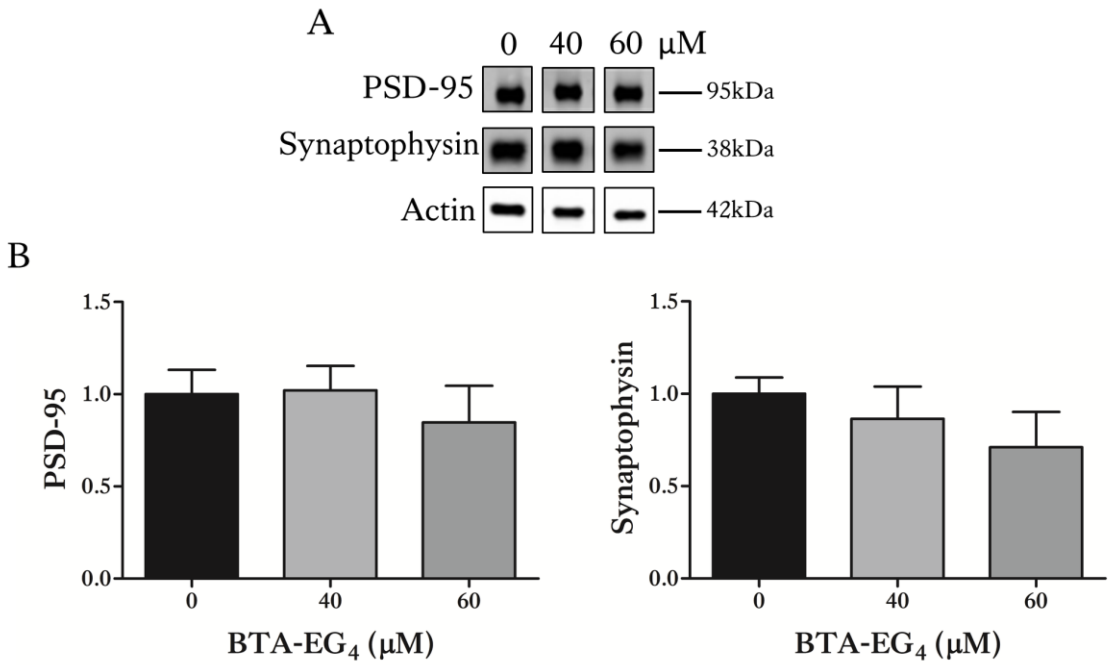

Figure 4.32: Treatment of 3xTg-AD slice cultures with BTA-EG$_4$ does not affect levels of the pre- and post-synaptic markers, synaptophysin and PSD-95
(A) Representative western blots of synaptosome fractions isolated from BTA-EG$_4$ and control (DMSO) treated 3xTg-AD slice cultures probed with antibodies against synaptophysin (38 kDa) and PSD-95 (95 kDa). Blots were also probed with an antibody against β-actin (42 kDa) as a loading control. (B) Bar charts show amounts of PSD-95 and synaptophysin, following normalisation to β-actin levels in each sample. Data are shown as fold change from control. Data is mean ± SEM, (n=9 wells from three independent experiments).

4.4.29 BTA-EG$_4$ does not affect levels of APP or tau at the synapse in 3xTg-AD slice cultures

Increased synaptic tau has been reported here in young 3xTg-AD mice and 14 *div* 3xTg-AD slice cultures (chapter 3), therefore the effect of BTA-EG4 treatment on the presence of these proteins in 3xTg-AD slices was investigated in the synaptosomal fractions by immunoblotting. Treatment of 3xTg-AD slice cultures with BTA-EG$_4$ did not affect amounts of tau nor APP in the enriched synaptosomal pellets compared to vehicle-

treated controls (Figure 4.33). Taken together, these results indicate that BTA-EG_4 causes reduction in tau phosphorylation at specific sites in 3xTg-AD brain slice cultures that are not related to changes in Aβ production or tau localisation in synapses.

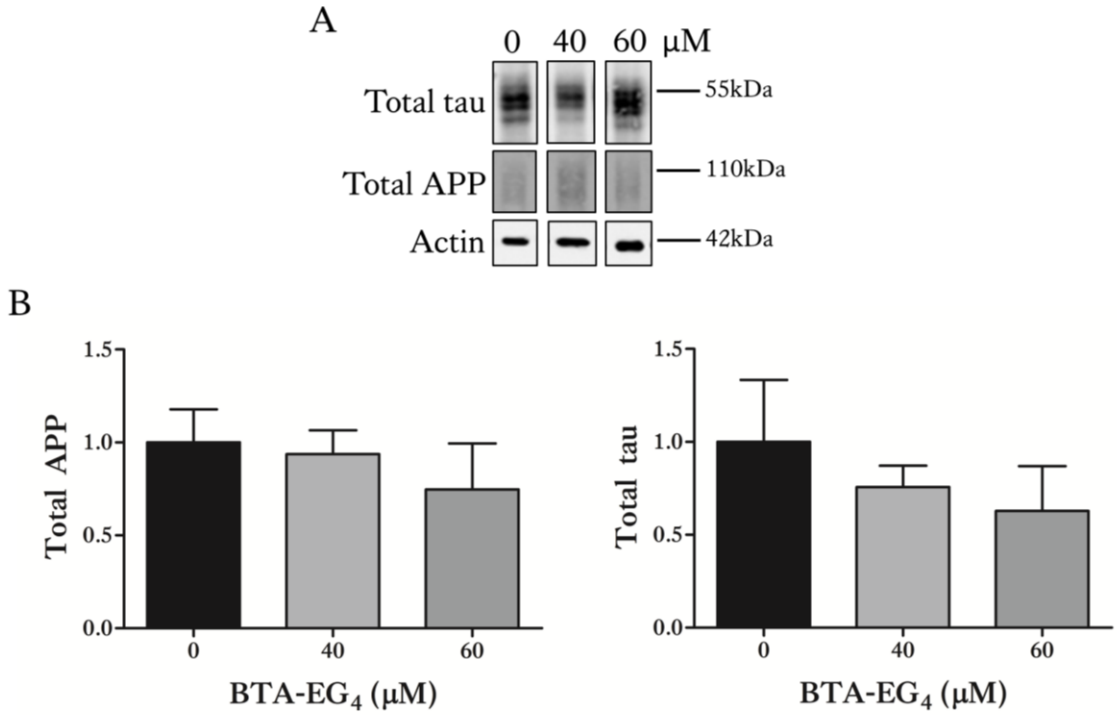

Figure 4.33: Treatment of 3xTg-AD slice cultures with BTA-EG_4 does not affect amounts of tau and APP in synaptosomes
(A) Representative western blots of synaptosome fractions isolated from BTA-EG_4-and control (DMSO)-treated 3xTg-AD slice cultures probed with antibodies against APP (90-120 kDa) and tau (50-55 kDa). Blots were also probed with an antibody against β-actin (42 kDa) as a loading control. (B) Bar charts show amounts of total tau and total APP following normalisation to β-actin amounts in each sample. Data are shown as fold change from control. Data is mean ± SEM, (n=9 wells from three independent experiments).

4.5 Summary

The work presented in this chapter aimed to provide information regarding the potential of 3xTg-AD slice cultures as an alternative to *in vivo* testing for some studies investigating potential AD therapeutics. The main findings were that:

- 3xTg-AD slice cultures treated with LiCl show reduced tau phosphorylation at sites also shown to be affected by LiCl treatment *in vivo* (Caccamo et al., 2007). APP phosphorylation at thr 668 was also shown to be reduced by LiCl treatment in these cultures. However, it was not possible to demonstrate GSK-3 inhibition, and therefore these effects may have been mediated by a GSK-3-independent mechanism.

- 3xTg-AD slice cultures treated with the octapeptide NAPVSIPQ show reduced phosphorylation of tau at thr 231, in agreement with previous 3xTg-AD *in vivo* studies (Matsuoka et al., 2007, Matsuoka et al., 2008) through an, as yet, unidentified mechanism. The effect on tau was not related to NAPVSIPQ promoting microtubule stabilisation.

- 3xTg-AD slice cultures treated with the amyloid-binding agent BTA-EG_4, show no change in APP or Aβ amounts, but did reveal novel inhibitory effects of this compound on tau phosphorylation at ser 202 and GSK-3 activity.

4.6 Discussion

4.6.1 LiCl reduces tau phosphorylation and APP phosphorylation in 3xTg-AD slice cultures but not through phosphorylation of ser 21/9 GSK-3

Initial experiments in primary cortical neurons established a disease-relevant, non-toxic dose of LiCl to take into 3xTg-AD slice cultures (20mM) in an attempt to mimic previous *in vivo* findings that LiCl treatment reduces disease-associated tau phosphorylation.

In vivo treatment of 3xTg-AD mice with LiCl has previously been reported to reduce GSK-3 activity and tau phosphorylation at several sites; thr 181, ser 202/thr 205, thr 231, and thr 212/ser 214. However, treatment of this cohort of 3xTg-AD mice with LiCl did not affect phosphorylation of tau at ser 396/404, levels of soluble and insoluble Aβ-40 and Aβ-42, levels of Aβ-positive plaques, nor did it affect working memory (Caccamo et al., 2007). In 3xTg-AD slice cultures, a 4 hour treatment with 20mM LiCl significantly reduced total tau amounts, tau phosphorylation at ser 396/404 and ser 199/202 and thr205, and reduced the phosphorylation of APP at thr 668. It was not possible to conclude that these effects were mediated by inactivation of GSK-3, as indicated by increased GSK-3 ser 21/9 phosphorylation, since phosphorylation at these inhibitory phosphorylation sites was actually significantly decreased by LiCl application to 3xTg-AD slice cultures.

Thus, treatment of 3xTg-AD slice cultures with LiCl only recapitulated some of the *in vivo* findings. Reduced tau phosphorylation at ser 202/thr205 was observed in both models, however in the slice culture model, reduction in total tau levels and reduced phosphorylation of tau at ser 396/404 was also observed, in contrast to findings *in vivo* (Caccamo et al., 2007). Lithium has previously been demonstrated to decrease tau protein levels and levels of tau phosphorylation in primary neuronal cultures independently of proteolytic processes including calpains, caspases and proteasome or neuronal loss but through reduced GSK-3 activity (Rametti et al., 2008, Martin et al., 2009). This reduction in total tau amounts observed in slice cultures was not through inhibition of GSK-3 at pser21/9 but could well be through tau undergoing autophagy as a result of lithium treatment (Motoi et al., 2014). It is plausible that phosphorylated or

aggregated tau species undergo autophagy and this could be why both a reduction in total tau and phosphorylated tau amounts are observed in slice cultures (Krüger et al., 2012). As phosphorylated tau amounts are standardised to total tau amounts in the analysis, lithium treatment reduces both phosphorylated tau and total tau in 3xTg-AD slice cultures. *In vivo,* reduced phosphorylation of tau in 3xTg-AD mice was attributed to reduced GSK-3 activity through increased phosphorylation of ser 21/9 GSK-3 (Caccamo et al., 2007), but no change in the inhibitory phosphorylation of GSK-3 was observed here. The tau sites investigated in these studies are all targets of GSK-3 (Sperbera et al., 1995, Lovestone et al., 1996), but can also be phosphorylated by other kinases such as cdk5 (Kimura et al., 2014). It is also well established that GSK-3 activity can be regulated by cdk5 activity and vice versa, and that this relationship can change during the progression of neurodegenerative tauopathies (Engmann and Giese, 2009). It is possible that the complex relationship between GSK-3 and cdk5 may thus have precluded detection of reduced GSK-3 activity upon LiCl treatment in 3xTg-AD slices. Alternatively, LiCl can also inhibit GSK-3 activity by competing with magnesium ions (Ryves and Harwood, 2001), and GSK-3 activity can be regulated by phosphorylation at other ser/thr and tyr sites (Wang et al., 1994). These mechanisms were not investigated here and therefore, an effect of LiCl on GSK-3 cannot be discounted in these studies. Finally, it is well known that LiCl can affect the activity of other kinases, and it is possible that these actions might be responsible for the reductions in tau phosphorylation observed in 3xTg-AD slice cultures (Lenox and Wang, 2003).

Levels of insoluble and soluble Aβ-40 and Aβ-42, and Aβ-positive plaques, were unaffected by LiCl treatment *in vivo* in 3xTg-AD mice (Caccamo et al., 2007). Due to restraints with time and resources Aβ was not specifically quantified in the 3xTg-AD slice cultures after treatment, however, LiCl treatment of 3xTg-AD slice cultures was found to significantly reduce levels of APP phosphorylation at thr 668. Reduced phosphorylation at this APP site increases its propensity to be processed via the non-amyloidogenic pathway, precluding the formation of Aβ-42 (Lee et al., 2003), therefore suggesting that LiCl treatment in slice cultures may have reduced levels of Aβ, should they have been quantified here. Whether LiCl treatment can affect APP processing and Aβ production in AD is unclear as some studies, both *in vitro* and *in vivo,* suggest an ability of lithium to reduce Aβ levels (Su et al., 2004), although this was not seen following LiCl treatment of 3xTg-AD mice (Caccamo et al., 2007).

4.6.2 NAPVSIPQ reduces tau phosphorylation in 3xTg-AD slice cultures, but does not affect microtubule stabilisation

Initial experiments carried out in primary cortical neurons established several non-toxic doses of the octapeptide NAPVSIPQ. The non-toxic dose of 1 x 10-7 M NAPVSIPQ, which was found to significantly reduce tau phosphorylation in cultured cells, was selected for treatments in 3xTg-AD slice cultures.

NAPVSIPQ was previously reported to lower levels of Aβ-40 and Aβ-42, reduced tau phosphorylation and improved memory impairments in 9 to 12 month old 3xTg-AD mice (Matsuoka et al., 2007). In 12 to 18 month old mice, reduced tau phosphorylation and

cognitive improvements were again observed, but at this age no effects on Aβ-40 and Aβ-42 were detected (Matsuoka et al., 2008). *In vitro* treatment of 3xTg-AD slice cultures with NAPVSIPQ replicated some of these *in vivo* findings.

In 3xTg-AD slice cultures, NAPVSIPQ reduced tau phosphorylation at thr 231, in agreement with *in vivo* studies (Matsuoka et al., 2007, Matsuoka et al., 2008). However, phosphorylation of tau at ser199/202 and thr205 was unaffected by NAPVSIPQ treatment in 3xTg-AD slice cultures, despite phosphorylation at these sites being reduced by NAPVSIPQ treatment *in vivo* (Matsuoka et al., 2007, Matsuoka et al., 2008). This discrepancy could perhaps be attributed to levels of tau phosphorylation in the 3xTg-AD slice cultures being higher than those observed in aged mice, and therefore possibly less amenable to treatment with NAPVSIPQ. Another important difference is that the slice cultures were only treated once with NAPVSIPQ, whereas the 3xTg-AD mice were dosed every day for 4 weeks (Matsuoka et al., 2007) or every day over 3 to 6 months (Matsuoka et al., 2008). It is possible that chronic exposure to NAPVSIPQ is needed to reduce tau phosphorylation at sites other than thr 231.

No mechanisms to explain reductions in tau phosphorylation and insoluble tau resulting from NAPVSIPQ treatment in mouse models of tauopathies have yet been described (Matsuoka et al., 2007, Matsuoka et al., 2008, Shiryaev et al., 2009). *In vitro* experiments show that NAPVSIPQ can increase the probability of microtubules becoming stabilised (Gozes and Divinski, 2004, Divinski et al., 2006). The microtubule binding assays conducted here and assessments of acetylated α-tubulin levels indicate that NAPVSIPQ

does not increase the amounts of tau bound to microtubules in primary cortical cultures or 3xTg-AD mice, and therefore it is unlikely that NAPVSIPQ is mediating its effects on tau through alterations in microtubule stability. Similarly, others have shown that NAPVSIPQ does not directly affect the polymerization or dynamics of purified tubulin or microtubules (Yenjerla et al., 2010).

4.6.3 BTA-EG_4 reduces GSK-3 activity and tau phosphorylation at ser 202 in 3xTg-AD slice cultures

A non-toxic, concentration of up to 60 μM BTA-EG_4 was identified in primary cortical neurons as causing significant reductions in tau phosphorylation, and this was further investigated in 3xTg-AD slice cultures. This neuroprotective, amyloid-binding compound (Inbar et al., 2006, Habib et al., 2010) had previously been reported to have positive effects on memory and at the synapse in both WT and 3xTg-AD mice (Megill et al., 2013, Song et al., 2014). Until now, effects of BTA-EG_4 on kinase activity and tau phosphorylation have not been reported.

No effects of BTA-EG_4 on total amounts of APP were observed in treated 3xTg-AD slice cultures, in agreement with previous findings *in vivo* in WT mice (Megill et al., 2013). In 3xTg-AD slice cultures, no effects of BTA-EG_4 on levels of Aβ-42, Aβ-40 or the Aβ-42/40 ratio were detected. This is in contrast to *in vivo* studies in WT mice and 3xTg-AD mice, where BTA-EG_4 was shown to significantly reduce levels of Aβ-40 (Megill et al., 2013, Song et al., 2014), however this effect was lost in older 3xTg-AD mice (Song et al., 2014). Taken together, these findings suggest that in the very early stages of AD development,

where only small over-production of Aβ is observed, BTA-EG_4 can reduce Aβ levels, but that this protective effect is lost in later disease stages, at times when Aβ has accumulated. Extrapolating these findings might suggest that perhaps BTA-EG_4 had no effect on Aβ in 28 *div* 3xTg-AD cultures since these already show significant over-production of Aβ.

In 3xTg-AD slice cultures, BTA-EG_4 was shown for the first time to significantly reduce GSK-3 activity, and tau phosphorylation at ser 202, but not ser 396/404. Cdk5 activity was unaffected by BTA-EG_4 treatment in 3xTg-AD slice cultures. Significant reductions in phosphorylation of tau at ser 199/202 and thr 205, ser 202 and ser 396/404 were observed following BTA-EG_4 treatment of primary cortical neurons, although in this case cdk5, rather than GSK-3 activity, was found to be reduced. The discrepancy in kinase activities might be related to interactions between GSK-3 and cdk5, which differ depending on whether the system contains pathological tau (3xTg-AD slice cultures) or more physiological tau (WT primary cortical neurons), as discussed above. Taken together, these findings suggest that treatment with BTA-EG_4 can reduce tau phosphorylation at several AD-relevant sites, but its effect is likely to be highly dependent on disease stage. Nevertheless, these findings support further investigations into the use of BTA-EG_4 and similar compounds in the treatment of tauopathies. They also highlight the importance of the disease stage of models when determining the effectiveness of potential therapies.

4.6.4 Limitations of this work

28 *div* slice cultures were used in this study. These show increased tau phosphorylation at several AD-relevant sites, an increased abundance of high molecular weight tau and increased Aβ-42. If time had permitted, it would have been interesting to determine the effects of treatments on slices cultured for shorter and longer times to further investigate the effects of disease stage on the effectiveness of each treatment.

Additionally, to corroborate findings of (Megill et al., 2013) on the effects of BTA-EG_4 on sAPPα and sAPPβ, several antibodies were used to try to detect these proteins, but unfortunately in the time of the project these were unable to be examined.

4.6.5 Conclusions

The findings presented in this chapter suggest that treatment of 3xTg-AD organotypic brain slice cultures with the AD-relevant therapies - LiCl and NAPVSIPQ - faithfully recapitulate the majority of findings obtained when these treatments were investigated *in vivo* in 3xTg-AD mice. Together, these results suggest that 3xTg-AD slice cultures are a suitable *ex vivo* alternative for some *in vivo* drug development and discovery projects. It is well established that lithium is an inhibitor of GSK-3; findings here suggest that lithium may also act to reduce tau phosphorylation by the inhibition of other kinases or the promotion of autophagy as previously reported (Lenox and Wang, 2003, Motoi et al., 2014). Furthermore, experiments in 3xTg-AD slice cultures have demonstrated that NAPVSIPQ does not act to reduce tau phosphorylation via increasing microtubule stability, which is the only mode of action which has been suggested for NAPVSIPQ

previously (Quraishe et al., 2013). It is plausible to speculate that NAPVSIPQ may inhibit the major tau kinases - GSK-3 and cdk5 to reduce tau phosphorylation and this could easily be addressed in future experiments in 3xTg-AD slice cultures. Finally, treatment of 3xTg-AD slice cultures with the amyloid-binding agent BTA-EG_4 has allowed identification of novel actions on GSK-3 activity, as well as its previously identified effects on Ras activity and the prevention of amyloid interactions (Megill et al., 2013, Habib et al., 2010). Overall, 3xTg-AD slice cultures provide an excellent novel platform in which to test compounds on AD-like disease features and to investigate the mechanisms by which they act. In the next chapter 3xTg-AD slice cultures are used as a model in which to investigate additional disease mechanisms, namely mechanisms of tau release and propagation in AD.

Chapter 5 : Understanding mechanisms of physiological and pathological tau release using organotypic brain slice cultures

5.1 Introduction

Understanding the mechanisms of tau release and propagation in tauopathy brain is likely to be critical for developing new strategies to treat these diseases. Several studies have shown that pathological tau species can be seeded and transmitted *in vivo* from brain region to region and from cell to cell through anatomical connections in a spatiotemporal manner (Clavaguera et al., 2009, de Calignon et al., 2012, Clavaguera et al., 2013, Sanders et al., 2014). Research in this area has expanded over the last several years, as we seek to understand the mechanisms underlying the release and propagation of "normal" tau in basal conditions and that of "pathological" tau in disease models, as well as the implications of tau propagation for neurodegeneration. The latter has recently come into question since removing endogenous tau from a transgenic model of tau propagation was shown not to prevent tau propagation but removes its toxicity (Wegmann et al., 2015).

Low levels of tau have been found in the CSF and ISF of normal individuals (Hampel et al., 2010) as well as in the CSF and ISF of healthy mice (Barten et al., 2011, Yamada et al., 2011) suggesting that tau release is a normal physiological process and that extracellular tau is not found only as a result of passive tau release from degenerating neurons. Considerable evidence from cell and animal models adds support to this hypothesis. For

example, tau is found in the medium of healthy primary cultured mouse and human neurons (Chai et al., 2012, Pooler et al., 2013, Kanmert et al., 2015) with tau release shown to occur through mechanisms not involving classical secretion pathways (Chai et al., 2012), or association of tau with exosomes (Chai et al., 2012, Kanmert et al., 2015), although small amounts of secreted tau have been found in association with ectosomes, vesicles that originate from plasma membranes (Dujardin et al., 2014). Furthermore, the increased physiological secretion of tau from neurons can be increased upon neuronal stimulation with KCl and AMPA (Pooler et al., 2013). Synaptic activity has been further implicated in this process since blocking neuronal activity and pre-synaptic vesicle release with tetrodotoxin and tetanus toxin was found to block calcium-dependent tau release in these studies (Pooler et al., 2013). Similar findings have since been reported in healthy WT mice (Yamada et al., 2014).

There has been considerable interest in determining the species of tau released from neurons and some conflicting data exists in the literature. Endogenous tau species released from cultured rat neurons are predominantly dephosphorylated when compared to tau species found intracellularly (Pooler et al., 2013), although phosphorylation at thr 181 was detected in extracellular tau released from human iPSC-derived neurons (Chai et al., 2012). In addition, several studies report that extracellular endogenous tau contains predominantly full-length tau species (Chai et al., 2012, Pooler et al., 2013), however, C-terminally truncated tau species have been reported as released from neurons in other studies (Kanmert et al., 2015). While the function of this extracellular tau is not well understood, its clearance from wild-type mouse brain can

take many days (Yamada et al., 2014), and exogenously applied extracellular tau species have been shown to activate muscarinic receptors (Gómez-Ramos et al., 2008, Gómez-Ramos et al., 2009) suggesting a signalling function of extracellular tau.

In disease, the levels of both total and phosphorylated tau are elevated in the CSF and ISF of individuals with AD relative to controls (Blennow et al., 1995, Meredith Jr et al., 2013), and the CSF from AD patients contains increased amounts of N-terminal tau fragments, with no evidence of full-length or C-terminal fragments of tau compared to controls (Meredith Jr et al., 2013). Moreover, elevated total and phosphorylated tau protein levels can be detected in exosomes prepared from blood from MCI and AD patients. Neural exosomes were prepared through differential centrifugation using an ExoQuick™ (System Biosciences, USA) precipitation method followed by immunochemical enrichment with antibodies for the neuronal adhesion proteins L1 and NCAM. ELISAs were then used to detect levels of total and phosphorylated tau in the enriched neuronal exosomes (Fiandaca et al., 2015). This finding suggests that there are alterations to normal tau secretion pathways that may underlie tau propagation in neurodegenerative tauopathies. The trans-synaptic spread of tau pathology has been elegantly demonstrated *in vivo* (Liu et al., 2012, de Calignon et al., 2012) and many *in vitro* experiments have since been conducted to elucidate the mechanisms underlying these events.

It has been demonstrated that unlike normal endogenous tau, exogenously expressed abnormally phosphorylated or aggregated “pathological” tau released from cultured

neural cells is commonly associated with exosomes in the extracellular space (Saman et al., 2012, Simón et al., 2012, Asai et al., 2015) and can be full-length or C-terminally truncated (Plouffe et al., 2012). In addition, in models in which the cell to cell propagation of tau species has been studied, tau capable of transmission has been identified as largely soluble and oligomeric, but not fibrillar since PHFs have been demonstrated to not propagate (Lasagna-Reeves et al., 2012, Iba et al., 2013), and one recent paper has shown that rare and very highly phosphorylated tau multimers are integral to this process (Takeda et al., 2015). Since tau species released under physiological conditions are largely dephosphorylated, this raises questions about whether or not tau release under physiological and disease conditions occurs through the same or alternative mechanisms.

Finally, the effects of Aβ on the propagation of pathological tau are still under investigation since this may be highly relevant for the spread of tau pathology across AD brain. *In vivo*, the presence of Aβ dramatically increases the speed and distance of tau propagation and increases tau-induced neurotoxicity (Pooler et al., 2015). Furthermore, when neuronal injury by Aβ is caused, the extracellular levels of both aggregation-prone microtubule binding region-containing fragments of tau and full-length tau are increased (Kanmert et al., 2015).

It is important that we further elucidate any similarities and differences between the release of tau under physiological and pathological conditions as this will increase understanding of the relevance of tau propagation in neurodegenerative diseases since

targeting the spread of extracellular tau could be useful in preventing the progression of AD and tauopathies. In addition, it is useful to better understand the function of tau released under physiological conditions since it is possible that dysregulation of normal tau release may also have damaging effects in disease.

5.2 Aims and objectives

The primary aims of the studies presented in this chapter were to begin to gain a better understanding of the mechanisms of physiological and pathological tau release in slice cultures prepared from WT and 3xTg-AD mice. The specific aims of this chapter were to:

- Measure basal levels of tau release from WT and 3xTg-AD slice cultures.

- Determine the effect of stimulating neuronal activity on tau release from WT and 3xTg-AD slice cultures.

- Assess the effects of inhibiting neuronal activity on the secretion of tau from WT and 3xTg-AD slice cultures.

- Investigate the relationship between tau localisation in neurons and its release by examining tau content in the cytosol and membrane under basal conditions and following neuronal stimulation.

5.3 Methods

The methods used for this work are detailed in Chapter 2. In brief, organotypic brain slice cultures were prepared from postnatal day 8 or 9 WT and 3xTg-AD mice and cultured for 28 days. At this point, total amounts of tau released into culture medium under basal conditions or following treatment to stimulate neuronal activity and/or block pre-synaptic vesicle release was measured by a total tau ELISA, developed in-house. LDH release from these slice cultures was used as a measurement of cell death. Cytosol and membrane fractions from slice cultures were also prepared using differential centrifugation, and tau species in these fractions were assessed by immunoblotting.

5.4 Results

5.4.1 Basal tau release from 3xTg-AD slice cultures is significantly increased compared to that from WT slice cultures

Basal tau release from both WT and 3xTg-AD slice cultures was assessed to determine any differences in tau release from an AD model in which disease-related changes in tau phosphorylation are apparent (Chapter 3). Total amounts of tau released into fresh culture medium over a period of 30 minutes were measured using an in-house total tau ELISA that uses two commercially available tau antibodies with epitopes in the middle region (BT2) and C-terminal portion (DAKO) of tau. Intracellular tau amounts were determined in the same cultures by immunoblotting, as described previously (Chapter 3). The amounts of tau detected in culture medium were then normalised to amounts of intracellular tau in the same sample to control for the effects of tau over-expression in

the 3xTg-AD slices and allow determination of the proportion of total tau released from slices to be determined. In addition, the amount of LDH released into the media from the same slices was measured to ensure that changes in tau release were not a result of increased cell death. The LDH content in culture medium was calculated as a proportion of the total LDH in the slice culture lysates plus that measured in medium.

The results of these analyses revealed that there were no significant differences in the amounts of LDH released from WT and 3xTg-AD slice cultures, (Figure 5.1). In contrast, the medium of 3xTg-AD slice cultures was found to contain significantly increased tau amounts when compared to WT slice cultures, indicating increased basal tau release from 3xTg-AD slices (Figure 5.1, $p<0.05$). Since no changes in LDH release were observed, these results indicate that the increased tau release from 3xTg-AD slices did not result from increased cell death in 3xTg-AD cultures.

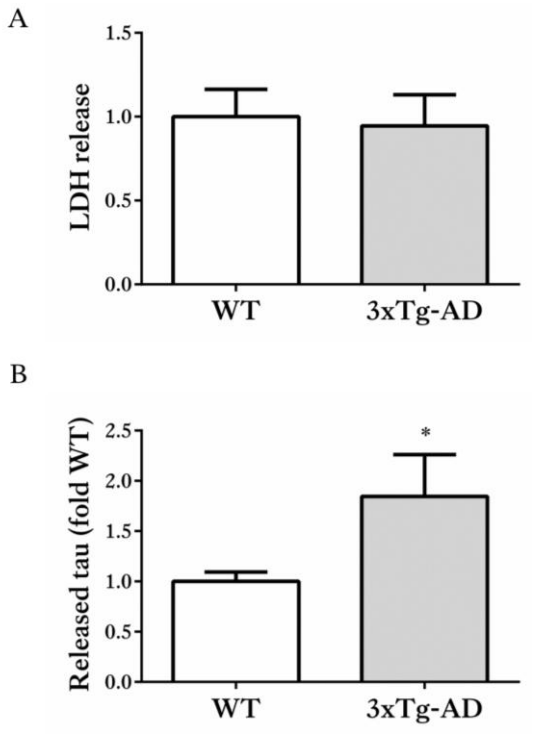

Figure 5.1: Basal tau release is significantly increased in 3xTg-AD slice cultures.
Tau and LDH release into the culture medium of 28 *div* WT and 3xTg-AD slice cultures was measured over a period of 30 minutes. (A) Release of LDH was measured to assess slice viability. LDH in culture medium was determined as a proportion of total LDH (LDH in lysates plus that in culture medium). Bar chart shows medium/total LDH as fold change from WT slice cultures. (B) Amounts of total tau released into the media were measured by ELISA and were standardised to total intracellular tau amounts in the same sample. Data are shown as fold change from WT slice cultures. Data is mean ± SEM, (n=24 wells from four independent experiments, *p<0.05).

5.4.2 Neuronal stimulation increases the release of tau from WT but not 3xTg-AD slice cultures

To assess the effects of neuronal stimulation on the release of normal and disease-associated tau from both WT and 3xTg-AD slice cultures, 50mM KCl was applied to depolarise neurons and stimulate neuronal activity over a period of 30 minutes. This had previously been shown to increase tau release from rat primary cortical neurons (Pooler et al., 2013). As described above, tau release into the media was detected by ELISA and

standardised to intracellular tau amounts, and LDH release was also measured to account for any tau release by cell death.

No significant differences in amounts of LDH release between depolarised and non-depolarised WT and 3xTg-AD slice cultures were identified, suggesting any increased tau release was not a result of increased cell death (Figure 5.2). When stimulated with KCl, WT slice cultures showed significant increases in extracellular tau release compared to non-stimulated WT slice cultures (Figure 5.2, $p<0.05$), in agreement with published data from rat primary cortical neurons (Pooler et al., 2013). In stark contrast, 3xTg-AD slice cultures stimulated with KCl did not demonstrate any further release of tau when compared to non-stimulated 3xTg-AD slice cultures (Figure 5.2). These findings suggest that possibly different mechanisms control the release of normal and disease-associated tau.

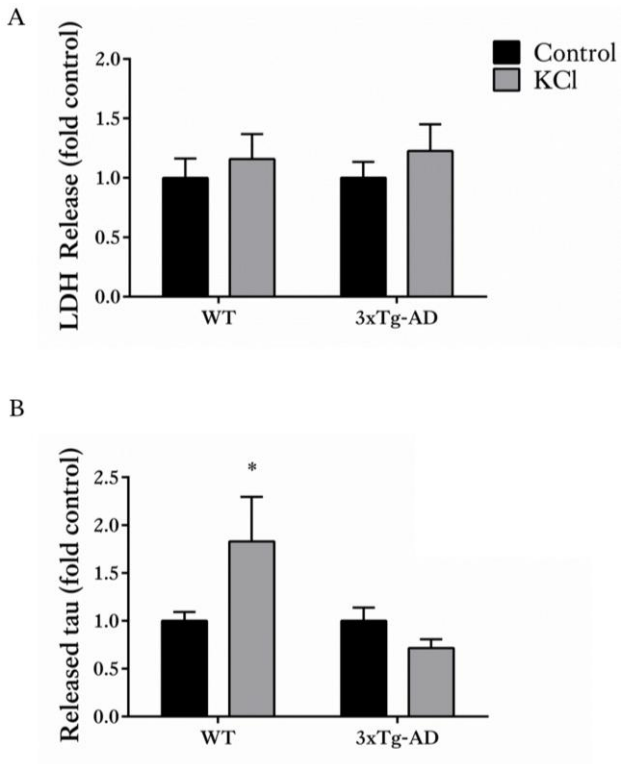

Figure 5.2: Neuronal stimulation with KCl significantly increases tau release from WT but not 3xTg-AD slice cultures.
Tau and LDH release into the media from 28 *div* WT and 3xTg-AD slice cultures, stimulated with 50 mM KCl, or control (non-stimulated) was measured over a period of 30 minutes. (A) Release of LDH was measured to assess slice viability. LDH in culture medium was determined as a proportion of total LDH (LDH in lysates plus that in culture medium). Bar chart shows medium/total LDH as fold change from control-treated slice cultures. (B) Amounts of total tau released into the media were measured by ELISA and standardised to total intracellular tau amounts. Data are shown as fold change from control-treated slice cultures. Data is mean ± SEM, (n=24 wells from four independent experiments, *p<0.05).

5.4.3 3xTg-AD slice cultures have increased amounts of dephosphorylated tau at the membrane

Mislocalisation of tau is a prominent feature of diseased brain (Noble et al., 2013). Although generally thought of as cytosolic, a significant proportion of tau is associated with plasma membranes (Brandt et al., 1995, Pooler et al., 2013). Membrane-associated tau is predominantly dephosphorylated at ser/thr residues compared to cytosolic tau

(Arrasate et al., 2000, Pooler et al., 2012), and since some of the vesicles (ectosomes, exosomes) associated with tau release originate at the plasma membrane it was of interest to investigate the proportions of tau at membranes in WT and 3xTg-AD slices to determine if there may be any association with levels of tau release. Therefore, differential centrifugation was used to prepare membrane and cytosol fractions from the slice culture lysates cultured in fresh medium for 30 minutes prior to measurement of tau released into culture medium. The method to prepare membrane and cytosol fractions has been reported previously and the majority of the tau in the membrane fraction was determined to be plasma membrane-associated (Pooler et al., 2012). These fractions were then immunoblotted with total (phosphorylated and non-phosphorylated) tau and phosphorylation-dependent tau primary antibodies. In 3xTg-AD slice cultures the ratio of total tau present in the membrane fraction relative to the cytosolic fraction was significantly decreased compared to WT slice cultures (Figure 5.3, $p<0.05$). However, the ratio of tau dephosphorylated at ser 199/202 and thr 205 (following normalisation to total tau) present in the membrane fraction relative to the cytosolic fraction was significantly increased in 3xTg-AD slices compared to that in WT slice cultures (Figure 5.3, $p<0.05$). In agreement with this finding, the ratio of tau phosphorylated at ser 396/404 (as a proportion of total tau) present in the membrane fraction relative to the cytosolic fraction was significantly decreased compared to WT slice cultures (Figure 5.3, $p<0.01$). These findings show that in 3xTg-AD slices, although overall there is a decreased total proportion of tau associated with membranes, there is an increased pool of membrane-associated dephosphorylated tau under basal

conditions, an environment in which these slices also show elevated tau release relative to that of WT slices.

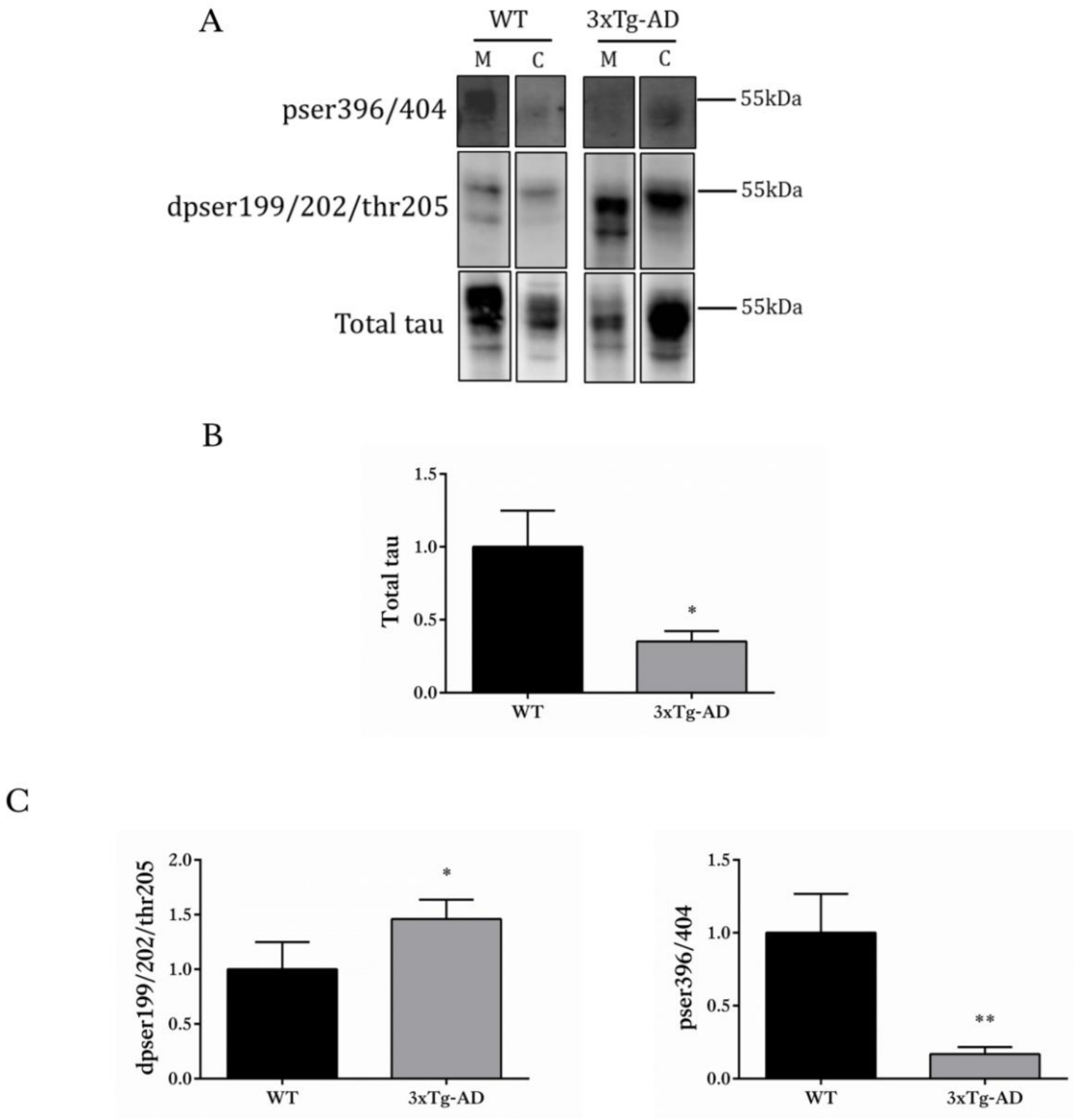

Figure 5.3: 3xTg-AD slice cultures contain less total membrane-associated tau, yet an increased presence of a dephosphorylated tau pool at membranes.
(A) Representative western blots of membrane and cytosol fractions prepared from WT and 3xTg-AD slice cultures showing total (phosphorylated and non-phosphorylated) tau, tau phosphorylated at ser 396/404 (PHF-1) and dephosphorylated at ser 199/202 and thr 205 (Tau-1), all at ~50-64 kDa. Bar charts show (B) the ratio of total tau present in the membrane fraction relative to the cytosolic fraction, and (C) the ratio of tau dephosphorylated at ser 199/202 and thr 205 or tau phosphorylated at ser 396/404 present in the membrane fraction relative to the cytosolic fraction all normalised to total tau amounts in the same fraction of the same sample. Data is shown as fold change from

WT slice cultures. Data is mean ± SEM, (n=12 wells from two independent experiments, *p<0.05, **p<0.01).

5.4.4 Both N-terminal and C-terminal fragments of tau are present in the membrane in WT and 3xTg-AD slice cultures

The cleavage of tau is a post-translational modification which can affect tau function, with some fragments acting as seeds which promote tau aggregation (Wang et al., 2014). Tau cleaved at both its N- and C-termini has been detected in AD brain (Garcia-Sierra et al., 2008). This truncation of tau is catalysed predominantly by caspases, calpains and asparagine endopeptidases (Rissman et al., 2004, Ferreira and Bigio, 2011, Zhang et al., 2014).

Currently, no consensus exists on whether N-terminally or C-terminally truncated or intact tau is the species of tau that propagates, as discussed above. Endogenous tau released under basal conditions from primary cortical rat neurons has been demonstrated to be predominantly full length (Pooler et al., 2013), although some truncated species have been identified together with full-length tau (Dujardin et al., 2014). However, others show that only C-terminally truncated forms of endogenous tau are secreted from unstimulated human and rodent neurons (Kanmert et al., 2015). In contrast, pathological extracellular tau in a rat model of tauopathy contains tau lacking the C-terminus but containing the N-terminus (Dujardin et al., 2014), and C-terminally truncated tau is also released from AD synaptosomes (Sokolow et al., 2015).

Additionally, exogenously expressed hyperphosphorylated tau secreted from non-neuronal cells was demonstrated to be C-terminally cleaved (Plouffe et al., 2012).

To determine which species of tau are associated with membranes, the membrane fractions prepared from 28 *div* WT and 3xTg-AD slice cultures were immunoblotted with primary antibodies directed against the N-terminus (TP007) and C-terminus (TP70) of tau. As can be seen in Figure 5.4, membranes of both WT and 3xTg-AD slice cultures contain predominantly full length tau species of 50-64 kDa with intact N- and C- termini. However, some smaller tau species of approximately 35-40 kDa and 28-30 kDa were detected by the TP007 and TP70 antibodies, respectively indicating the presence of some C-terminally and N-terminally truncated tau present at membranes in both WT and 3xTg-AD slices. There were no marked differences in the tau species detected between genotypes.

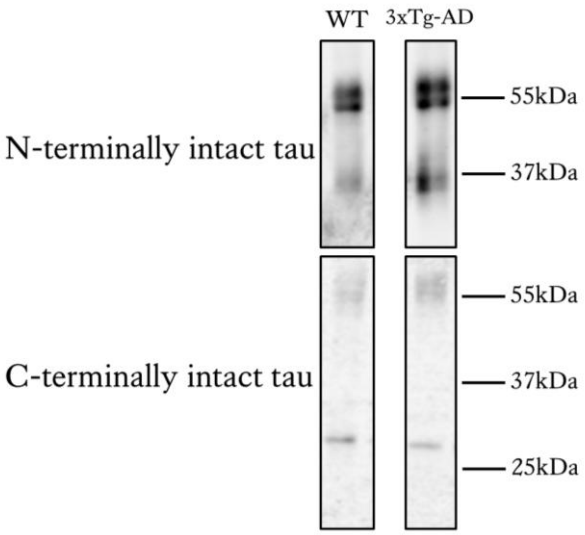

Figure 5.4: Membrane-associated tau is largely intact in both WT and 3xTg-AD slice cultures.
Representative western blots of membrane fractions prepared from 28 *div* WT and 3xTg-AD slice cultures showing N-terminally intact (TP007) and C-terminally intact (TP70) tau at 50-64 kDa representing full-length tau, and some smaller fragments of ~28-40 kDa.

5.4.5 Neuronal stimulation of WT and 3xTg-AD slice cultures has differential effects on the pool of dephosphorylated tau associated with membranes

Membrane and cytosolic fractions were prepared from WT and 3xTg-AD slice cultures at 28 *div* treated with control or 50 mM KCl to induce depolarisation. These fractions were immunoblotted with total tau (phosphorylated and non-phosphorylated) and tau phosphorylation-dependent primary antibodies. In both WT and 3xTg-AD slice cultures treated with KCl, the ratio of total tau present in the membrane fraction relative to the cytosolic fraction did not differ from control treatment (Figure 5.5). However, in WT slice cultures treated with KCl, the ratio of tau phosphorylated at ser 396/404 (following normalisation to total tau) present in the membrane fraction relative to the cytosolic fraction was significantly decreased compared to control treatment (Figure 5.5, $p<0.05$). Similarly, the ratio of tau dephosphorylated at ser 199/202 and thr 205 (following normalisation to total tau) present in the membrane fraction relative to the cytosolic fraction was significantly increased compared to control treatment (Figure 5.5, $p<0.01$), showing an increased association of dephosphorylated tau with membranes following neuronal stimulation, conditions under which tau release was increased.

In contrast, in 3xTg-AD slice cultures treated with KCl, the ratio of tau phosphorylated at ser 396/404 (normalised to total tau) present in the membrane fraction relative to the cytosolic fraction was significantly increased compared to control treatment (Figure 5.5, $p<0.05$), and the ratio of tau dephosphorylated at ser 199/202 and thr 205 (normalised to total tau) present in the membrane fraction relative to the cytosolic fraction did not

differ from the control treatment (Figure 5.5). These data show no increase in the pool of dephosphorylated tau associated with membranes upon neuronal stimulation of 3xTg-AD slices, conditions under which tau release was not increased above basal levels. Taken together, these data indicate that conditions leading to an increased pool of dephosphorylated tau at membranes are associated with tau release from slice cultures. In addition, these data further suggest that differences in the effect of neuronal stimulation on tau release from tissues containing normal or disease-associated tau might be related to the subcellular localisation of pools of dephosphorylated tau.

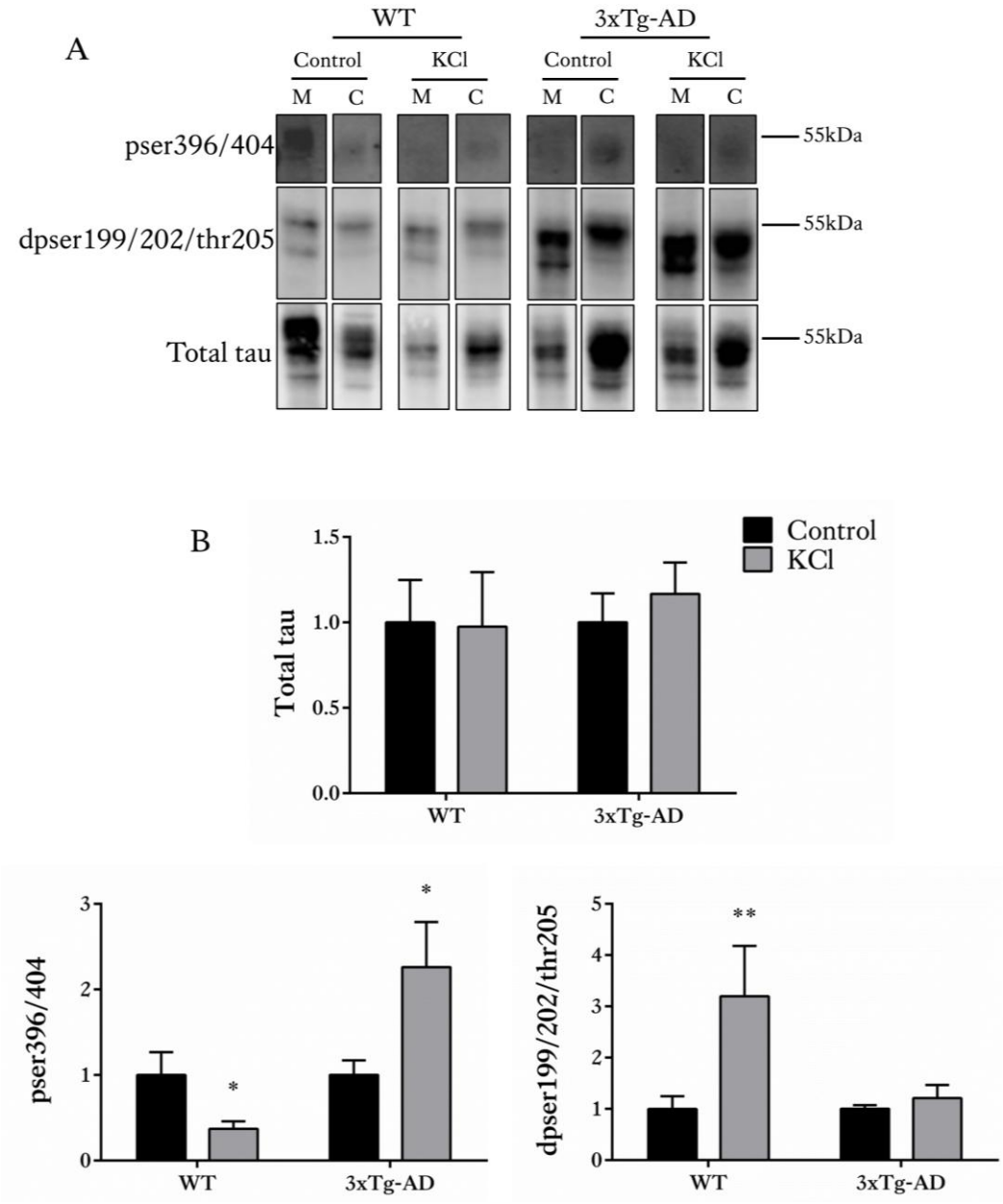

Figure 5.5: Increased amounts of dephosphorylated tau at the membrane upon neuronal stimulation of WT, but not 3xTg-AD slice cultures.

(A) Representative western blots of membrane and cytosol fractions prepared from WT and 3xTg-AD slice cultures treated with 50mM KCl or control (non-stimulated) for 30 mins showing total (phosphorylated and non-phosphorylated) tau, tau phosphorylated at ser 396/404 (PHF-1) and dephosphorylated at ser 199/202 and thr 205 (Tau-1), all at ~50-64 kDa. Bar charts show (B) the ratio of total tau present in the membrane fraction relative to the cytosolic fraction, and the ratio of tau dephosphorylated at ser 199/202 and thr 205 or tau phosphorylated at ser 396/404 present in the membrane fraction relative to the cytosolic fraction all normalised to total tau amounts in the same fraction of the same sample. Data is shown as fold change from control-treated slice cultures.

Data is mean ± SEM, (n=12 wells from two independent experiments, *p<0.05, **p<0.01).

5.4.6 Physiological tau release but not pathological tau release can be inhibited by blocking pre-synaptic vesicle release

To further investigate the mechanisms underlying tau release from slice cultures, slices were treated with TTX prior to KCl application. TTX is a neurotoxin which blocks voltage-gated Na^+ channels, thereby preventing pre-synaptic vesicle release and the propagation of action potentials (Lee and Ruben, 2008). Previous research has suggested that pre-treatment with TTX blocks the increased release of endogenous tau that occurs when neuronal activity is stimulated *in vitro* in primary neurons (Pooler et al., 2013), and *in vivo* in mice (Yamada et al., 2014). However, basal tau release was not significantly reduced *in vivo* in mice treated with TTX (Yamada et al., 2014).

Therefore, 28 *div* WT and 3xTg-AD slice cultures were pre-treated with 2 µM TTX or control for 1 hour, followed by a 30 minute control or KCl treatment. 2 µM TTX treatment of primary cortical neurons has previously been demonstrated as an effective non-toxic dose to inhibit neuronal activity (Pooler et al., 2013). As before, total amounts of tau released into the media were measured by ELISA and standardised to amounts of intracellular tau. Due to time restraints, the data presented for this experiment represents results from only one experiment with a group size of 2-6 resulting from some unhealthy cultures not being analysed. Nevertheless, the results of this work suggest that pre-treatment with TTX in WT slice cultures prevents the KCl-induced increases in tau release, but does not lower basal levels of tau release. In 3xTg-AD slice cultures, in which KCl did not increase levels of tau release, pre-treatment with TTX does

not affect tau release in either stimulated or non-stimulated conditions (Figure 5.6). These data further suggest that there are different mechanisms underlying tau release from normal and diseased tissues.

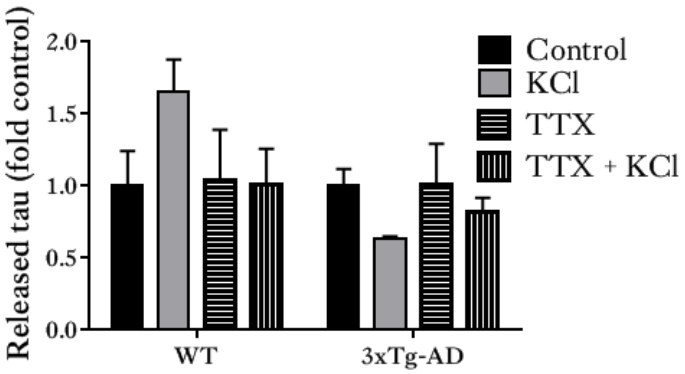

Figure 5.6: Increased tau release with neuronal stimulation can be inhibited by TTX in WT, but not 3xTg-AD slice cultures
28 *div* WT and 3xTg-AD slice cultures were pre-treated with TTX or control for 1 hour, followed by a 30 minute control or KCl treatment to stimulate neuronal activity. Amounts of total tau released into the media were measured by ELISA and standardised to total intracellular tau amounts. Data are shown as fold change from control-treated slice cultures. Data is mean ± SEM, (n=2-6 wells from one independent experiment).

5.5 Summary

The main findings presented in this chapter are that:

- Organotypic brain slice cultures from 3xTg-AD mice show significantly increased basal release of tau compared to WT slice cultures.

- Neuronal stimulation of WT, but not 3xTg-AD, slice cultures significantly increases tau release.

- Inhibiting neuronal activity with TTX prevents KCl-induced increases in tau release from WT slice cultures, but does not affect tau release from 3xTg-AD slice cultures.

- The increased presence of dephosphorylated tau at membranes is associated with tau release.

5.6 Discussion

5.6.1 3xTg-AD slice cultures release increased amounts of tau compared to WT slice cultures under basal conditions and this is associated with an increased presence of dephosphorylated tau at membranes

The results presented show for the first time that slice cultures from 3xTg-AD mice release almost two-fold the amount of tau released by WT slice cultures in basal conditions, after controlling for tau over-expression in 3xTg-AD slices. It is likely that this release of tau, by an as yet undefined mechanism, into the extracellular space contributes to tau propagation in disease, the latter having been demonstrated previously in several AD and tauopathy models (Clavaguera et al., 2009, de Calignon et al., 2012, Clavaguera et al., 2013, Sanders et al., 2014).

The results also demonstrate that 3xTg-AD slice cultures contain a greater proportion of dephosphorylated tau at membranes as shown by an increased abundance of tau dephosphorylated at ser 199/202 and thr 205 and decreases in amounts of tau phosphorylated at ser 396/404 in this fraction. While it is has not been possible to

explore the exact relationship between membrane-associated tau and tau release in this work, previous studies have suggested that tau is held at the membrane before it is released, potentially in association with exosomes (Saman et al., 2012, Simón et al., 2012, Asai et al., 2015) or ectosomes (Dujardin et al., 2014). In agreement with the data shown here, tau species at the membrane have previously been identified as being predominantly dephosphorylated at ser/thr residues as compared to cytosolic tau (Pooler et al., 2012), and increased phosphorylation of tau, particularly at N-terminal residues, reduces it association with the membrane (Arrasate et al., 2000). Taken together, this suggests that these largely dephosphorylated species of tau may be awaiting secretion, as it has been demonstrated that both physiological and pathological extracellular tau species are predominantly dephosphorylated compared to species found intracellularly (Plouffe et al., 2012, Pooler et al., 2013). Additionally, 3xTg-AD slice cultures show overall increases in tau phosphorylation (chapter 3), but have increased pools of dephosphorylated tau at their membranes, and the reasons for this remain unclear.

It remains to be determined which species of tau are released by 3xTg-AD slice cultures, and also the mechanism by which they are released. There is some suggestion that pathological tau can be released in association within vesicles (Simón et al., 2012, Saman et al., 2012, Dujardin et al., 2014), and this may be related to the tran-synaptic propagation of tau (Liu et al., 2012, Calafate et al., 2015). Additional studies using slice cultures may allow further investigation of the precise mechanisms involved in tau release from WT and 3xTg-AD slices under basal conditions. Additionally, in both WT and

3xTg-AD slice cultures, full-length and N- and C- terminal fragments of tau were detected at the membrane. Full length, N-terminally truncated and C-terminally truncated tau species have all been found extracellularly in previous studies (Pooler et al., 2013, Dujardin et al., 2014, Bright et al., 2015, Kanmert et al., 2015).

5.6.2 Neuronal stimulation increases tau release from WT slice cultures and this is associated with an increased presence of dephosphorylated tau at membranes

Stimulating neuronal activity with KCl was shown here to significantly increase tau release from WT slice cultures, but not to stimulate any further increases in tau release from 3xTg-AD slice cultures. Increased release of tau upon KCl treatment has previously been shown in both WT rat primary cortical neurons (Pooler et al., 2013) and *in vivo* in WT mice (Yamada et al., 2014). The reasons why KCl does not stimulate further tau release from 3xTg-AD slices is not clear. Increased tau release was found to occur upon KCl depolarisation of synaptosomes isolated from human AD brain, but not control brain (Sokolow et al., 2015), in apparent disagreement with the data shown here. However, this published work used a different model that measured tau release from the synapse only, compared to the entire neural cells present in slice cultures. Additionally, differences in the species of tau released from the synapse in physiological (Pooler et al., 2013, Yamada et al., 2014) and pathological (Liu et al., 2012, Calafate et al., 2015) conditions have been described, in addition to differential association of extracellular tau with vesicles (Simón et al., 2012, Chai et al., 2012, Saman et al., 2012, Dujardin et al., 2014, Asai et al., 2015). It is possible that the increased overall phosphorylation of tau demonstrated in the 3xTg-AD slice cultures (chapter 3) changes its subcellular

distribution such that an increased pool of tau is docked at membranes in readiness for release, and this cannot be further increased by neuronal stimulation. In partial support of this idea, increased tau release upon KCl treatment of WT slices was associated with increased amounts of membrane-associated tau dephosphorylated at ser 199/202 and thr 205 and decreased amounts of membrane-associated tau phosphorylated at ser 396/404. There were no changes in the amounts of dephosphorylated tau at membranes upon KCl stimulation of 3xTg-AD slices, and increases in membrane-associated tau phosphorylated at ser 396/404 were identified, conditions under which no elevated tau release was observed. Additionally, neuronal hyperactivity has been demonstrated in AD (Quiroz et al., 2010), and it could be that KCl cannot elicit any further tau release under conditions where neurons are already over-stimulated.

5.6.3 KCl-induced increases in tau release, but not basal tau release, can be inhibited by blocking pre-synaptic vesicle release

The preliminary findings presented in this chapter suggest that pre-treatment of WT slice cultures with TTX prior to KCl application prevents the increased tau release that results from neuronal stimulation. In both WT and 3xTg-AD slices basal levels of tau release were not affected by TTX. Unfortunately, this data only represented results from one experiment with each group size being 2-6, but the general trend towards significance supports the validity of these findings. In particular, despite the small group numbers, the variability within groups is small, and the findings from one experiment recapitulate those of previous experiments where KCl was shown to stimulate increased tau release from WT slice cultures, but not 3xTg-AD slice cultures.

Data from others support these preliminary findings by showing that basal tau release in WT mice cannot be reduced by preventing neuronal activity (Yamada et al., 2014), suggesting both neuronal activity-dependent and non-dependent mechanisms of tau release exist. The data presented here highlights additional differences in normal and diseased brain tissues.

Importantly, the half-life of physiologically released tau has been demonstrated to be approximately 11 days (Yamada et al., 2014), suggesting that the clearance of extracellular tau is a slow process. This clearance of extracellular tau may be even slower in AD due to the increased presence of extracellular tau (Blennow et al., 1995, Meredith Jr et al., 2013). If this tau is required for tau propagation, then therapeutic approaches that reduce tau release could be a very efficacious treatment. Therefore, experiments aimed at increasing knowledge about the mechanisms of tau release are warranted, and the data presented here suggests that brain slice cultures might represent an ideal model with which to probe these processes further.

5.6.4 Limitations of this work

Although the work presented in this chapter increases our knowledge of some aspects of both physiological and pathological tau release, further experiments are required to build upon this data.

Firstly, the association of released tau with vesicles has been highlighted in some studies (Saman et al., 2012, Dujardin et al., 2014, Asai et al., 2015). Unfortunately, studies where

the media from both WT and 3xTg-AD slice cultures, treated with control or KCl was going to be concentrated in order to identify any vesicular-associated tau were not able to be completed due to technical difficulties combined with time constraints. Slice cultures were prepared but unfortunately died from reasons beyond my control before the 28 *div* treatment day.

Similarly, this media would have been column concentrated to allow examination of the tau species present (full-length, N- and C-terminally truncated species), as well as phosphorylation status. It would have been interesting to identify whether there were any differences in phosphorylation or truncation of extracellular tau in WT and 3xTg-AD slice medium.

Finally, it is clear that the interplay between Aβ and tau is important for the propagation of tau (Pooler et al., 2015, Bright et al., 2015). The presence of both increased amounts of Aβ and tau in 3xTg-AD slice cultures lends themselves to understand the effect of Aβ on tau release, but this was not exploited in this project. Specifically, Aβ production could have been suppressed, for example, with inhibitors of γ-secretase or antibodies to deplete Aβ, and any changes in tau release could have been explored.

5.6.5 Conclusions

The results in this chapter suggest that pathological tau, that is tau with AD-related properties such as increased phosphorylation, as found in 3xTg-AD slice cultures is released in higher amounts compared to normal WT tau released from WT slices, yet in

both models the release of tau is associated with the presence of dephosphorylated tau at membranes. In addition, neuronal activity regulates the release of WT tau, but appears not to affect the release of disease-associated tau, indicating that physiological and pathological tau release is likely mediated by alternative mechanisms.

Chapter 6 : Discussion

The studies presented in this thesis demonstrate that slice cultures produced from 3xTg-AD mice develop both biochemical and physiological features of AD, which recapitulate those observed *in vivo* in 3xTg-AD brain, as well as in post-mortem human AD brain. Importantly, many of these AD-like changes appeared to be accelerated with respect to those observed *in vivo*. In addition, the utility of slice cultures as a drug screening tool was demonstrated, as well as their potential to be used to understand mechanisms of physiological and pathological tau release.

6.1 Organotypic brain slice cultures as an AD research tool

6.1.1 Organotypic brain slice cultures as an alternative model for AD research

A multitude of approaches can be taken to understand AD. Currently, the majority of scientists approach AD research using transgenic mouse models of AD. Although none of the transgenic mouse models currently available develop the full spectrum of neurodegenerative changes seen in human AD (Radde et al., 2008, Puzzo et al., 2015), they have been successfully used to identify some of the mechanisms and pathways involved in the disease. The most commonly used transgenic mouse models of AD commonly over-express one or more FAD- or FTLD- causing mutations in human *APP* and/or *PS1/2* and/or *MAPT* to allow development of Aβ- and/or tau-associated neurodegeneration that is characteristic of AD (LaFerla and Green, 2012). Although the causes of sporadic and familial AD clearly differ, they share common characteristics such as the progressive development of abnormal APP and tau processing, tau

mislocalisation, Aβ plaques, intracellular NFTs, widespread synaptic and neuronal loss, inflammation, calcium dyshomeostasis and oxidative injury that precedes cognitive and behavioural changes (Hardy and Selkoe, 2002). Therefore, in the absence of rodent models that spontaneously develop human AD features, these transgenic lines are the best we have available for AD research, at least until other better alternatives are developed.

Mice have several features that make them very useful for investigating the progressive neurodegeneration that characterises AD and other neurodegenerative conditions. Namely, their genome is very similar to humans – approximately 97.5% of working DNA is shared (Waterston et al., 2002), they are readily amenable to genetic modification, and are suitable for a range of cognitive and behavioural tests to reveal abnormalities observed in human diseases. Additionally, their average 2 year life-span allows monitoring of progressive disease phenotypes with age. Finally, they allow for pre-clinical investigation of AD therapies in an intact organism, an essential step before clinical testing can commence. However, there are obvious ethical issues with using mouse models in biomedical research, and the utility of lower (less sentient) organisms must also be considered.

Several alternatives to transgenic mice exist for studying AD, each with their own advantages and disadvantages. The most common of these will be discussed here, but this is not an exhaustive list. Alternative *in vivo* models include *Drosophila melanogaster, Caenorhabditis elegans* and zebrafish (Jucker, 2010). All of these organisms have a much

shorter life-span than mice, which reduces both costs and time, and a much less complex nervous system which allows easier study of neuronal circuitry. However, it could be argued that the latter point makes these organisms unsuitable for researching human neurodegenerative disorders since relevant brain regions (such as the cortex) are not present in at least some of these model species (Friedrich et al., 2010). Drosophila are the most used alternative to rodents for investigating neurodegenerative diseases, and these have particular utility as models for screening genetic modifiers of disease (Shulman et al., 2014). They have also been used to provide some useful information regarding the role of tau in neurodegeneration (Wittmann et al., 2001) - seminal studies that were later reproduced in mice (SantaCruz et al., 2005). However, their utility for examining the mechanisms underlying AD is questionable since the drosophila homolog of APP does not contain an Aβ-42 domain (Prüβing et al., 2013), and other important pathways such as the activation of cdk5 are not the same as in mammals (Lin et al., 2006).

In vitro models, including neuronal cell lines and primary neuronal cultures, are also invaluable for understanding aspects of AD (Shastry et al., 2001). These are easy to obtain and maintain, readily susceptible to genetic and pharmacological information, and are an easily replaceable source of protein and genetic material. However, cell lines, even neuronal cell lines, usually require modification to express exogenous proteins, and even then they do not always demonstrate the same trafficking pathways as neurons (Usardi et al., 2011). Moreover, the brain is a complex organ, composed of multiple cell types, in precise arrangements, with important anatomical and functional connectivity

that cannot be readily replicated *in vitro*; therefore, the use of these *in vitro* systems can often be too simplistic and the data often do not translate to more complex systems.

Recent advances in iPSC technology has allowed the investigation of disease processes in neurons differentiated from iPSCs derived from familial and sporadic AD patient and control tissues (Israel et al., 2012). The generation of human neurons, and in particular those from AD patients, has allowed investigation of disease processes in highly relevant cell models, particularly since they have been shown to conserve the downstream effects of AD-causing mutant genes (Israel et al., 2012, Nieweg et al., 2015) and can be used to identify risk haplotypes (Soldner and Jaenisch, 2015) and gene regulatory networks (Hossini et al., 2015) in sporadic cases. However, these are still not ideal since several groups have reported that their human AD iPSCs only produce small amounts of 4R tau (Iovino et al., 2010), and that this takes a long time (one year) to appear (Sposito et al., 2015) indicating that iPSC-derived neurons have an immature phenotype for long periods of time which is not ideal for investigating a disease that typically affects those in mid-late life. Together with the fact that methods to generate all neural cell types believed to be implicated in AD, including microglia and astrocytes (Gentleman, 2013, Phillips et al., 2014, Tejera and Heneka, 2015) are not yet fully established, it is clear that further work is required to develop iPSC-based models before they can be fully utilised in AD research (Ovchinnikov and Wolvetang, 2014). More recently, a three-dimensional human neural progenitor cell derived 'organoid' transfected with known FAD mutations has also been described (Choi et al., 2014). These show development of some astrocytes, however, these 'organoids' still do not represent the elaborate connectivity

and architecture of regions of the human brain and cell types involved in AD, as they are just cultures of several layers of cells (Choi et al., 2014).

Although it cannot be considered a "model" per se, a great deal of AD research is conducted using post-mortem human brain tissue (Bell et al., 2008). As more and more research institutes develop banks of brain tissue from control, AD and other neurodegenerative conditions, these have become an increasingly useful resource to study biochemical and neuropathological changes in diseased human brain relative to age- and gender-matched controls. This can be particularly useful for back translation of findings e.g. investigating the mechanisms leading to the development of pathologies observed in human brain (Wray et al., 2008). Indeed, this type of work is responsible for decades of investigation into the implications of tangles and plaques in AD (Braak et al., 2011). However, there are several disadvantages to using post-mortem brain tissue in isolation to draw conclusions, and careful consideration to these has to be made. Firstly, most research is conducted using relatively small sample sizes which is not ideal since human brain is known to be highly heterogeneous (Atherton et al., 2014). Additionally, post-mortem delay, brain pH and storage temperature can considerably affect findings for several reasons including freeze-thawing, activation of proteases and protein, DNA and RNA degradation (Ferrer et al., 2008). Furthermore, age-matched controls are vital for comparisons to AD brain; however these are often obtained from people suffering other acute or chronic conditions which could ultimately affect the brain and confound results and interpretations. Perhaps most importantly, most brains available for study

are at the end-stages of disease, or at least a fixed stage of disease, making temporal assessment of progressive alterations impossible.

This thesis outlines the use of *ex vivo* organotypic brain slice cultures as a model for AD research. The preparation of brain slice cultures is a well-documented technique in neuroscience research (Gähwiler et al., 1997), and here we provide, to the best of our knowledge, the first evidence of an organotypic brain slice culture model of AD that progressively develops both Aβ and tau abnormalities, together with other representative features of human AD. These *ex vivo* organotypic brain slice cultures offer several advantages over alternative *in vitro* systems as they can replicate many aspects of the progressive development of disease phenotypes observed in an *in vivo* context, and they are amenable to manipulation and can be used in unison with techniques which are invasive *in vivo*.

The results presented in this thesis have demonstrated the utility of 3xTg-AD brain slice cultures as a model that can be used to understand the mechanisms and pathways underlying the development and progression of AD, as well as a drug screening and development tool for developing novel AD therapeutics. 3xTg-AD slice cultures rapidly develop important features of *in vivo* brain in the 3xTg-AD mice from which they are derived as well as human AD. The most interesting findings in 3xTg-AD slice cultures which recapitulate human AD, and that were found to develop more rapidly *ex vivo* than *in vivo* are discussed below. These findings suggest that 3xTg-AD slice cultures have utility for investigating therapeutic strategies that are directed at reducing levels of Aβ

and post-translationally modified tau as well as those which inhibit p25/cdk5 activity. The results of this work all suggest that 3xTg-AD slices are suited to research aimed at understanding mechanisms involved in the interplay between Aβ and tau in AD, which are still relatively poorly understood.

By 14 *div,* 3xTg-AD slice cultures were found to have accumulated substantial amounts of Aβ-42, a major feature of human AD brain (O'Brien and Wong, 2011), that is not apparent in 3xTg-AD mice *in vivo* until 6 months of age (Oddo et al., 2003a). In addition, 3xTg-AD slice cultures display highly phosphorylated tau and high molecular weight tau species by 21 *div*, which are a major feature of human AD (Iqbal et al., 2005), but are only found to develop *in vivo* at 12 to 15 months of age (Oddo et al., 2003a, Oddo et al., 2003b). 3xTg-AD slice cultures also show an increased p25 activation of cdk5 from 28 *div*, which is also a feature found in human AD brain (Tseng et al., 2002), although this finding is somewhat contentious (Tandon et al., 2003). Again, *in vivo* in the 3xTg-AD mice, increased cdk5 activity is not observed until 12 months of age (Sy et al., 2011). Thus, the seemingly rapid development of important AD features in 3xTg-AD brain slice cultures compared to those observed in this model *in vivo* suggests that the slice culture model is a sensitive system to be used in AD research that will allow investigations to be conducted in a shorter, more efficient time-scale, and one that avoids aging of animals until harmful phenotypes develop.

6.1.2 Advantages of organotypic brain slice cultures for AD research

As an alternative to *in vivo* research in 3xTg-AD mice, slice cultures derived from this line hold several advantages. Firstly, as described above, 3xTg-AD slice cultures show a much more rapid development of AD-relevant changes with features such as highly phosphorylated tau species being present at 21 to 28 *div* in slice cultures as opposed to 12 to 15 months *in vivo* (Oddo et al., 2003a, Oddo et al., 2003b). The use of 14-28 *div* slice cultures avoids ageing mice for long periods of time, where the disease phenotype can become a lot more severe and cause harm to the animal, and this technique also allows smaller breeding colonies of mice to be maintained since slices are prepared from mice, pre-weaning, at postnatal day 8 or 9. This significantly reduces the time and cost and *in vivo* implications of AD research. Overall, the use of slice cultures is highly relevant to the implementation of the 3Rs in neurodegeneration research; the numbers of animals for particular AD experiments can be reduced by greater than 90%, a huge number of experiments investigating the molecular mechanisms underlying AD or drug screening for AD can be conducted in slice cultures, thereby replacing some animal research, and procedures which may be invasive *in vivo* can be performed *ex vivo* instead, thus refining AD research.

Specifically, when compared to *in vivo* research, the numbers of mice used is considerably reduced since one 3xTg-AD pup is used to produce 36 slice cultures containing the hippocampus and cortex (typically used in experiments in groups of 3). This enables the study of up to 12 compounds at once, or observations of several disease-related changes over time in brain tissue derived from the same mouse, a

system that also reduces inter-animal variation. Furthermore, compared to pre-clinical *in vivo* research, treatment paradigms are much easier to implement and results can be obtained more rapidly from 3xTg-AD slice cultures. For example, treatment of 3xTg-AD slice cultures with LiCl led to reduced tau phosphorylation after a 4 hour period in 28 *div* cultures. *In vivo,* 3xTg-AD mice were aged to 15 months of age and then treated for a 4 week period with LiCl (Caccamo et al., 2007). It is clear that *in vivo* studies using transgenic models of neurodegeneration require a long treatment protocol after a prolonged aging period, and this prevents a rapid clinical translation of AD therapies, which instead can be accelerated using 3xTg-AD slice cultures. In addition, further advantages of brain slice cultures lie in their ease of use. For example, drug treatments or other manipulators can be easily added to their external environment. Further convenience lies in the fact that many slice cultures can be produced and maintained in relative short time frames, and experiments can be easily and rapidly conducted using supplies of slices maintained in tissue culture incubators, removing some of the technical problems associated with maintaining large groups of age-matched mice for prolonged periods of time. Thus, overall, long-term 3xTg-AD slice cultures provide a means to replace, refine and reduce some aspects of *in vivo* AD research, as suggested for other AD brain slice models (Humpel, 2015a), in addition to providing a more readily tractable and considerably cheaper alternative to *in vivo* transgenic studies.

Ex vivo organotypic brain slice cultures also provide several advantages over more common *in vitro* models. *Ex vivo* organotypic brain slice cultures show preservation of three-dimensional organisation and architecture of the tissue from which they are

derived (Humpel, 2015a). In particular, the 3xTg-AD slice cultures reported here contain both the cortex and hippocampus, and therefore a range of cell types which are not represented in single cell lines or primary neural cell cultures unless an advanced co-culture method, and scaffolding matrices are employed (Chwalek et al., 2015). Even then, co-culture systems do not usually contain all of the cell types of the region from which they are derived and in the correct proportions. The presence of astrocytes in 3xTg-AD slice cultures has been demonstrated here (chapter 3) and other published reports suggest that all glia develop normally in organotypic cultures, in approximately the same proportions as observed *in vivo* (Hailer et al., 1996), which is particularly important as astrocytes and microglia are implicated in the progression of AD (Gentleman, 2013, Phillips et al., 2014, Tejera and Heneka, 2015) so it is imperative as much of the original cytoarchitecture is maintained in order to correctly model the disease. Additionally, although transfection techniques can be employed in slice cultures, and Aβ or other manipulators could be added to the external environment of slice cultures prepared from wild-type or other AD transgenic lines, 3xTg-AD slice cultures express the human mutant *PS1, MAPT,* and *APP* transgenes, leading to overexpression of APP and tau proteins, and Aβ overproduction, so do not require any further transfection of proteins of interest.

In vitro alternatives to 3xTg-AD slice cultures are also less ideal for pre-clinical screening of AD therapeutics because despite a compound often showing efficacy and hitting a desired target *in vitro* these often do not translate to intact organisms, particularly mammals, due to the lack of biological complexity (Sundstrom et al., 2005). In

comparison to high-content screening in cell cultures, treatment of 3xTg-AD slice cultures should enable a more robust selection of lead compounds to investigate *in vivo* since they are more biologically relevant than dissociated primary cells or cell lines (Sundstrom et al., 2005).

Finally, 3xTg-AD organotypic brain slice cultures lend themselves to the exploitation of various other exciting techniques. Although not demonstrated in this thesis, slice cultures can be easily biolistically or virally transfected (McAllister, 2004). For example, this would be useful to examine the effects of upregulation or knockdown of inflammatory mediators implicated in AD (Sastre et al., 2011) as demonstrated *in vivo* (Chakrabarty et al., 2015). The electrical activity of 3xTg-AD slice cultures could be probed over long durations using single or multi-electrode arrays (Plenz et al., 2011), this would be useful to investigate the presence or absence of any abhorrent electrical activity in AD (Quiroz et al., 2010). Additionally, this slice culture model of AD could easily be used in a wide range of live imaging setups (Goldberg and Yuste, 2009), in particular, the imaging of any calcium dyshomeostasis in the slice cultures could increase our understanding of this aspect of AD (Egorova et al., 2015).

In summary, *ex vivo* 3xTg-AD slice cultures hold several advantages as a sensitive and tractable model of AD that has the capacity and potential to provide an alternative system to *in vivo* research, but at a lower cost and at a more rapid pace, and with more biological reliability and relevance than other *in vitro* systems. Due to the numerous advantages of this 3xTg-AD slice culture system it is likely they will be useful to

understand the basic science underpinning AD as well as in the discovery and development of new AD drugs in the future.

6.1.3 Disadvantages of organotypic brain slice cultures to study AD

It is also important to point out that there are some disadvantages to brain slice culture systems, and that other models are more appropriate for studying certain aspects of AD.

Firstly, most studies have identified that organotypic slice cultures are synaptically similar to acute preparations, however increased axonal branching and higher order dendrites have been reported in these organotypic cultures (De Simoni et al., 2003), suggesting an increased synaptic integrity in slice cultures. Similarly, an increased frequency of synaptic miniature currents, suggesting an increased number of synapses has also been reported (De Simoni et al., 2003). These differences are likely accounted for during the initial preparation and culture of these slices where several axons are cut, and it is likely that recovery would be seen over long-term culture, as suggested in previous publications (De Simoni et al., 2003). It is important, however, to be aware of these potential synaptic differences which may confound results, particularly since synaptic degeneration is a key feature of human AD. Specifically, this potential for an increased synaptic integrity in slice cultures may mean synapses in slice cultures are more resistant to degeneration.

Secondly, as with all *ex vivo* or *in vitro* preparations, the main prolific symptoms of AD - loss of memory and cognition, cannot be assessed in slice cultures, so *in vivo* studies will

inevitably have to take place to examine the effects of treatments or other manipulations on behaviour and cognitive function. However, *ex vivo* slice cultures should allow screening of potential therapeutics before they are tested in vivo so that only the most specific and biologically relevant strategies are taken *in vivo* (Sundstrom et al., 2005).

Additionally, although slice cultures contain multiple cell types in relevant proportions and can contain several brain regions (e.g. hippocampus and cortex), they are not fully intact brain; therefore the full extent of the spatiotemporal progression of disease cannot be explored.

Finally, the generation and manipulation of slice cultures is technically demanding, requires substantial training and exacting conditions, so at present there is no possibility of automation of any experiments. Therefore, organotypic slice cultures still require a modest amount of time, and some relatively substantial costs are required to generate and maintain them.

6.2 Organotypic brain slice cultures as a model to study the mechanisms underlying AD

The findings presented in this thesis demonstrate the rapid progression of pathological changes in 3xTg-AD slice cultures that are relevant to the progression and development of AD. Therefore, this supports their application in research aimed at studying the mechanisms and pathways involved in AD, and particularly the interplay between Aβ

and tau in a much more rapid timescale than other approaches. In particular, the work presented here shows that tau is redistributed to the synapse at relative early disease stages in 3xTg-AD slice cultures and this may be an early change that contributes to further neurodegenerative changes in AD. Such events could be further investigated in 3xTg-AD slice cultures.

6.2.1 Studying AD-like abnormalities in tau and Aβ in 3xTg-AD brain slice cultures

Tau, APP and Aβ all independently hold physiological and pathological effects at the synapse (section 1.5). In addition, the interplay between Aβ and tau at the synapse is highly relevant in AD. Indeed, Aβ can drive the missorting of tau to dendritic compartments causing microtubule breakdown, calcium dyshomeostasis and spine loss (Zempel et al., 2010). Similarly, other studies have shown that tau mislocalisation and the phosphorylation of tau at the synapse may be required to mediate Aβ-induced synaptotoxicity (Mairet-Coello et al., 2013, Miller et al., 2014). In addition, tau enables Aβ to exert its toxic effects at the synapse, as removal of tau reduces excitotoxicity, improves memory function and synaptic deficits (Roberson et al., 2007, Roberson et al., 2011, Ittner et al., 2010), implicating tau at dendritic spines in Aβ-induced synaptic dysfunction.

The results presented here show for the first time that total amounts of tau are significantly increased at the synapse in 3xTg-AD slices at 14 *div*, indicating a redistribution of tau from its normal cytoplasmic localisation at an early disease stage. Significantly increased total tau amounts were found in synaptosomes prepared from

3xTg-AD slice cultures at 14 *div* but not at 21 or 28 *div*. This is similar to changes observed in synaptosomes isolated from 3xTg-AD mice here, where increased total tau amounts were found at 1 and 2 months of age, but not at 4, 9 or 12 months of age. The pathological relevance of these findings is not clear; however, in end-stage human AD brain, it has been reported that total tau amounts at the synapse do not differ from those found in control human brain (Tai et al., 2012, Tai et al., 2014). However, it has been shown that tau at the synapse is phosphorylated and misfolded in human AD (Henkins et al., 2012, Tai et al., 2014) and also in mice which express FTD-causing P301L mutant human tau (Harris et al., 2012, Kopeikina et al., 2013). Additionally, it has been demonstrated that P301L tau, but not WT tau, is targeted to dendritic spines (Xia et al., 2015). Taken together, these findings suggest that increases in total amounts of tau at the synapse may be an early disease feature in AD, and at later stages of the disease, some of the tau may have been transported to an alternative neuronal compartment or released from the neurons, with the remainder being misfolded or phosphorylated at the synapse. This synaptic tau may be synaptotoxic and prevent physiological functions of tau at the synapse, as suggested by (Hoover et al., 2010) leading to the decline in cognition and memory that occurs in AD. Unfortunately, these are all mechanisms that are poorly understood at present (Crimins et al., 2013).

Increased amounts of APP were also found in synaptosomes prepared from the hippocampus of 3xTg-AD mice at 1, 2 and 9 months, but no increased amounts of APP were found at the synapse in 3xTg-AD slice cultures at 14, 21 or 28 *div.* In human AD brain, no increases in total amounts of APP are found at the synapse compared to

control brain (Gylys et al., 2004); however increased amounts of Aβ are found at the synapse in human AD brain (Fein et al., 2008). Taken together, this might suggest that early increases in APP amounts at synapses in AD may precede APP processing via the amyloidogenic pathway (Zhang et al., 2011b) to generate increased amounts of Aβ which are retained at the synapses throughout AD. This build-up of Aβ is likely detrimental to synapse health and function in AD (Sheng et al., 2012). In particular, Aβ can drive internalisation of NMDA and AMPA receptors, causing LTD as well as driving NMDA-dependent excitotoxicity (Hsieh et al., 2006, Shankar et al., 2007, Shankar et al., 2008). Alternatively, Aβ is suggested by many to exert synaptotoxicity through disruptions in calcium homeostasis and altering neuronal excitability (Kuchibhotla et al., 2008). In addition, tau may also be involved in driving this Aβ-toxicity in the dendritic compartment through its trafficking of Fyn to the dendrites postsynaptic and its role in NMDAR-mediated signalling (Ittner et al., 2010).

6.2.2 Organotypic slice culture models for investigating tau release and propagation

The data presented in this thesis also demonstrates the utility of WT and 3xTg-AD slice cultures as a suitable and relevant model with which to investigate the mechanisms of physiological and pathological tau release. In brief, tau released from organotypic brain slice cultures can be measured in the extracellular culture medium, allowing us to understand differences between tau release from WT slices containing normal (physiological) tau and that from 3xTg-AD slice cultures which contain AD-like (pathological) tau.

The data presented here highlights differences between the release of tau from normal and diseased brain tissues under basal conditions. Tau release was manipulated here by adding pharmacological agents that stimulate or block neuronal activity to the slice culture environment. As more is elucidated about potential mechanisms involved in tau release, additional agents could be further investigated in a similar way.

The work described in this thesis has focussed on tau release, which is likely related to the ability of tau to propagate across diseased brain. Tau propagation has previously been demonstrated both *in vitro* and *in vivo* in seeding experiments (Clavaguera et al., 2009, Clavaguera et al., 2013, Sanders et al., 2014), as well as *in vivo* through controlled expression of human FTD-causing P301L tau only in the entorhinal cortex, which spreads, trans-synaptically, to regions downstream of the entorhinal cortex in a spatiotemporal manner (de Calignon et al., 2012).

It is likely that slice cultures from WT, 3xTg-AD mice and other transgenic models of neurodegeneration could also be used for tau seeding experiments, which tend to be conducted *in vivo* or in single cell lines, and/or as a mode of tau propagation which is largely studied *in vivo*. It is conceivable that tau seeds from human AD or tauopathy brain can be applied on to the slice cultures, and propagation from cell to cell and region to region can be assessed using histological or advanced live imaging methods more rapidly in slice cultures than *in vivo*, enabling a greater understanding of propagation of tau in AD. In addition, adeno-associated virus (AAV) technology (Chakrabarty et al., 2015) could be used to express tau in one specific region of the slice cultures, and its

spread could also be rapidly identified. Furthermore, pharmacological methods to block this release of tau and propagation could be efficiently explored in slice culture models, particularly antibodies against extracellular tau are of interest (Bright et al., 2015).

6.2.3 Mechanisms of physiological tau release

Recent studies have indicated that endogenous tau is released from neurons (Chai et al., 2012, Pooler et al., 2013, Yamada et al., 2014). While the reasons for this and potential functions of extracellular tau are not well understood, tau may act as a mediator of extracellular signalling by binding to and activating muscarinic receptors (Gómez-Ramos et al., 2008, Gómez-Ramos et al., 2009). It has not yet been investigated whether or not this novel function of tau is disrupted in disease conditions. WT slice cultures have been used in this thesis to further investigate the release of endogenous wild-type tau.

Firstly, corroborating previous findings from both WT rat primary cortical neurons (Pooler et al., 2013) and *in vivo* experiments in WT mice (Yamada et al., 2014), the results presented here show that small amounts of tau are released from WT slice cultures under basal conditions. Moreover, neuronal stimulation using KCl was found to significantly increase tau release from WT slice cultures. Previous research has shown that tau is released from neurons via an unconventional secretion pathway (Chai et al., 2012). Since extracellular tau is largely dephosphorylated (Pooler et al., 2013) and a pool of dephosphorylated tau exists at membranes (Pooler et al., 2012) the amounts and phosphorylation status of membrane-associated tau was also investigated in WT slice cultures. It was shown here that the increased tau release that results from neuronal

stimulation occurred concurrently with reduced presence of tau phosphorylated at ser 199/202 and thr 205 and ser 396/404 at membranes. Neuronal stimulation of WT slice cultures did not change overall tau amounts at the membrane. Overall, this suggests that perhaps the pool of dephosphorylated endogenous tau that is held at membranes is that which is released upon neuronal stimulation. The mechanisms that are involved in this process are as yet undetermined.

Preliminary findings presented in this thesis also suggest that pre-treatment of WT slice cultures with TTX to inhibit pre-synaptic vesicle release, prior to KCl application, prevents neuronal-activity induced increases in tau release. This is in agreement with data showing that pre-treatment of WT primary cortical neurons and WT mice with TTX prevents KCl-induced action potentials, and therefore increases in extracellular tau amounts (Pooler et al., 2013, Yamada et al., 2014). In addition, others have shown release of tau is dependent on neuronal activity (Karch et al., 2012, Frandemiche et al., 2014). However, basal levels of tau release from WT slice cultures were not affected by treatment with TTX, as has also been previously demonstrated *in vivo* in WT mice (Yamada et al., 2014). Taken together, this suggests both neuronal activity-dependent and non-dependent mechanisms of endogenous tau release.

6.2.4 Mechanisms of pathological tau release

3xTg-AD slice cultures containing pathological tau species release almost two-fold the amount of tau compared to WT slice cultures in basal conditions. This increased release of extracellular tau may enable its propagation through the brain which has been

demonstrated previously in several AD and tauopathy models (Clavaguera et al., 2009, de Calignon et al., 2012, Clavaguera et al., 2013, Sanders et al., 2014).

Furthermore, the results presented here demonstrate that the increased release of basal tau amounts from 3xTg-AD slice cultures is also associated with a reduced pool of tau phosphorylated at ser 199/202 and thr 205 and at ser 396/404 at the membrane. This further suggests an association between membrane-associated dephosphorylated tau and tau release, as discussed above. However, unlike in WT slice cultures, stimulation with KCl did not elicit any further increases in amounts of extracellular tau release from 3xTg-AD slices, and additionally, KCl treatment resulted in increased presence of tau phosphorylated at ser 396/404 at the membrane. This in part suggests that the translocation of phosphorylated tau species to the membrane may prevent any further increases in tau release in pathological 3xTg-AD slice cultures. One could speculate that increased basal tau release in 3xTg-AD slice cultures may be as a result of increased neuronal activity as reported in early stages of AD (Quiroz et al., 2010), potentially through altered excitatory glutamatergic neurotransmission (Gonzalez et al., 2015) with further neuronal stimulation from KCl treatment not eliciting any further tau release, due to synapses already being over-stimulated. However, findings from preliminary experiments where 3xTg-AD slice cultures did not show any attenuation in basal amounts of tau release upon pre-treatment with TTX suggest that pathological tau release is likely not mediated through increased neuronal activity.

Despite adding to our understanding of physiological and pathological tau release, a multitude of questions relating to this topic still need to be explored. In particular, more research into how tau is taken up and released both physiologically and pathologically needs to be understood. Evidence so far suggests that endogenously expressed tau is not contained within vesicles when it is released, and that it is secreted via non-classical mechanisms (Chai et al., 2012) which are likely dependent on neuronal activity and calcium (Pooler et al., 2013). Pathological tau, especially when exogenously expressed is released in association with vesicles (Saman et al., 2012, Simón et al., 2012, Asai et al., 2015), and spreads trans-synaptically (Liu et al., 2012, de Calignon et al., 2012). Little is known about how tau is taken up into cells, but misfolded tau species can be taken up by endocytosis and axonally transported (Wu et al., 2013). Additionally, a role for the microglial uptake of tau by phagocytosis and subsequent exosomal release of tau in AD has recently emerged (Asai et al., 2015).

Furthermore, the identification of which species of tau are released and propagated needs to be determined. Most evidence demonstrates that endogenous extracellular tau species are predominantly dephosphorylated compared to tau found intracellularly (Plouffe et al., 2012, Pooler et al., 2013), although some reports indicate that tau is phosphorylated at thr 181 (Chai et al., 2012). Most endogenously released tau species have been demonstrated to be full-length or C-terminally truncated (Pooler et al., 2013, Kanmert et al., 2015). Pathologically released tau species have also been demonstrated as full-length and N- or C-terminally truncated (Plouffe et al., 2012, Bright et al., 2015). In addition, it has been demonstrated that pathological tau species which propagate are

largely soluble and oligomeric, but not fibrillar since PHFs have been demonstrated to not propagate (Lasagna-Reeves et al., 2012, Iba et al., 2013). Additionally, recent evidence has suggested that rare and highly phosphorylated multimers of tau can also propagate (Takeda et al., 2015). However, the removal of endogenous tau does not prevent the propagation of tau, but does reduce neuronal death (Wegmann et al., 2015).

Lastly, further work is required to explore the effects of Aβ on the propagation of pathological tau. It has been demonstrated that Aβ dramatically increases the speed and distance of tau propagation and increases tau-induced neurotoxicity *in vivo* (Pooler et al., 2015). Additionally, when inducing neuronal injury with Aβ is caused, the release of extracellular tau species is also increased (Kanmert et al., 2015). Furthermore, extracellular tau drives aberrations in neuronal excitability, likely increasing the production of Aβ driving an increased release of tau and further hyperactivity in a feed-forward mechanism (Bright et al., 2015). Slice cultures from 3xTg-AD mice lend themselves to studying this aspect of pathological tau release.

It is important that we further elucidate the mechanisms by which tau is released under physiological and pathological conditions and determine how this relates to the propagation of tau that is observed in neurodegenerative conditions. This should clarify whether targeting the spread of extracellular tau is therapeutically relevant, or whether it is actually dysfunctions in normal tau release that should be targeted.

In summary, 3xTg-AD slice cultures recapitulate important pathological features of *in vivo* brain, and here have been used to identify novel early changes in APP and tau at the synapse, whilst also identifying a possible association between the accumulation of pools of dephosphorylated tau at the membrane and the release of tau. In conclusion, this slice culture model lends itself to investigate disease mechanisms underlying the progression and development of AD, including tau release and propagation/transmission.

6.3 Organotypic brain slice cultures in novel AD drug discovery and development

As described above 3xTg-AD slice cultures lend themselves to applications to discover novel therapies targeted against Aβ-42, tau phosphorylation and high molecular weight tau, as well as inhibitors of p25/cdk5.

6.3.1 Validation of AD slice cultures to develop novel AD therapeutics and new understanding of previously used compounds

Data presented in this thesis demonstrate that treatment of 3xTg-AD organotypic brain slice cultures with LiCl and NAPVSIPQ yielded results which recapitulate those reported by others when used *in vivo* in 3xTg-AD mice (Caccamo et al., 2007, Matsuoka et al., 2007, Matsuoka et al., 2008). Additionally, treatment of 3xTg-AD slice cultures with these compounds has increased our knowledge of new AD-relevant properties of LiCl, as well as, identification of mechanisms by which NAPVSIPQ does not act.

In brief, a 20 mM 4 hour treatment of 28 *div* 3xTg-AD slice cultures reduced total tau amounts, tau phosphorylation at ser 396/404 and at ser 199/202 and thr 205, and APP phosphorylation at thr 668. It is difficult to conclude that these effects were solely mediated by reduced GSK-3 activity since no increases in GSK-3 phosphorylation at the inhibitory residues ser 21/9 phosphorylation were observed. In fact, phosphorylation at these GSK-3 sites was actually significantly decreased by LiCl treatment in 3xTg-AD slice cultures. Thus, LiCl treatment of 3xTg-AD slice cultures recapitulated some, but not all of the findings presented by (Caccamo et al., 2007) who treated 3xTg-AD mice with LiCl. Treatment of slice cultures confirmed the reduction of tau phosphorylation at ser199/202 and thr205 reported by Caccamo et al., but also resulted in reduced phosphorylation at ser 396/404, which was not observed *in vivo*. Additionally, the inhibitory phosphorylation of GSK-3 at ser 21/9 was shown *in vivo,* but this was not recapitulated in slice cultures. Reasons for the discrepancies between these findings could be that GSK-3 was inhibited by LiCl through other mechanisms in slice cultures, for example, by competition with magnesium (Ryves and Harwood, 2001), or regulatory phosphorylation at other ser/thr and tyr sites (Wang et al., 1994). It also cannot be ruled out that the changes in phosphorylated tau could have been mediated by changes in cdk5 activity since there is complex interplay between GSK-3 and cdk5 (Engmann and Giese, 2009, Kimura et al., 2014) or also through changes in the activity of other kinases by LiCl (Lenox and Wang, 2003). Alternatively the effects of LiCl on tau may be through the enhancement of autophagy by lithium, driving an increased autophagy and degradation of phosphorylated tau amounts and aggregation-prone tau, as previously reported (Shimada et al., 2012, Motoi et al., 2014).

Additionally, LiCl treatment of 3xTg-AD slice cultures resulted in reduced levels of APP phosphorylation at thr 668. Reduced phosphorylation at this APP site increases its propensity to be processed via the non-amyloidogenic pathway, precluding the formation of Aβ-42 (Lee et al., 2003). This finding therefore suggests that LiCl treatment of slice cultures may have reduced levels of Aβ, should they have been quantified here. The effects of lithium on APP processing and Aβ production in AD are currently unclear. Previous studies, both *in vitro* and *in vivo*, suggest an ability of lithium to reduce Aβ levels (Phiel et al., 2003, Su et al., 2004), although no changes in Aβ levels were observed following LiCl treatment of 3xTg-AD mice (Caccamo et al., 2007). These findings also support those of others where lithium treatment of neuroblastoma cells prevents phosphorylation of APP at thr 668, reducing axonal transport of APP (Acevedo et al., 2014). This axonal transport is necessary to enable the transport of APP for physiological functions at the synapse (Hoe et al., 2012) as well as in other neuronal compartments. However, increased amounts of APP phosphorylation at thr 668 are found in AD brain, and are thought to be associated with synaptic deficits and memory loss in AD (Shin et al., 2007, Lombino et al., 2013), suggesting that reduced phosphorylation of APP at thr 668 may be beneficial in AD. Thus, although the mechanism of action is not clear, the results presented here, and by others, suggests that LiCl could have beneficial effects in AD by reducing both tau and APP phosphorylation.

To further validate slice cultures as a tool for drug discovery, 3xTg-AD slice cultures were treated for 24 hours with 1×10^{-7} M NAPVSIPQ. Treatment of the slice cultures reduced tau phosphorylation at thr 231, a site thought to be involved in microtubule binding and

stabilisation (Sengupta et al., 1998). This finding recapitulated previous *in vivo* findings in 3xTg-AD mice, where phosphorylation of tau at thr 231 was also attenuated by NAPVSIPQ treatment (Matsuoka et al., 2007, Matsuoka et al., 2008). Conversely, phosphorylation of tau at ser 199/202 and thr 205 in 3xTg-AD slice cultures was not affected by NAPVSIPQ treatment, despite phosphorylation at these sites being reduced by NAPVSIPQ treatment *in vivo* (Matsuoka et al., 2007, Matsuoka et al., 2008). Again, the reasons for the discrepancies between these results is not clear, but it is possible that NAPVSIPQ treatment of 3xTg-AD slice cultures did not affect tau phosphorylation at ser 199/202 and thr 205 because chronic exposure may be required to reduce phosphorylation at these sites and only one dose of NAPVSIPQ was applied to slices unlike the several doses given *in vivo*. Alternatively, levels of tau phosphorylation at these sites may have been higher in 3xTg-AD slice cultures than *in vivo* so these may have been less readily responsive to treatment.

NAPVSIPQ is widely reported as a microtubule interacting agent (Quraishe et al., 2013). However, the results presented here using 3xTg-AD slice cultures have shown that NAPVSIPQ does not increase the binding of tau to microtubules, nor does it rescue microtubule destabilisation after treatment with nocodazole, a microtubule destabilising agent (Samson et al., 1979). This suggests that positive effects of NAPVSIPQ on tau phosphorylation are not mediated through changes in microtubule stability. This is in agreement with others who have demonstrated that NAPVSIPQ does not directly affect the polymerisation or dynamics of microtubules (Yenjerla et al., 2010), but disagrees with *in vitro* findings that have shown that NAPVSIPQ can increase microtubule stability

(Gozes and Divinski, 2004, Divinski et al., 2006). Previous *in vivo* work in mouse models of tauopathies has also not been able to uncover the mechanisms by which NAPVSIPQ treatment leads to reduced tau phosphorylation and lowering of insoluble tau amounts (Matsuoka et al., 2007, Matsuoka et al., 2008, Shiryaev et al., 2009). Here, we have shown that the reductions in tau phosphorylation at thr 231 that result from NAPVSIPQ treatment does not cause changes in the binding of tau to microtubules. The mechanisms underlying the tau-targeted effects of NAPVSIPQ remain to be established.

6.3.2 BTA-EG_4 as a novel AD drug

Previous research has highlighted that BTA-EG_4 may hold potential as a novel AD therapeutic. BTA-EG_4 has amyloid-binding properties (Inbar et al., 2006), and is neuroprotective *in vitro* against Aβ preparations and associated subsequent hydrogen peroxide release (Habib et al., 2010). BTA-EG_4 readily crosses the blood-brain-barrier and is soluble in aqueous environments (Inbar et al., 2006) making it an ideal candidate for pre-clinical studies into its potential use in the treatment of AD or other tauopathies.

Several beneficial effects of BTA-EG_4 relevant to AD have been identified in this thesis and by others. Firstly, BTA-EG_4 treatment reduces the production of Aβ-40 *in vivo* in adult WT mice and young 3xTg-AD mice (Megill et al., 2013, Song et al., 2014). Production of Aβ-42 was not assessed in these published studies, however treatment with BTA-EG_4 in this work did not attenuate levels of Aβ-42 and nor did it affect the ratio of Aβ-42 to Aβ-40 or Aβ-40 levels in 3xTg-AD slice cultures at 28 *div*, a time at which Aβ-42 is significantly overproduced in these cultures,. Additionally, BTA-EG_4 increases the

production of sAPPα and reduces production of sAPPβ in WT mice (Megill et al., 2013), suggesting BTA-EG_4 is able to drive less β-secretase cleavage of APP under certain conditions. Therefore positive effects against Aβ and reduced β-secretase cleavage of APP in some systems are likely relevant to the treatment of AD before the build-up of Aβ-containing plaques in AD (O'Brien and Wong, 2011). Taken together with the findings that amounts of Aβ-40 are attenuated in young but not old 3xTg-AD mice (Song et al., 2014), it is likely that the stage of AD in which BTA-EG_4 is given is important for its effects on Aβ amounts since APP processing changes as AD progresses (Stockley and O'Neill, 2007, O'Brien and Wong, 2011). Secondly, BTA-EG_4 increases spine density, the number of functional synapses and overall synaptic function, as measured by an increased frequency of miniature excitatory postsynaptic currents (mEPSCs) in the cortex and hippocampus in WT mice. These synaptic improvements are also accompanied by improved cognitive performance in WT mice (Megill et al., 2013). BTA-EG_4 treatment of 3xTg-AD mice also increases spine density and spine size in the cortex and hippocampus, alongside improving cognitive performance compared to untreated 3xTg-AD mice (Song et al., 2014). These positive effects of BTA-EG_4 at synaptic and behavioural levels further support the likely beneficial effects of this treatment for AD (Terry et al., 1991, Sheng et al., 2012). Lastly, in 3xTg-AD slice cultures, BTA-EG_4 was shown here for the first time to significantly reduce tau phosphorylation at ser 202, but not ser 396/404. Again, the stage of AD at which BTA-EG_4 is given is suggested to be critical, as in primary cortical neurons, where there is no accumulation of pathological tau, the phosphorylation of tau at ser 199/202 and thr 205, ser 202 and ser 396/404 is attenuated with BTA-EG_4. These novel effects of BTA-EG_4 on tau are also likely relevant to the treatment of AD since

changes in tau are most closely associated with dementia in AD (Perez-Nievas et al., 2013) and tau is necessary for Aβ-induced neuronal loss (Rapoport et al., 2002) and deficits in LTP (Shipton et al., 2011).

Several mechanisms for the mode of action of BTA-EG_4 have been proposed so far. Firstly, BTA-EG_4 has been shown to increase the cell surface expression of APP (Megill et al., 2013), which enhances preferential cleavage by α-secretase to preclude Aβ formation (Hyman, 2011). Increased synaptic density observed with BTA-EG_4 both in WT and 3xTg-AD mice was shown to be as a result of APP-dependent increases in Ras activity as well as downstream Ras signalling (Megill et al., 2013, Song et al., 2014). Lastly, data presented in this thesis has shown that BTA-EG_4 significantly reduces GSK-3 activity in 3xTg-AD slice culture but does not affect cdk5 activity. However, in WT primary cortical neurons, p35 activation of cdk5, rather than GSK-3 activity, was found to be reduced. This discrepancy in the effect of BTA-EG_4 on cdk5 and GSK-3 activity in these different model systems is unclear, but might be related to interactions between GSK-3 and cdk5 (Engmann and Giese, 2009), which likely differ depending on whether the system contains physiological tau (WT primary cortical neurons) or pathological tau (3xTg-AD slice cultures).

Taken together, these findings support further investigation into the potential beneficial effects of BTA-EG_4 and similar compounds in the treatment of AD, particularly since BTA-EG_4 appears to have positive effects at the synapse, on Aβ and tau, and also improving cognition. Finally, the results discussed here indicate that for all treatments, it is

important to assess the disease stage of models when interpreting the effectiveness of potential therapies as this is likely to be relevant to successful outcomes in clinical trials.

6.4 Limitations of this work

For all of the work presented in this thesis, the utmost effort was taken to ensure that the experimental work carried out was well designed, planned and controlled. However, it is important to discuss some of the limitations of this work.

6.4.1 Slice Culture survival

At the outset of the project, it was planned that slice cultures would be cultured for longer durations of time, as culture periods of up to 6 months had previously been reported (Duff et al., 2002). However, WT and 3xTg-AD slice cultures showed a rapid death rate beyond 28 *div*. Most slice cultures were found to suddenly die at approximately 30 *div*, and only a few slice cultures were found to survive up to 2-3 months *in vitro*. Throughout the course of this project, reasons for this sudden death were explored, however, it was not possible to identify a specific reason for this sudden death. Further optimisation of methods to prepare slice cultures could potentially enable slices to survive for longer periods of time.

Levels of Aβ and phosphorylated tau species were assessed here using biochemical methods, but it is likely that if slice cultures were able to survive for longer durations in culture allowing the disease phenotype to further develop, that aggregated Aβ and tau species may also have been detected using histological methods, as reported by (Duff et

al., 2002). Additionally, longer culture periods would allow other important disease characteristics such as synaptic integrity to be monitored over time, as well as allowing the assessment of treatment effects in cultures maintained for time periods beyond 28 *div*, representing later disease stages.

6.4.2 Limitations of antibodies

Despite using different dilutions, dilution buffers, incubation periods, alternative epitopes and suppliers, several primary antibodies for western blotting, ELISA or immunohistochemistry did not detect the protein of interest. This prevented certain proteins from being detected in 3xTg-AD slice cultures to allow a greater breadth of characterisation of the slice cultures.

Specifically, antibodies were used to detect PS1, sAPPα, sAPPβ, C83, C99, Aβ-40, Aβ-42 but none of these were detected in organotypic brain slice cultures using western blotting. Additionally, several antibodies against additional tau phosphorylation sites were used to try and establish a direct ELISA that would enable simultaneous analysis of several samples; however, some of these antibodies did not work at all in direct ELISAs and others did not produce reproducible, reliable results. Since ELISAs are well established in the laboratory, this is likely not to be a general problem with the methodology, yet again reflects difficulties in obtaining reliable signals with some commercially available antibodies. Finally, some antibodies were used successfully to detect phosphorylated tau in organotypic brain slice cultures from mice using immunohistochemistry, however the tau antibodies; MC1, tau-1, Tg3 and TOC1 were

not able to be successfully optimised for this work, despite these antibodies being previously published for this type of use (Brion et al., 1999, Oh et al., 2010, Ward et al., 2014).

6.4.3 Tau release mechanisms

As described in chapter 5, several experiments were planned to be conducted in WT and 3xTg-AD slice cultures, however, due to time constraints and unexpected slice culture death they were not able to be carried out, or were carried out only once.

Specifically, media from control or KCl-treated WT and 3xTg-AD slice cultures was planned to be concentrated in order to identify any extracellular vesicular-associated tau, phosphorylated or dephosphorylated tau and any N-terminal or C-terminal truncated or intact species to understand the species of tau associated with physiological and pathological tau release. In addition, experiments exploring the effect of neuronal activity on physiological and pathological tau release were only performed once, with small group sizes, allowing no statistical tests to be performed on the data, and only allowing assumptions rather than conclusions to be drawn from the gathered data.

6.5 Future directions

A lot of the work presented in this thesis involved the development of the 3xTg-AD slice culture model and subsequent characterisation of AD-relevant features. Now that this model is well characterised, it lends itself to further optimisation, as well as for the

development of techniques designed to exploit this slice culture system in further research to understand the mechanisms involved in AD. The following section outlines some of the experiments that could be conducted to extend from the work presented in this thesis.

6.5.1 Optimise slice culture survival

Methods presented in this thesis enabled both WT and 3xTg-AD organotypic brain slice cultures to survive up to 30 *div*. 3xTg-AD slice cultures showed progressive increases in tau phosphorylation at several AD-relevant sites, an increased abundance of high molecular weight tau, as well as increased levels of Aβ-42 and other AD-relevant proteins. However, beyond 30 *div* slice cultures showed a rapid release of LDH and subsequent death. It would be interesting to further optimise the culture of organotypic brain slices to allow investigation of AD-related changes and the effects of drug treatments beyond this time-point. Approaches which could optimise the survival of slice cultures for longer durations would include:

1. **Alternative medium composition.** Slice culture medium containing less horse serum (20%), or B27 supplement as an alternative, alongside altered levels of sugars and salts have also been shown to promote long-term culture (Opitz-Araya and Barria, 2011, Mewes et al., 2012). These culture mediums may be more suited to promoting the survival of 3xTg-AD slice cultures.
2. **Alternative membrane inserts.** The Millipore inserts used in these experiments are made from polytetrafluoroethylene (PTFE) and are marketed as supporting culture for up to 40 *div.* Other inserts made from polyethylene

terephthalate (PET) were tested when developing the slice culture model but did not support slice culture survival. Other inserts made from Anopore™ are available and it is possible that these may support longer-term culture.

3. **Preparing thinner slice cultures.** Slices cultured at 200 µm thickness compared to 300 µm thickness show a 30–50 % higher metabolism rate likely through a better nutrition supply and show reduced levels of cell death (Mewes et al., 2012).

4. **Culturing at a lower temperature.** Slices cultured at 32 ^{o}C instead of 35 ^{o}C show a better survival rate, likely through reduced levels of ischaemia (Frantseva et al., 1999, Mewes et al., 2012).

6.5.2 Optimise imaging methods for examining pathological changes in 3xTg-AD slice cultures

As discussed above, should slice culture methods be optimised such that they can survive beyond 30 *div,* it is likely they may develop aggregates of tau or Aβ, as previously demonstrated after long periods of culture in mice overexpressing mutant APP or tau (Duff et al., 2002). An optimised protocol to detect plaques using thioflavin s or congo red (Rajamohamedsait and Sigurdsson, 2012) and to detect NFTs using gallyas staining (Kuninaka et al., 2015) in organotypic brain slice cultures would be useful to identify these neuropathological features of AD.

In addition, slice cultures lend themselves to other advanced imaging techniques which could be used to underpin the progression of AD-relevant changes in the slice cultures.

For example, array tomography could be used to more closely look at the effects of Aβ, tau and APP at the synapse in slice cultures (Micheva and Smith, 2007, Koffie et al., 2009). In addition, using live imaging of calcium to identify any changes in slice cultures would also increase our knowledge of this aspect of AD (Goldberg and Yuste, 2009).

6.5.3 Investigate different time points of drug intervention

Due to time constraints of the project, treatments were provided to 3xTg-AD slice cultures at 28 *div,* when significant amounts of Aβ-42, phosphorylated tau and high molecular weight tau had accumulated. Future work should elucidate the effects of treatments on slices cultured for shorter and longer times to further investigate the effects of disease stage on the effectiveness of each treatment. In particular, 3xTg-AD slice cultures treated at 28 *div* with BTA-EG_4 did not show any changes in levels of Aβ-42, but one may speculate that had slice cultures been treated at 14 *div* when only a small overproduction of Aβ-42 is evident, treatment with BTA-EG_4 may have shown different effects since treatment of young but not old 3xTg-AD mice with BTA-EG_4 reduces levels of Aβ-40 (Song et al., 2014). Consequently, this is highly relevant to the treatment of AD in humans, particularly concerning the need for an early and accurate diagnosis of the disease (Schaffer et al., 2015) for certain treatments to be effective, as well as a demand for other treatments which can be used if the diagnosis of the disease is received much later in the disease course.

6.5.4 Investigate BTA-EG_4 and other benzothiazole derivatives *ex vivo* and *in vivo*

3xTg-AD slice cultures treated with BTA-EG_4 showed reduced activation of GSK-3 and this was associated with reductions in the phosphorylation of tau at ser 202. Additionally, primary cortical neurons treated with BTA-EG_4 showed reductions in tau phosphorylation at ser 199/292 and thr 205 and ser 396/404 that were associated with inactivation of cdk5. This suggests that the differential effects of BTA-EG_4 on tau and kinase activity are apparent in different disease states of a system, as discussed above. However, these results also suggest that exploring the effects of BTA-EG_4 on tau *in vivo* could be an important focus of future experiments. Additionally, other benzothiazole derivatives similar to BTA-EG_4 have been confirmed with better blood-brain-barrier penetration, a lower toxicity and an increased solubility (Jerry Yang, personal communication), suggesting these could also be investigated as potential AD therapeutics which target disease-associated changes in tau.

6.5.5 Develop a further understanding of mechanisms of pathological and physiological tau release

Due to time constraints and problems with slice culture survival, some planned experiments to investigate physiological and pathological tau release in organotypic brain slice cultures were not performed, so these would be a focus of future work. Specifically, medium from both WT and 3xTg-AD, control and KCl-treated slice cultures should be concentrated and examined for tau associated with vesicles, full-length, N- and C-terminally truncated tau species, as well as phosphorylated and dephosphorylated species of tau, to begin to investigate the role of these tau species physiologically and in

disease. The media could also be used to examine species of tau release via alternative methods including ELISA (Kanmert et al., 2015) or mass spectrometry (Bright et al., 2015).

Additionally, experiments using the pre-treatment of TTX to inhibit neuronal stimulation of WT and 3xTg-AD slice cultures were only performed once so should be repeated to fully understand the effects of neuronal activity on physiological and pathological tau release. In addition, slice cultures lend themselves to electrophysiology studies, so any changes in neuronal hyperactivity accompanying release could be assessed using this method (Plenz et al., 2011, Bright et al., 2015).

Furthermore, 3xTg-AD slice cultures lend themselves to study the interplay between Aβ and tau in the propagation of tau in AD. Specifically, treatment of 3xTg-AD slice cultures with γ-secretase inhibitors to prevent the formation of Aβ species (Golde et al., 2013) or applying antibodies to the slice cultures against Aβ would provide novel information to understand the role of Aβ in the propagation and release of extracellular tau in AD. In addition, slice cultures also provide an appropriate platform to study therapies targeting extracellular tau, including antibodies against extracellular tau (Bright et al., 2015).

Finally, it is conceivable that slice cultures could be used for tau seeding experiments, where tau seeds from human AD or tauopathy brain can be applied on to the slice cultures, and propagation from cell to cell and region to region can be assessed using histological or advanced live imaging methods more rapidly in slice cultures than *in vivo*,

but in more intact brain than *in vitro* studies (Sanders et al., 2014) enabling a greater understanding of propagation of tau in AD. In addition, AAV technology (Chakrabarty et al., 2015) could be used to express tau in one specific region of the slice cultures, and its spread could also be rapidly identified. Taken together, this series of experiments which could be easily and efficiently conducted in slice cultures would dramatically increase our knowledge of tau release and its role in tau propagation. A summary of experiments to investigate tau release and propagation in organotypic brain slice cultures can be seen in **Figure 6.1**.

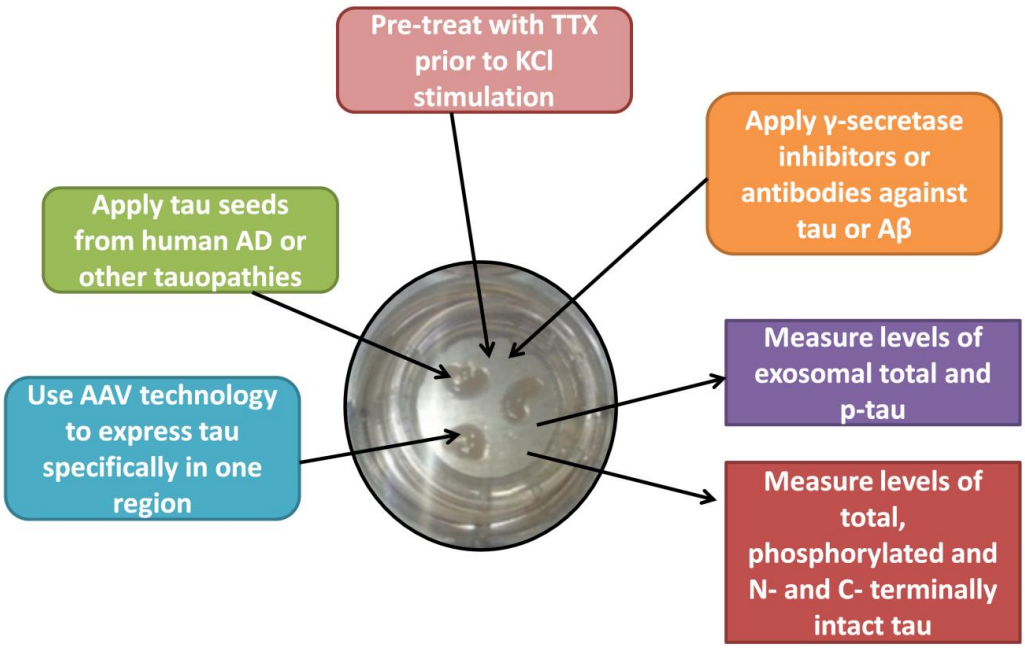

Figure 6.1: Visualisation of experiments to investigate tau propagation in organotypic brain slice cultures.
Both WT and 3xTg-AD slice cultures can be used to investigate tau release and propagation. Tau seeds could be applied to slice cultures or AAV technology could be used to express tau in one region of a slice culture; any propagation of tau could then be assessed by histological or advanced imaging methods. To investigate whether tau is released at the synapse, the application of TTX prior to depolarisation with KCl would block this release should it be synaptic. Furthermore, interactions between Aβ and tau in the release and propagation of tau could be investigated using γ-secretase inhibitors or antibodies against tau or Aβ. In all these situations, levels of total, phosphorylated and cleaved tau and exosomal total and phosphorylated tau should be measured in the media by western blotting, ELISA or mass spectrometry.

6.5.6 Determine whether increased total tau amounts are found at the synapse in early AD

Previous research assessing tau at the synapse has been performed in both control and advanced-staged AD brain. These findings suggest that there are no differences in total tau amounts at the synapse between AD and non-diseased brain (Tai et al., 2012, Tai et al., 2014), however, increased amounts of phosphorylated and misfolded tau are found at the synapse in AD (Tai et al., 2014). Results both *in vivo* and *ex vivo* in 3xTg-AD mice and slice cultures, respectively, suggest an early increase in total tau amounts at the synapse, which progressively returns to control levels, thus suggesting the redistribution of tau from the synapse to other compartments or the extracellular space and/or post-translational modifications of tau at the synapse at later stages of AD. As we have access to post-mortem human brain diagnosed at all the Braak stages of AD (Braak and Braak, 1991, Braak and Braak, 1995), it would be interesting to prepare synaptosomes from this brain tissue and determine whether this early but not sustained increases in tau at the synapse is also found in human AD brain. Furthermore, array tomography could be used to study interactions between Aβ species and tau species at the synapse at the different Braak stages (Kay et al., 2013). It would also be interesting to identify whether dephosphorylated tau is also present at the membrane in human tissue preparations as found *in vitro* (Arrasate et al., 2000, Pooler et al., 2012) and *ex vivo* in slice cultures, as this may be associated with the propagation of tau in AD.

6.6 Final Conclusions

Overall, the data presented in this thesis demonstrates that organotypic brain slice cultures prepared from 3xTg-AD mice provide a reliable *ex vivo* model of AD which rapidly develops progressive AD-related changes. This slice culture system can be used effectively to understand mechanisms and pathways underlying the development and progression of AD, as well as in pre-clinical testing of potential AD therapeutics. In particular, slice cultures have been exploited here to increase understanding of the mechanisms implicated in physiological and pathological tau release and to understand the novel tau-targeted effects of the amyloid-binding agent BTA-EG_4.

In conclusion, this novel slice culture model of AD, developed using NC3Rs funding, should significantly reduce the number of animals required for neurodegeneration research, refine experiments into AD by reducing variability, whilst also reducing and replacing the need for invasive *in vivo* studies. Therefore, this novel experimental model should accelerate studies underpinning the mechanisms of AD and the discovery of novel therapeutics for AD and other neurodegenerative conditions.

References

Abramov, E., Dolev, I., Fogel, H., Ciccotosto, G. D., Ruff, E. & Slutsky, I. 2009. Amyloid-[beta] as a positive endogenous regulator of release probability at hippocampal synapses. *Nature Neuroscience,* 12**,** 1567-1576.

Acevedo, K. M., Opazo, C. M., Norrish, D., Challis, L. M., Li, Q.-X., White, A. R., Bush, A. I. & Camakaris, J. 2014. Phosphorylation of Amyloid Precursor Protein at Threonine 668 Is Essential for Its Copper-responsive Trafficking in SH-SY5Y Neuroblastoma Cells. *The Journal of Biological Chemistry,* 289**,** 11007-11019.

Ackerley, S., Grierson, A. J., Brownlees, J., Thornhill, P., Anderton, B. H., Leigh, P. N., Shaw, C. E. & Miller, C. C. J. 2000. Glutamate Slows Axonal Transport of Neurofilaments in Transfected Neurons. *The Journal of Cell Biology,* 150**,** 165-176.

Ahmed, M., Davis, J., Aucoin, D., Sato, T., Ahuja, S., Aimoto, S., Elliott, J. I., Van Nostrand, W. E. & Smith, S. O. 2010. Structural conversion of neurotoxic amyloid-β(1–42) oligomers to fibrils. *Nature structural & molecular biology,* 17**,** 561-567.

Allen, B., Ingram, E., Takao, M., Smith, M. J., Jakes, R., Virdee, K., Yoshida, H., Holzer, M., Craxton, M., Emson, P. C., Atzori, C., Migheli, A., Crowther, R. A., Ghetti, B., Spillantini, M. G. & Goedert, M. 2002. Abundant Tau Filaments and Nonapoptotic Neurodegeneration in Transgenic Mice Expressing Human P301S Tau Protein. *The Journal of Neuroscience,* 22**,** 9340-9351.

Alonso, A. D. C., Mederlyova, A., Novak, M., Grundke-Iqbal, I. & Iqbal, K. 2004. Promotion of Hyperphosphorylation by Frontotemporal Dementia Tau Mutations. *Journal of Biological Chemistry,* 279**,** 34873-34881.

Alzheimer's Society. 2015. *Statistics - Alzheimer's Society www.alzheimers.org.uk/statistics* [Online]. [Accessed 2nd October 2015.

Alzheimer, A. 1906. Über einen eigenartigen schweren Erkrankungsprozeß der Hirnrinde. *Neurologisches Centralblatt,* 23**,** 1129–3.

Andorfer, C., Kress, Y., Espinoza, M., De Silva, R., Tucker, K. L., Barde, Y.-A., Duff, K. & Davies, P. 2003. Hyperphosphorylation and aggregation of tau in mice expressing normal human tau isoforms. *Journal of Neurochemistry,* 86**,** 582-590.

Arrasate, M., Pérez, M. & Avila, J. 2000. Tau Dephosphorylation at Tau-1 Site Correlates with its Association to Cell Membrane. *Neurochemical Research,* 25**,** 43-50.

Asai, H., Ikezu, S., Tsunoda, S., Medalla, M., Luebke, J., Haydar, T., Wolozin, B., Butovsky, O., Kugler, S. & Ikezu, T. 2015. Depletion of microglia and inhibition of exosome synthesis halt tau propagation. *Nature Neuroscience,* 18**,** 1584-1593.

Ashur-Fabian, O., Segal-Ruder, Y., Skutelsky, E., Brenneman, D. E., Steingart, R. A., Giladi, E. & Gozes, I. 2003. The neuroprotective peptide NAP inhibits the aggregation of the beta-amyloid peptide. *Peptides,* 24**,** 1413-1423.

Atherton, J., Kurbatskaya, K., Bondulich, M., Croft, C. L., Garwood, C. J., Chhabra, R., Wray, S., Jeromin, A., Hanger, D. P. & Noble, W. 2014. Calpain cleavage and inactivation of the sodium calcium exchanger-3 occur downstream of Aβ in Alzheimer's disease. *Aging Cell,* 13**,** 49-59.

Barghorn, S., Zheng-Fischhöfer, Q., Ackmann, M., Biernat, J., Von Bergen, M., Mandelkow, E. M. & Mandelkow, E. 2000. Structure, Microtubule Interactions, and Paired Helical Filament Aggregation by Tau Mutants of Frontotemporal Dementias†. *Biochemistry,* 39**,** 11714-11721.

Barnes, C. A. 1999. Do synaptic markers provide a window on synaptic effectiveness in the aged hippocampus? *Neurobiology of Aging,* 20**,** 349-351.

Barten, D. M., Cadelina, G. W., Hoque, N., Decarr, L. B., Guss, V. L., Yang, L., Sankaranarayanan, S., Wes, P. D., Flynn, M. E., Meredith, J. E., Ahlijanian, M. K. & Albright, C. F. 2011. Tau transgenic mice as models for cerebrospinal fluid tau biomarkers. *Journal of Alzheimers Disease,* 24 Suppl 2**,** 127-41.

Bayer, T. A., Cappai, R., Masters, C. L., Beyreuther, K. & Multhaup, G. 1999. It all sticks together--the APP-related family of proteins and Alzheimer's disease. *Molecular Psychiatry,* 4**,** 524-8.

Bayer, T. A. & Wirths, O. 2008. Review on the APP/PS1KI mouse model: intraneuronal Abeta accumulation triggers axonopathy, neuron loss and working memory impairment. *Genes Brain Behaviour,* 7 Suppl 1**,** 6-11.

Bell, J., Alafuzoff, I., Al-Sarraj, S., Arzberger, T., Bogdanovic, N., Budka, H., Dexter, D., Falkai, P., Ferrer, I., Gelpi, E., Gentleman, S., Giaccone, G., Huitinga, I., Ironside, J., Kliloueva, N., Kovacs, G., Meyronet, D., Palkovits, M., Parchi, P., Patsouris, E., Reynolds, R., Riederer, P., Roggendorf, W., Seilhean, D., Schmitt, A., Schmitz, P., Streichenberger, N., Schwalber, A. & Kretzschmar, H. 2008. Management of a twenty-first century brain bank: experience in the BrainNet Europe consortium. *Acta Neuropathologica,* 115**,** 497-507.

Beurel, E., Grieco, S. F. & Jope, R. S. 2015. Glycogen synthase kinase-3 (GSK3): Regulation, actions, and diseases. *Pharmacology & Therapeutics,* 148**,** 114-131.

Biernat, J. & Mandelkow, E.-M. 1999. The Development of Cell Processes Induced by tau Protein Requires Phosphorylation of Serine 262 and 356 in the Repeat Domain and Is Inhibited by Phosphorylation in the Proline-rich Domains. *Molecular Biology of the Cell,* 10**,** 727-740.

Billings, L. M., Oddo, S., Green, K. N., Mcgaugh, J. L. & La Ferla, F. M. 2005. Intraneuronal Aβ Causes the Onset of Early Alzheimer's Disease-Related Cognitive Deficits in Transgenic Mice. *Neuron,* 45**,** 675-688.

Binder, L. I., Guillozet-Bongaarts, A. L., Garcia-Sierra, F. & Berry, R. W. 2005. Tau, tangles, and Alzheimer's disease. *Biochimica et Biophysica Acta (BBA) - Molecular Basis of Disease,* 1739**,** 216-223.

Bittner, T., Fuhrmann, M., Burgold, S., Ochs, S. M., Hoffmann, N., Mitteregger, G., Kretzschmar, H., Laferla, F. M. & Herms, J. 2010. Multiple Events Lead to Dendritic Spine Loss in Triple Transgenic Alzheimer's Disease Mice. *PLoS ONE,* 5**,** e15477.

Blennow, K., Wallin, A., Agren, H., Spenger, C., Siegfried, J. & Vanmechelen, E. 1995. Tau protein in cerebrospinal fluid: a biochemical marker for axonal degeneration in Alzheimer disease? *Molecular Chemical Neuropathology,* 26**,** 231-45.

Bolmont, T., Clavaguera, F., Meyer-Luehmann, M., Herzig, M. C., Radde, R., Staufenbiel, M., Lewis, J., Hutton, M., Tolnay, M. & Jucker, M. 2007. Induction of Tau Pathology by Intracerebral Infusion of Amyloid-β-Containing Brain Extract and by Amyloid-β Deposition in APP × Tau Transgenic Mice. *The American Journal of Pathology,* 171**,** 2012-2020.

Braak, H. & Braak, E. 1991. Neuropathological stageing of Alzheimer-related changes. *Acta Neuropathologica,* 82**,** 239-259.

Braak, H. & Braak, E. 1995. Staging of alzheimer's disease-related neurofibrillary changes. *Neurobiology of Aging,* 16**,** 271-278.

Braak, H., Thal, D. R., Ghebremedhin, E. & Del Tredici, K. 2011. Stages of the pathologic process in Alzheimer disease: age categories from 1 to 100 years. *Journal of Neuropathology and Experimental Neurology,* 70**,** 960-9.

Brandt, R. & Lee, G. 1994. Orientation, assembly, and stability of microtubule bundles induced by a fragment of tau protein. *Cell Motility and the Cytoskeleton,* 28**,** 143-54.

Brandt, R., Léger, J. & Lee, G. 1995. Interaction of tau with the neural plasma membrane mediated by tau's amino-terminal projection domain. *The Journal of Cell Biology,* 131**,** 1327-1340.

Bright, J., Hussain, S., Dang, V., Wright, S., Cooper, B., Byun, T., Ramos, C., Singh, A., Parry, G., Stagliano, N. & Griswold-Prenner, I. 2015. Human secreted tau increases amyloid-beta production. *Neurobiology of Aging,* 36**,** 693-709.

Brion, J.-P., Couck, A.-M., Robertson, J., Loviny, T. L. F. & Anderton, B. H. 1993. Neurofilament Monoclonal Antibodies RT97 and 8D8 Recognize Different Modified Epitopes in Paired Helical Filament-τ in Alzheimer's Disease. *Journal of Neurochemistry,* 60**,** 1372-1382.

Brion, J.-P., Tremp, G. & Octave, J.-N. 1999. Transgenic Expression of the Shortest Human Tau Affects Its Compartmentalization and Its Phosphorylation as in the Pretangle Stage of Alzheimer's Disease. *The American Journal of Pathology,* 154**,** 255-270.

Broadstock, M., Ballard, C. & Corbett, A. 2014. Latest treatment options for Alzheimer's disease, Parkinson's disease dementia and dementia with Lewy bodies. *Expert Opinion on Pharmacotherapy,* 15**,** 1797-1810.

Bruce, A. J., Malfroy, B. & Baudry, M. 1996. beta-Amyloid toxicity in organotypic hippocampal cultures: protection by EUK-8, a synthetic catalytic free radical scavenger. *Proceedings of the National Academy of Sciences of the United States of America,* 93**,** 2312-2316.

Buée, L., Bussière, T., Buée-Scherrer, V., Delacourte, A. & Hof, P. R. 2000. Tau protein isoforms, phosphorylation and role in neurodegenerative disorders. *Brain Research Reviews,* 33**,** 95-130.

Butterfield, D. A. 2002. Amyloid beta-peptide (1-42)-induced oxidative stress and neurotoxicity: implications for neurodegeneration in Alzheimer's disease brain. A review. *Free Radical Research,* 36**,** 1307-13.

Butterfield, D. A., Griffin, S., Munch, G. & Pasinetti, G. 2002. Amyloid beta-peptide and amyloid pathology are central to the oxidative stress and inflammatory cascades under which Alzheimer's disease brain exists. *Journal of Alzheimers disease,* 4**,** 193-202.

Caccamo, A., Oddo, S., Tran, L. X. & La Ferla, F. M. 2007. Lithium Reduces Tau Phosphorylation but Not Aβ or Working Memory Deficits in a Transgenic Model with Both Plaques and Tangles. *The American Journal of Pathology,* 170**,** 1669-1675.

Calafate, S., Buist, A., Miskiewicz, K., Vijayan, V., Daneels, G., De strooper, B., De wit, J., Verstreken, P. & Moechars, D. 2015. Synaptic Contacts Enhance Cell-to-Cell Tau Pathology Propagation. *Cell Reports,* 11**,** 1176-1183.

Cárdenas-Aguayo, M. D. C., Gómez-Virgilio, L., Derosa, S. & Meraz-Ríos, M. A. 2014. The Role of Tau Oligomers in the Onset of Alzheimer's Disease Neuropathology. *ACS Chemical Neuroscience,* 5**,** 1178-1191.

Chai, X., Dage, J. L. & Citron, M. 2012. Constitutive secretion of tau protein by an unconventional mechanism. *Neurobiology of Disease,* 48**,** 356-366.

Chakrabarty, P., Li, A., Ceballos-Diaz, C., Eddy, James a., Funk, Cory c., Moore, B., Dinunno, N., Rosario, Awilda m., Cruz, Pedro e., Verbeeck, C., Sacino, A., Nix, S., Janus, C., Price, Nathan d., Das, P. & Golde, Todd e. 2015. IL-10 Alters Immunoproteostasis in APP Mice, Increasing Plaque Burden and Worsening Cognitive Behavior. *Neuron,* 85**,** 519-533.

Chapman, P. F., White, G. L., Jones, M. W., Cooper-Blacketer, D., Marshall, V. J., Irizarry, M., Younkin, L., Good, M. A., Bliss, T. V. P., Hyman, B. T., Younkin, S. G. & Hsiao, K. K. 1999.

Impaired synaptic plasticity and learning in aged amyloid precursor protein transgenic mice. *Nature Neuroscience,* 2**,** 271-276.

Chen, Y., Zhao, Y., Dai, C.-L., Liang, Z., Run, X., Iqbal, K., Liu, F. & Gong, C.-X. 2014. Intranasal insulin restores insulin signaling, increases synaptic proteins, and reduces Aβ level and microglia activation in the brains of 3xTg-AD mice. *Experimental Neurology,* 261**,** 610-619.

Choi, S. H., Kim, Y. H., Hebisch, M., Sliwinski, C., Lee, S., D/'Avanzo, C., Chen, H., Hooli, B., Asselin, C., Muffat, J., Klee, J. B., Zhang, C., Wainger, B. J., Peitz, M., Kovacs, D. M., Woolf, C. J., Wagner, S. L., Tanzi, R. E. & Kim, D. Y. 2014. A three-dimensional human neural cell culture model of Alzheimer's disease. *Nature,* 515**,** 274-278.

Choy, R. W.-Y., Cheng, Z. & Schekman, R. 2012. Amyloid precursor protein (APP) traffics from the cell surface via endosomes for amyloid β (Aβ) production in the trans-Golgi network. *Proceedings of the National Academy of Sciences of the United States of America,* 109**,** E2077-E2082.

Chung, C.-W., Song, Y.-H., Kim, I.-K., Yoon, W.-J., Ryu, B.-R., Jo, D.-G., Woo, H.-N., Kwon, Y.-K., Kim, H.-H., Gwag, B.-J., Mook-Jung, I.-H. & Jung, Y.-K. 2001. Proapoptotic Effects of Tau Cleavage Product Generated by Caspase-3. *Neurobiology of Disease,* 8**,** 162-172.

Chwalek, K., Sood, D., Cantley, W. L., White, J. D., Tang-Schomer, M. & Kaplan, D. L. 2015. Engineered 3D Silk-collagen-based Model of Polarized Neural Tissue. *Journal of Visualized Experiments***,** e52970.

Clavaguera, F., Akatsu, H., Fraser, G., Crowther, R. A., Frank, S., Hench, J., Probst, A., Winkler, D. T., Reichwald, J., Staufenbiel, M., Ghetti, B., Goedert, M. & Tolnay, M. 2013. Brain homogenates from human tauopathies induce tau inclusions in mouse brain. *Proceedings of the National Academy of Sciences of the United States of America,* 110**,** 9535-9540.

Clavaguera, F., Bolmont, T., Crowther, R. A., Abramowski, D., Frank, S., Probst, A., Fraser, G., Stalder, A. K., Beibel, M., Staufenbiel, M., Jucker, M., Goedert, M. & Tolnay, M. 2009. Transmission and spreading of tauopathy in transgenic mouse brain. *Nature cell biology,* 11**,** 909-913.

Corder, E. H., Saunders, A. M., Risch, N. J., Strittmatter, W. J., Schmechel, D. E., Gaskell, P. C., Rimmler, J. B., Locke, P. A., Conneally, P. M., Schmader, K. E., Small, G. W., Roses, A. D., Haines, J. L. & Pericak-Vance, M. A. 1994. Protective effect of apolipoprotein E type 2 allele for late onset Alzheimer disease. *Nature Genetics,* 7**,** 180-184.

Corder, E. H., Saunders, A. M., Strittmatter, W. J., Schmechel, D. E., Gaskell, P. C., Small, G. W., Roses, A. D., Haines, J. L. & Pericak-Vance, M. A. 1993. Gene dose of apolipoprotein E type 4 allele and the risk of Alzheimer's disease in late onset families. *Science,* 261**,** 921-3.

Corse, A. M., Bilak, M. M., Bilak, S. R., Lehar, M., Rothstein, J. D. & Kuncl, R. W. 1999. Preclinical Testing of Neuroprotective Neurotrophic Factors in a Model of Chronic Motor Neuron Degeneration. *Neurobiology of Disease,* 6**,** 335-346.

Crews, L. & Masliah, E. 2010. Molecular mechanisms of neurodegeneration in Alzheimer's disease. *Human Molecular Genetics,* 19**,** R12-R20.

Crimins, J. L., Pooler, A., Polydoro, M., Luebke, J. I. & Spires-Jones, T. L. 2013. The intersection of amyloid beta and tau in glutamatergic synaptic dysfunction and collapse in Alzheimer's disease. *Ageing research reviews,* 12**,** 757-763.

Cruts, M., Theuns, J. & Van Broeckhoven, C. 2012. Locus-specific mutation databases for neurodegenerative brain diseases. *Human Mutation,* 33**,** 1340-1344.

Cruz, J. C., Tseng, H.-C., Goldman, J. A., Shih, H. & Tsai, L.-H. 2003. Aberrant Cdk5 Activation by p25 Triggers Pathological Events Leading to Neurodegeneration and Neurofibrillary Tangles. *Neuron,* 40**,** 471-483.

Cuchillo-Ibanez, I., Seereeram, A., Byers, H. L., Leung, K. Y., Ward, M. A., Anderton, B. H. & Hanger, D. P. 2008. Phosphorylation of tau regulates its axonal transport by controlling its binding to kinesin. *The FASEB Journal,* 22**,** 3186-95.

Davis, D. R., Brion, J. P., Couck, A. M., Gallo, J. M., Hanger, D. P., Ladhani, K., Lewis, C., Miller, C. C., Rupniak, T., Smith, C. & Et Al. 1995. The phosphorylation state of the microtubule-associated protein tau as affected by glutamate, colchicine and beta-amyloid in primary rat cortical neuronal cultures. *Biochemical Journal,* 309 (Pt 3)**,** 941-9.

Dawkins, E. & Small, D. H. 2014. Insights into the physiological function of the β-amyloid precursor protein: beyond Alzheimer's disease. *Journal of Neurochemistry,* 129**,** 756-769.

De Calignon, A., Polydoro, M., Suárez-Calvet, M., William, C., Adamowicz, D. H., Kopeikina, K. J., Pitstick, R., Sahara, N., Ashe, K. H., Carlson, G. A., Spires-Jones, T. L. & Hyman, B. T. 2012. Propagation of tau pathology in a model of early Alzheimer's disease. *Neuron,* 73**,** 685-697.

De Simoni, A., Griesinger, C. B. & Edwards, F. A. 2003. Development of rat CA1 neurones in acute Versus organotypic slices: role of experience in synaptic morphology and activity. *The Journal of Physiology,* 550**,** 135-147.

De Simoni, A. & My Yu, L. 2006. Preparation of organotypic hippocampal slice cultures: interface method. *Nature Protocols,* 1**,** 1439-1445.

Dickson, D. W., Crystal, H. A., Bevona, C., Honer, W., Vincent, I. & Davies, P. 1995. Correlations of synaptic and pathological markers with cognition of the elderly. *Neurobiology of Aging,* 16**,** 285-298.

Divinski, I., Holtser-Cochav, M., Vulih-Schultzman, I., Steingart, R. A. & Gozes, I. 2006. Peptide neuroprotection through specific interaction with brain tubulin. *Journal of Neurochemistry,* 98**,** 973-984.

Dixit, R., Ross, J. L., Goldman, Y. E. & Holzbaur, E. L. F. 2008. Differential Regulation of Dynein and Kinesin Motor Proteins by Tau. *Science,* 319**,** 1086-1089.

Duff, K., Knight, H., Refolo, L. M., Sanders, S., Yu, X., Picciano, M., Malester, B., Hutton, M., Adamson, J., Goedert, M., Burki, K. & Davies, P. 2000. Characterization of Pathology in Transgenic Mice Over-Expressing Human Genomic and cDNA Tau Transgenes. *Neurobiology of Disease,* 7**,** 87-98.

Duff, K., Noble, W., Gaynor, K. & Matsuoka, Y. 2002. Organotypic slice cultures from transgenic mice as disease model systems. *Journal of Molecular Neuroscience,* 19**,** 317-320.

Dujardin, S., Bégard, S., Caillierez, R., Lachaud, C., Delattre, L., Carrier, S., Loyens, A., Galas, M.-C., Bousset, L., Melki, R., Aurégan, G., Hantraye, P., Brouillet, E., Buée, L. & Colin, M. 2014. Ectosomes: A New Mechanism for Non-Exosomal Secretion of Tau Protein. *PLoS ONE,* 9**,** e100760.

Egorova, P., Popugaeva, E. & Bezprozvanny, I. 2015. Disturbed calcium signaling in spinocerebellar ataxias and Alzheimer's disease. *Seminars in Cell & Developmental Biology,* 40**,** 127-133.

Engmann, O. & Giese, K. P. 2009. Crosstalk between Cdk5 and GSK3β: Implications for Alzheimer's Disease. *Frontiers in Molecular Neuroscience,* 2**,** 2.

Falcon, B., Cavallini, A., Angers, R., Glover, S., Murray, T. K., Barnham, L., Jackson, S., O'neill, M. J., Isaacs, A. M., Hutton, M. L., Szekeres, P. G., Goedert, M. & Bose, S. 2015. Conformation Determines the Seeding Potencies of Native and Recombinant Tau Aggregates. *The Journal of Biological Chemistry,* 290**,** 1049-1065.

Fath, T., Eidenmuller, J. & Brandt, R. 2002. Tau-mediated cytotoxicity in a pseudohyperphosphorylation model of Alzheimer's disease. *The Journal of Neuroscience,* 22**,** 9733-41.

Fein, J. A., Sokolow, S., Miller, C. A., Vinters, H. V., Yang, F., Cole, G. M. & Gylys, K. H. 2008. Co-Localization of Amyloid Beta and Tau Pathology in Alzheimer's Disease Synaptosomes. *The American Journal of Pathology,* 172**,** 1683-1692.

Fernandez, M. A., Klutkowski, J. A., Freret, T. & Wolfe, M. S. 2014. Alzheimer Presenilin-1 Mutations Dramatically Reduce Trimming of Long Amyloid β-Peptides (Aβ) by γ-Secretase to Increase 42-to-40-Residue Aβ. *Journal of Biological Chemistry*.

Ferreira, A. & Bigio, E. H. 2011. Calpain-Mediated Tau Cleavage: A Mechanism Leading to Neurodegeneration Shared by Multiple Tauopathies. *Molecular Medicine,* 17**,** 676-685.

Ferrer, I., Martinez, A., Boluda, S., Parchi, P. & Barrachina, M. 2008. Brain banks: benefits, limitations and cautions concerning the use of post-mortem brain tissue for molecular studies. *Cell and Tissue Banking,* 9**,** 181-194.

Fiandaca, M. S., Kapogiannis, D., Mapstone, M., Boxer, A., Eitan, E., Schwartz, J. B., Abner, E. L., Petersen, R. C., Federoff, H. J., Miller, B. L. & Goetzl, E. J. 2015. Identification of preclinical Alzheimer's disease by a profile of pathogenic proteins in neurally derived blood exosomes: A case-control study. *Alzheimer's & Dementia: The Journal of the Alzheimer's Association,* 11**,** 600-607.e1.

Flores-Rodríguez, P., Ontiveros-Torres, M. A., Cárdenas-Aguayo, M. C., Luna-Arias, J. P., Meraz-Ríos, M. A., Viramontes-Pintos, A., Harrington, C. R., Wischik, C. M., Mena, R., Florán-Garduño, B. & Luna-Muñoz, J. 2015. The relationship between truncation and phosphorylation at the C-terminus of tau protein in the paired helical filaments of Alzheimer's disease. *Frontiers in Neuroscience,* 9**,** 33.

Force, T. & Woodgett, J. R. 2009. Unique and Overlapping Functions of GSK-3 Isoforms in Cell Differentiation and Proliferation and Cardiovascular Development. *The Journal of Biological Chemistry,* 284**,** 9643-9647.

Frandemiche, M. L., De Seranno, S., Rush, T., Borel, E., Elie, A., Arnal, I., Lanté, F. & Buisson, A. 2014. Activity-Dependent Tau Protein Translocation to Excitatory Synapse Is Disrupted by Exposure to Amyloid-Beta Oligomers. *The Journal of Neuroscience,* 34**,** 6084-6097.

Frantseva, M. V., Carlen, P. L. & El-Beheiry, H. 1999. A submersion method to induce hypoxic damage in organotypic hippocampal cultures. *Journal of Neuroscience Methods,* 89**,** 25-31.

Friedhoff, P., Von Bergen, M., Mandelkow, E. M., Davies, P. & Mandelkow, E. 1998. A nucleated assembly mechanism of Alzheimer paired helical filaments. *Proceedings of the National Academy of Sciences of the United States of America,* 95**,** 15712-15717.

Friedrich, R. W., Jacobson, G. A. & Zhu, P. 2010. Circuit Neuroscience in Zebrafish. *Current Biology,* 20**,** R371-R381.

Fukushima, N., Furuta, D., Hidaka, Y., Moriyama, R. & Tsujiuchi, T. 2009. Post-translational modifications of tubulin in the nervous system. *Journal of Neurochemistry,* 109**,** 683-693.

Gagnon, L. G. & Belleville, S. 2011. Working memory in mild cognitive impairment and Alzheimer's disease: Contribution of forgetting and predictive value of complex span tasks. *Neuropsychology,* 25**,** 226-236.

Gähwiler, B. H. 1981. Organotypic monolayer cultures of nervous tissue. *Journal of Neuroscience Methods,* 4**,** 329-342.

Gähwiler, B. H., Capogna, M., Debanne, D., Mckinney, R. A. & Thompson, S. M. 1997. Organotypic slice cultures: a technique has come of age. *Trends in Neurosciences,* 20**,** 471-477.

Gamblin, T. C., Chen, F., Zambrano, A., Abraha, A., Lagalwar, S., Guillozet, A. L., Lu, M., Fu, Y., Garcia-Sierra, F., Lapointe, N., Miller, R., Berry, R. W., Binder, L. I. & Cryns, V. L. 2003. Caspase cleavage of tau: Linking amyloid and neurofibrillary tangles in Alzheimer's disease. *Proceedings of the National Academy of Sciences of the United States of America,* 100**,** 10032-10037.

Garcia-Sierra, F., Mondragon-Rodriguez, S. & Basurto-Islas, G. 2008. Truncation of tau protein and its pathological significance in Alzheimer's disease. *Journal of Alzheimer's Disease,* 14**,** 401-9.

Garg, S., Timm, T., Mandelkow, E.-M., Mandelkow, E. & Wang, Y. 2011. Cleavage of Tau by calpain in Alzheimer's disease: the quest for the toxic 17 kD fragment. *Neurobiology of Aging,* 32**,** 1-14.

Garwood, C. J., Pooler, A. M., Atherton, J., Hanger, D. P. & Noble, W. 2011. Astrocytes are important mediators of Aβ-induced neurotoxicity and tau phosphorylation in primary culture. *Cell Death and Disease,* 2**,** e167.

Gentleman, S. M. 2013. Microglia in protein aggregation disorders: friend or foe? *Neuropathology and applied neurobiology,* 39**,** 45-50.

Girão Da Cruz, M. T., Jordão, J., Dasilva, K. A., Ayala-Grosso, C. A., Ypsilanti, A., Weng, Y.-Q., Laferla, F. M., Mclaurin, J. & Aubert, I. 2012. Early Increases in Soluble Amyloid-β Levels Coincide with Cholinergic Degeneration in 3xTg-AD Mice. *Journal of Alzheimer's Disease,* 32**,** 267-272.

Glenner, G. G. & Wong, C. W. 1984. Alzheimer's disease: Initial report of the purification and characterization of a novel cerebrovascular amyloid protein. *Biochemical and Biophysical Research Communications,* 120**,** 885-890.

Goate, A., Chartier-Harlin, M.-C., Mullan, M., Brown, J., Crawford, F., Fidani, L., Giuffra, L., Haynes, A., Irving, N., James, L., Mant, R., Newton, P., Rooke, K., Roques, P., Talbot, C., Pericak-Vance, M., Roses, A., Williamson, R., Rossor, M., Owen, M. & Hardy, J. 1991. Segregation of a missense mutation in the amyloid precursor protein gene with familial Alzheimer's disease. *Nature,* 349**,** 704-706.

Goedert, M., Spillantini, M. G., Jakes, R., Rutherford, D. & Crowther, R. A. 1989. Multiple isoforms of human microtubule-associated protein tau: sequences and localization in neurofibrillary tangles of Alzheimer's disease. *Neuron,* 3**,** 519-526.

Gogolla, N., Galimberti, I., Depaola, V. & Caroni, P. 2006. Staining protocol for organotypic hippocampal slice cultures. *Nature Protocols,* 1**,** 2452-2456.

Goldberg, J. H. & Yuste, R. 2009. Two-Photon Calcium Imaging of Spines and Dendrites. *Cold Spring Harbor Protocols,* 6.

Golde, T. E. 2006. Disease modifying therapy for AD? *Journal of Neurochemistry,* 99**,** 689-707.

Golde, T. E., Koo, E. H., Felsenstein, K. M., Osborne, B. A. & Miele, L. 2013. γ-Secretase Inhibitors and Modulators. *Biochimica et biophysica acta,* 1828**,** 2898-907.

Gómez-Ramos, A., Díaz-Hernández, M., Rubio, A., Díaz-Hernández, J. I., Miras-Portugal, M. T. & Avila, J. 2009. Characteristics and consequences of muscarinic receptor activation by tau protein. *European Neuropsychopharmacology,* 19**,** 708-717.

Gómez-Ramos, A., Díaz-Hernández, M., Rubio, A., Miras-Portugal, M. T. & Avila, J. 2008. Extracellular tau promotes intracellular calcium increase through M1 and M3 muscarinic receptors in neuronal cells. *Molecular and Cellular Neuroscience,* 37**,** 673-681.

Gong, C.-X., Shaikh, S., Wang, J.-Z., Zaidi, T., Grundke-Iqbal, I. & Iqbal, K. 1995. Phosphatase Activity Toward Abnormally Phosphorylated τ: Decrease in Alzheimer Disease Brain. *Journal of Neurochemistry,* 65**,** 732-738.

Gonzalez, J., Jurado-Coronel, J. C., Avila, M. F., Sabogal, A., Capani, F. & Barreto, G. E. 2015. NMDARs in neurological diseases: a potential therapeutic target. *International Journal of Neuroscience,* 125**,** 315-27.

Götz, J., Chen, F., Van Dorpe, J. & Nitsch, R. M. 2001. Formation of Neurofibrillary Tangles in P301L Tau Transgenic Mice Induced by Aβ42 Fibrils. *Science,* 293**,** 1491-1495.

Gozes, I. & Divinski, I. 2004. The femtomolar-acting NAP interacts with microtubules: Novel aspects of astrocyte protection. *Journal of Alzheimer's Disease,* 6**,** S37-S41.

Greenberg, S. G. & Davies, P. 1990. A preparation of Alzheimer paired helical filaments that displays distinct tau proteins by polyacrylamide gel electrophoresis. *Proceedings of the National Academy of Sciences of the United States of America,* 87**,** 5827-5831.

Grundke-Iqbal, I., Iqbal, K., Quinlan, M., Tung, Y. C., Zaidi, M. S. & Wisniewski, H. M. 1986. Microtubule-associated protein tau. A component of Alzheimer paired helical filaments. *Journal of Biological Chemistry,* 261**,** 6084-6089.

Guerreiro, R. & Hardy, J. 2014. Genetics of Alzheimer's Disease. *Neurotherapeutics,* 11**,** 732-737.

Guerreiro, R., Wojtas, A., Bras, J., Carrasquillo, M., Rogaeva, E., Majounie, E., Cruchaga, C., Sassi, C., Kauwe, J. S. K., Younkin, S., Hazrati, L., Collinge, J., Pocock, J., Lashley, T., Williams, J., Lambert, J.-C., Amouyel, P., Goate, A., Rademakers, R., Morgan, K., Powell, J., St. George-Hyslop, P., Singleton, A. & Hardy, J. 2012. TREM2 Variants in Alzheimer's Disease. *New England Journal of Medicine,* 368**,** 117-127.

Guo, Q., Fu, W., Sopher, B. L., Miller, M. W., Ware, C. B., Martin, G. M. & Mattson, M. P. 1999. Increased vulnerability of hippocampal neurons to excitotoxic necrosis in presenilin-1 mutant knock-in mice. *Nature Medicine,* 5**,** 101-106.

Gylys, K. H., Fein, J. A., Yang, F., Wiley, D. J., Miller, C. A. & Cole, G. M. 2004. Synaptic Changes in Alzheimer's Disease : Increased Amyloid-β and Gliosis in Surviving Terminals Is Accompanied by Decreased PSD-95 Fluorescence. *The American Journal of Pathology,* 165**,** 1809-1817.

Haass, C. & Selkoe, D. J. 2007. Soluble protein oligomers in neurodegeneration: lessons from the Alzheimer's amyloid [beta]-peptide. *Nature Reviews Molecular Cell Biology,* 8**,** 101-112.

Habib, L. K., Lee, M. T. C. & Yang, J. 2010. Inhibitors of Catalase-Amyloid Interactions Protect Cells from β-Amyloid-Induced Oxidative Stress and Toxicity. *Journal of Biological Chemistry,* 285**,** 38933-38943.

Hailer, N. P., Järhult, J. D. & Nitsch, R. 1996. Resting microglial cells in vitro: Analysis of morphology and adhesion molecule expression in organotypic hippocampal slice cultures. *Glia,* 18**,** 319-331.

Hampel, H., Blennow, K., Shaw, L. M., Hoessler, Y. C., Zetterberg, H. & Trojanowski, J. Q. 2010. Total and Phosphorylated Tau Protein as Biological Markers of Alzheimer's Disease. *Experimental gerontology,* 45**,** 30.

Hanger, D. P., Anderton, B. H. & Noble, W. 2009. Tau phosphorylation: the therapeutic challenge for neurodegenerative disease. *Trends in Molecular Medicine,* 15**,** 112-119.

Hanger, D. P., Byers, H. L., Wray, S., Leung, K.-Y., Saxton, M. J., Seereeram, A., Reynolds, C. H., Ward, M. A. & Anderton, B. H. 2007. Novel Phosphorylation Sites in Tau from Alzheimer Brain Support a Role for Casein Kinase 1 in Disease Pathogenesis. *Journal of Biological Chemistry,* 282**,** 23645-23654.

Hanger, D. P., Hughes, K., Woodgett, J. R., Brion, J.-P. & Anderton, B. H. 1992. Glycogen synthase kinase-3 induces Alzheimer's disease-like phosphorylation of tau: Generation of paired helical filament epitopes and neuronal localisation of the kinase. *Neuroscience Letters,* 147**,** 58-62.

Hanger, Diane p. & Wray, S. 2010. Tau cleavage and tau aggregation in neurodegenerative disease. *Biochemical Society Transactions,* 38**,** 1016-1020.

Hardy, J. 2009. The amyloid hypothesis for Alzheimer's disease: a critical reappraisal. *Journal of Neurochemistry,* 110**,** 1129-1134.

Hardy, J. & Selkoe, D. J. 2002. The Amyloid Hypothesis of Alzheimer's Disease: Progress and Problems on the Road to Therapeutics. *Science,* 297**,** 353-356.

Hardy, J. A. & Higgins, G. A. 1992. Alzheimer's disease: the amyloid cascade hypothesis. *Science,* 256**,** 184-185.

Harris, J. A., Koyama, A., Maeda, S., Ho, K., Devidze, N., Dubal, D. B., Yu, G.-Q., Masliah, E. & Mucke, L. 2012. Human P301L-Mutant Tau Expression in Mouse Entorhinal-Hippocampal Network Causes Tau Aggregation and Presynaptic Pathology but No Cognitive Deficits. *PLoS ONE,* 7**,** e45881.

Hedberg, M. M., Clos, M. V., Ratia, M., Gonzalez, D., Unger Lithner, C., Camps, P., Muñoz-Torrero, D., Badia, A., Giménez-Llort, L. & Nordberg, A. 2010. Effect of Huprine X on β-Amyloid, Synaptophysin and α7 Neuronal Nicotinic Acetylcholine Receptors in the Brain of 3xTg-AD and APPswe Transgenic Mice. *Neurodegenerative Diseases,* 7**,** 379-388.

Henkins, K. M., Sokolow, S., Miller, C. A., Vinters, H. V., Poon, W., Cornwell, L. B., Saing, T. & Gylys, K. H. 2012. Extensive p-tau pathology and SDS-stable p-tau oligomers in Alzheimer's cortical synapses. *Brain pathology,* 22**,** 826-833.

Hernández, F. & Avila, J. 2008. The role of glycogen synthase kinase 3 in the early stages of Alzheimers' disease. *FEBS Letters,* 582**,** 3848-3854.

Himmler, A. 1989. Structure of the bovine tau gene: alternatively spliced transcripts generate a protein family. *Molecular and Cellular Biology,* 9**,** 1389-1396.

Himmler, A., Drechsel, D., Kirschner, M. W. & Martin, D. W. 1989. Tau consists of a set of proteins with repeated C-terminal microtubule-binding domains and variable N-terminal domains. *Molecular and Cellular Biology,* 9**,** 1381-1388.

Hoe, H.-S., Lee, H.-K. & Pak, D. T. S. 2012. The Upside of APP at Synapses. *CNS Neuroscience & Therapeutics,* 18**,** 47-56.

Holcomb, L., Gordon, M. N., Mcgowan, E., Yu, X., Benkovic, S., Jantzen, P., Wright, K., Saad, I., Mueller, R., Morgan, D., Sanders, S., Zehr, C., O'campo, K., Hardy, J., Prada, C.-M., Eckman, C., Younkin, S., Hsiao, K. & Duff, K. 1998. Accelerated Alzheimer-type phenotype in transgenic mice carrying both mutant amyloid precursor protein and presenilin 1 transgenes. *Nature Medicine,* 4**,** 97-100.

Hoover, B. R., Reed, M. N., Su, J., Penrod, R. D., Kotilinek, L. A., Grant, M. K., Pitstick, R., Carlson, G. A., Lanier, L. M., Yuan, L.-L., Ashe, K. H. & Liao, D. 2010. Tau Mislocalization to Dendritic Spines Mediates Synaptic Dysfunction Independently of Neurodegeneration. *Neuron,* 68**,** 1067-1081.

Horowitz, P. M., Patterson, K. R., Guillozet-Bongaarts, A. L., Reynolds, M. R., Carroll, C. A., Weintraub, S. T., Bennett, D. A., Cryns, V. L., Berry, R. W. & Binder, L. I. 2004. Early N-terminal changes and caspase-6 cleavage of tau in Alzheimer's disease. *The Journal of Neuroscience,* 24**,** 7895-902.

Hossini, A., Megges, M., Prigione, A., Lichtner, B., Toliat, M., Wruck, W., Schroter, F., Nuernberg, P., Kroll, H., Makrantonaki, E., Zoubouliss, C. & Adjaye, J. 2015. Induced pluripotent stem cell-derived neuronal cells from a sporadic Alzheimer's disease donor as a model for investigating AD-associated gene regulatory networks. *BMC Genomics,* 16**,** 84.

Hsiao, K., Chapman, P., Nilsen, S., Eckman, C., Harigaya, Y., Younkin, S., Yang, F. & Cole, G. 1996. Correlative memory deficits, Abeta elevation, and amyloid plaques in transgenic mice. *Science,* 274**,** 99-102.

Hsieh, H., Boehm, J., Sato, C., Iwatsubo, T., Tomita, T., Sisodia, S. & Malinow, R. 2006. AMPA-R Removal Underlies Aβ-induced Synaptic Depression and Dendritic Spine Loss. *Neuron,* 52**,** 831-843.

Hu, J., Akama, K. T., Krafft, G. A., Chromy, B. A. & Van Eldik, L. J. 1998. Amyloid-β peptide activates cultured astrocytes: morphological alterations, cytokine induction and nitric oxide release. *Brain Research,* 785**,** 195-206.

Hubbert, C., Guardiola, A., Shao, R., Kawaguchi, Y., Ito, A., Nixon, A., Yoshida, M., Wang, X.-F. & Yao, T.-P. 2002. HDAC6 is a microtubule-associated deacetylase. *Nature,* 417**,** 455-458.

Humpel, C. 2015a. Organotypic brain slice cultures: A review. *Neuroscience,* 305**,** 86-98.

Humpel, C. 2015b. Organotypic vibrosections from whole brain adult Alzheimer mice (overexpressing amyloid-precursor-protein with the Swedish-Dutch-Iowa mutations) as a model to study clearance of beta-amyloid plaques. *Frontiers in Aging Neuroscience,* 7.

Humpel, C. & Weis, C. 2002. Nerve growth factor and cholinergic CNS neurons studied in organotypic brain slices: Implication in Alzheimer's disease? *Journal of Neural Transmission, Supplement***,** 253-263.

Hutton, M., Lendon, C. L., Rizzu, P., Baker, M., Froelich, S., Houlden, H., Pickering-Brown, S., Chakraverty, S., Isaacs, A., Grover, A., Hackett, J., Adamson, J., Lincoln, S., Dickson, D., Davies, P., Petersen, R. C., Stevens, M., De Graaff, E., Wauters, E., Van Baren, J., Hillebrand, M., Joosse, M., Kwon, J. M., Nowotny, P., Che, L. K., Norton, J., Morris, J. C., Reed, L. A., Trojanowski, J., Basun, H., Lannfelt, L., Neystat, M., Fahn, S., Dark, F., Tannenberg, T., Dodd, P. R., Hayward, N., Kwok, J. B. J., Schofield, P. R., Andreadis, A., Snowden, J., Craufurd, D., Neary, D., Owen, F., Oostra, B. A., Hardy, J., Goate, A., Van Swieten, J., Mann, D., Lynch, T. & Heutink, P. 1998. Association of missense and 5'-splice-site mutations in tau with the inherited dementia FTDP-17. *Nature,* 393**,** 702-705.

Hyman, B. T. 2011. Amyloid-dependent and amyloid-independent stages of alzheimer disease. *Archives of Neurology,* 68**,** 1062-1064.

Iba, M., Guo, J. L., Mcbride, J. D., Zhang, B., Trojanowski, J. Q. & Lee, V. M. Y. 2013. Synthetic Tau Fibrils Mediate Transmission of Neurofibrillary Tangles in a Transgenic Mouse Model of Alzheimer's-like Tauopathy. *The Journal of Neuroscience,* 33**,** 1024-1037.

Inbar, P., Li, C. Q., Takayama, S. A., Bautista, M. R. & Yang, J. 2006. Oligo(ethylene glycol) Derivatives of Thioflavin T as Inhibitors of Protein–Amyloid Interactions. *ChemBioChem,* 7**,** 1563-1566.

Iovino, M., Patani, R., Watts, C., Chandran, S. & Spillantini, M. G. 2010. Human Stem Cell-Derived Neurons: A System to Study Human Tau Function and Dysfunction. *PLoS ONE,* 5**,** e13947.

Iqbal, K., Del C. Alonso, A., Chen, S., Chohan, M. O., El-Akkad, E., Gong, C.-X., Khatoon, S., Li, B., Liu, F., Rahman, A., Tanimukai, H. & Grundke-Iqbal, I. 2005. Tau pathology in Alzheimer disease and other tauopathies. *Biochimica et Biophysica Acta (BBA) - Molecular Basis of Disease,* 1739**,** 198-210.

Israel, M. A., Yuan, S. H., Bardy, C., Reyna, S. M., Mu, Y., Herrera, C., Hefferan, M. P., Van Gorp, S., Nazor, K. L., Boscolo, F. S., Carson, C. T., Laurent, L. C., Marsala, M., Gage, F. H., Remes, A. M., Koo, E. H. & Goldstein, L. S. B. 2012. Probing sporadic and familial Alzheimer's disease using induced pluripotent stem cells. *Nature,* 482**,** 216-220.

Ittner, L. M., Ke, Y. D., Delerue, F., Bi, M., Gladbach, A., Van Eersel, J., Wölfing, H., Chieng, B. C., Christie, M. J., Napier, I. A., Eckert, A., Staufenbiel, M., Hardeman, E. & Götz, J. 2010. Dendritic Function of Tau Mediates Amyloid-β Toxicity in Alzheimer's Disease Mouse Models. *Cell,* 142**,** 387-397.

Jicha, G. A., Bowser, R., Kazam, I. G. & Davies, P. 1997. Alz-50 and MC-1, a new monoclonal antibody raised to paired helical filaments, recognize conformational epitopes on recombinant tau. *Journal of Neuroscience Research,* 48**,** 128-132.

Johnson, G. V. W., Jope, R. S. & Binder, L. I. 1989. Proteolysis of tau by calpain. *Biochemical and Biophysical Research Communications,* 163**,** 1505-1511.

Jonsson, T., Atwal, J. K., Steinberg, S., Snaedal, J., Jonsson, P. V., Bjornsson, S., Stefansson, H., Sulem, P., Gudbjartsson, D., Maloney, J., Hoyte, K., Gustafson, A., Liu, Y., Lu, Y., Bhangale, T., Graham, R. R., Huttenlocher, J., Bjornsdottir, G., Andreassen, O. A., Jonsson, E. G., Palotie, A., Behrens, T. W., Magnusson, O. T., Kong, A., Thorsteinsdottir, U., Watts, R. J. & Stefansson, K. 2012. A mutation in APP protects against Alzheimer/'s disease and age-related cognitive decline. *Nature,* 488**,** 96-99.

Jucker, M. 2010. The benefits and limitations of animal models for translational research in neurodegenerative diseases. *Nature Medicine,* 16**,** 1210-1214.

Kanmert, D., Cantlon, A., Muratore, C. R., Jin, M., O'malley, T. T., Lee, G., Young-Pearse, T. L., Selkoe, D. J. & Walsh, D. M. 2015. C-Terminally Truncated Forms of Tau, But Not Full-Length Tau or Its C-Terminal Fragments, Are Released from Neurons Independently of Cell Death. *The Journal of Neuroscience,* 35**,** 10851-10865.

Karch, C. M., Jeng, A. T. & Goate, A. M. 2012. Extracellular Tau Levels Are Influenced by Variability in Tau That Is Associated with Tauopathies. *The Journal of Biological Chemistry,* 287**,** 42751-42762.

Kay, K. R., Smith, C., Wright, A. K., Serrano-Pozo, A., Pooler, A. M., Koffie, R., Bastin, M. E., Bak, T. H., Abrahams, S., Kopeikina, K. J., Mcguone, D., Frosch, M. P., Gillingwater, T. H., Hyman, B. T. & Spires-Jones, T. L. 2013. Studying synapses in human brain with array tomography and electron microscopy. *Nature protocols,* 8**,** 1366-1380.

Kazim, S. F., Blanchard, J., Dai, C.-L., Tung, Y.-C., Laferla, F. M., Iqbal, I.-G. & Iqbal, K. 2014. Disease modifying effect of chronic oral treatment with a neurotrophic peptidergic compound in a triple transgenic mouse model of Alzheimer's disease. *Neurobiology of Disease,* 71**,** 110-130.

Kelleher, I., Garwood, C., Hanger, D. P., Anderton, B. H. & Noble, W. 2007. Kinase activities increase during the development of tauopathy in htau mice. *Journal of Neurochemistry,* 103**,** 2256-2267.

Khatoon, S., Grundke-Iqbal, I. & Iqbal, K. 1994. Levels of normal and abnormally phosphorylated tau in different cellular and regional compartments of Alzheimer disease and control brains. *FEBS Letters,* 351**,** 80-84.

Kimura, T., Ishiguro, K. & Hisanaga, S.-I. 2014. Physiological and pathological phosphorylation of tau by Cdk5. *Frontiers in Molecular Neuroscience,* 7.

Klein, A. M., Kowall, N. W. & Ferrante, R. J. 1999. Neurotoxicity and Oxidative Damage of Beta Amyloid 1–42 versus Beta Amyloid 1–40 in the Mouse Cerebral Cortex. *Annals of the New York Academy of Sciences,* 893**,** 314-320.

Koffie, R. M., Hyman, B. T. & Spires-Jones, T. L. 2011. Alzheimer's disease: synapses gone cold. *Molecular Neurodegeneration,* 6**,** 63-63.

Koffie, R. M., Meyer-Luehmann, M., Hashimoto, T., Adams, K. W., Mielke, M. L., Garcia-Alloza, M., Micheva, K. D., Smith, S. J., Kim, M. L., Lee, V. M., Hyman, B. T. & Spires-Jones, T. L. 2009. Oligomeric amyloid β associates with postsynaptic densities and correlates with excitatory synapse loss near senile plaques. *Proceedings of the National Academy of Sciences of the United States of America,* 106**,** 4012-4017.

Koo, E. H., Sisodia, S. S., Archer, D. R., Martin, L. J., Weidemann, A., Beyreuther, K., Fischer, P., Masters, C. L. & Price, D. L. 1990. Precursor of amyloid protein in Alzheimer disease undergoes fast anterograde axonal transport. *Proceedings of the National Academy of Sciences of the United States of America,* 87**,** 1561-1565.

Kopeikina, K. J., Carlson, G. A., Pitstick, R., Ludvigson, A. E., Peters, A., Luebke, J. I., Koffie, R. M., Frosch, M. P., Hyman, B. T. & Spires-Jones, T. L. 2011. Tau Accumulation Causes Mitochondrial Distribution Deficits in Neurons in a Mouse Model of Tauopathy and in Human Alzheimer's Disease Brain. *The American Journal of Pathology,* 179**,** 2071-2082.

Kopeikina, K. J., Polydoro, M., Tai, H.-C., Yaeger, E., Carlson, G. A., Pitstick, R., Hyman, B. T. & Spires-Jones, T. L. 2013. Synaptic alterations in the rTg4510 mouse model of tauopathy. *Journal of Comparative Neurology,* 521**,** 1334-1353.

Kopke, E., Tung, Y. C., Shaikh, S., Alonso, A. C., Iqbal, K. & Grundke-Iqbal, I. 1993. Microtubule-associated protein tau. Abnormal phosphorylation of a non-paired helical filament pool in Alzheimer disease. *The Journal of Biological Chemistry,* 268**,** 24374-84.

Krüger, U., Wang, Y., Kumar, S. & Mandelkow, E.-M. 2012. Autophagic degradation of tau in primary neurons and its enhancement by trehalose. *Neurobiology of Aging,* 33**,** 2291-2305.

Kuchibhotla, K. V., Goldman, S. T., Lattarulo, C. R., Wu, H.-Y., Hyman, B. T. & Bacskai, B. J. 2008. Aβ Plaques Lead to Aberrant Regulation of Calcium Homeostasis In Vivo Resulting in Structural and Functional Disruption of Neuronal Networks. *Neuron,* 59**,** 214-225.

Kuninaka, N., Kawaguchi, M., Ogawa, M., Sato, A., Arima, K., Murayama, S. & Saito, Y. 2015. Simplification of the modified Gallyas method. *Neuropathology,* 35**,** 10-15.

Kusakawa, G., Saito, T., Onuki, R., Ishiguro, K., Kishimoto, T. & Hisanaga, S. 2000. Calpain-dependent proteolytic cleavage of the p35 cyclin-dependent kinase 5 activator to p25. *The Journal of Biological Chemistry,* 275**,** 17166-72.

Lacor, P. N., Buniel, M. C., Furlow, P. W., Sanz Clemente, A., Velasco, P. T., Wood, M., Viola, K. L. & Klein, W. L. 2007. Aβ Oligomer-Induced Aberrations in Synapse Composition, Shape, and Density Provide a Molecular Basis for Loss of Connectivity in Alzheimer's Disease. *The Journal of Neuroscience,* 27**,** 796-807.

Laferla, F. M. & Green, K. N. 2012. Animal Models of Alzheimer Disease. *Cold Spring Harbor Perspectives in Medicine,* 2.

Laferla, F. M., Green, K. N. & Oddo, S. 2007. Intracellular amyloid-[beta] in Alzheimer's disease. *Nature Reviews Neuroscience,* 8**,** 499-509.

Lambert, J.-C., Ibrahim-Verbaas, C. A., Harold, D., Naj, A. C., Sims, R., Bellenguez, C., Jun, G., Destefano, A. L., Bis, J. C., Beecham, G. W., Grenier-Boley, B., Russo, G., Thornton-Wells, T. A., Jones, N., Smith, A. V., Chouraki, V., Thomas, C., Ikram, M. A., Zelenika, D., Vardarajan, B. N., Kamatani, Y., Lin, C.-F., Gerrish, A., Schmidt, H., Kunkle, B., Dunstan, M. L., Ruiz, A., Bihoreau, M.-T., Choi, S.-H., Reitz, C., Pasquier, F., Hollingworth, P., Ramirez, A., Hanon, O., Fitzpatrick, A. L., Buxbaum, J. D., Campion, D., Crane, P. K., Baldwin, C., Becker, T., Gudnason, V., Cruchaga, C., Craig, D., Amin, N., Berr, C., Lopez, O. L., De Jager, P. L., Deramecourt, V., Johnston, J. A., Evans, D., Lovestone, S., Letenneur, L., Morón, F. J., Rubinsztein, D. C., Eiriksdottir, G., Sleegers, K., Goate, A. M., Fiévet, N., Huentelman, M. J., Gill, M., Brown, K., Kamboh, M. I., Keller, L., Barberger-Gateau, P., Mcguinness, B., Larson, E. B., Green, R., Myers, A. J., Dufouil, C., Todd, S., Wallon, D., Love, S., Rogaeva, E., Gallacher, J., St George-Hyslop, P., Clarimon, J., Lleo, A., Bayer, A., Tsuang, D. W., Yu, L., Tsolaki, M., Bossù, P., Spalletta, G., Proitsi, P., Collinge, J., Sorbi, S., Sanchez-Garcia, F., Fox, N. C., Hardy, J., Deniz Naranjo, M. C., Bosco, P., Clarke, R., Brayne, C., Galimberti, D., Mancuso, M., Matthews, F., European Alzheimer's Disease, I., Genetic, Environmental Risk in Alzheimer's, D., Alzheimer's Disease Genetic, C., et al.

2013. Meta-analysis of 74,046 individuals identifies 11 new susceptibility loci for Alzheimer's disease. *Nature genetics,* 45**,** 1452-1458.

Lasagna-Reeves, C. A., Castillo-Carranza, D. L., Sengupta, U., Guerrero-Munoz, M. J., Kiritoshi, T., Neugebauer, V., Jackson, G. R. & Kayed, R. 2012. Alzheimer brain-derived tau oligomers propagate pathology from endogenous tau. *Scientific Reports,* 2**,** 700.

Lee, C. H. & Ruben, P. C. 2008. Interaction between voltage-gated sodium channels and the neurotoxin, tetrodotoxin. *Channels,* 2**,** 407-412.

Lee, G., Newman, S. T., Gard, D. L., Band, H. & Panchamoorthy, G. 1998. Tau interacts with src-family non-receptor tyrosine kinases. *Journal of Cell Science,* 111**,** 3167-3177.

Lee, J., Retamal, C., Cuitiã±O, L., Caruano-Yzermans, A., Shin, J.-E., Van Kerkhof, P., Marzolo, M.-P. & Bu, G. 2008. Adaptor Protein Sorting Nexin 17 Regulates Amyloid Precursor Protein Trafficking and Processing in the Early Endosomes. *The Journal of Biological Chemistry,* 283**,** 11501-11508.

Lee, K. J., Moussa, C. E. H., Lee, Y., Sung, Y., Howell, B. W., Turner, R. S., Pak, D. T. S. & Hoe, H.-S. 2010. Beta amyloid-independent role of amyloid precursor protein in generation and maintenance of dendritic spines. *Neuroscience,* 169**,** 344-356.

Lee, M.-S., Kao, S.-C., Lemere, C. A., Xia, W., Tseng, H.-C., Zhou, Y., Neve, R., Ahlijanian, M. K. & Tsai, L.-H. 2003. APP processing is regulated by cytoplasmic phosphorylation. *The Journal of Cell Biology,* 163**,** 83-95.

Lee, M.-S., Kwon, Y. T., Li, M., Peng, J., Friedlander, R. M. & Tsai, L.-H. 2000. Neurotoxicity induces cleavage of p35 to p25 by calpain. *Nature,* 405**,** 360-364.

Lee, S. & Shea, T. B. 2012. Caspase-mediated truncation of tau potentiates aggregation. *International Journal of Alzheimers Disease,* 2012**,** 731063.

Lenox, R. H. & Wang, L. 2003. Molecular basis of lithium action: integration of lithium-responsive signaling and gene expression networks. *Molecular Psychiatry,* 8**,** 135-144.

Leroy, K., Yilmaz, Z. & Brion, J. P. 2007. Increased level of active GSK-3β in Alzheimer's disease and accumulation in argyrophilic grains and in neurones at different stages of neurofibrillary degeneration. *Neuropathology and Applied Neurobiology,* 33**,** 43-55.

Levy-Lahad, E., Wasco, W., Poorkaj, P., Romano, D. M., Oshima, J., Pettingell, W. H., Yu, C. E., Jondro, P. D., Schmidt, S. D., Wang, K. & Al, E. 1995. Candidate gene for the chromosome 1 familial Alzheimer's disease locus. *Science,* 269**,** 973-977.

Lew, J., Huang, Q. Q., Qi, Z., Winkfein, R. J., Aebersold, R., Hunt, T. & Wang, J. H. 1994. A brain-specific activator of cyclin-dependent kinase 5. *Nature,* 371**,** 423-6.

Lewis, J., Dickson, D. W., Lin, W.-L., Chisholm, L., Corral, A., Jones, G., Yen, S.-H., Sahara, N., Skipper, L., Yager, D., Eckman, C., Hardy, J., Hutton, M. & Mcgowan, E. 2001. Enhanced Neurofibrillary Degeneration in Transgenic Mice Expressing Mutant Tau and APP. *Science,* 293**,** 1487-1491.

Lewis, J., Mcgowan, E., Rockwood, J., Melrose, H., Nacharaju, P., Van Slegtenhorst, M., Gwinn-Hardy, K., Murphy, M. P., Baker, M., Yu, X., Duff, K., Hardy, J., Corral, A., Lin, W.-L., Yen, S.-H., Dickson, D. W., Davies, P. & Hutton, M. 2000. Neurofibrillary tangles, amyotrophy and progressive motor disturbance in mice expressing mutant (P301L) tau protein. *Nature Genetics,* 25**,** 402-405.

Lin, H., Lin, T. Y. & Juang, J. L. 2006. Abl deregulates Cdk5 kinase activity and subcellular localization in Drosophila neurodegeneration. *Cell Death and Differentiation,* 14**,** 607-615.

Liu, C.-W. A., Lee, G. & Jay, D. G. 1999. Tau is required for neurite outgrowth and growth cone motility of chick sensory neurons. *Cell motility and the cytoskeleton,* 43**,** 232-242.

Liu, L., Drouet, V., Wu, J. W., Witter, M. P., Small, S. A., Clelland, C. & Duff, K. 2012. Trans-synaptic spread of tau pathology in vivo. *PLoS ONE,* 7**,** e31302.

Lombino, F., Biundo, F., Tamayev, R., Arancio, O. & D'adamio, L. 2013. An Intracellular Threonine of Amyloid-β Precursor Protein Mediates Synaptic Plasticity Deficits and Memory Loss. *PLoS ONE,* 8**,** e57120.

Lopresti, P., Szuchet, S., Papasozomenos, S. C., Zinkowski, R. P. & Binder, L. I. 1995. Functional implications for the microtubule-associated protein tau: Localization in oligodendrocytes. *Proceedings of the National Academy of Sciences of the United States of America,* 92**,** 10369-10373.

Lovestone, S., Hartley, C. L., Pearce, J. & Anderton, B. H. 1996. Phosphorylation of tau by glycogen synthase kinase-3β in intact mammalian cells: The effects on the organization and stability of microtubules. *Neuroscience,* 73**,** 1145-1157.

Lucas, J. J., Hernández, F., Gómez-Ramos, P., Morán, M. A., Hen, R. & Avila, J. 2001. Decreased nuclear β-catenin, tau hyperphosphorylation and neurodegeneration in GSK-3β conditional transgenic mice. *The EMBO Journal,* 20**,** 27-39.

Lund, E. T., Mckenna, R., Evans, D. B., Sharma, S. K. & Mathews, W. R. 2001. Characterization of the in vitro phosphorylation of human tau by tau protein kinase II (cdk5/p20) using mass spectrometry. *Journal of Neurochemistry,* 76**,** 1221-1232.

Macdonald, B. T., Tamai, K. & He, X. 2009. Wnt/β-catenin signaling: components, mechanisms, and diseases. *Developmental cell,* 17**,** 9-26.

Maezawa, I., Zimin, P. I., Wulff, H. & Jin, L.-W. 2011. Amyloid-β Protein Oligomer at Low Nanomolar Concentrations Activates Microglia and Induces Microglial Neurotoxicity. *Journal of Biological Chemistry,* 286**,** 3693-3706.

Magdesian, M. H., Carvalho, M. M. V. F., Mendes, F. A., Saraiva, L. M., Juliano, M. A., Juliano, L., Garcia-Abreu, J. & Ferreira, S. T. 2008. Amyloid-β binds to the extracellular cysteine-rich domain of frizzled and inhibits Wnt/β-catenin signaling. *Journal of Biological Chemistry,* 283**,** 9359-9368.

Mairet-Coello, G., Courchet, J., Pieraut, S., Courchet, V., Maximov, A. & Polleux, F. 2013. The CAMKK2-AMPK Kinase Pathway Mediates the Synaptotoxic Effects of Aβ Oligomers through Tau Phosphorylation. *Neuron,* 78**,** 94-108.

Manaye, K., Mouton, P., Xu, G., Drew, A., Lei, D.-L., Sharma, Y., Rebeck, G. W. & Turner, S. 2013. Age-related loss of noradrenergic neurons in the brains of triple transgenic mice. *AGE,* 35**,** 139-147.

Mandelkow, E. M., Stamer, K., Vogel, R., Thies, E. & Mandelkow, E. 2003. Clogging of axons by tau, inhibition of axonal traffic and starvation of synapses. *Neurobiology of Aging,* 24**,** 1079-85.

Mandell, J. W. & Banker, G. A. 1995. The microtubule cytoskeleton and the development of neuronal polarity. *Neurobiology of Aging,* 16**,** 229-237.

Mark, R. J., Hensley, K., Butterfield, D. A. & Mattson, M. P. 1995. Amyloid β-peptide impairs ion-motive ATPase activities: Evidence for a role in loss of neuronal Ca2+ homeostasis and cell death. *Journal of Neuroscience,* 15**,** 6239-6249.

Martin, L., Magnaudeix, A., Esclaire, F., Yardin, C. & Terro, F. 2009. Inhibition of glycogen synthase kinase-3β downregulates total tau proteins in cultured neurons and its reversal by the blockade of protein phosphatase-2A. *Brain Research,* 1252**,** 66-75.

Masliah, E., Mallory, M., Alford, M., Deteresa, R., Hansen, L. A., Mckeel, D. W. & Morris, J. C. 2001. Altered expression of synaptic proteins occurs early during progression of Alzheimer's disease. *Neurology,* 56**,** 127-129.

Mastrangelo, M. & Bowers, W. 2008. Detailed immunohistochemical characterization of temporal and spatial progression of Alzheimer's disease-related pathologies in male triple-transgenic mice. *BMC Neuroscience,* 9**,** 81.

Matsuoka, Y., Gray, A., Hirata-Fukae, C., Minami, S. S., Waterhouse, E., Mattson, M., Laferla, F., Gozes, I. & Aisen, P. 2007. Intranasal NAP administration reduces accumulation of amyloid peptide and tau hyperphosphorylation in a transgenic mouse model of Alzheimer's disease at early pathological stage. *Journal of Molecular Neuroscience,* 31**,** 165-170.

Matsuoka, Y., Jouroukhin, Y., Gray, A. J., Ma, L., Hirata-Fukae, C., Li, H.-F., Feng, L., Lecanu, L., Walker, B. R., Planel, E., Arancio, O., Gozes, I. & Aisen, P. S. 2008. A Neuronal Microtubule-Interacting Agent, NAPVSIPQ, Reduces Tau Pathology and Enhances Cognitive Function in a Mouse Model of Alzheimer's Disease. *Journal of Pharmacology and Experimental Therapeutics,* 325**,** 146-153.

Mattson, M. P., Partin, J. & Begley, J. G. 1998. Amyloid β-peptide induces apoptosis-related events in synapses and dendrites. *Brain Research,* 807**,** 167-176.

Mattson, M. P., Tomaselli, K. J. & Rydel, R. E. 1993. Calcium-destabilizing and neurodegenerative effects of aggregated β-amyloid peptide are attenuated by basic FGF. *Brain Research,* 621**,** 35-49.

Mcallister, A. K. 2004. Biolistic Transfection of Cultured Organotypic Brain Slices. *Methods in Molecular Biology,* 245**,** 197-206.

Meda, L., Cassatella, M. A., Szendrei, G. I., Otvos, L., Baron, P., Villalba, M., Ferrari, D. & Rossi, F. 1995. Activation of microglial cells by [beta]-amyloid protein and interferon-[gamma]. *Nature,* 374**,** 647-650.

Megill, A., Lee, T., Dibattista, A. M., Song, J. M., Spitzer, M. H., Rubinshtein, M., Habib, L. K., Capule, C. C., Mayer, M., Turner, R. S., Kirkwood, A., Yang, J., Pak, D. T. S., Lee, H.-K. & Hoe, H.-S. 2013. A Tetra(Ethylene Glycol) Derivative of Benzothiazole Aniline Enhances Ras-Mediated Spinogenesis. *The Journal of Neuroscience,* 33**,** 9306-9318.

Meraz-Ríos, M. A., Lira-De León, K. I., Campos-Peña, V., De Anda-Hernández, M. A. & Mena-López, R. 2010. Tau oligomers and aggregation in Alzheimer's disease. *Journal of Neurochemistry,* 112**,** 1353-1367.

Meredith Jr, J. E., Sankaranarayanan, S., Guss, V., Lanzetti, A. J., Berisha, F., Neely, R. J., Slemmon, J. R., Portelius, E., Zetterberg, H., Blennow, K., Soares, H., Ahlijanian, M. & Albright, C. F. 2013. Characterization of Novel CSF Tau and ptau Biomarkers for Alzheimer's Disease. *PLoS ONE,* 8**,** e76523.

Mewes, A., Franke, H. & Singer, D. 2012. Organotypic Brain Slice Cultures of Adult Transgenic P301S Mice - A Model for Tauopathy Studies. *PLoS ONE,* 7**,** e45017.

Micheva, K. D. & Smith, S. J. 2007. Array tomography: A new tool for imaging the molecular architecture and ultrastructure of neural circuits. *Neuron,* 55**,** 25-36.

Miller, E. C., Teravskis, P. J., Dummer, B. W., Zhao, X., Huganir, R. L. & Liao, D. 2014. Tau phosphorylation and tau mislocalization mediate soluble Aβ oligomer-induced AMPA glutamate receptor signaling deficits. *The European journal of neuroscience,* 39**,** 1214-1224.

Mitchison, T. & Kirschner, M. 1984. Dynamic instability of microtubule growth. *Nature,* 312**,** 237-242.

Mondragón-Rodríguez, S., Trillaud-Doppia, E., Dudilot, A., Bourgeois, C., Lauzon, M., Leclerc, N. & Boehm, J. 2012. Interaction of Endogenous Tau Protein with Synaptic Proteins Is Regulated by N-Methyl-d-aspartate Receptor-dependent Tau Phosphorylation. *The Journal of Biological Chemistry,* 287**,** 32040-32053.

Moreno, H., Choi, S., Yu, E., Brusco, J., Avila, J., Moreira, J. E., Sugimori, M. & Llinás, R. R. 2011. Blocking Effects of Human Tau on Squid Giant Synapse Transmission and Its Prevention by T-817 MA. *Frontiers in Synaptic Neuroscience,* 3**,** 3.

Morris, G., Clark, I. & Vissel, B. 2014. Inconsistencies and Controversies Surrounding the Amyloid Hypothesis of Alzheimer's Disease. *Acta Neuropathologica Communications,* 2**,** 135.

Motoi, Y., Shimada, K., Ishiguro, K. & Hattori, N. 2014. Lithium and Autophagy. *ACS Chemical Neuroscience,* 5**,** 434-442.

Mucke, L. & Selkoe, D. J. 2012. Neurotoxicity of Amyloid β-Protein: Synaptic and Network Dysfunction. *Cold Spring Harbor Perspectives in Medicine,* 2**,** a006338.

Muñoz-Montaño, J. R., Moreno, F. J., Avila, J. & Diaz-Nido, J. 1997. Lithium inhibits Alzheimer's disease-like tau protein phosphorylation in neurons. *FEBS Letters,* 411**,** 183-188.

Nieweg, K., Andreyeva, A., Van Stegen, B., Tanriöver, G. & Gottmann, K. 2015. Alzheimer's disease-related amyloid-β induces synaptotoxicity in human iPS cell-derived neurons. *Cell Death & Disease,* 6**,** e1709.

Nisbet, R. M., Polanco, J.-C., Ittner, L. M. & Götz, J. 2015. Tau aggregation and its interplay with amyloid-β. *Acta Neuropathologica,* 129**,** 207-220.

Noble, W., Hanger, D. P., Miller, C. C. J. & Lovestone, S. 2013. The Importance of Tau Phosphorylation for Neurodegenerative Diseases. *Frontiers in Neurology,* 4**,** 83.

Noble, W., Olm, V., Takata, K., Casey, E., Mary, O., Meyerson, J., Gaynor, K., Lafrancois, J., Wang, L., Kondo, T., Davies, P., Burns, M., Veeranna, Nixon, R., Dickson, D., Matsuoka, Y., Ahlijanian, M., Lau, L.-F. & Duff, K. 2003. Cdk5 Is a Key Factor in Tau Aggregation and Tangle Formation In Vivo. *Neuron,* 38**,** 555-565.

Noble, W., Planel, E., Zehr, C., Olm, V., Meyerson, J., Suleman, F., Gaynor, K., Wang, L., Lafrancois, J., Feinstein, B., Burns, M., Krishnamurthy, P., Wen, Y., Bhat, R., Lewis, J., Dickson, D. & Duff, K. 2005. Inhibition of glycogen synthase kinase-3 by lithium correlates with reduced tauopathy and degeneration in vivo. *Proceedings of the National Academy of Sciences of the United States of America,* 102**,** 6990-6995.

Nordstedt, C., Gandy, S. E., Alafuzoff, I., Caporaso, G. L., Iverfeldt, K., Grebb, J. A., Winblad, B. & Greengard, P. 1991. Alzheimer beta/A4 amyloid precursor protein in human brain: aging-associated increases in holoprotein and in a proteolytic fragment. *Proceedings of the National Academy of Sciences of the United States of America,* 88**,** 8910-8914.

O'brien, R. J. & Wong, P. C. 2011. Amyloid Precursor Protein Processing and Alzheimer's Disease. *Annual review of neuroscience,* 34**,** 185-204.

Oddo, S., Caccamo, A., Kitazawa, M., Tseng, B. P. & Laferla, F. M. 2003a. Amyloid deposition precedes tangle formation in a triple transgenic model of Alzheimer's disease. *Neurobiology of Aging,* 24**,** 1063-1070.

Oddo, S., Caccamo, A., Shepherd, J. D., Murphy, M. P., Golde, T. E., Kayed, R., Metherate, R., Mattson, M. P., Akbari, Y. & Laferla, F. M. 2003b. Triple-Transgenic Model of Alzheimer's Disease with Plaques and Tangles: Intracellular Aβ and Synaptic Dysfunction. *Neuron,* 39**,** 409-421.

Oddo, S., Caccamo, A., Tseng, B., Cheng, D., Vasilevko, V., Cribbs, D. H. & Laferla, F. M. 2008. Blocking Aβ42 Accumulation Delays the Onset and Progression of Tau Pathology via the C Terminus of Heat Shock Protein70-Interacting Protein: A Mechanistic Link between Aβ and Tau Pathology. *The Journal of Neuroscience,* 28**,** 12163-12175.

Oh, K.-J., Perez, S. E., Lagalwar, S., Vana, L., Binder, L. & Mufson, E. J. 2010. Staging of Alzheimer's Pathology in Triple Transgenic Mice: A Light and Electron Microscopic Analysis. *International Journal of Alzheimer's Disease,* 2010**,** 780102.

Olabarria, M., Noristani, H. N., Verkhratsky, A. & Rodríguez, J. J. 2010. Concomitant astroglial atrophy and astrogliosis in a triple transgenic animal model of Alzheimer's disease. *Glia,* 58**,** 831-838.

Opitz-Araya, X. & Barria, A. 2011. Organotypic Hippocampal Slice Cultures. *Journal of Visualized Experiments : JoVE***,** 2462.

Ovchinnikov, D. A. & Wolvetang, E. J. 2014. Opportunities and Limitations of Modelling Alzheimer's Disease with Induced Pluripotent Stem Cells. *Journal of Clinical Medicine,* 3**,** 1357-1372.

Palazzo, A., Ackerman, B. & Gundersen, G. G. 2003. Cell biology (Communication arising): Tubulin acetylation and cell motility. *Nature,* 421**,** 230-230.

Papasozomenos, S. C. & Binder, L. I. 1987. Phosphorylation determines two distinct species of Tau in the central nervous system. *Cell motility and the cytoskeleton,* 8**,** 210-226.

Patrick, G. N., Zukerberg, L., Nikolic, M., De La Monte, S., Dikkes, P. & Tsai, L. H. 1999. Conversion of p35 to p25 deregulates Cdk5 activity and promotes neurodegeneration. *Nature,* 402**,** 615-22.

Patzke, H. & Tsai, L. H. 2002. Calpain-mediated cleavage of the cyclin-dependent kinase-5 activator p39 to p29. *Journal of Biological Chemistry,* 277**,** 8054-60.

Peck, A., Sargin, M. E., Lapointe, N. E., Rose, K., Manjunath, B. S., Feinstein, S. C. & Wilson, L. 2011. Tau isoform-specific modulation of kinesin-driven microtubule gliding rates and trajectories as determined with tau-stabilized microtubules. *Cytoskeleton,* 68**,** 44-55.

Pei, J.-J., Tanaka, T., Tung, Y.-C., Braak, E., Iqbal, K. & Grundke-Iqbal, I. 1997. Distribution, Levels, and Activity of Glycogen Synthase Kinase-3 in the Alzheimer Disease Brain. *Journal of Neuropathology & Experimental Neurology,* 56**,** 70-78.

Perez-Nievas, B. G., Stein, T. D., Tai, H.-C., Dols-Icardo, O., Scotton, T. C., Barroeta-Espar, I., Fernandez-Carballo, L., De Munain, E. L., Perez, J., Marquie, M., Serrano-Pozo, A., Frosch, M. P., Lowe, V., Parisi, J. E., Petersen, R. C., Ikonomovic, M. D., López, O. L., Klunk, W., Hyman, B. T. & Gómez-Isla, T. 2013. Dissecting phenotypic traits linked to human resilience to Alzheimer's pathology. *Brain,* 136**,** 2510-2526.

Perl, D. P. 2010. Neuropathology of Alzheimer's Disease. *The Mount Sinai Journal of Medicine,* 77**,** 32-42.

Phiel, C. J., Wilson, C. A., Lee, V. M. Y. & Klein, P. S. 2003. GSK-3[alpha] regulates production of Alzheimer's disease amyloid-[beta] peptides. *Nature,* 423**,** 435-439.

Phillips, E. C., Croft, C. L., Kurbatskaya, K., O'neill, M. J., Hutton, M. L., Hanger, D. P., Garwood, C. J. & Noble, W. 2014. Astrocytes and neuroinflammation in Alzheimer's disease. *Biochemical Society Transactions,* 42**,** 1321-1325.

Plenz, D., Stewart, C. V., Shew, W., Yang, H., Klaus, A. & Bellay, T. 2011. Multi-electrode Array Recordings of Neuronal Avalanches in Organotypic Cultures. *Journal of Visualized Experiments***,** e2949.

Plouffe, V., Mohamed, N.-V., Rivest-Mcgraw, J., Bertrand, J., Lauzon, M. & Leclerc, N. 2012. Hyperphosphorylation and Cleavage at D421 Enhance Tau Secretion. *PLoS ONE,* 7**,** e36873.

Polydoro, M., Acker, C. M., Duff, K., Castillo, P. E. & Davies, P. 2009. Age-Dependent Impairment of Cognitive and Synaptic Function in the htau Mouse Model of Tau Pathology. *The Journal of Neuroscience,* 29**,** 10741-10749.

Pooler, A. M., Phillips, E. C., Lau, D. H. W., Noble, W. & Hanger, D. P. 2013. Physiological release of endogenous tau is stimulated by neuronal activity. *EMBO Reports,* 14**,** 389-394.

Pooler, A. M., Polydoro, M., Maury, E. A., Nicholls, S. B., Reddy, S. M., Wegmann, S., William, C., Saqran, L., Cagsal-Getkin, O., Pitstick, R., Beier, D. R., Carlson, G. A., Spires-Jones, T. L. & Hyman, B. T. 2015. Amyloid accelerates tau propagation and toxicity in a model of early Alzheimer's disease. *Acta Neuropathologica Communications,* 3**,** 14.

Pooler, A. M., Usardi, A., Evans, C. J., Philpott, K. L., Noble, W. & Hanger, D. P. 2012. Dynamic association of tau with neuronal membranes is regulated by phosphorylation. *Neurobiology of Aging,* 33**,** 431.e27-431.e38.

Prince, M., Knapp, M., Guerchet, M., Mccrone, P., Prina, M., Comas-Herrera, A., Wittenberg, R., Adelaja, B., Hu, B., King, D., Rehill, A. & Salimkumar, D. 2014. Dementia UK: Update Second Edition.

Pringle, A. K., Iannotti, F., Wilde, G. J. C., Chad, J. E., Seeley, P. J. & Sundstrom, L. E. 1997. Neuroprotection by both NMDA and non-NMDA receptor antagonists in in vitro ischemia. *Brain Research,* 755**,** 36-46.

Proctor, D. T., Coulson, E. J. & Dodd, P. R. 2010. Reduction in post-synaptic scaffolding PSD-95 and SAP-102 protein levels in the Alzheimer inferior temporal cortex is correlated with disease pathology. *Journal of Alzheimer's Disease,* 21**,** 795-811.

Prüβing, K., Voigt, A. & Schulz, J. 2013. Drosophila melanogaster as a model organism for Alzheimer's disease. *Molecular Neurodegeneration,* 8**,** 35.

Puzzo, D., Gulisano, W., Palmeri, A. & Arancio, O. 2015. Rodent models for Alzheimer's disease drug discovery. *Expert opinion on drug discovery,* 10**,** 703-711.

Quiroz, Y. T., Budson, A. E., Celone, K., Ruiz, A., Newmark, R., Castrillón, G., Lopera, F. & Stern, C. E. 2010. Hippocampal Hyperactivation in Presymptomatic Familial Alzheimer's Disease. *Annals of neurology,* 68**,** 865-875.

Quraishe, S., Cowan, C. M. & Mudher, A. 2013. NAP (davunetide) rescues neuronal dysfunction in a Drosophila model of tauopathy. *Molecular Psychiatry,* 18**,** 834-842.

Radde, R., Duma, C., Goedert, M. & Jucker, M. 2008. The value of incomplete mouse models of Alzheimer's disease. *European Journal of Nuclear Medicine and Molecular Imaging,* 35**,** 70-74.

Rajamohamedsait, H. B. & Sigurdsson, E. M. 2012. Histological Staining of Amyloid and Pre-Amyloid Peptides and Proteins in Mouse Tissue. *Methods in molecular biology (Clifton, N.J.),* 849**,** 10.1007/978-1-61779-551-0_28.

Rametti, A., Esclaire, F., Yardin, C., Cogné, N. & Terro, F. 2008. Lithium down-regulates tau in cultured cortical neurons: A possible mechanism of neuroprotection. *Neuroscience Letters,* 434**,** 93-98.

Rao, M. V., Mohan, P. S., Peterhoff, C. M., Yang, D. S., Schmidt, S. D., Stavrides, P. H., Campbell, J., Chen, Y., Jiang, Y., Paskevich, P. A., Cataldo, A. M., Haroutunian, V. & Nixon, R. A. 2008. Marked calpastatin (CAST) depletion in Alzheimer's disease accelerates cytoskeleton disruption and neurodegeneration: neuroprotection by CAST overexpression. *The Journal of Neuroscience,* 28**,** 12241-54.

Rapoport, M., Dawson, H. N., Binder, L. I., Vitek, M. P. & Ferreira, A. 2002. Tau is essential to β-amyloid-induced neurotoxicity. *Proceedings of the National Academy of Sciences of the United States of America,* 99**,** 6364-6369.

Reddy, P. H. 2011. Abnormal Tau, Mitochondrial Dysfunction, Impaired Axonal Transport of Mitochondria, and Synaptic Deprivation in Alzheimer's Disease. *Brain research,* 1415**,** 136-148.

Revilla, S., Suñol, C., García-Mesa, Y., Giménez-Llort, L., Sanfeliu, C. & Cristòfol, R. 2014. Physical exercise improves synaptic dysfunction and recovers the loss of survival factors in 3xTg-AD mouse brain. *Neuropharmacology,* 81**,** 55-63.

Rissman, R. A., Poon, W. W., Blurton-Jones, M., Oddo, S., Torp, R., Vitek, M. P., Laferla, F. M., Rohn, T. T. & Cotman, C. W. 2004. Caspase-cleavage of tau is an early event in Alzheimer disease tangle pathology. *Journal of Clinical Investigation,* 114**,** 121-130.

Rivest, S. 2015. TREM2 enables amyloid [beta] clearance by microglia. *Cell Research,* 25**,** 535-536.

Roberson, E. D., Halabisky, B., Yoo, J. W., Yao, J., Chin, J., Yan, F., Wu, T., Hamto, P., Devidze, N., Yu, G.-Q., Palop, J. J., Noebels, J. L. & Mucke, L. 2011. Amyloid-β/Fyn–Induced Synaptic, Network, and Cognitive Impairments Depend on Tau Levels in Multiple Mouse Models of Alzheimer's Disease. *The Journal of Neuroscience,* 31**,** 700-711.

Roberson, E. D., Scearce-Levie, K., Palop, J. J., Yan, F., Cheng, I. H., Wu, T., Gerstein, H., Yu, G.-Q. & Mucke, L. 2007. Reducing Endogenous Tau Ameliorates Amyloid ß-Induced Deficits in an Alzheimer's Disease Mouse Model. *Science,* 316**,** 750-754.

Rochefort, N. L. & Konnerth, A. 2012. Dendritic spines: from structure to in vivo function. *EMBO reports,* 13**,** 699-708.

Ryves, W. J. & Harwood, A. J. 2001. Lithium Inhibits Glycogen Synthase Kinase-3 by Competition for Magnesium. *Biochemical and Biophysical Research Communications,* 280**,** 720-725.

Saito, K., Elce, J. S., Hamos, J. E. & Nixon, R. A. 1993. Widespread activation of calcium-activated neutral proteinase (calpain) in the brain in Alzheimer disease: a potential molecular basis for neuronal degeneration. *Proceedings of the National Academy of Sciences of the United States of America,* 90**,** 2628-32.

Saman, S., Kim, W., Raya, M., Visnick, Y., Miro, S., Saman, S., Jackson, B., Mckee, A. C., Alvarez, V. E., Lee, N. C. Y. & Hall, G. F. 2012. Exosome-associated Tau Is Secreted in Tauopathy Models and Is Selectively Phosphorylated in Cerebrospinal Fluid in Early Alzheimer Disease. *The Journal of Biological Chemistry,* 287**,** 3842-3849.

Samson, F., Donoso, J. A., Heller-Bettinger, I., Watson, D. & Himes, R. H. 1979. Nocodazole action on tubulin assembly, axonal ultrastructure and fast axoplasmic transport. *Journal of Pharmacology and Experimental Therapeutics,* 208**,** 411-417.

Sanchez, J. F., Sniderhan, L. F., Williamson, A. L., Fan, S., Chakraborty-Sett, S. & Maggirwar, S. B. 2003. Glycogen Synthase Kinase 3β-Mediated Apoptosis of Primary Cortical Astrocytes Involves Inhibition of Nuclear Factor κB Signaling. *Molecular and Cellular Biology,* 23**,** 4649-4662.

Sanders, D. W., Kaufman, S. K., Devos, S. L., Sharma, A. M., Mirbaha, H., Li, A., Barker, S. J., Foley, A., Thorpe, J. R., Serpell, L. C., Miller, T. M., Grinberg, L. T., Seeley, W. W. & Diamond, M. I. 2014. Distinct tau prion strains propagate in cells and mice and define different tauopathies. *Neuron,* 82**,** 1271-1288.

Santacruz, K., Lewis, J., Spires, T., Paulson, J., Kotilinek, L., Ingelsson, M., Guimaraes, A., Deture, M., Ramsden, M., Mcgowan, E., Forster, C., Yue, M., Orne, J., Janus, C., Mariash, A., Kuskowski, M., Hyman, B., Hutton, M. & Ashe, K. H. 2005. Tau Suppression in a Neurodegenerative Mouse Model Improves Memory Function. *Science,* 309**,** 476-481.

Sastre, M., Richardson, J. C., Gentleman, S. M. & Brooks, D. J. 2011. Inflammatory risk factors and pathologies associated with Alzheimer's disease. *Current Alzheimer Research,* 8**,** 132-41.

Satizabal, C. L., Beiser, A. S., Chouraki, V., Chêne, G., Dufouil, C. & Seshadri, S. 2016. Incidence of Dementia over Three Decades in the Framingham Heart Study. *New England Journal of Medicine,* 374**,** 523-532.

Saul, A., Sprenger, F., Bayer, T. A. & Wirths, O. 2013. Accelerated tau pathology with synaptic and neuronal loss in a novel triple transgenic mouse model of Alzheimer's disease. *Neurobiology of Aging,* 34**,** 2564-2573.

Schaffer, C., Sarad, N., Decrumpe, A., Goswami, D., Herrmann, S., Morales, J., Patel, P. & Osborne, J. 2015. Biomarkers in the Diagnosis and Prognosis of Alzheimer's Disease. *Journal of Laboratory Automation,* 20**,** 589-600.

Scheff, S. W., Price, D. A., Schmitt, F. A., Dekosky, S. T. & Mufson, E. J. 2007. Synaptic alterations in CA1 in mild Alzheimer disease and mild cognitive impairment. *Neurology,* 68**,** 1501-1508.

Schmechel, D. E., Saunders, A. M., Strittmatter, W. J., Crain, B. J., Hulette, C. M., Joo, S. H., Pericak-Vance, M. A., Goldgaber, D. & Roses, A. D. 1993. Increased amyloid beta-peptide deposition in cerebral cortex as a consequence of apolipoprotein E genotype in late-onset Alzheimer disease. *Proceedings of the National Academy of Sciences,* 90**,** 9649-9653.

Schweers, O., Schönbrunn-Hanebeck, E., Marx, A. & Mandelkow, E. 1994. Structural studies of tau protein and Alzheimer paired helical filaments show no evidence for beta-structure. *Journal of Biological Chemistry,* 269**,** 24290-24297.

Selkoe, D. J. 2002. Alzheimer's Disease Is a Synaptic Failure. *Science,* 298**,** 789-791.

Sengupta, A., Kabat, J., Novak, M., Wu, Q., Grundke-Iqbal, I. & Iqbal, K. 1998. Phosphorylation of Tau at Both Thr 231 and Ser 262 Is Required for Maximal Inhibition of Its Binding to Microtubules. *Archives of Biochemistry and Biophysics,* 357**,** 299-309.

Seshadri S., Fitzpatrick A. L., Ikram M., Destefano A. L., Gudnason V., Boada M., Bis J. C., Smith A. V., Carassquillo M. M., Lambert J. C., Harold D., Schrijvers E. M., Ramirez-Lorca R., Debette S., Longstreth W. T. Jr, Janssens A. C., Pankratz V. S., Dartigues J. F., Hollingworth P., Aspelund T., Hernandez I., Beiser A., Kuller L. H., Koudstaal P. J., Dickson D. W., Tzourio C., Abraham R., Antunez C., Du Y., Rotter J. I., Aulchenko Y. S., Harris T. B., Petersen R. C., Berr C., Owen M. J., Lopez-Arrieta J., Varadarajan B. N., Becker J. T., Rivadeneira F., Nalls M. A., Graff-Radford N. R., Campion D., Auerbach S., Rice K., Hofman A., Jonsson P. V., Schmidt H., Lathrop M., Mosley T. H., Au R., Psaty B. M., Uitterlinden A. G., Farrer L. A., Lumley T., Ruiz A., Williams J., Amouyel P., Younkin S. G., Wolf P. A., Launer L. J., Lopez O. L., Van Duijn C. M., Breteler M. M., Charge Consortium, Gerad1 Consortium & Eadi1 Consortium 2010. Genome-wide analysis of genetic loci associated with alzheimer disease. *Journal of the American Medical Association,* 303**,** 1832-1840.

Shankar, G. M., Bloodgood, B. L., Townsend, M., Walsh, D. M., Selkoe, D. J. & Sabatini, B. L. 2007. Natural Oligomers of the Alzheimer Amyloid-β Protein Induce Reversible Synapse Loss by Modulating an NMDA-Type Glutamate Receptor-Dependent Signaling Pathway. *The Journal of Neuroscience,* 27**,** 2866-2875.

Shankar, G. M., Li, S., Mehta, T. H., Garcia-Munoz, A., Shepardson, N. E., Smith, I., Brett, F. M., Farrell, M. A., Rowan, M. J., Lemere, C. A., Regan, C. M., Walsh, D. M., Sabatini, B. L. & Selkoe, D. J. 2008. Amyloid β-Protein Dimers Isolated Directly from Alzheimer Brains Impair Synaptic Plasticity and Memory. *Nature Medicine,* 14**,** 837-842.

Shastry, P., Basu, A. & Rajadhyaksha, M. S. 2001. Neuroblastoma Cell Lines-A Versatile in Vitro Model in Neurobiology. *International Journal of Neuroscience,* 108**,** 109-126.

Sheng, M., Sabatini, B. L. & Südhof, T. C. 2012. Synapses and Alzheimer's Disease. *Cold Spring Harbor Perspectives in Biology,* 4**,** a005777.

Sherrington, R., Rogaev E. I., Liang Y., Rogaeva E. A., Levesque G., Ikeda M., Chi H., Lin C., Li G., Holman K., Tsuda T., Mar L., Foncin J. F., Bruni A. C., Montesi M. P., Sorbi S., Rainero I., Pinessi L., Nee L., Chumakov I., Pollen D., Brookes A., Sanseau P., Polinsky R. J., Wasco W., Da Silva H. A., Haines J. L., Perkicak-Vance M. A., Tanzi R. E., Roses A. D., Fraser P. E., Rommens J. M. & H., S. G.-H. P. 1995. Cloning of a gene bearing missense mutations in early-onset familial Alzheimer's disease. *Nature,* 375**,** 754-760.

Shimada, K., Motoi, Y., Ishiguro, K., Kambe, T., Matsumoto, S.-E., Itaya, M., Kunichika, M., Mori, H., Shinohara, A., Chiba, M., Mizuno, Y., Ueno, T. & Hattori, N. 2012. Long-term oral lithium treatment attenuates motor disturbance in tauopathy model mice: Implications of autophagy promotion. *Neurobiology of Disease,* 46**,** 101-108.

Shin, R.-W., Ogino, K., Shimabuku, A., Taki, T., Nakashima, H., Ishihara, T. & Kitamoto, T. 2007. Amyloid precursor protein cytoplasmic domain with phospho-Thr668 accumulates in Alzheimer's disease and its transgenic models: a role to mediate interaction of Aβ and tau. *Acta Neuropathologica,* 113**,** 627-636.

Shipton, O. A., Leitz, J. R., Dworzak, J., Acton, C. E. J., Tunbridge, E. M., Denk, F., Dawson, H. N., Vitek, M. P., Wade-Martins, R., Paulsen, O. & Vargas-Caballero, M. 2011. Tau protein is required for amyloid β-induced impairment of hippocampal long-term potentiation. *The Journal of Neuroscience,* 31**,** 1688-92.

Shiryaev, N., Jouroukhin, Y., Giladi, E., Polyzoidou, E., Grigoriadis, N. C., Rosenmann, H. & Gozes, I. 2009. NAP protects memory, increases soluble tau and reduces tau hyperphosphorylation in a tauopathy model. *Neurobiology of Disease,* 34**,** 381-388.

Shulman, J. M., Imboywa, S., Giagtzoglou, N., Powers, M. P., Hu, Y., Devenport, D., Chipendo, P., Chibnik, L. B., Diamond, A., Perrimon, N., Brown, N. H., De Jager, P. L. & Feany, M. B. 2014. Functional screening in Drosophila identifies Alzheimer's disease susceptibility genes and implicates Tau-mediated mechanisms. *Human Molecular Genetics,* 23**,** 870-877.

Simón, D., García-García, E., Royo, F., Falcón-Pérez, J. M. & Avila, J. 2012. Proteostasis of tau. Tau overexpression results in its secretion via membrane vesicles. *FEBS Letters,* 586**,** 47-54.

Sjogren, M., Davidsson, P., Tullberg, M., Minthon, L., Wallin, A., Wikkelso, C., Granerus, A., Vanderstichele, H., Vanmechelen, E. & Blennow, K. 2001. Both total and phosphorylated tau are increased in Alzheimer's disease. *Journal of Neurology, Neurosurgery, and Psychiatry,* 70**,** 624-630.

Sjogren, T., Sjogren, H. & Lindgren, A. G. 1952. Morbus Alzheimer and morbus Pick, a genetic, clinical and patho-anatomical study. *Acta Psychiatrica et Neurologica Scandinavica. Supplementum,* 82**,** 1-152.

Smith, M. A., Hirai, K., Hsiao, K., Pappolla, M. A., Harris, P. L., Siedlak, S. L., Tabaton, M. & Perry, G. 1998. Amyloid-β Deposition in Alzheimer Transgenic Mice Is Associated with Oxidative Stress. *Journal of Neurochemistry,* 70**,** 2212-2215.

Sokolow, S., Henkins, K. M., Bilousova, T., Gonzalez, B., Vinters, H. V., Miller, C. A., Cornwell, L., Poon, W. W. & Gylys, K. H. 2015. Pre-synaptic C-terminal truncated tau is released from cortical synapses in Alzheimer's disease. *Journal of Neurochemistry,* 133**,** 368-379.

Soldner, F. & Jaenisch, R. 2015. Dissecting Risk Haplotypes in Sporadic Alzheimer's Disease. *Cell Stem Cell,* 16**,** 341-342.

Song, J. M., Dibattista, A. M., Sung, Y. M., Ahn, J. M., Turner, R. S., Yang, J., Pak, D. T. S., Lee, H.-K. & Hoe, H.-S. 2014. A tetra(ethylene glycol) derivative of benzothiazole aniline ameliorates dendritic spine density and cognitive function in a mouse model of Alzheimer's disease. *Experimental Neurology,* 252**,** 105-113.

Sperbera, B. R., Leight, S., Goedert, M. & Lee, V. M. Y. 1995. Glycogen synthase kinase-3β phosphorylates tau protein at multiple sites in intact cells. *Neuroscience Letters,* 197**,** 149-153.

Spires-Jones, Tara l. & Hyman, Bradley t. 2014. The Intersection of Amyloid Beta and Tau at Synapses in Alzheimer's Disease. *Neuron,* 82**,** 756-771.

Sposito, T., Preza, E., Mahoney, C. J., Setó-Salvia, N., Ryan, N. S., Morris, H. R., Arber, C., Devine, M. J., Houlden, H., Warner, T. T., Bushell, T. J., Zagnoni, M., Kunath, T., Livesey, F. J., Fox, N. C., Rossor, M. N., Hardy, J. & Wray, S. 2015. Developmental regulation of tau splicing is disrupted in stem cell-derived neurons from frontotemporal dementia patients with the 10 + 16 splice-site mutation in MAPT. *Human Molecular Genetics,* 24**,** 5260-5269.

Standen, C. L., Brownlees, J., Grierson, A. J., Kesavapany, S., Lau, K.-F., Mcloughlin, D. M. & Miller, C. C. J. 2001. Phosphorylation of thr668 in the cytoplasmic domain of the Alzheimer's disease amyloid precursor protein by stress-activated protein kinase 1b (Jun N-terminal kinase-3). *Journal of Neurochemistry,* 76**,** 316-320.

Sterniczuk, R., Antle, M. C., Laferla, F. M. & Dyck, R. H. 2010a. Characterization of the 3xTg-AD mouse model of Alzheimer's disease: Part 2. Behavioral and cognitive changes. *Brain Research,* 1348**,** 149-155.

Sterniczuk, R., Dyck, R. H., Laferla, F. M. & Antle, M. C. 2010b. Characterization of the 3xTg-AD mouse model of Alzheimer's disease: Part 1. Circadian changes. *Brain Research,* 1348**,** 139-148.

Stockley, J. H. & O'neill, C. 2007. The proteins BACE1 and BACE2 and β-secretase activity in normal and Alzheimer's disease brain. *Biochemical Society Transactions,* 35**,** 574-576.

Stoothoff, W. H. & Johnson, G. V. W. 2005. Tau phosphorylation: physiological and pathological consequences. *Biochimica et Biophysica Acta (BBA) - Molecular Basis of Disease,* 1739**,** 280-297.

Stoppini, L., Buchs, P. A. & Muller, D. 1991. A simple method for organotypic cultures of nervous tissue. *Journal of Neuroscience Methods,* 37**,** 173-182.

Sturchler-Pierrat, C., Abramowski, D., Duke, M., Wiederhold, K.-H., Mistl, C., Rothacher, S., Ledermann, B., Burki, K., Frey, P., Paganetti, P. A., Waridel, C., Calhoun, M. E., Jucker, M., Probst, A., Staufenbiel, M. & Sommer, B. 1997. Two amyloid precursor protein transgenic mouse models with Alzheimer disease-like pathology. *Proceedings of the National Academy of Sciences of the United States of America,* 94**,** 13287-13292.

Su, J. H., Cummings, B. J. & Cotman, C. W. 1994. Early phosphorylation of tau in Alzheimer's disease occurs at Ser-202 and is preferentially located within neurites. *NeuroReport,* 5**,** 2358-2362.

Su, Y., Ryder, J., Li, B., Wu, X., Fox, N., Solenberg, P., Brune, K., Paul, S., Zhou, Y., Liu, F. & Ni, B. 2004. Lithium, a Common Drug for Bipolar Disorder Treatment, Regulates Amyloid-β Precursor Protein Processing. *Biochemistry,* 43**,** 6899-6908.

Sundaram, J. R., Poore, C. P., Sulaimee, N. H. B., Pareek, T., Asad, A. B. M. A., Rajkumar, R., Cheong, W. F., Wenk, M. R., Dawe, G. S., Chuang, K.-H., Pant, H. C. & Kesavapany, S. 2013. Specific Inhibition of p25/Cdk5 Activity by the Cdk5 Inhibitory Peptide Reduces Neurodegeneration In Vivo. *The Journal of Neuroscience,* 33**,** 334-343.

Sundstrom, L., Pringle, A., Morrison, B. & Bradley, M. 2005. Organotypic cultures as tools for functional screening in the CNS. *Drug Discovery Today,* 10**,** 993-1000.

Sutherland, C., Leighton, I. A. & Cohen, P. 1993. Inactivation of glycogen synthase kinase-3 beta by phosphorylation: new kinase connections in insulin and growth-factor signalling. *Biochemical Journal,* 296**,** 15-19.

Sy, M., Kitazawa, M., Medeiros, R., Whitman, L., Cheng, D., Lane, T. E. & Laferla, F. M. 2011. Inflammation Induced by Infection Potentiates Tau Pathological Features in Transgenic Mice. *The American Journal of Pathology,* 178**,** 2811-2822.

Tai, H.-C., Serrano-Pozo, A., Hashimoto, T., Frosch, M. P., Spires-Jones, T. L. & Hyman, B. T. 2012. The Synaptic Accumulation of Hyperphosphorylated Tau Oligomers in Alzheimer Disease Is Associated With Dysfunction of the Ubiquitin-Proteasome System. *The American Journal of Pathology,* 181**,** 1426-1435.

Tai, H.-C., Wang, B. Y., Serrano–Pozo, A., Frosch, M. P., Spires-Jones, T. L. & Hyman, B. T. 2014. Frequent and symmetric deposition of misfolded tau oligomers within presynaptic and postsynaptic terminals in Alzheimer's disease. *Acta Neuropathologica Communications,* 2**,** 146.

Takeda, S., Wegmann, S., Cho, H., Devos, S. L., Commins, C., Roe, A. D., Nicholls, S. B., Carlson, G. A., Pitstick, R., Nobuhara, C. K., Costantino, I., Frosch, M. P., Muller, D. J., Irimia, D. & Hyman, B. T. 2015. Neuronal uptake and propagation of a rare phosphorylated high-molecular-weight tau derived from Alzheimer's disease brain. *Nature Communications,* 6.

Takuma, H., Arawaka, S. & Mori, H. 2003. Isoforms changes of tau protein during development in various species. *Developmental brain research,* 142**,** 121-127.

Tandon, A., Yu, H., Wang, L., Rogaeva, E., Sato, C., Chishti, M. A., Kawarai, T., Hasegawa, H., Chen, F., Davies, P., Fraser, P. E., Westaway, D. & St George-Hyslop, P. H. 2003. Brain levels of CDK5 activator p25 are not increased in Alzheimer's or other

neurodegenerative diseases with neurofibrillary tangles. *Journal of Neurochemistry,* 86**,** 572-581.

Tang, D., Yeung, J., Lee, K.-Y., Matsushita, M., Matsui, H., Tomizawa, K., Hatase, O. & Wang, J. H. 1995. An Isoform of the Neuronal Cyclin-dependent Kinase 5 (Cdk5) Activator. *Journal of Biological Chemistry,* 270**,** 26897-26903.

Tanzi, R. E. 2012. The Genetics of Alzheimer Disease. *Cold Spring Harbor Perspectives in Medicine,* 2.

Tejera, D. & Heneka, M. T. 2015. Microglia in Alzheimer's disease: the good, the bad and the ugly. *Current Alzheimer Research,* 13.

Terry, R. D. & Davies, P. 1980. Dementia of the Alzheimer Type. *Annual Review of Neuroscience,* 3**,** 77-95.

Terry, R. D., Masliah, E., Salmon, D. P., Butters, N., Deteresa, R., Hill, R., Hansen, L. A. & Katzman, R. 1991. Physical basis of cognitive alterations in alzheimer's disease: Synapse loss is the major correlate of cognitive impairment. *Annals of Neurology,* 30**,** 572-580.

Terwel, D., Lasrado, R., Snauwaert, J., Vandeweert, E., Van Haesendonck, C., Borghgraef, P. & Van Leuven, F. 2005. Changed Conformation of Mutant Tau-P301L Underlies the Moribund Tauopathy, Absent in Progressive, Nonlethal Axonopathy of Tau-4R/2N Transgenic Mice. *Journal of Biological Chemistry,* 280**,** 3963-3973.

Townsend, M., Mehta, T. & Selkoe, D. J. 2007. Soluble Aβ inhibits specific signal transduction cascades common to the insulin receptor pathway. *Journal of Biological Chemistry,* 282**,** 33305-33312.

Tsai, L.-H., Lee, M.-S. & Cruz, J. 2004. Cdk5, a therapeutic target for Alzheimer's disease? *Biochimica et Biophysica Acta (BBA) - Proteins and Proteomics,* 1697**,** 137-142.

Tseng, H.-C., Zhou, Y., Shen, Y. & Tsai, L.-H. 2002. A survey of Cdk5 activator p35 and p25 levels in Alzheimer's disease brains. *FEBS Letters,* 523**,** 58-62.

Usardi, A., Pooler, A. M., Seereeram, A., Reynolds, C. H., Derkinderen, P., Anderton, B., Hanger, D. P., Noble, W. & Williamson, R. 2011. Tyrosine phosphorylation of tau regulates its interactions with Fyn SH2 domains, but not SH3 domains, altering the cellular localization of tau. *FEBS Journal,* 278**,** 2927-2937.

Vassar, R., Bennett, B. D., Babu-Khan, S., Kahn, S., Mendiaz, E. A., Denis, P., Teplow, D. B., Ross, S., Amarante, P., Loeloff, R., Luo, Y., Fisher, S., Fuller, J., Edenson, S., Lile, J., Jarosinski, M. A., Biere, A. L., Curran, E., Burgess, T., Louis, J.-C., Collins, F., Treanor, J., Rogers, G. & Citron, M. 1999. β-Secretase Cleavage of Alzheimer's Amyloid Precursor Protein by the Transmembrane Aspartic Protease BACE. *Science,* 286**,** 735-741.

Villemagne, V. L., Pike, K. E., Chételat, G., Ellis, K. A., Mulligan, R. S., Bourgeat, P., Ackermann, U., Jones, G., Szoeke, C., Salvado, O., Martins, R., O'keefe, G., Mathis, C. A., Klunk, W. E., Ames, D., Masters, C. L. & Rowe, C. C. 2011. Longitudinal assessment of Aβ and cognition in aging and Alzheimer disease. *Annals of Neurology,* 69**,** 181-192.

Vossel, K. A., Xu, J. C., Fomenko, V., Miyamoto, T., Suberbielle, E., Knox, J. A., Ho, K., Kim, D. H., Yu, G.-Q. & Mucke, L. 2015. Tau reduction prevents Aβ-induced axonal transport deficits by blocking activation of GSK3β. *The Journal of Cell Biology,* 209**,** 419-433.

Walsh, D. M., Tseng, B. P., Rydel, R. E., Podlisny, M. B. & Selkoe, D. J. 2000. The Oligomerization of Amyloid β-Protein Begins Intracellularly in Cells Derived from Human Brain. *Biochemistry,* 39**,** 10831-10839.

Walsh, D. T., Montero, R. M., Bresciani, L. G., Jen, A. Y. T., Leclercq, P. D., Saunders, D., El-Amir, A. N., Gbadamoshi, L., Gentleman, S. M. & Jen, L.-S. 2002. Amyloid-Beta Peptide Is Toxic to Neurons In Vivo via Indirect Mechanisms. *Neurobiology of Disease,* 10**,** 20-27.

Wang, J.-Z., Gong, C.-X., Zaidi, T., Grundke-Iqbal, I. & Iqbal, K. 1995. Dephosphorylation of Alzheimer Paired Helical Filaments by Protein Phosphatase-2A and −2B. *Journal of Biological Chemistry,* 270**,** 4854-4860.

Wang, J. Z., Gao, X. & Wang, Z. H. 2014. The physiology and pathology of microtubule-associated protein tau. *Essays in Biochemistry,* 56**,** 111-23.

Wang, Q., Walsh, D. M., Rowan, M. J., Selkoe, D. J. & Anwyl, R. 2004. Block of Long-Term Potentiation by Naturally Secreted and Synthetic Amyloid β-Peptide in Hippocampal Slices Is Mediated via Activation of the Kinases c-Jun N-Terminal Kinase, Cyclin-Dependent Kinase 5, and p38 Mitogen-Activated Protein Kinase as well as Metabotropic Glutamate Receptor Type 5. *The Journal of Neuroscience,* 24**,** 3370-3378.

Wang, Q. M., Fiol, C. J., Depaoli-Roach, A. A. & Roach, P. J. 1994. Glycogen synthase kinase-3 beta is a dual specificity kinase differentially regulated by tyrosine and serine/threonine phosphorylation. *Journal of Biological Chemistry,* 269**,** 14566-14574.

Ward, S. M., Himmelstein, D. S., Ren, Y., Fu, Y., Yu, X.-W., Roberts, K., Binder, L. I. & Sahara, N. 2014. TOC1: A valuable tool in assessing disease progression in the rTg4510 mouse model of tauopathy. *Neurobiology of disease,* 67**,** 37-48.

Waterston, R. H., Mouse Genome Sequencing, C., Lindblad-Toh, K., Birney, E., Rogers, J., Abril, J. F., Agarwal, P., Agarwala, R., Ainscough, R., Alexandersson, M., An, P., Antonarakis, S. E., Attwood, J., Baertsch, R., Bailey, J., Barlow, K., Beck, S., Berry, E., Birren, B., Bloom, T., Bork, P., Botcherby, M., Bray, N., Brent, M. R., Brown, D. G., Brown, S. D., Bult, C., Burton, J., Butler, J., Campbell, R. D., Carninci, P., Cawley, S., Chiaromonte, F., Chinwalla, A. T., Church, D. M., Clamp, M., Clee, C., Collins, F. S., Cook, L. L., Copley, R. R., Coulson, A., Couronne, O., Cuff, J., Curwen, V., Cutts, T., Daly, M., David, R., Davies, J., Delehaunty, K. D., Deri, J., Dermitzakis, E. T., Dewey, C., Dickens, N. J., Diekhans, M., Dodge, S., Dubchak, I., Dunn, D. M., Eddy, S. R., Elnitski, L., Emes, R. D., Eswara, P., Eyras, E.,

Felsenfeld, A., Fewell, G. A., Flicek, P., Foley, K., Frankel, W. N., Fulton, L. A., Fulton, R. S., Furey, T. S., Gage, D., Gibbs, R. A., Glusman, G., Gnerre, S., Goldman, N., Goodstadt, L., Grafham, D., Graves, T. A., Green, E. D., Gregory, S., Guigo, R., Guyer, M., Hardison, R. C., Haussler, D., Hayashizaki, Y., Hillier, L. W., Hinrichs, A., Hlavina, W., Holzer, T., Hsu, F., Hua, A., Hubbard, T., Hunt, A., Jackson, I., Jaffe, D. B., Johnson, L. S., Jones, M., Jones, T. A., Joy, A., Kamal, M., et al. 2002. Initial sequencing and comparative analysis of the mouse genome. *Nature,* 420**,** 520-62.

Weaver, C. L., Espinoza, M., Kress, Y. & Davies, P. 2000. Conformational change as one of the earliest alterations of tau in Alzheimer's disease. *Neurobiology of Aging,* 21**,** 719-727.

Webster, S. J., Bachstetter, A. D., Nelson, P. T., Schmitt, F. A. & Van Eldik, L. J. 2014. Using mice to model Alzheimer's dementia: an overview of the clinical disease and the preclinical behavioral changes in ten mouse models. *Frontiers in Genetics,* 5.

Wegmann, S., Maury, E. A., Kirk, M. J., Saqran, L., Roe, A., Devos, S. L., Nicholls, S., Fan, Z., Takeda, S., Cagsal-Getkin, O., William, C. M., Spires-Jones, T. L., Pitstick, R., Carlson, G. A., Pooler, A. M. & Hyman, B. T. 2015. Removing endogenous tau does not prevent tau propagation yet reduces its neurotoxicity. *The EMBO Journal*.

Weingarten, M. D., Lockwood, A. H., Hwo, S. Y. & Kirschner, M. W. 1975. A protein factor essential for microtubule assembly. *Proceedings of the National Academy of Sciences of the United States of America,* 72**,** 1858-1862.

Willem, M., Tahirovic, S., Busche, M. A., Ovsepian, S. V., Chafai, M., Kootar, S., Hornburg, D., Evans, L. D. B., Moore, S., Daria, A., Hampel, H., Muller, V., Giudici, C., Nuscher, B., Wenninger-Weinzierl, A., Kremmer, E., Heneka, M. T., Thal, D. R., Giedraitis, V., Lannfelt, L., Muller, U., Livesey, F. J., Meissner, F., Herms, J., Konnerth, A., Marie, H. & Haass, C. 2015. η-Secretase processing of APP inhibits neuronal activity in the hippocampus. *Nature,* 526**,** 443-447.

Wittmann, C. W., Wszolek, M. F., Shulman, J. M., Salvaterra, P. M., Lewis, J., Hutton, M. & Feany, M. B. 2001. Tauopathy in Drosophila: Neurodegeneration Without Neurofibrillary Tangles. *Science,* 293**,** 711-714.

Wolozin, B. L., Pruchnicki, A., Dickson, D. W. & Davies, P. 1986. A neuronal antigen in the brains of Alzheimer patients. *Science,* 432**,** 648-50.

Wray, S., Saxton, M., Anderton, B. H. & Hanger, D. P. 2008. Direct analysis of tau from PSP brain identifies new phosphorylation sites and a major fragment of N-terminally cleaved tau containing four microtubule-binding repeats. *Journal of Neurochemistry,* 105**,** 2343-2352.

Wu, J. W., Herman, M., Liu, L., Simoes, S., Acker, C. M., Figueroa, H., Steinberg, J. I., Margittai, M., Kayed, R., Zurzolo, C., Di Paolo, G. & Duff, K. E. 2013. Small Misfolded Tau Species Are Internalized via Bulk Endocytosis and Anterogradely and Retrogradely Transported in Neurons. *The Journal of Biological Chemistry,* 288**,** 1856-1870.

Xia, D., Li, C. & Götz, J. 2015. Pseudophosphorylation of Tau at distinct epitopes or the presence of the P301L mutation targets the microtubule-associated protein Tau to dendritic spines. *Biochimica et Biophysica Acta (BBA) - Molecular Basis of Disease,* 1852**,** 913-924.

Yamada, K., Cirrito, J. R., Stewart, F. R., Jiang, H., Finn, M. B., Holmes, B. B., Binder, L. I., Mandelkow, E.-M., Diamond, M. I., Lee, V. M. Y. & Holtzman, D. M. 2011. In Vivo Microdialysis Reveals Age-Dependent Decrease of Brain Interstitial Fluid Tau Levels in P301S Human Tau Transgenic Mice. *The Journal of Neuroscience,* 31**,** 13110-13117.

Yamada, K., Holth, J. K., Liao, F., Stewart, F. R., Mahan, T. E., Jiang, H., Cirrito, J. R., Patel, T. K., Hochgräfe, K., Mandelkow, E.-M. & Holtzman, D. M. 2014. Neuronal activity regulates extracellular tau in vivo. *The Journal of Experimental Medicine,* 211**,** 387-393.

Yang, L.-S. & Ksiezak-Reding, H. 1995. Calpain-Induced Proteolysis of Normal Human Tau and Tau Associated with Paired Helical Filaments. *European Journal of Biochemistry,* 233**,** 9-17.

Yankner, B. A. & Lu, T. 2009. Amyloid β-Protein Toxicity and the Pathogenesis of Alzheimer Disease. *The Journal of Biological Chemistry,* 284**,** 4755-4759.

Yates, D. & Mcloughlin, D. M. 2008. The molecular pathology of Alzheimer's disease. *Psychiatry,* 7**,** 1-5.

Yatin, S., Varadarajan, S., Link, C. & Butterfield, D. 1999. In vitro and in vivo oxidative stress associated with Alzheimer's amyloid ß-peptide (1–42). *Neurobiology of Aging,* 20**,** 325-30.

Yeh, C.-Y., Verkhratsky, A., Terzieva, S. & Rodríguez, J. 2013. Glutamine synthetase in astrocytes from entorhinal cortex of the triple transgenic animal model of Alzheimer's disease is not affected by pathological progression. *Biogerontology,* 14**,** 777-787.

Yenjerla, M., Lapointe, N. E., Lopus, M., Cox, C., Jordan, M. A., Feinstein, S. C. & Wilson, L. 2010. The Neuroprotective Peptide NAP Does Not Directly Affect Polymerization or Dynamics of Reconstituted Neural Microtubules. *Journal of Alzheimer's Disease,* 19**,** 1377-1386.

Zemlyak, I., Furman, S., Brenneman, D. E. & Gozes, I. 2000. A Novel peptide prevents death in enriched neuronal cultures. *Regulatory Peptides,* 96**,** 39-43.

Zempel, H., Thies, E., Mandelkow, E. & Mandelkow, E. M. 2010. Abeta oligomers cause localized Ca(2+) elevation, missorting of endogenous Tau into dendrites, Tau phosphorylation, and destruction of microtubules and spines. *The Journal of Neuroscience,* 30**,** 11938-50.

Zhang, F., Su, B., Wang, C., Siedlak, S. L., Mondragon-Rodriguez, S., Lee, H.-G., Wang, X., Perry, G. & Zhu, X. 2015a. Posttranslational modifications of α-tubulin in alzheimer disease. *Translational Neurodegeneration,* 4**,** 9.

Zhang, H., Jarjour, A. A., Boyd, A. & Williams, A. 2011a. Central nervous system remyelination in culture — A tool for multiple sclerosis research. *Experimental Neurology,* 230**,** 138-148.

Zhang, Y.-W., Thompson, R., Zhang, H. & Xu, H. 2011b. APP processing in Alzheimer's disease. *Molecular Brain,* 4**,** 3-3.

Zhang, Z., Song, M., Liu, X., Kang, S. S., Kwon, I.-S., Duong, D. M., Seyfried, N. T., Hu, W. T., Liu, Z., Wang, J.-Z., Cheng, L., Sun, Y. E., Yu, S. P., Levey, A. I. & Ye, K. 2014. Cleavage of tau by asparagine endopeptidase mediates the neurofibrillary pathology in Alzheimer's disease. *Nature Medicine,* 20**,** 1254-1262.

Zhang, Z., Song, M., Liu, X., Su Kang, S., Duong, D. M., Seyfried, N. T., Cao, X., Cheng, L., Sun, Y. E., Ping Yu, S., Jia, J., Levey, A. I. & Ye, K. 2015b. Delta-secretase cleaves amyloid precursor protein and regulates the pathogenesis in Alzheimer's disease. *Nature Communications,* 6**,** 8762.